University of Southampton

Online Condition Monitoring of HV Cable Circuits

By

Ping Wang

A thesis submitted for the Degree of

Doctor of Philosophy

In

The School of Electronics and Computer Science

July 2004

UNIVERSITY OF SOUTHAMPTON

ABSTRACT

FACULTY OF ENGINEERING SCIENCE AND MATHEMATICS

SCHOOL OF ELECTRONICS AND COMPUTER SCIENCE

Doctor of Philosophy

ONLINE CONDITION MONITORING OF HV CABLE CIRCUITS

by Ping Wang

This thesis is concerned with the development of online condition monitoring methods for high voltage cables and accessories. In particular the detection and measurement of partial discharge activities has been investigated in detail as it is an important metric and a clear symptom of insulation degradation.

Acoustic methods have been widely applied for partial discharge detection in power apparatus. Initial studies were undertaken to assess the suitability of PVDF as a piezoelectric sensor for detecting acoustic emission signals due to partial discharge activities in high voltage cable accessories. However, experimentation revealed that in this application the sensor output is due to electrical coupling rather than measuring a detectable acoustic emission signal.

As an alternative approach, the use of capacitive couplers for partial discharge detection has been further considered. Although widely applied a suitably accurate method of calibration when used in the field has not been developed. Assessment of various pulse based calibration techniques yielded the conclusion that these approaches are inaccurate because they cannot account for the influence of stray capacitance. This has led to the development of a new method of calibration based on frequency response analysis and the use of simulation model. Results obtained are in good agreement with values determined using a terminal injection method.

Consideration has also been given to methods of discriminating between internal partial discharge activities and external sources of noise such as corona discharge, synchronous pulses or random noise. The use of wavelets for signals discrimination and to improve the signal to noise ratio has proved successful.

Contents

List of Figures

List of Tables

List of Symbols and Abbreviations

Symbols

ζ	damping ratio
ω	frequency in radian/s
ω_P	Pole corner frequency in radian/s
ω_Z	zero corner frequency in radian/s
A	integration (area) of voltage $U_m(t)$ across a load
B	transmission input of network analyser
C_0	injection capacitor
C_A	capacitance of dielectrics
C_B	capacitance of the sound dielectrics
C_C	capacitance of the void, capacitive coupler capacitance
C_f	capacitance of piezo film
C_k	coupling capacitance
C_S	stray capacitance
C_x	capacitance of the test object
D	detector
G	low frequency gain
$H(\omega)$	transfer function model
$H_a(\omega)$	approximate transfer function model
i(t)	output transient current from calibrator
I_2	output current of a current source pulse generator
R	reference output of network analyser
R_f	internal film resistance
R_M	measuring impedance

P	discharge power
Q	charge developed over PVDF film electrodes, injected charge
q	apparent charge
q_A	apparent charge across the whole dielectrics
q_C	real discharge across the void
U_0	voltage magnitude of pulse generator
U_A	applied high voltage across the dielectrics
U_C	internal voltage across the cavity
U_{CB}	breakdown voltage $U_p$discharge pulse
U_e	discharge extinguish voltage
U_i	discharge inception voltage
$U_m(t)$	transient voltage across a load
U_r	remnant voltage
U_s	inverse voltage due to discharge
U~	high voltage supply
V	voltage developed over PVDF film electrodes, voltage magnitude of pulse generator
V_0	discharge magnitude detected by capacitive coupler
V_1	output voltage from a current source pulse generator
V_2	output voltage across the external load
V_I	discharge voltage magnitude occurred between cable core conductor and earth
V_X	voltage across the test object
W	discharge energy
Z_0	characteristic impedance of the cable
Z_{mi}	impedance of the measuring system

Abbreviations

AC	Alternating current
AE	acoustic emission
BM	breakdown maintenance
CBM	condition based maintenance
CCS	coaxial cable sensor
CD	coupling device

CT	current transducer
DC	direct current
DCS	directional coupler sensor
DGA	dissolved gas analysis
DSI	discrete spectral interference
ERA	Electric Research Association
EPR	propylene rubber
FFT	fast Fourier transform
FRA	frequency response analyser
GIS	gas insulated switchgear
GPIB	general-purpose interface board
HFCT	high frequency current transformer
HV	high voltage
IEC	Electro-technical Commission
LDPE	low density polyethylene
MI	measuring instrument
NA	network analyser
OWT	oscillating wave test
PD	partial discharge
PE	polyethylene
PG	pulse generator
PVC	polyvinyl chloride
PVDF	polyvinylidene fluoride
RC	resistor and capacitor circuit measuring impedance
REDI	resonance type partial discharge
RF	radio frequency
RLC	resistor inductor and capacitor circuit measuring impedance
sgp	surge protector
TBM	time based maintenance
TDR	time domain reflectometry
VHF	very high frequency
VLF	very low frequency
XLPE	cross-linked polyethylene

Acknowledgements

My acknowledgement must go to Dr Paul Lewin for his guidance and support and encouragement throughout every part of this work, without which the completion of this thesis would not be possible.

My gratitude must also go to the technical staff of high voltage laboratory for their support and assistance during the experimental work of the project in particular Mr N Palmer and Mr M Smith. I would also like to express my appreciation to my colleges in high voltage group for their assistance, support and valuable discussions during the whole process of the work. Special thanks go to Dr Yuan Tian and Dr Baojia Han. The help from Dr George Chen for guidance is highly appreciated.

My gratitude is also extended to National Grid Transco, plc for sponsoring this project, especially Dr Simon Sutton for advice and support.

Special appreciation goes to Professor Tony Davies and Mr Roland for their guidance and support in the initial stage of this work. Their sudden death is great loss to everyone in HV group.

Last but not least, thanks must go to my parents, my husband Yisheng and my daughter Jenny for their love, support and encouragement through my study in UK.

Chapter 1

Introduction

High Voltage (HV) cables are necessary and important equipment for industrial power transmission and distribution. Hence, the long-term reliability of cable systems especially the condition of their insulation is of great importance. During manufacture, installation and operation, the thermal, electrical and mechanical stresses together with environmental factors can combine to degrade electrical insulation [1]. Degraded insulation will eventually lead to breakdown that may result in system failure and significant economical loss. So from both an economical and technical point of view, the maintenance strategies for cable systems are gradually shifting from passive Breakdown Maintenance (BM), Time Based Maintenance (TBM) towards more active Condition Based Maintenance (CBM), i.e. preventive maintenance depending on the actual conditions [2, 3]. Condition monitoring of cable systems is becoming an important means to assess insulation deterioration, various techniques have been developed and several parameters that indicate insulation deterioration such as inception voltage, dielectric properties and partial discharge activities are being studied [4-8]. Among them partial discharge (PD) measurements have become an important metric and an internationally accepted method for condition monitoring of insulation systems because PD is both a dominant preceding symptom and cause of deterioration within solid electric insulation [4,5,8].

Since PD activities result in high frequency current pulses and radio frequency emission, the detection of PD under laboratory conditions is relatively straightforward and PD measurements have become the dominant basis for quality

control testing of high voltage apparatus which employs solid insulation. This is so called traditional off-line PD testing which is usually performed within a well-screened laboratory with the equipment disconnected from the power system for the duration of the test. The applied high voltage is usually higher than the normal operating voltage. It has become a standard method and widely used for quality control testing when the equipment is in development by a manufacturer. PD detection will identify defects such as voids, metallic impurities inside the insulation and insulating surface contamination. The relevant standards for PD tests have been established for more than 50 years and the latest (third) version was published in 2000 [9]. However, this approach requires an increased power supply, connection of a coupling capacitor for isolation from the operating voltage, and it can only be performed under laboratory conditions.

An alternative for the traditional off-line test is on-line testing where the high voltage apparatus operates normally, i.e. without an outage for PD testing. Therefore, the interruption of the operating voltage is avoided and the operators' costs are drastically reduced. Online test systems have been successfully used on HV equipment such as power generators, transformers and gas insulated substations (GIS) [1, 10, 11]. Online PD detection techniques are especially useful for detecting defects that occur during the installation of cable accessories such as joints and terminations, which have to be installed on site often in unideal conditions. Normal service defects due to the environmental factors such as thermal stresses and chemical changes can also be detected.

Online versus offline detection methods and their advantages and disadvantages have been vigorously debated in recent years especially with the advancement of online detection techniques [11-13]. Generally speaking, PD measurements are preferably undertaken online during regular operation for several reasons: Firstly online PD measurements are conducted under realistic stresses. Offline measurements are carried out at an elevated test voltage, which could cause damage to the insulation material. The level of damage that a PD can cause is proportional to the power (energy per unit time) per unit area of insulation (power density) involved in the discharge. Therefore, it is misleading to assume that offline PD tests using elevated stresses are non-destructive. Offline testing can reduce the remaining life of a cable

system and introduce some types of defects. It can also initiate electrical trees from existing water trees [12]. Secondly online PD measurements provide early detection of possible failures. Online PD measurements are based on the permanent installation of PD sensors which provide continuous condition monitoring of HV components. Therefore inspection of the condition is possible at every instant e.g. before instead of during a revision, before and after repair. Therefore catastrophic failures can be successfully avoided. However, online PD measurements are based on non-conventional field techniques. They are relatively new and no international standards are available regarding the procedures of online PD measurements and the quantification of measured results from online systems remains a controversial topic. Another challenge associated with online PD measurements is coping with excessive background noise and interference. As online PD tests are carried out on-site where no specific measures have been employed to avoid external interference from radio transmissions, communications and ambient electrical devices, suppression of background noise is important in order to improve online detection credibility and measurement sensitivity.

Several non-conventional techniques such as capacitive coupling and inductive coupling as well as acoustic emission methods have been developed for online PD detection and some of them have been applied [14-20]. This project focuses on a popular non-conventional field coupling technique i.e. very high frequency (VHF) capacitive coupling. The structure and characteristics of capacitive couplers used to detect PD in HV cables will be discussed, and in particular the calibration of the measured results and signal post-processing techniques regarding the signals obtained by capacitive couplers will be investigated. Another non-conventional PD detection technique - acoustic emission technique using PVDF polymer film sensor has also been examined.

It is widely accepted that capacitive coupler sensors are very sensitive and effective in detecting PD activities online [21, 22]. Compared to the conventional electrical method, they are cheap and easy to apply. The application of capacitive couplers has been reported not only on HV cables but also on other HV equipment such as transformers and rotating machines [23-26]. However the measured results have been referred only in voltage (mV or μV) term rather than charge values in picoColoumbs

(pC) due to lack of an established calibration method and subsequent international standard.

Another problem regarding online onsite PD detection is coping with excessive background noise and interference. Noise and interference includes PD and corona from the power system, arcing between adjacent metallic components and poor contact, power line carrier communication systems, thyristor switching and radio transmissions [1]. The latter three sources of interference tend to generate frequency components which can be eliminated through suitable frequency domain filtering or pulses which occur at fixed positions of ac cycle can be deleted by time domain filtering (gating). Thus these sources of noise are not difficult to identify and remove. Other noise sources can cause significant problems for PD detection since they have characteristics in common with the PD signal being measured in that they involve brief bursts of current flow across short gas gaps, just as PD occurring in a cavity within a solid dielectric. The existence of the noise and interference significantly reduces the measurement sensitivity and results in false indication. In extreme cases, online PD tests are impossible. Thus to ensure reliable online PD testing without false indication, PD pulses from test objects must be distinguished from such extreme electrical interference.

1.1 Contents of this thesis

Based on the present problems regarding the use of capacitive couplers as a means to monitor the condition of HV cables online, this project is concerned with solving these problems. Within this in mind, fundamental studies regarding the use of capacitive couplers especially calibration of capacitive couplers have been investigated in detail. A possible acoustic PD online detection method has also been examined. A brief review of fundamentals of PD and detection methods in cable systems is presented in Chapter 2. Chapter 3 investigates a possible acoustic emission method for online detection of partial discharges in cables using a new piezoelectric material. The issues relevant to the use of capacitive couplers especially evaluation of injected charge and available calibration methods for capacitive coupler sensors are presented in Chapter 4. Chapter 5 presents a new calibration method based on a simulation model of a specific capacitive coupler/cable system,

which is established through frequency response analysis (FRA) of the coupler/cable system. To further investigate this method, two real PD experiments have been undertaken and their calibration results and comparison with the conventional apparent charge are presented in Chapter 6. Chapter 7 investigates de-noising techniques applied to signals obtained using capacitive couplers. Wavelet analysis is found to be effective in discriminating between internal PD pulses and external corona interference as well as some other forms of pulse-like interference. Finally Conclusions and Further Work are presented in Chapter 8.

Chapter 2

Partial Discharge and Detection in HV Cables

As an important tool for assessing the quality and performance characteristics of HV equipment, partial discharge testing has been employed for more than 50 years. Over this time research into partial discharge phenomena has been undertaken and it is now considered to be a well-developed field. Investigations related to PD mechanisms, physical and chemical effects, detection and measurement techniques have been widely reported [27]. It has been the main non-destructive test for HV cable insulation especially since the introduction of polymeric extruded cables into the power distribution network in the early 1950s. These cables include polyethylene (PE), cross-linked polyethylene (XLPE), Polyvinyl Chloride (PVC) and Ethylene Propylene Rubber (EPR) insulation. While partial discharge testing is important for both oil-impregnated paper cables and extruded polymeric cables, it is crucial to polymeric cables. Compared to oil/paper insulation cables, polymeric cables are highly susceptible to PD induced degradation and cannot operate in the presence of PD without undergoing eventual failure. This is due to the following reasons [28, 29]: Firstly partial discharge can originate from voids, impurities and protrusions within the cable insulation or at the interface between the insulation and the semiconducting screen layer due to improper manufacture. Secondly, the discharge endurance performance of extruded polymer insulation can be weak. For example, the hydrogen atom within the polyethylene molecule may cause an oxidation reaction and degrade insulation performance. Thirdly, since the 1960s, long-term tests and practical experience have indicated that ageing and breakdown of the extruded plastic cable insulation is due to treeing such as electrical trees, water trees and electrochemical trees, which are closely linked to the partial discharge activities.

Due to the high demands and requirements for polymeric cables, partial discharge detection techniques and testing standards to assess the reliability of these cables have rapidly developed. Typical partial discharge measurement instruments such as those manufactured by Robinson (UK), Hiptronics and Biddle (USA), Haefely and Tettex (Switzerland) have been developed worldwide. The standard textbook "Discharge Detection in High Voltage Equipment" regarding the fundamentals of partial discharge detection and measurements by Dr. F. H. Kreuger was first published in 1964 [30]. The relevant standards about partial discharge measurements have been revised 3 times and the third edition was published in 2000. In the new edition recently developed techniques such as digital techniques and the use of ultra-wideband instruments as well as non-conventional detection methods have been included. Digital techniques based on the widespread usage of computers provide more flexibility in the treatment of partial discharge test data and associated signal processing techniques. Ultra-wideband instruments such as oscilloscopes of very high bandwidth and spectrum analysers together with some appropriate coupling devices have become popular online partial discharge detection tools.

Generally, cables and accessories are tested and inspected at factories prior to being transported to customers. Most manufacturing defects can be detected during the factory tests. However, transportation and field installation damage can still occur, where the most vulnerable time for a cable circuit is the field installation of cables and their accessories. Defects could also be introduced during the service operation due to environmental factors such as temperature variation and chemical reaction. Cable accessories such as joints and terminations are usually installed on site. Consequently defects leading to partial discharges are more likely to occur at these locations and online partial discharge detection is therefore focused on cable accessories.

In this chapter, fundamentals regarding partial discharge and its mechanism are presented and detection and measurement techniques in HV equipment especially in HV cables are reviewed.

2.1 PD Fundamentals

PD is defined by IEC 60270 (Partial Discharge Measurements) as a localised electrical discharge that only partially bridges the insulation between conductors and is confined in some way that does not permit complete failure of the system [9]. It can result from mechanisms such as breakdown of gas in a cavity, or breakdown of gas in an electrical tree channel, or breakdown between an energized electrode and a metal impurity. In HV cables PD are mainly caused by a local field enhancement due to the imperfections inside the insulation such as gas-filled cavities or voids and cracks caused during installation or normal service conditions. To interpret PD phenomena it is necessary to consider gaseous PD mechanisms.

2.1.1 PD Mechanisms

There are two basic theoretical mechanisms to explain gaseous partial discharge phenomena, namely Townsend theory and streamer theory [27-31].

2.1.1.1 Townsend Theory

Free electrons within a void are accelerated under the electric field and collide with neutral gaseous molecules. When the impact of electrons is high enough, new electrons and positive ions will be formed. Newly formed electrons and the original free electrons gain speed in the electric field and ionise more neutral molecules by impact. This process produces more free electrons and positive ions and leads to electron avalanche. The produced electrons move towards anode and leaving behind positive ions that move towards the cathode, thereby forming a passage of current through the gas. The positive ions enhance the electric field around the cathode and will cause the cathode emit more electrons called secondary electrons. Consequently, the electron avalanche is self-maintained by cathode emission without depending on free electrons.

2.1.1.2 Streamer Theory

The streamer discharge is initially caused by the simple Townsend theory. When an avalanche is formed under a high voltage, the electrical field between two electrodes is different. The head and tail of an avalanche near the electrodes is stronger than the middle part of the avalanche which can be considered as a plasma with a weak electrical field. When more ions and electrons are produced, it leads to the recombination of ions and electrons in this plasma area and creates photon emission. The photons enter both ends of the avalanche and ionise more neutral molecules and emit more electrons. The electrons move towards the anode and form a secondary avalanche. The secondary avalanche will connect to the original one and enlarge the plasma column. When the enlarged plasma area bridges the anode and cathode, gaseous discharge with a narrow channel is formed and this is a streamer discharge.

Streamer discharge usually takes place within long gaps when the number of space charges is high enough. As gaps within the insulation are usually thin and small the dominating partial discharge mechanism is explained using Townsend theory inside the insulation. The speed of the streamer discharge is faster than that of Townsend discharges as the speed of photoionization is much faster than the ionisation caused by electrons. The distinguishing features of steamer discharges are their independence on cathode emission and their dependence upon photoionization in the gas volume.

2.1.2 Types of Partial Discharges in Gas

Basically there are two types of gas discharge namely pulse discharge (e.g. spark) and pulse-less discharges. In most cases partial discharges are pulse like discharges, in which separate pulses can be observed during some phases of the applied voltage. Pulse-less discharges generally occur in small gaps where air pressure is low. No separate pulses can be observed, but discharges can be detected acoustically and optically. Between these basic two types of discharge, a third kind of discharge called pseudoglow discharge can sometimes occur with a group of small amplitude pulses with comparatively long duration which are generally difficult to be observed [28].

2.1.3 Process of Gas Discharges

Discharges are processes involving any kinds of ionisation; partial discharge belongs to a far greater group of gas discharges that do not completely bridge the electrodes. Generally gas discharge processes are different depending on the situations where gas partial discharges happen; they can be internal discharges, surface discharges or corona discharges [28, 30].

2.1.3.1 Internal discharge process

Internal discharges can occur inside voids or cavities within solid dielectrics. Most partial discharges within HV cable systems are internal discharges. Traditionally internal discharges are described in the context of the 'ABC' model using the equivalent circuit model of internal discharge as shown in Figure 2.1, where C_C is the equivalent capacitance of the cavity C, C_B the equivalent capacitance of the dielectric in contact with the void and C_A the capacitance of the rest of the sample [32].

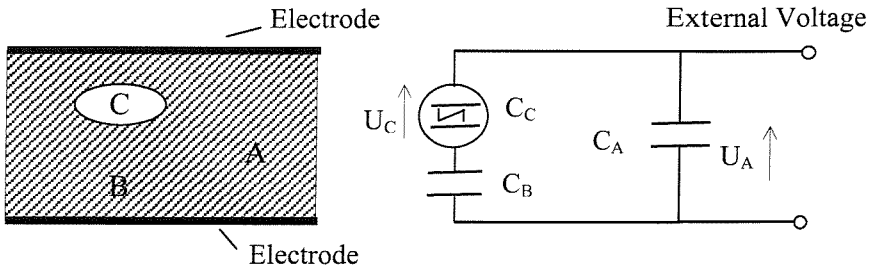

Figure 2.1 Equivalent circuit representation of a cavity in a dielectric

The applied AC high voltage across the dielectric is denoted as U_A, and corresponding internal voltage across the cavity is U_C. When the internal high voltage has not reached the breakdown voltage (U_{CB}) of the cavity, the voltage inside the cavity will change with the applied external high voltage. When U_C reaches the breakdown voltage U_{CB} a discharge takes place inside the cavity producing large amount of positive ions, negative ions and electrons. These space charges move in the opposite directions to the internal electrical field under the applied high voltage and form an internal voltage of $-\Delta U_C$ which reduces the voltage drop to its remnant voltage U_r, where

$$U_r = U_{CB} - \Delta U_C < U_{CB} \qquad (2.1)$$

This is below the breakdown voltage; therefore the discharge process is extinguished. This process lasts for a few nanoseconds and is extremely short compared to the

period of a 50Hz power voltage and therefore the voltage drop may be regarded as a step function. With an increase of the applied high voltage, a second discharge will occur when it reaches the breakdown voltage of the cavity again. As a result, more space charges are produced and an internal voltage twice of the original internal voltage $-2\Delta U_C$ is formed. This reduces the voltage across the cavity and extinguishes the discharge again. If the discharge process occurs n times before the applied voltage reaches its peak value, the internal voltage of $-n\Delta U_C$ will be formed due to the space charge accumulation. Uc drops after the applied voltage passes its peak and the discharge process restarts when the cavity voltage reaches - U_{CB}, i.e.

$$-n\Delta U_C + Uc = - U_{CB} \qquad (2.2)$$

However this time, the direction of the internal electrical field inside the cavity is determined by the superposition of the present discharge and previous accumulation of space discharges. Some of the space charges may be neutralised and therefore the internal voltage will drop and the discharge will be extinguished. With the decrease of the applied voltage, another discharge starts. After the applied voltage passes zero, the accumulated space charges disappear and another half cycle of discharges will start again. In this way groups of regular recurrent discharges can be observed from PD detectors. The whole process is as illustrated in Figure 2.2.

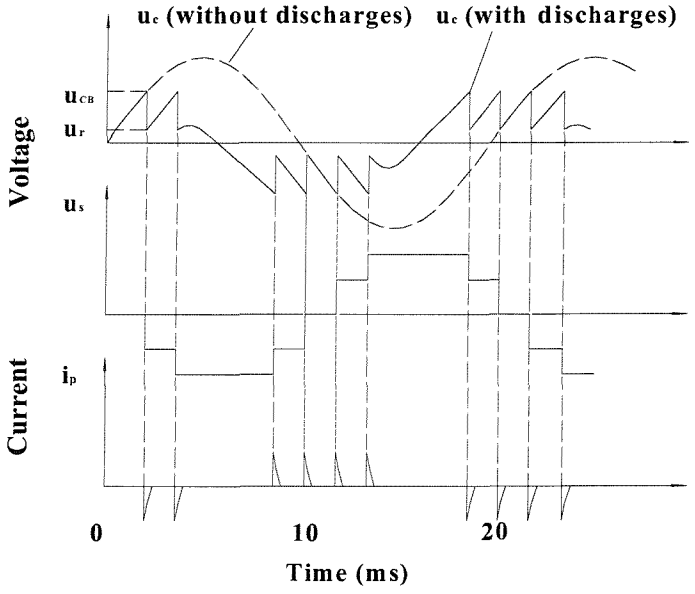

Us - potential difference across the capacitor C_B

Figure 2.2 Internal discharge process

Generally discharge patterns in positive and negative half cycles have symmetry and most discharge pulses occur in the increasing quadrants of the power cycle (first and third quadrants) as shown in Figure 2.3. The bandwidth of the original PD pulse is very wide and can range from a few hundreds of Hz to several GHz.

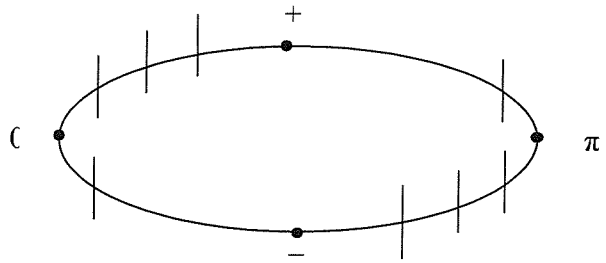

0, π - zero-crossing of the applied voltage, + - positive half cycle, _ - negative half cycle

Figure 2.3 Internal discharge pattern

2.1.3.2 Surface discharge process

The process of surface discharge is similar to that of internal discharges except it occurs between an electrode and a dielectric surface. The equivalent circuit model describing internal discharge can be applied to surface discharges as illustrated in Figure 2.4, where C_C represents the capacitance between the electrode and dielectric surface. The difference is that only one side of the gap is the electrode and the other side is a dielectric surface therefore produced space charges can only accumulate near the electrode on the surface.

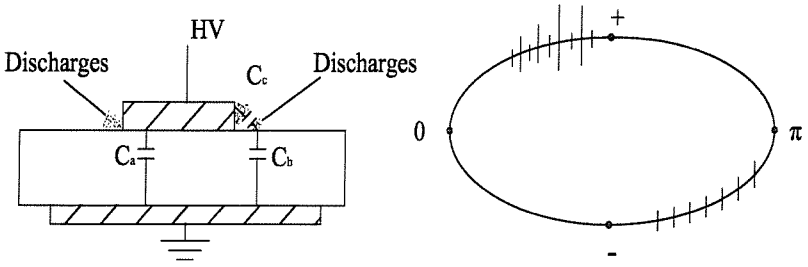

Figure 2.4 Surface discharge and its pattern

The surface discharge pattern depends on the shape of the electrode system. If the electrode system is symmetrical so that the electrical fields near the electrode and dielectric are equal then the discharge pattern is symmetrical. But in most cases, the electrode system is not symmetrical and therefore the discharge pattern is asymmetric. Figure 2.4 shows a surface discharge arrangement and the

corresponding discharge pattern that is in the first and third quadrants of the power cycle.

2.1.3.3 Corona discharge

Corona discharge occurs around sharp points or edges surrounded by gas at high voltage. The process of corona discharge is different from that of internal discharge as it occurs in gas environments with free moving molecules. The typical process of corona discharge can be described by a point-plane electrode system as shown in Figure 2.5, when the plane electrode is at a large distance from a point electrode. When the applied voltage reaches the breakdown voltage of the gas near the point, a discharge occurs. It takes place during the negative half cycle of the applied voltage due to the easy emission of electrons when the electrode is negative (cathode). At the same time positive ions move towards the electrode and release more electrons (secondary emission by the Townsend mechanism), causing a cloud of positive ions near the point and negative electrons travelling away from the point. During this process radiation occurs which causes photoionization at the surface of the point; a lateral extension of the ionised region takes place until so-called cathode spot is formed from which the corona discharge emanates. At greater distances from the cathode the electrons slow down and attach themselves to the oxygen molecules in air. Two regions with space charges have been formed by now and this reduces the electrical field near the point and the discharge is extinguished. With the increase of the voltage or negative ions moving towards the plane, a second discharge starts to occur.

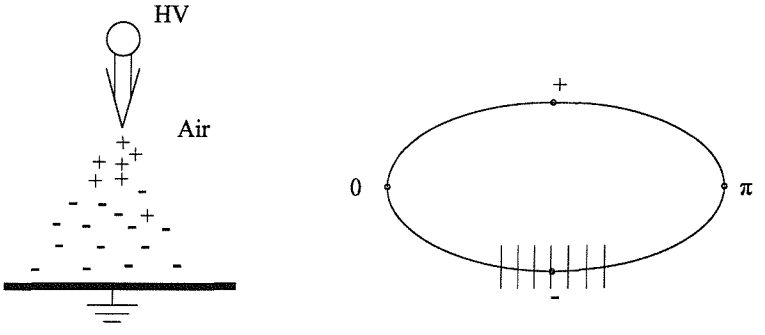

Figure 2.5 Corona discharge and its pattern

Corona discharge always first appears during the negative half cycle around the 270 degree phase angle and almost symmetrical about the negative peak voltage. The

discharge pulses are almost equal in magnitude and equally spaced. As the applied voltage is increased, a small number of discharge pulses with large magnitude can be observed in the positive half cycle as well as in the negative half cycle. The corona discharge process is slower than that of internal discharges. The time interval of a corona discharge within 0.1 mm from the point is of the order of 10 nanoseconds [30]. Therefore the signal bandwidth of corona discharge is lower than that of internal discharge measurement signals.

The above three kinds of discharge are basic processes of partial discharge and occur frequently in high voltage equipment. Other forms of discharge that may occur include floating discharges due to a floating conductor in the electrical field and contact discharges due to a bad contact between a conductor and dielectric or other conductors.

2.2 PD Quantities

Partial discharges are complicated phenomena and there are several quantities available to describe them according to IEC 60270 [9]. These quantities include apparent charge q, charge repetition rate n, discharge energy, and discharge power as well as inception and extinction voltage. Among them, apparent charge is widely used.

2.2.1 Apparent Charge q

Apparent charge is defined as the charge transfer between two electrodes when a partial discharge takes place inside the insulation.

Based on the equivalent circuit model of the internal discharge shown in Figure 2.1, when a discharge occurs, the voltage change inside the cavity is ΔU_C, so the total charge change within the cavity is

$$q_C = \Delta U_C (C_C + \frac{C_A C_B}{C_A + C_B}) \qquad (2.3)$$

Under the condition of $C_A >> C_B$, which generally exists because the cavity is very small compared to the whole dielectric, assuming

$$\frac{C_A C_B}{C_A + C_B} = \frac{C_B}{1 + \frac{C_B}{C_A}} \approx C_B \qquad (2.4)$$

Equation 2.3 becomes

$$q_C \approx \Delta U_C (C_C + C_B) \qquad (2.5)$$

Which represents the real discharge magnitude occurring inside the cavity. The problem is that the value of the capacitances C_C, C_B and the voltage change ΔU_C are not readily known. So the real discharge magnitude is difficult to determine using Equation 2.5. However, the charge transfer on the electrodes of the test object can be determined by the following method. The voltage drop inside the cavity causes voltage drop on the electrodes of the test object in a very short time, therefore the charges within the void are redistributed among capacitor C_C and C_A, as

$$\Delta U_C = \Delta U_A + \Delta U_B = \Delta U_A \frac{C_A + C_B}{C_B} \qquad (2.6)$$

Hence $$\Delta U_A = \Delta U_C \frac{C_B}{C_A + C_B} \qquad (2.7)$$

The charge transfer on the test object is

$$q_A = \Delta U_A (C_A + \frac{C_C C_B}{C_C + C_B}) \approx \Delta U_A (C_A + C_C) \approx \Delta U_A C_A \approx \Delta U_C C_B \qquad (2.8)$$

q_A is called apparent charge, expressed in pico Coulombs. It is the most important discharge quantity used for the evaluation of partial discharge. The relationship between the real charge and the apparent charge can therefore be expressed as

$$q_A = \frac{C_B}{C_C + C_B} q_C \qquad (2.9)$$

Equation 2.9 indicates that the apparent charge is smaller than the real charge inside the cavity, but it is proportional to the real discharge.

2.2.2 Discharge Repetition Rate

This is the average number of discharges per second occurring during the period of measured time and is another important quantity to describe the discharge activity especially under DC voltage conditions as the discharge can extinguish itself under DC conditions [28]. The deterioration effect on insulation caused by discharges is closely related to the discharge repetition rate. If the discharge repetition rate is low,

discharges even with high magnitude are less likely to have a detrimental effect on the insulation.

2.2.3 Discharge Energy

Discharge energy, W, is the energy released during a discharge event, which can be calculated as

$$W = \frac{1}{2}(C_C + \frac{C_A C_B}{C_A + C_B})(U_{CB}^2 - U_r^2) \approx \frac{1}{2}(C_C + C_B)(U_{CB}^2 - U_r^2) \qquad (2.10)$$

Where U_{CB} is the breakdown voltage of a void and U_r is the remnant voltage inside the void after a discharge (Figure 2.2). Using Equation 2.5, Equation 2.7 can be rewritten as

$$W = \frac{1}{2} q_C (U_{CB} + U_r) = \frac{1}{2} q_C \frac{C_C + C_B}{C_B} (U_{CB} + U_r) \qquad (2.11)$$

Given the applied voltage between the electrodes is U_i when the electrical field inside the cavity reaches its discharge voltage U_{CB}, the relationship between U_i and U_{CB} is

$$U_{CB} = \frac{C_B}{C_C + C_B} U_i \qquad (2.12)$$

Thus the discharge energy is

$$W = \frac{1}{2} q_A \frac{U_i}{U_{CB}} (U_{CB} + U_r) \qquad (2.13)$$

If $U_r \approx 0$, then

$$W \approx \frac{1}{2} q_A U_i \qquad (2.14)$$

Therefore the discharge energy usually expressed in μJ can be approximately determined from the apparent charge and applied external voltage.

2.2.4 Discharge Power

This is a derived quantity that is the average pulse power fed into the terminals of the test object due to apparent charge magnitude q_i during a chosen reference time interval T_{ref}, such that the discharge power, P, is defined as

$$P = \frac{1}{T_{ref}} (q_1 u_1 + q_2 u_2 + ... + q_i u_i) \qquad (2.15)$$

where u_1, u_2 ... u_i are instantaneous values of the test voltage at the instants of the occurrence t_i of the individual apparent charge magnitudes q_i. The sign of the individual values must be observed. The discharge power is generally expressed in Watts (W).

2.2.5 Discharge Inception and Extinction Voltage

Partial discharge inception voltage U_i is the applied voltage at which repetitive partial discharges are first observed in the test object, when the voltage applied to the object is gradually increased to a higher value at which PD pulse quantities are observed. While the partial discharge extinction voltage U_e is the applied voltage at which repetitive partial discharges cease to occur in the test object, when the voltage applied to the object is gradually decreased from a higher value at which PD pulse quantities are observed.

Besides the above widely applied quantities, other discharge quantities used for condition assessment include average discharge current, phase angle and time of occurrence of a PD pulse and largest repeatedly occurring PD magnitude.

The partial discharge phenomenon is complicated itself and fundamentals regarding its mechanism, signal generation as well as detection have been researched for many years [31, 32, 33, 34]. For partial discharges occurring within solid dielectrics such as cable insulation the real discharge magnitude is related to factors that include the sample geometry, cavity size, shape and position of the cavity within the sample [32]. Although attempts have been made to determine PD magnitude based on theoretical models for some typical cavity shapes such as spherical and ellipsoidal voids [32, 35], the real PD magnitude that occurs within a cavity can never be known because not all of the parameters of the cavity are determinable. Only the apparent charge of the PD can be measured externally. Furthermore, the PD signal that can be detected outside the object depends on the nature of the connection between the point of generation and external world and the chosen detection method.

2.3 PD under DC Stress

PD characteristics under direct voltage (DC) are quite different from those under alternating voltage (AC). During the increase of the applied DC voltage the discharge process is similar to that of AC voltage. However when the applied DC voltage magnitude becomes constant, discharges occur less frequently. The main differences can be summarized as follows [9]: Firstly, the discharge pulse repetition rate may be very low for direct voltage applied to solid insulation, because the time interval between discharges at each discharge site is determined by the relaxation time constants of the insulation. Secondly, numerous discharges may occur when the applied voltage is changed. In particular, polarity reversal during test can cause numerous discharges in low voltage, but subsequently the pulse repetition rate will decrease to the steady-state condition. Finally the PD characteristics of test objects may be affected by ripple on the test voltage.

If the discharge repetition rate is very low, discharges even with high magnitude will not have a detrimental effect on the insulation. Therefore the discharge repetition rate is the most important parameter for discharges under DC voltage. The discharge repetition rate increases with the applied voltage, the conductivity of the dielectric under test and temperature. Usually the conductivity of the insulation is low and therefore the discharge repetition rate is also low. Generally discharges under DC voltage are less harmful to the insulation than under AC stresses. However, due to the increase in voltage rating of DC power apparatus and the correspondingly increase of the operating temperature, it is important that partial discharge measurements under DC stress are undertaken as part of the development process of DC power equipment [28, 29].

2.4 Effects of PD on Insulation Performance

Partial discharge activity will eventually result in the complete breakdown of the insulation due to electrical ageing. Electrical ageing is a complicated process of insulation deterioration and is closely related to partial discharge activities which cause series of physical and chemical transformations within the insulation [28-30]. Firstly, ion and electron bombardment can break the molecular structure of the insulation when discharge occurs. Secondly, high temperatures can be generated as a

result of partial discharge activities at the discharge site. Burning and melting can be observed in a dissected insulation sample which has undergone a long term ageing process without breakdown. High temperatures will result in thermal cracking and increase of the insulation loss which in turn will accelerate the ageing process and lead to final breakdown. Thirdly, formation of chemical products such as ozone and nitric acid cause further chemical reactions inside the insulation and corrode the insulation material. Furthermore, partial discharges give rise to some phenomena such as photon emission including ultraviolet rays, X rays and γ rays. These rays may break the main bond and decompose the high molecule into a monomer. For some kinds of material, these rays can damage the cross-linking among molecules and make them brittle. Finally the mechanical force caused by the high-pressure gas and acoustic waves produced by intermittent and blasting discharges may crack the insulation and form new discharge sites.

The above effects often combine together to degrade insulation performance simultaneously. However, one mechanism may dominate for different materials and working conditions. Obviously the bombardment effect will dominate the degradation of insulation under high electrical fields and large void situations. While in high temperature environments, thermal effects will dominate insulation degradation especially for lossy materials.

The ageing process of the insulation is closely related to the formation of electrical trees inside the insulation. Electrical trees are the tracks of insulation carbonification due to discharge activities. The typical growing process of an electrical tree is shown in Figure 2.6. Figure 2.6(a) shows the initial tree with a few branches; 2.6(b) indicates that the tree is growing with more branches; and in 2.6(c) some thin branches reach the other electrode but no breakdown occurs; 2.6(d) shows the final breakdown of the channel between two electrodes when a large and destructive current flows through it [28].

When an electrical tree is first initiated, the growing speed is quite slow and it maybe undergo a long slow process until some branches reach between the two electrodes. Then a rapid growing process happens and a breakdown channel forms leading to the complete with the completely breakdown of the insulation.

The speed of electrical ageing is related to many factors. Besides the characteristics of the insulation material itself, there are many external factors which affect the ageing. These factors include the strength of the applied electrical field, frequency of the applied voltage, ambient temperature and humidity as well as the mechanical stress applied to the insulation material. High electrical fields lead to a great number of discharges with high discharge magnitudes. While the higher the frequency of the applied voltage, the higher the discharge repetition rate. The effect of ambient temperature on the insulation is different under different situations. Generally, high temperatures will accelerate chemical reactions that result from partial discharges and the thermal cracking process. Therefore high temperatures lead to short insulation life. But in some circumstances, higher temperature can retard the deterioration process. High ambient humidity will increase insulation life due to the high conductivity and dielectric constant of water which will improve the electrical field distribution and weaken the discharge. All these factors are related to the discharge process inside the insulation and have great effect on the rate of insulation ageing [28].

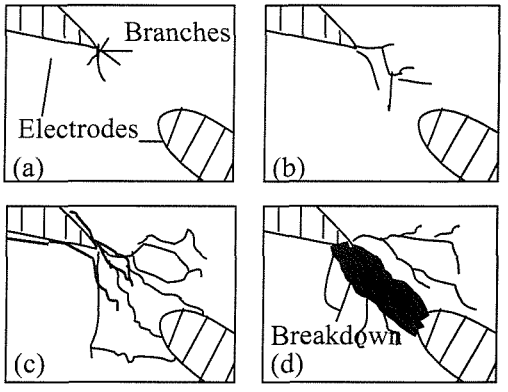

Figure 2.6 Growing process of electrical tree
(a) Initial (b) branches (c) reach to other electrode (d) breakdown

2.5 Representation of PD Information

Partial discharge phenomena occurring in a dielectric medium are inherently complicated stochastic processes and basic PD quantities such as apparent charge and charge repetition rate alone are not enough to represent the overall deterioration

of the insulation allowing diagnostic interpretation. Therefore it is necessary to take statistical information into account in order to perform any analysis.

2.5.1 Statistical quantities

Several statistical quantities have been defined to describe the PD distribution over the AC phase position. These quantities include the pulse count distribution $H_n(\varphi)$, which represents the number of observed discharges in each phase window as a function of the phase angle φ; $H_{qmax}(\varphi)$, which represents the maximal discharge amplitude in each phase window and the mean pulse height distribution $H_{qn}(\varphi)$, which represents the average discharge amplitude in each phase window as a function of the phase angle. $H_{qn}(\varphi)$ is derived from the total discharge quantity in each phase window divided by the total number of discharges in the same phase window. The resolution of the phase angle axis is determined by the number of phase windows. Large number of the phase windows gives high phase resolution, but it requires more computational capability and large computer memory. It has been found that 200 phase windows give reasonable and sufficient accuracy for pulse phase distribution quantities and 50 were found to be a reasonable number for magnitude window [28, 29].

According to several authors, the time dependence of the pulse phase distribution $H_n(\varphi)$ and the mean pulse height distribution $H_{qn}(\varphi)$ provide a good description of changes in discharge patterns [36-39]. The $H_n(\varphi)$ quantity contains information of the intensity of discharges as a function of their phase angle. The $H_{qn}(\varphi)$ quantity allows noise reduction due to the difference between the statistical characteristics of the discharge pulses and that of noise pulses as a function of phase angle.

In addition to the three two-dimensional statistical quantities discussed above, a three-dimensional statistical quantity called Phase-Charge-Number (φ-q-n) pattern has been used to analyse the discharge signals [38-40]. This is the characterization of the partial discharges by their angular position on the AC cycle (φ), their relative magnitude (q) and occurring frequency per unit time (n). These three parameters may be used to construct a three-dimensional surface from which important features may

be extracted. Based on these features, the overall insulation conditions can be diagnosed and important decisions can be made.

2.5.2 Statistical operators

Partial discharge patterns occurring in positive half voltage cycles and negative half voltage cycles may be different according to different occurring situations as described in section 2.2.3. To discriminate the pattern difference between the two half cycles, the statistical quantities $H_n(\varphi)$ and $H_{qn}(\varphi)$ can be characterised by both distributions: $H_n^+(\varphi)$, $H_{qn}^+(\varphi)$ for the positive half cycle and $H_n^-(\varphi)$, $H_{qn}^-(\varphi)$ for the negative half cycle. To study the difference between both half cycles several statistical operators have been defined.

2.5.2.1 Discharge asymmetry Q

The discharge asymmetry Q is the quotient of the mean discharge level of the $H_{qn}(\varphi)$ distribution in the positive and in the negative half of voltage cycle:

$$Q = \frac{Q^-/N^-}{Q^+/N^+} \tag{2.16}$$

Where Q^+ and Q^- are the sum of signal amplitudes of the $H_{qn}(\varphi)$ distribution in the positive and negative half of the voltage cycle; N+ and N- are the number of discharges of the $H_{qn}(\varphi)$ distribution in the positive and negative half of the voltage cycle.

2.5.2.2 Phase asymmetry Φ

The phase asymmetry Φ is used to study the difference in inception voltage of the $H_{qn}(\varphi)$ distribution in the positive and negative half of the voltage cycle:

$$\Phi = \frac{\varphi_{in}^-}{\varphi_{in}^+} \tag{2.17}$$

Where φ_{in}^+ and φ_{in}^- are the inception phases of the $H_{qn}(\varphi)$ distribution in the positive and in the negative half of the voltage cycle.

2.5.2.3 Cross-correlation factor CC

The cross-correlation factor CC is employed to evaluate the difference between the shape of the distribution $H_{qn}^{+}(\varphi)$ and $H_{qn}^{-}(\varphi)$. The following formula is used to calculate the cross-correlation factor:

$$CC = \frac{\sum xy - \sum x \sum y/n}{\sqrt{\left[\sum x^2 - \left(\sum x\right)^2/n\right]\left[\sum y^2 - \left(\sum y\right)^2/n\right]}} \qquad (2.18)$$

Where x is the mean signal amplitude in a phase window in the positive half voltage cycle; y is the mean signal amplitude in the corresponding phase window in the negative half voltage cycle and n is the number of phase windows per half cycle. CC=1 means 100% shape symmetry and CC=0 means total asymmetry.

Thus, three independent parameters have been defined to describe the difference of discharge distribution between positive half cycle and negative half cycle: phase asymmetry Φ, discharge asymmetry Q and cross-correlation factor CC. The first two parameters are also defined in such a way that they are equal to 1 in the case of fully symmetry and smaller than 1 in the case of asymmetry. These three parameters can be combined to form a new quantity called modified cross-correlation factor (MCC) by multiplication:

$$MCC = \Phi \cdot Q \cdot CC \qquad (2.19)$$

MCC is used to evaluate the overall differences between positive discharge distribution pattern and negative discharge distribution pattern.

In the case of single defect, discharge parameters can be fairly well described by a normal distribution process [29]. Therefore to get a better evaluation of statistical quantities $H_n(\varphi)$ and $H_{qn}(\varphi)$, the following statistical parameters for a normal distribution can also be used.

2.5.2.4 Skewness Sk and Kurtosis Ku

Skewness is an indicator of the asymmetry of a distribution with respect to a normal distribution and defined as:

$$Sk = \frac{\sum_{i}^{n} (x_i - \mu)^3 f(x_i)}{\sigma^3 \sum_{i}^{n} f(x_i)} \tag{2.20}$$

And kurtosis Ku is the indicator for the deviation from the normal distribution:

$$Ku = \frac{\sum (x_i - \mu)^4 \cdot f(x_i)}{\sigma^4 \sum f(x_i)} - 3 \tag{2.21}$$

Where x_i is a random variable, $f(x_i)$ is its probability distribution function; μ is the mean value of the distribution, and σ is the standard deviation of the distribution:

$$\sigma^2 = \frac{\sum_{i=1}^{n} (x_i - \mu)^2 f(x_i)}{\sum_{i=1}^{n} f(x_i)} \tag{2.22}$$

$$\mu = \frac{\sum_{i=1}^{n} x_i f(x_i)}{\sum_{i=1}^{n} f(x_i)} \tag{2.23}$$

Skewness (Sk) describes the asymmetry of the distribution. Sk is zero for a symmetric distribution, positive when the distribution is asymmetric to the left, and negative when the distribution is asymmetric to the right. Kurtosis (Ku) indicates the sharpness of the distribution. Ku is zero for a normal distribution, for a sharper than normal distribution Ku is positive and for a flatter than normal distribution Ku is negative. Figure 2.7 shows some examples of different skewness and kurtosis respect to normal distribution.

These statistical parameters and operators reflect the overall PD information and they are important quantities leading to diagnosis of insulation conditions and application of maintenance strategies. With the advancement of computer technology, computer-aided PD measurements based on real-time signal post-processing techniques and statistical information have become important means for overall insulation condition monitoring especially for online condition monitoring [28, 41-43].

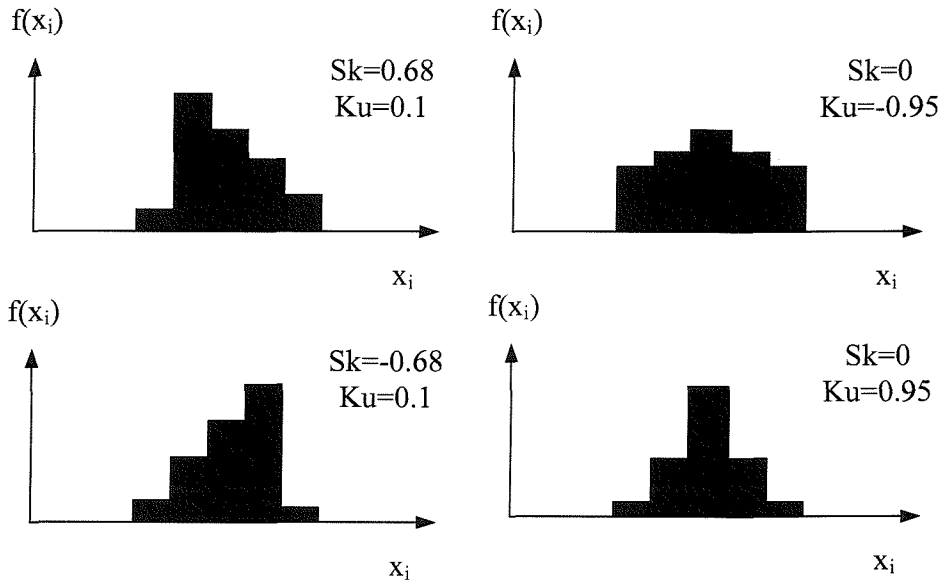

Figure 2.7 Distribution with different Sk and Ku

2.6 PD Detection Methods for HV Cables

Partial discharges give rise to phenomena that may be used for detection. These phenomena include electrical phenomena such as electrical impulses, dielectric losses, electromagnetic radiation and non-electrical phenomena such as light, heat, acoustic emission and chemical transformations. These can be divided into two main categories of related detection methods namely electrical and non-electrical PD detection.

2.6.1 Electrical PD Detection

The detection of electrical phenomena is the most common approach for partial discharge detection. There are several electrical methods available to detect the electrical impulses emitted during the partial discharge process. Generally these methods can be classified either as conventional electrical detection or non-conventional electrical methods. The conventional electrical method is a well-developed method and is widely used in factories and laboratories for quality control of various HV apparatus such as power capacitors, transformers and cables [28-30]. It requires a discharge free power supply and additional coupling capacitors.

Electrical detection of partial discharge can also be realized using field coupling techniques. Unlike conventional electrical coupling, non-conventional field coupling techniques can avoid interruption of the operating voltage and can be carried out under service conditions. Ideas on this procedure were first proposed by Koske in the 1930s [44], but the application of these methods only appeared in recent years with the development of new equipment allowing improved signal-to-noise ratios.

The basic principle of field coupling methods is that the electromagnetic field radiated from the PD source can be detected by means of antennas under the condition that the frequency response of the receiving antenna (sensor) is of the same order with the frequency spectrum of the original PD pulse. These sensors include inductive sensors, which couple the magnetic field of PD sources, capacitive coupler sensors, which couple the electrical field of PD sources and directional coupler sensors, which couple both magnetic and electrical field of PD sources. For PD detection in HV cables and accessories, several non-conventional techniques are popular and widely used.

2.6.1.1 Conventional electrical PD detection

The conventional electrical PD detection method has been employed for more than 50 years. It is usually used in factories and laboratories for quality control of various HV apparatus such as transformers, power capacitors, electrical machines and gas insulated substations (GIS). It is also the basic PD detection method for HV cables and accessories. The first industrial standard, International Electro-technical Commission (IEC) Publication 270 'Partial Discharge Measurement' was issued in 1968. The third (latest) edition was issued in 2000[9]. There are various kinds of commercial PD detectors available such as the Robinson PD Detector (UK), Hipotronics (USA), and Haefely and Tettex (Switzerland). Commercially available PD detection systems have been compared and reviewed [33]. The test circuit proposed by Electric Research Association (ERA) using the conventional electrical method for a short piece of cable (less than 300m in length, can be treated as a capacitor) is illustrated in Figure 2.8 although some variations of this circuit are also specified in IEC 60270[9]. Where C_x is the capacitance of the cable under test, C_k the discharge free coupling capacitor, which couples the discharge pulses from test object and removes power frequency voltages. The input unit acts as the

measurement impedance to high frequency discharge pulses and suppresses the power frequency and low frequency harmonic signals. To ensure maximum sensitivity the input unit must be chosen to match the capacitance of the test object and the coupling capacitor. The output signal of the input unit is fed into the PD detector and displayed as an oscillograph.

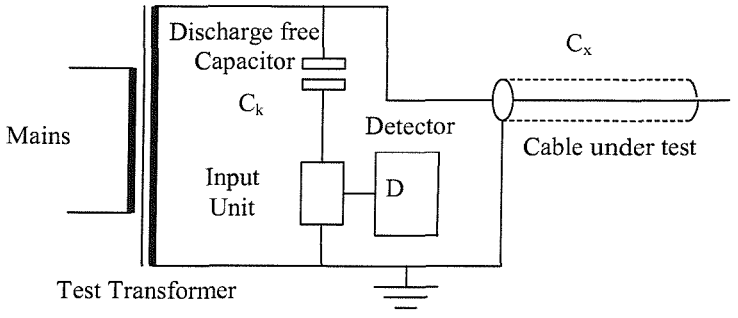

Figure 2.8 Basic diagram of electrical method

Longer cables have to be treated as transmission lines and should be tested with the circuit shown in Figure 2.9, where the far end of the cable is terminated in its characteristic impedance R in series with a discharge free capacitor. The capacitor serves both to reduce the power rating of the resistor and the consumption at power frequency while maintaining the correct impedance within the pass band of the discharge detector. The near end of the cable is coupled to the input unit via the discharge free capacitor C_k [29].

The frequency spectrum of the PD pulse itself inside the insulation is wideband and can reach up to 1GHz. But PD signals that can be detected depend on the nature of connection between the point of pulse generation and the external world and in most cases only limited sensitivities can be achieved [34]. The bandwidth of the conventional PD detection system varies with different PD detectors [33], but generally, PD signals are detected with a bandwidth of several hundreds kHz or less, and the time parameters of the detection system are much longer than the PD pulse time parameters so that the detector acts as a low pass filter or integrator.

The conventional electrical method is a highly sensitive and reliable method that has a history of successful use. The disadvantages are that it is prone to excessive

electromagnetic interference therefore can only be implemented under laboratory conditions; it is an off-line method that requires an external power supply and HV coupling equipment. Another drawback of the conventional electrical method is that it fails to provide any information on PD location.

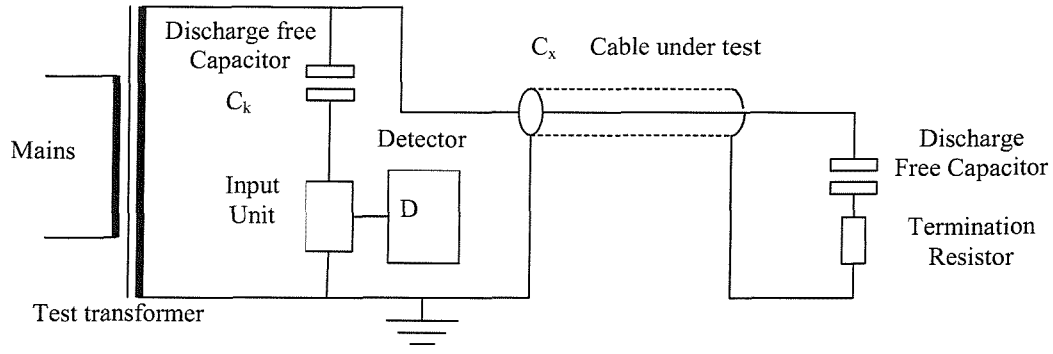

Figure 2.9 PD test circuit for longer cables

2.6.1.2 Non-conventional electrical detection using capacitive couplers

The capacitive coupling technique is one of the most popular non-conventional techniques used for PD detection. For detection of PD in cables and their accessories, capacitive couplers are usually implemented by placing metallic foils above semicon layers, but it is also possible to use stress cones or semicon layers around a joint as pick up electrodes [23, 24, 45]. Another solution is to place permanent electrodes inside cable accessories during the design of cable joints and terminations. This technique has been successfully applied in Japanese 275kV high voltage cross-linked polyethylene cable lines for condition monitoring and after-laying tests [14, 15]. Recently, it has been put into the directly buried cable system in China for online condition monitoring [16]. The shape of the metallic foils can be patches or cylinders around the cable as shown in Figure 2.10 [45, 21]. In practice two differential capacitive sensors are usually used in order to discriminate the internal PD from external interference and provide accurate PD locations [21,45,46].

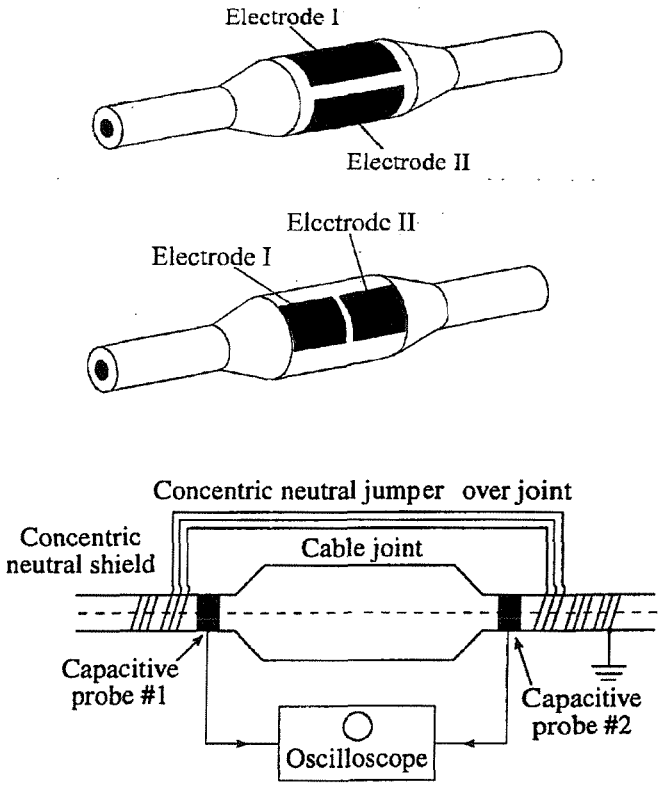

Figure 2.10 Shapes and positions of capacitive couplers [21, 45]

2.6.1.3 Non-conventional electrical detection using inductive couplers

Inductive couplers couple energy from the magnetic field of the PD pulse into the measurement system. There are several kinds of inductive couplers available depending on the applicability and cable construction. For cables having a wire sheath, detection can be achieved using the outside of the cable, because the magnetic field is not perfectly confined within the interior of the cable. The spiral winding of the wire causes an axial magnetic field component that can be measured as shown in Figure 2.11(a) [45, 47, 48]. For the case of a nearly perfectly shielded cable (Aluminium foil, lead, or corrugated aluminium sheath) sensors have to be installed between the sheath and the outer semicon layer or at the cable termination. Because the magnetic field will not have axial components, Rogowski coils are usually used [45, 49, 50] and Figure 2.11(b) shows the principle of the Rogowski coil [45], If a ferrite core is used, a rather flat frequency response can be achieved, but care must be taken to avoid saturation of the ferrite in on-line measurements.

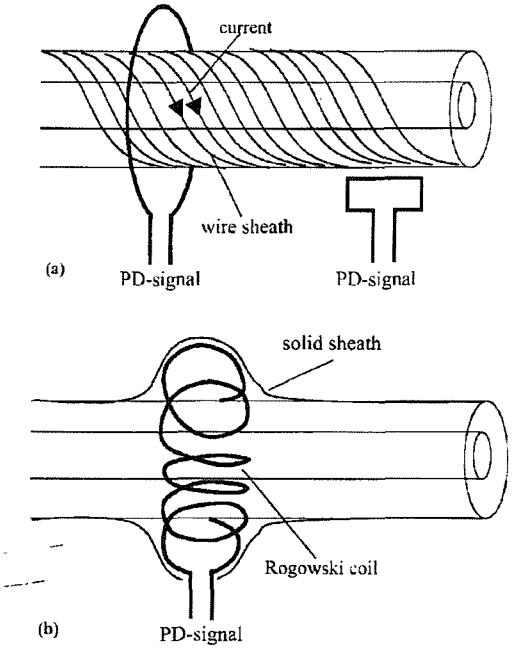

Figure 2.11 Inductive Coupling of PD Pulses [48] (a) two methods for wire sheath cables, (b) a method for a cable with a RF tight sheath

Another kind of widely used current coupler is high frequency current transducers (HFCT) [51-53], which usually clamped around the metallic ground screen of the cable in order to detect the discharge current flowing through it. The typical transfer impedance of the HFCT and its application in cable PD detection are shown in Figure 2.12[51]. Alternatively, it can be clamped around the outer sheath of the cable joint [17]. If the outer sheath of a cable joint is connected to earth through copper braids, the HFCT can be clamped around the copper braids. The output signal of the sensor can then be filtered and/or amplified for further processing. This method is non-intrusive and convenient to use. It does not require any connection to live apparatus and can be applied in most field tests without necessarily taking equipment out of service.

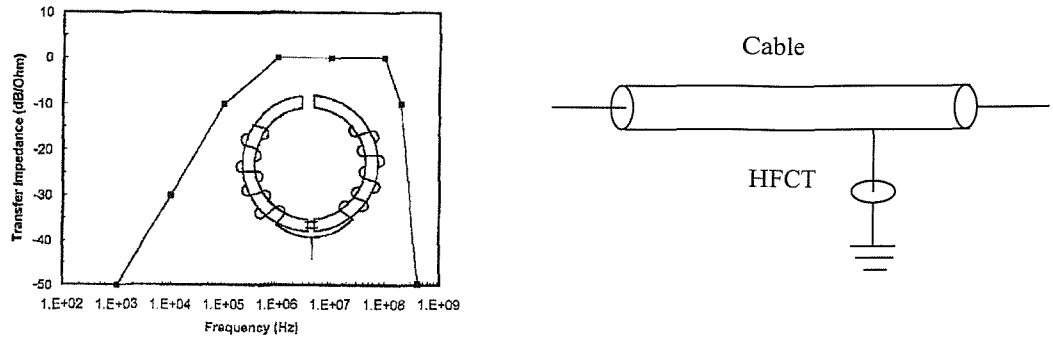

Figure 2.12 HFCT characteristics and using HFCT to detect PD in cables [51]

2.6.1.4 Non-conventional electrical detection using directional couplers

Directional coupler sensors (DCS) are widely used for detection and location of PD pulses for cables and cable accessories under onsite conditions, at the same time discrimination of PD pulses from other noise pulses can be implemented by the directivity that the sensors provide [45, 54, 55]. They are passive components that require no power supply and can be used for long-term condition monitoring of cables and accessories.

Theoretically a directional coupler couples both electrical field and inductive field of a PD pulse travelling along a cable or waveguide into one or two ports. This is done such that energy travelling in one direction in the cable or waveguide mainly causes a signal at one of the two output ports of the directional coupler. Energy that travels in the other direction will mainly couple to the other output port. Such a coupler is characterized by its coupling factor and directivity. The coupling factor describes how much energy is coupled from the cable into the output ports. Directivity quantifies the ability to distinguish between the forward and backward propagating pulses. Strong coupling leads to good coupling factor and a balance between both couplings is needed to achieve high directivity. To avoid any degradation of HV performance of the cables, the directional coupler is installed between the outer semicon layer and the metallic cable sheath. A short strip of metal is placed on the outer semicon layer (with or without contact) and attached to two output connectors [45].

To apply this methodology to cable joint, sensors are placed to the left and to the right of a cable joint as shown in Figure 2.13[45]. Signals propagating forward are coupled to ports A and C, while signals propagating backward are coupled to ports B and D. PD pulses in the joint will be coupled to ports B and C. The sensors can be within the joint housing or can be mounted after joint installation close to the joint.

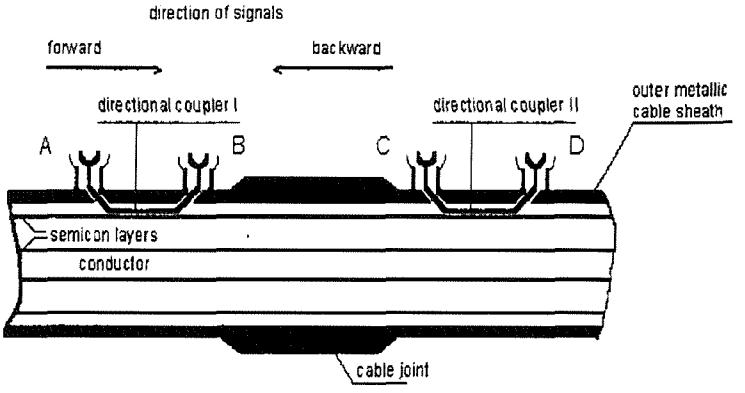

Figure 2.13 Principal arrangement of two directional couplers at a Joint [45]

Compared to capacitive couplers and current transducers, directional coupler sensors may provide more information about PD sources such as directivity of the pulse. They are easy to apply in homogenous dielectrics. But for HV cables that use semicon layers to smooth the electrostatic field, the dielectric constant of such material is complex and frequency dependent which makes the application of the broadband directional couplers more complicated [54].

2.6.1.5 Non-conventional electrical detection using other techniques

There are also some other forms of non-conventional electrical PD detection techniques such as coaxial cable sensors [56], which are typically positioned in a cable joint and similar to capacitive coupler in principle, resonance type partial discharge sensors [57] and specialised PD sensors such as the one designed by DTE Energy Technologies [58], which is both an inductive and a capacitive sensor. Screen interruption is another technique used for PD detection in cables [47,59], this involves cutting the metal earth screen. It has a significant disadvantage as it limits the short circuit handling ability. Therefore for online measurements, it is necessary to either short the measurement impedance by an inductor or over voltage protection needs to be placed in parallel with the measurement impedance. Moreover, the open

structure of the screen interruption method means that it is easily influenced by external electromagnetic noise.

These sensors generally work over the very high frequency (VHF, 30-300MHz) range, as the cable semicon layers will attenuate ultra high frequency component of the PD pulse. The advantages of these methods are obvious due to their low cost, high sensitivity and applicability for online measurement. However, due to fundamental differences compared to the conventional electrical detection method, the evaluation of measured results is not directly comparable and quantification of sensor measurements has become a controversial topic. An international standard regarding VHF coupling PD detection methods has not yet been developed.

2.6.2 Non-electrical PD detection methods

Non-electrical methods of partial discharge detection include acoustic, optical and chemical methods and also the subsequent observation of the effects of any discharges on the test objects. Similar to the above non-conventional electrical PD detection methods, these methods are also not suitable for quantitative measurements. Therefore these methods can also be classified as non-conventional methods.

2.6.2.1 Acoustic Methods

Acoustic methods are among the most important non-destructive methods for mechanical structures and components. Acoustic discharge detection is based on detection of the mechanical signals emitted from the discharge. The discharge appears as a small 'explosion', which excites a mechanical wave that propagates throughout the insulation [60]. In the early history of PD detection, an insulation tube was used to guide the audible hissing sound from liquid-filled equipment and microphones were usually used for discharges in air or gases [61, 62]. Acoustic PD detection techniques have been studied and developed over a long period of time, and a substantial body of knowledge has been accumulated [60, 62]. In recent years, the acoustic emission (AE) method has gained popularity and being widely used for PD detection in power transformers [18, 19, 63-65], power capacitors [66, 67], gas insulated switchgear (GIS)[20] as well as HV cables and accessories [22, 68-71]. It is

a passive method that uses piezoelectric materials as acoustic transducers to detect PD signals emitted from the PD source.

In principle, acoustic methods have many advantages over electrical PD detection methods in that they are non-invasive and immune to electromagnetic noise, which can greatly reduce sensitivity of electrical methods especially when applied under field conditions. More importantly acoustic methods can be extended to facilitate PD location in many situations [60]. Therefore acoustic methods have become an important means for online condition monitoring. The disadvantage of acoustic methods is that they are generally less sensitive than electrical methods and difficult to calibrate. The possibility of acoustic emission PD detection in cables using a new piezoelectric polymer material has been investigated as part of this thesis and is discussed Chapter 3.

2.6.2.2 Optical detection

Optical or light detection methods can be carried out in a darkened room for surface discharges and photographic records. These methods can also be useful for internal discharge detection of translucent dielectrics. However for cable PD detection this method is seldom used.

2.6.2.3 Chemical methods

The presence of partial discharge in oil- or gas-insulated apparatus may be detected by analysis of decomposition products dissolved in the oil or in the gas. The dissolved gas analysis (DGA) method has been widely applied to transformer PD detection due to the simplicity in procedure and applicability for online detection [72, 73]. However when used for oil-filled cables and accessories, it requires removal of a small amount of dielectric fluid from the cable or cable accessory. Therefore, it requires outrage of service for safety reasons to allow access to fluid filled areas within the system components. Consequently, it is not suitable for online application. The sample is then sent to a laboratory for DGA testing using a chromatograph. Interpretation of dissolved gases is based on the type of gases present and their concentration. The primary indicator gases for partial discharge activity are hydrogen, acetylene and methane. Other gases of importance are ethane, ethylene, propane, propylene, isobutene, carbon monoxide, carbon dioxide, oxygen and

nitrogen. Based on the different levels of dissolved gases, different actions such as immediate repair, scheduled repair, monitor or retest, clean or no action at all, can be recommended [74].

The main disadvantage of this method is that it provides only an integrated measure of prevalent PD activity and that it can only roughly indicate the severity of the PD activity, but provides little or no indication about its nature, intensity or location. The nature of this method limits it to offline applications. Therefore it has not been widely used for PD detection in cables and cable accessories.

2.6.3 Summary

Of all above PD detection methods for cables and accessories, the conventional electrical method is a reliable and standard method used for offline tests. For online PD detection, capacitive couplers, high frequency current transducers (HFCT) and acoustic emission (AE) methods are good choices. Tian et al. [22] have compared these methods used for a cable joint PD detection. Generally, capacitive couplers are more sensitive than HFCTs, but they are easily influenced by electrical noise and interference; thus they need to be fully shielded and further signal processing such as filtering and gating is usually required. HFCTs are very convenient to apply, but the detection sensitivity is low as the PD signals are usually attenuated while traveling along the earth screen and detected signals are influenced by noise and interference. Acoustic emission methods are free from electrical interference, but have low sensitivity due to the significant attenuation of the acoustic wave within a cable joint.

2.6.4 Characteristics of HV Cables and Limitations of PD Tests

Since the introduction of solid dielectric cables in 1950's, PD tests have been established as the most effective and non-destructive means of quality control and service condition monitoring. Cables and accessories are usually tested in factories to identify manufacturing defects. However, damage may still occur during transportation and installation especially for cable joints or terminations. Therefore PD online tests concentrate on these cable accessories. There are limitations on PD detection due to the structure of the cable as well as the materials used. HV cables are usually long, having a cylindrically symmetric structure containing dielectrics

that operate at relatively high stress. The capacitance of such a structure is so high that only limited sensitivity can be achieved using the narrowband conventional electrical method [75]. Better sensitivity can only be achieved under circumstances where very wide bandwidth detection can be employed [34]. Furthermore, the semi-conducting layers of a solid dielectric cable cause substantial high frequency attenuation of PD pulses as they propagate from their source to the PD detector [76]. The PD pulse shape that can be detected is a function of the distance between the PD source and the detector as well as the properties of the semi-conducting layer [77]. For non-conventional PD detection techniques such as capacitive coupler sensors, the frequency response of these sensors is normally in VHF range (up to 500MHz), the results are more affected by distance and the semi-conducting layer than low frequency detecting.

Another limitation on long cable PD testing is the effect of PD pulse reflection. When a PD pulse occurs it will propagate away in both directions from its origin. Unless the remote ends are terminated (for high frequency) at the characteristic impedance of the cable, this pulse will reflect and return to the PD detector and be superimposed on the first pulse. This superposition can cause significant error in detected magnitude especially when looking for PD location [77, 78]. Therefore precautions must be taken to avoid such errors.

2.7 PD Location

Detection of PD in HV cables is generally of little value without determining the location of the PD source. During factory tests, it allows 'good' cable sections to be salvaged. As for online monitoring during normal service conditions, the determination of the location of PD improves the efficiency of preventive maintenance.

Traditionally PD location within HV cables has used the Time Domain Reflectometry (TDR) method. It was introduced by F. H. Kreuger in 1961 and has become a standard method for PD location [78]. It is based on the travelling wave theorem, the pulse of a partial discharge travels in two directions. The original pulse will travel directly towards the near end (where the measurement set is connected);

the other pulse will travel in the opposite direction. At the open remote cable-end, this pulse reflects and finally the first reflection of the original pulse travels in the direction of the measurement set. The time difference between the arrival of the original pulse and its first reflection can be used to determine the location of the PD in power cables. Over the years, the sensitivity and accuracy of TDR method has been greatly improved through the use of current test procedures such as ones developed by Mashikian et al. [79, 80] and digital techniques such as reported by Borsi [81]. The advantage of this method is that it can be performed onsite for buried cables and cables installed in ducts. However it requires temporary interruption of service and a separate power supply to energize the disconnected cables. The power (up to 10MVA [82]) required for onsite testing at 50(60) Hz is so great that the weight and cost of such a power supply is not financially practical especially for long cables with a large capacitance. Therefore several alternative energizing methods such as very low frequency (VLF) method [83-86], oscillating wave test (OWT) systems [87-90] and variable frequency AC voltage [82, 91-93] have been developed and some of them put into use for after-laying tests of cable systems. Obviously all of the HV equipment has to be discharge free to avoid any erroneous readings. Special attention should be paid when detecting and measuring PD at frequencies other than 50(60) Hz as the PD activity could be different under different energizing frequencies due to the failure mechanism under different frequencies may be different [94-97]. Relationships between PD activities at different frequencies are complicated issues and need to be established to guarantee the efficiency and validity of these onsite test methods.

With the development of non-conventional PD probe techniques such as the capacitive coupling, inductive coupling and acoustic emission techniques, PD location can also be accomplished by using these sensors [46, 21, 48, 54, 77, 78]. Unlike the TDR method, these techniques are intended for use on cables under operating conditions so service interruption can be avoided. While the high frequency losses of solid dielectric cables due to the existence of the semi-conducting layers tends to decrease the detection sensitivity for PD measurements, it can be used for PD location by determining the frequency dependent attenuation of a specific kind of cable. This can be done prior to testing by sending a known pulse down the cable, measuring the shape of the reflected pulse and computing the

transfer function between the input and reflected pulse. Given the length of the cable, the attenuation per unit length as a function of frequency can be calculated. Such a calibration can also give the electrical length of the cable and electromagnetic propagation velocity, which are necessary parameters for PD location [77, 98].

2.8 Post-processing of PD Signals

One of the main challenges associated with online PD measurements is coping with background noise and interference. A wide range of noise and interference can be encountered during onsite PD tests. This includes PD and corona from the power system, arcing between adjacent metallic components and poor contact, power line carrier communication systems, thyristor switching and radio transmissions [1, 99]. The presence of the noise and interference corrupts the PD signals and may result in false indications. Therefore post-processing of PD signals is necessary for online PD measurements especially with the advancement of several non-conventional detection techniques such as capacitive couplers and inductive couplers.

Various methods for post processing of PD signals have been reported with the development in digital techniques and signal processing techniques. These methods include designing of suitable filters (FIR and IIR), Fast Fourier Transform (FFT) based approaches, moving average, adaptive filtering as well as wavelet analysis. An overview paper [100] by Shim et al classified these methods as open loop systems and closed loop systems. As closed loop systems, adaptive filtering techniques are found to be very effective in suppressing sinusoidal noise and discrete spectral interferences (DSI). Hariri et al [101] and Mashikian et al [102] designed an adaptive noise mitigating system (ANMS) to suppress the amplitude modified (AM) interference for cable fault location instruments based on time-domain reflectrometry (TDR). Khan et al [103] have successfully adopted an adaptive linear predictor to suppress sinusoidal noise for online monitoring of PD on transformers using a current transducer (CT). The advantage of the adaptive filter is that it self learns, therefore no prior knowledge of the noise is needed. However, it needs a reference input of the ambient noise, which is somehow correlated to the noise in the primary input, but de-correlated to the signal in the primary input [104]. Zargari et al [105, 106] used two acoustic emission (AE) sensors positioned differently to ensure one detects only noise and another detects both noise and PD signals in transformer oil

tank PD detection. In most cases, an antenna is used as the reference sensor [101, 107, 108]. To overcome this problem, Su [109, 110] used a modified adaptive noise canceller with the terminal injected calibration pulse as the reference input for transformer oil tank PD detection. But this method is not applicable to online detection of PD on HV cables as terminals are not readily accessible.

For open loop systems, wavelet analysis has recently been found extremely efficient in partial discharge detection. It is not only effective for periodic noise and DSI but also effective for pulse-shaped interference, which is reported to be difficult to recognise and suppress. Satish et al [99] have successfully applied wavelet analysis to signals obtained using conventional PD detector in noisy environments. It shows that the wavelet-based de-noising technique is more powerful than traditional FIR and IIR filtering techniques. Ma et al [111-114] have interpreted various aspects of wavelet analysis and its application in PD detection in detail. These aspects include optimal wavelet selection for different PD pulses obtained using different coupling impedance circuits, i.e. RC and RLC circuits and automatic thresholding for de-noising. The advantage of the open loop system is that it is independent of the reference signals as it is based on the prior knowledge of the signal and noise [115]. Compared to other traditional de-noising methods such as FFT-based spectral analysis and pulse averaging, wavelet analysis can provide both time and frequency domain information, which is very significant for PD source location.

Most of the work mentioned above is with reference to the processing of signals acquired by the conventional PD detection method, which is useful for offline PD detection although it can be used onsite. For online PD detection, signal post processing techniques have only been applied to a few non-conventional PD detection sensors up to now. Basically, non-conventional PD sensors can be classified into two categories, i.e. capacitive sensors such as capacitive couplers (dividers) and antennas, which measure the voltage pulse of the PD, and inductive sensors such as current transducers (CT) and Rogowski coils, which measure the current pulse of the PD. Unlike conventional PD measuring systems they are generally broadband, sensitive and easy to apply (capacitive couplers can be integrated into the design of the cable accessories)[116]. In 2000, Borsi [116] introduced a PD measuring and evaluation system for non-conventional broadband

sensors for long term condition monitoring of HV equipment based on digital signal processing. Capacitive dividers and Rogowski coils have been discussed as basic sensors for the system, and several noise suppression techniques such as adaptive filtering techniques for continuous noise suppression and a PD pattern recognition algorithm for suppression of pulse shaped interferences have been discussed. PD signal processing methods applied to signals obtained using current transducers (CT) have also been reported using FFT-based de-noising, adaptive filtering techniques, wavelet and fractal theory as well as multi-band-pass filters [103, 117-119]. PD signal processing methods such as wavelet analysis, adaptive filtering and FIR filtering etc. applied to signals obtained using Rogowski coils have also been reported [116, 120-123]. However, for capacitive couplers, no further published work has been found for the post processing of noisy measurement signals. De-noising of data obtained by capacitive couplers requires consideration if they are to be practically applied under normal operating conditions.

Chapter 3

Partial Discharge Detection Using PVDF Film Sensor

Among several non-conventional partial discharge techniques applicable to online PD detection, the acoustic method has been an attractive option due to its immunity to electrical noise and interference. In the early days of PD detection, acoustic PD detection involved listening for hissing sounds emanated from liquid-filled equipment using an insulating tube and microphones were usually employed for PD detection in air and gases [61]. Recently a passive acoustic emission (AE) method using piezoelectric ceramic as the acoustic sensor has gained popularity and been widely applied for PD detection within HV equipment such as HV transformers [18, 19, 63-65], power capacitors [66, 67], and GIS [20]. Research and application of AE methods for HV cables and accessories have also been reported [68, 69]. At the University of Southampton, systematic studies have been conduced on AE detection of PD within cable insulation [22, 70, 71, 124, 125]. Compared to electrical field coupling methods such as capacitive coupling and inductive coupling, the acoustic emission method is easy to apply and free from electrical noise although relatively lower sensitivity has been reported due to the high acoustic impedance of cable insulation [22]. More recently, a new piezoelectric polymer material and its copolymer have been used as an alternative acoustic emission sensor in many non-destructive detection applications such as force-rate sensing [126], traffic sensors, musical instruments and sports scoring [127]. Interest is growing in the possibility of using an acoustic sensor based on polymeric materials to detect PD activity within HV cables.

3.1 Polyvinylidene fluoride (PVDF) Sensors

Polyvinylidene fluoride (PVDF) is a new piezoelectric material, which generates electrical charge when mechanically deformed. Piezoelectricity was first discovered by the Curie brothers more than 100 years ago. They found that quartz changed its dimensions when subjected to an electrical field, and conversely, generated electrical charge when mechanically deformed. Since then it has attracted various research interests and various practical applications have been reported. By the 1960's, researchers had discovered a weak piezoelectric effect in whale bone and tendon. This began an intensive search for other organic materials that might exhibit piezoelectricity. In 1969, Kawai found high piezo-activity in the polarized fluoropolymer, polyvinylidene fluoride (PVDF). While other materials, like nylon and PVC exhibit the effect, none are as highly piezoelectric as PVDF and its copolymers.

PVDF film, like all piezoelectric materials, is a dynamic material that develops an electrical charge proportional to a change in mechanical stress. The amplitude and frequency of the signal is directly proportional to the mechanical deformation of the film. The resulting deformation causes a change in the surface charge density of the material so that a voltage appears between electroded surfaces. When the force is reversed, the output voltage is of opposite polarity. A reciprocating force thus results in alternating output voltage.

PVDF film is one of the most popular piezoelectric polymers used in AE sensors. It has several advantages over conventional piezoelectric ceramic sensors. First the bandwidth of PVDF film is very wide (approximately 0-2GHz) and it is non-resonant, that means it picks up signals with equal sensitivity over a wide range of frequency. Whereas the bandwidth of piezoelectric ceramic sensors is generally below 1.5MHz and they are resonant, i.e. with high sensitivity within their resonant bandwidths. Second the acoustic impedance of PVDF is low (~ 4 Pas/m^3) compared to ceramics (~ 37 Pas/m^3), which enables efficient energy coupling into/from low acoustic impedance medium such as water, oil, plastics, and human tissue. Thirdly it has a high sensitivity due to its high stress constant ($g33 \sim 250 \times 10^{-3}$ Vm/N) when

compared to ceramics (g33~41×10^{-3} Vm/N for PZT 7A) [128]. In addition, it is mechanically flexible and can easily be fabricated into complex shapes [127, 128].

3.1.1 Equivalent Circuits of PVDF Film

The simplified equivalent circuit of the piezo film can be expressed either as voltage mode or charge mode depending on the interfacing electronic circuit. Figure 3.1 shows voltage mode and charge mode equivalent circuits of PVDF film, where Q represents the charge developed on piezo film and V is the open circuit voltage. The voltage mode of the piezo film consists of a voltage source in series with a capacitance. The series capacitance C_f represents piezo film capacitance which is proportional to the film permitivity and area and inversely proportional to film thickness. The voltage source is directly proportional to the applied stimulus (acoustic wave). When measured using an oscilloscope the probe of the oscilloscope can be modelled as a pure resistance to ground. Therefore the sensor and oscilloscope act as a high pass filter with a cut-off frequency effectively determined by the sensor dimensions and oscilloscope coupling resistance [127].

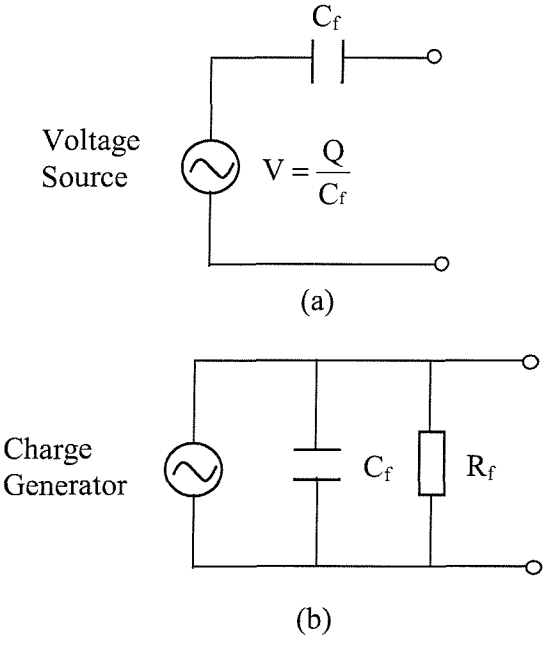

Figure 3.1 Simplified equivalent circuits of piezo film (a) Voltage mode (b) Charge mode

The charge mode equivalent circuit of the piezo film is illustrated in Figure 3.1(b). It consists of a charge generator in parallel with the capacitance of the film. The

induced charge Q is linearly proportional to the applied force and the capacitance C_f is the same capacitance in voltage mode. In low frequency applications, the internal impedance is very high and can be ignored. The open circuit output voltage can be found from the film capacitance; i.e. $V=Q/C_f$. In practice, the voltage mode is more commonly used in electrical circuit analysis.

3.2 Experiments

Experiments have been undertaken on two arrangements, firstly investigations were conducted on a three-layer sandwich of LDPE films with a void in the centre film to provide a PD source as shown in Figure 3.2. Then tests were carried out on a 132kV power cable joint containing a known PD source as shown in Figure 3.3. In order to compare the results from different sensors, a conventional electrical PD detector (Robinson model 5 type 700), a commercial ceramic AE sensor (manufactured by Physical Acoustics Ltd) and a PVDF film sensor were applied at the same time. The ceramic AE sensor used here employs a differential construction, which provides common mode rejection of unwanted signals in environments of high electromagnetic interference. A preamplifier (PAC1220A) was used to amplify the signal with a selectable 40/60 dB gain. The differential input of the preamplifier provides 24dB common-mode rejection to avoid picking up any EMI noise. A power unit, which can be operated by mains or by batteries, provided a 28 V dc supply to the preamplifier. The PVDF film sensor was made from a patch of PVDF film with metallic surfaces. A coaxial cable lead was connected to the film through tin tape foil electrodes, which was attached to PVDF film surface using silicon oil to ensure good contact. The whole sensor was mounted on the insulation surface using double-sided adhesive. The output of the PVDF film sensor was fed into a wideband amplifier with 20dB gain.

Similar results have been obtained from both experiment arrangements as shown in Figures 3.4 and 3.5 respectively. Both the conventional PD detector and ceramic AE sensor detect the PD pulse. The signal detected using conventional electrical detection is leading by a certain time the signal detected by the ceramic AE sensor as the propagation velocity of acoustic wave is slower than that of electrical pulses. This is in agreement with previous results obtained by other researchers [61].

However the signal detected using PVDF film sensor is not in the same time position as signals from the ceramic AE sensor that lag behind the conventional PD detection pulses. On the contrary, it slightly leads the electrical pulse. Therefore it can be concluded that the signal from the PVDF film sensor was not caused by acoustic waves. It is more likely an electrically coupled signal by the metallic coating or film electrodes. Further experiment confirmed this hypothesis by comparing results obtained using a capacitive coupler sensor. Hence, pulses obtained using the PVDF film sensor in this arrangement are actually caused by electrical coupling rather than acoustic waves. The present PVDF film sensor is not suitable for use in an electrically noisy environment. Further measures such as sensor shielding have to be adapted in order to apply the PVDF film sensor for PD detection.

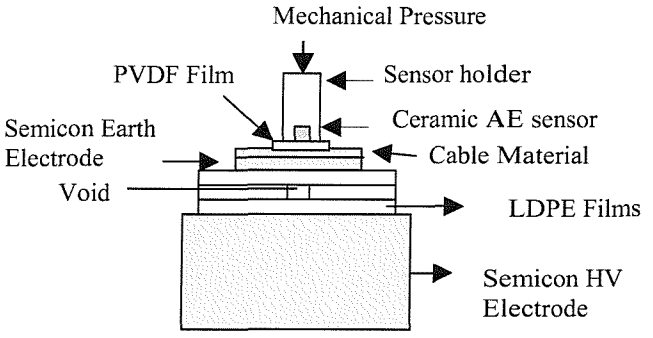

Figure 3.2 Three layers sandwich film PD experimental model

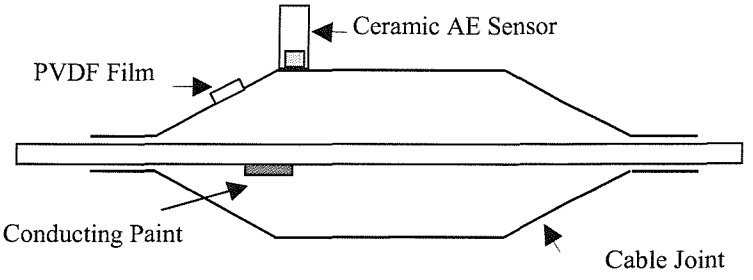

Figure 3.3 Cable joint AE PD detection experiment model

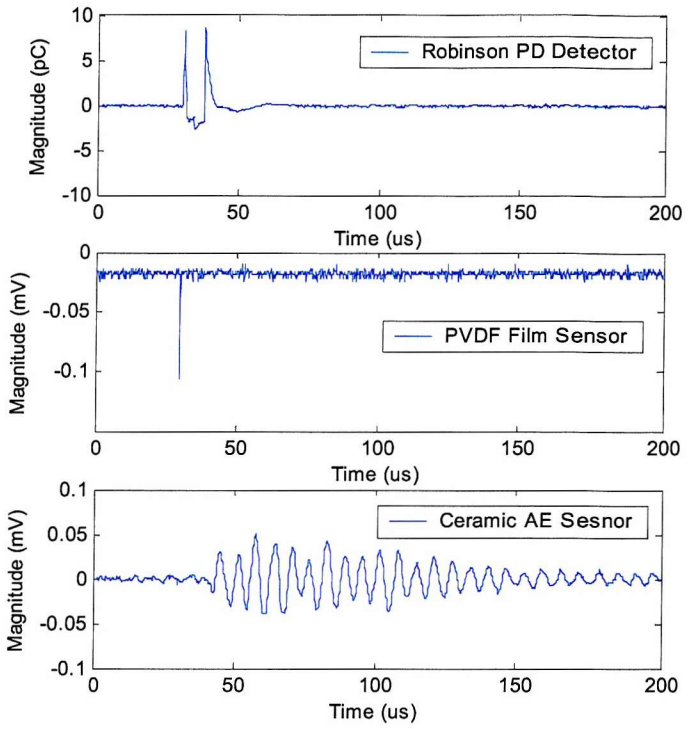

Figure 3.4 Signals detected on sandwich film void arrangement (1.8kV HV applied)

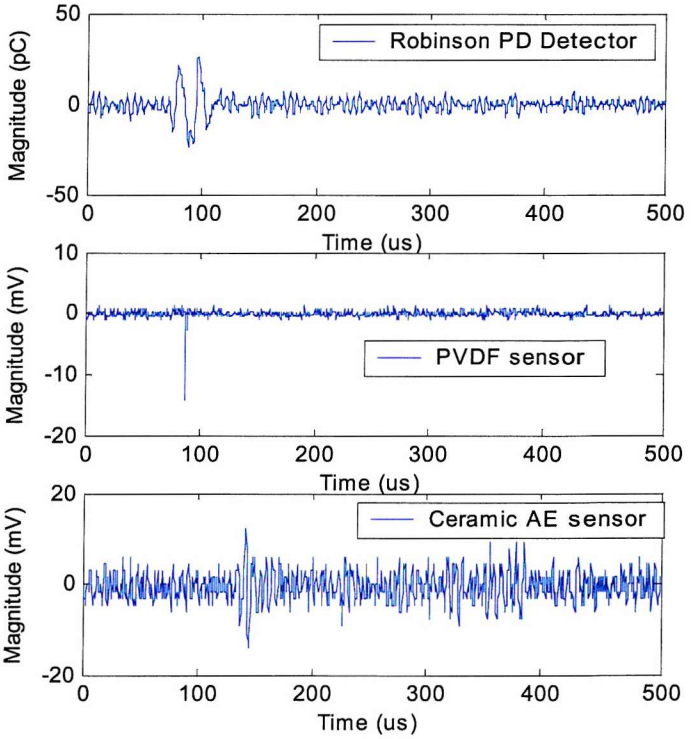

Figure 3.5 Signals detected on 132kv cable joint (49.8kV HV applied)

3.3 Shielded PVDF Sensor

In order to minimize the electrical coupling of the PVDF film, commercially shielded sensors (SDT1-028K, Measurement Specialties) were assessed. The sensor SDT1 and its frequency response are shown in Figure 3.6. According to manufacturers data, it is a fully shielded, low mass, surface mounted vibration sensor. It consists of a sensing element constructed of piezo film, a shielded cable and housing. However, it has never been used in such electrically noisy environments as in the case for partial discharge detection. Extensive experimentation revealed that it still acted as an electrical coupler. The obtained results were similar to Figures 3.4 and 3.5, which were obtained using ordinary PVDF film without special shielding.

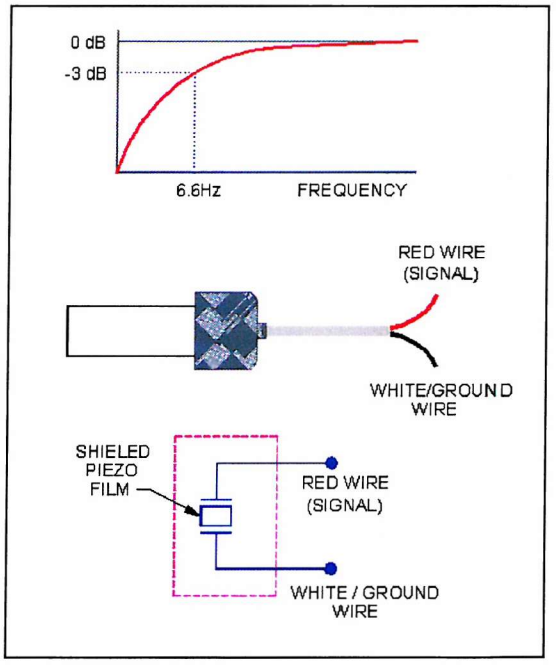

Figure 3.6 SDT1-28K Shielded piezo film sensor and its frequency response [127]

3.4 Mechanical Vibration Detection

Mechanical vibration detection was conducted using a hammer on a cable section with a PVDF film sensor and a ceramic AE sensor. The result showed that the sensor could detect the low frequency mechanical signal, and the signal is in agreement with signals obtained using a commercial AE sensor as shown in Figure 3.7. The acoustic signals arrive at both sensors almost simultaneously. The detection sensitivity of the

PVDF film sensor is quite high and no amplifier was used during the experiment. But the frequency components of the signal detected by the ceramic AE sensor is lower than that detected by PVDF film sensor probably due to its resonance within its resonant bandwidths.

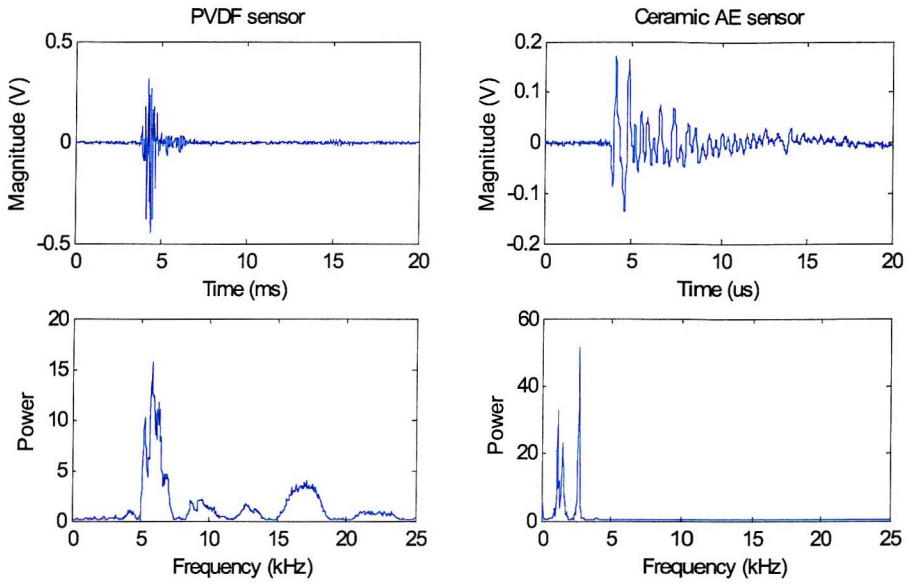

Figure 3.7 PVDF and commercial AE for mechanical impact detection

3.5 Summary

PVDF film sensors can be used to monitor mechanical vibration with higher sensitivity than ceramic AE sensors under laboratory conditions. However, they act as an electrically coupled sensor rather than acoustic sensors when used for PD detection due to the strong HF electromagnetic field environment. Therefore commercially available PVDF film sensors are not suitable for on-line PD monitoring or general PD detection. Further measures similar to those used for ceramic AE sensors such as electrical shielding, differential input sensors and amplifiers in order to reject the common mode noise need to be developed in the future if PVDF film-based sensors are to be applied to PD detection in HV cables.

Chapter 4

Online Partial Discharge Detection Using a Capacitive Coupler

Capacitive coupling is one of several popular non-conventional PD detection methods that are widely applied for online PD detection. The advantages of capacitive couplers are that they are sensitive, cheap and easy to apply. However, they have a major disadvantage in that the obtained output is generally difficult to quantify in terms of the conventional PD quantity, apparent charge. The measured results are usually expressed in voltage terms rather than in charge terms. This is not very convenient for assessment and diagnosis of the condition of the in service cable. Calibration of capacitive couplers becomes a necessary aspect of partial discharge measurement in order to effectively evaluate the conditions of the cable system.

According to IEC 60270 [9], the PD magnitude is its 'apparent charge' that is defined as the charge that, if injected instantaneously between the terminals of the test object, would momentarily change the voltage between its terminals by the same amount as the partial discharge itself. The apparent charge is generally expressed in pico-Coulombs. The purpose of calibration is to assure that if two different systems are used to measure the same sample, they measure the same 'apparent PD magnitude', which is the charge transfer on the sample electrodes. However, the measured effective apparent charge is related to the sample geometry and the size, shape, and position of the void within insulation [32], therefore the measured effective charge rarely has absolute meaning and no direct connection can be made between the measured PD magnitude and what is going on in the test sample [31].

According to IEC 60270 [9], for conventional electrical detection, calibration of the measuring system is intended for the measurement of apparent charge q and should be made by injecting current pulses by means of a calibrator as shown in Figure 4.1. The calibrator consists of a step voltage pulse generator (PG, voltage magnitude U_0) and a calibration capacitor C_0 ($C_0 < 0.1C_x$). In practice, it is not possible to produce ideal step voltage pulses, therefore pulses with fast rise times less than 60ns are recommended to ensure that the calibration pulse has similar frequency components to those of a real PD source. Calibrating pulses are injected into the terminals of the test object (C_x). If the requirements for the calibrator are met, the calibration pulse is then equivalent to a single-event discharge magnitude $q_0 = U_0C_0$.

Evolved from the conventional calibration method, the above terminal injection calibration method has been accepted as a standard method for calibration of capacitive couplers and is widely applied in laboratory conditions [14, 22, 44, 59]. However, for online measurement, alternative methods that are equivalent to the terminal injection method have to be developed, as terminals are not accessible if the cable is in service. In this chapter, several calibration methods suitable for online measurement are evaluated and their advantages and limitations discussed in detail.

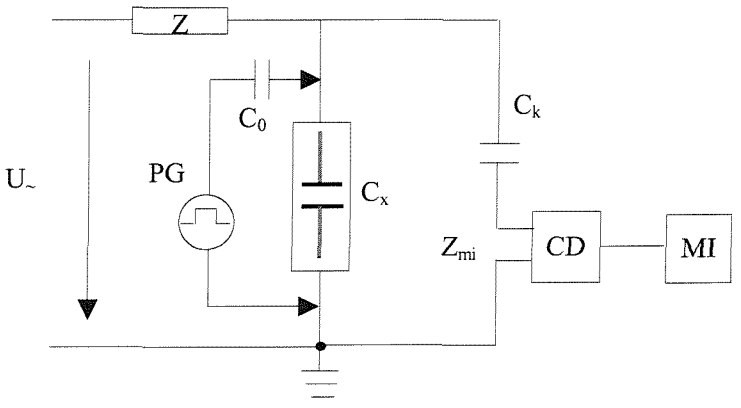

C_k coupling capacitance, C_0 calibration capacitor, PG step voltage generator, Z_{mi} input impedance of the measuring system, C_x test object, CD coupling device, Z filter, MI measuring instrument, U~ high voltage supply.

Figure 4.1 Conventional calibration of PD Measurement

4.1 Capacitive Coupler Basics

Capacitive couplers have been widely used for partial discharge detection in high voltage cables and their accessories. To further investigate the capacitive couplers it

is necessary to look into the basic principle and characteristics of capacitive coupling.

4.1.1 Principle of Capacitive Coupler Sensors

Capacitive coupler sensors work by coupling the electrical field radiated from PD sources inside test objects. They may consist of metallic cylinders or patches. As for well-shielded power cables, sensors have to be mounted outside the solid insulation and under the outer sheath in order to detect electrical field radiating from the insulation.

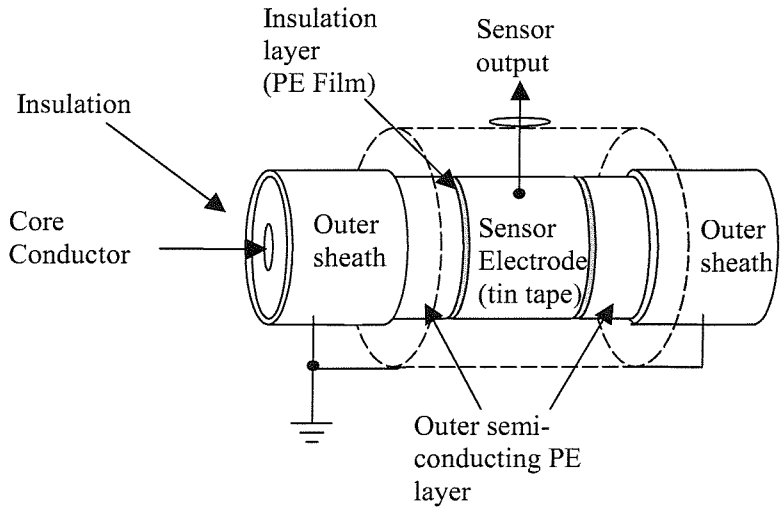

Figure 4.2 Capacitive coupler construction

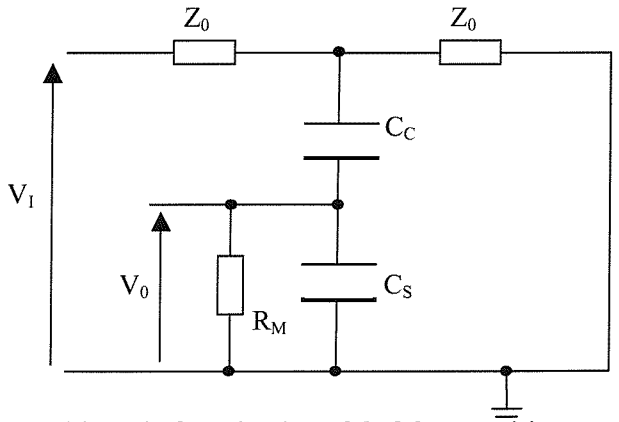

Figure 4.3 Equivalent circuit model of the capacitive coupler

Figure 4.2 shows the construction of a capacitive coupler mounted on a section of power cable used in the experiment. The HV power cable consists of a core conductor, insulation, inner and outer semi-conducting (semi-con) layers and an

outer shield. The capacitive coupler sensor is usually placed on the outer semi-con layer and consists of an insulation layer (PE film), the electrode (tin tape) and a dielectric substrate (bubble wrap) above the electrode. The sensor is completely covered by the outer sheath of the HV cable in order to keep the integrity of the cable coaxial structure and minimize the effect of external noise.

The sensor output signal is detected using a digital oscilloscope measuring between the sensor electrode and outer sheath of the cable. The lumped equivalent circuit model of the above capacitive coupler is shown in Figure 4.3, where Z_0 represents the characteristic impedance of the cable, and C_C represents the capacitance between the electrode of the capacitive coupler and cable core conductor. C_C can be approximately determined according to cable geometry and material used by Equation 4.1,

$$C_C = \frac{2\pi\varepsilon_0\varepsilon_r}{\ln\left(\frac{D_2}{D_1}\right)} L \qquad (4.1)$$

Where L is the length of the coupler, ε_0 is the dielectric constant (8.86×10^{-12} Fm^{-1}) in the vacuum, ε_r is the relative dielectric constant of the insulating material (assumed to be 2.3 for XLPE), D_2 is the outer diameter of the insulation, and D_1 is the inner diameter of the conductor.

The stray capacitance C_S between sensor electrode and the outer sheath of the cable and the input impedance (R_M) of the oscilloscope act as the coupling unit of the measurement system if compared to conventional electrical method. Obviously the measured discharge pulse magnitude V_0 is a function of the internal discharge voltage magnitude V_1, capacitance C_C and stray capacitance C_S.

4.1.2 Characteristics of Capacitive Couplers

In accordance to standard PD measurement, the pulse charge detected by capacitive coupler sensors can also be regarded as a measurement of space charge generated inside the PD source. However, due to the fundamental different coupling mechanism compared to the conventional method, only an unknown and strongly reduced part of the origin pulse charge is detectable. In order to distinguish the

standard PD quantity 'apparent charge', in 1993 Lemke and Schmiegel introduced a new quantity called 'reduced charge' if a specified calibration procedure is applied [44]. However, it can never be expected that the PD quantity 'reduced charge' will identically correspond to the 'apparent charge' even when the same origin PD event is considered.

Because capacitive couplers couple the electrical field radiated from the PD source, the dimensions of the sensor including the length of the coupler electrode, gap length between the electrode and outer sheath as well as the dimension of the coupler dielectric affect the obtained result. In practice, the reproducibility of capacitive coupler measurements is further restricted by the non-defined stray capacitance between the sensor and the test object. So any calibration result is sensor and cable specific, and can never be transferred from one sensor/cable combination to another.

In addition, some time-based parameters of the calibration pulse may significantly influence the calibration result of capacitive couplers. These parameters include rise time (10% to 90%) of the calibration pulse and decay time. Figure 4.4 shows the effect of different rise time calibration pulses on coupler output when the rise time of injected charge pulse is 1ns and 5ns respectively. The magnitude and the waveform of the two output pulses are significantly different although the same amount of charge has been injected (100pC). Whereas in the case of standardized PD measurement it has no significant influence if specified tolerance limits for time parameters are met. This is due to the fact that the capacitive coupler acts as a high pass filter and works in very high frequency (VHF) range, which is of the same order as the calibration pulse. Therefore the output of capacitive coupler is very sensitive to the rise time of the calibration pulse.

The use of capacitive couplers is relatively new, therefore it cannot be expected that well-established values exist to allow a general judgment of the risk of circuit failure due to PD activities. More experience is needed in this subject, any diagnosis based on the developing trend of the measured signal is considered to be more important than the absolute value of results.

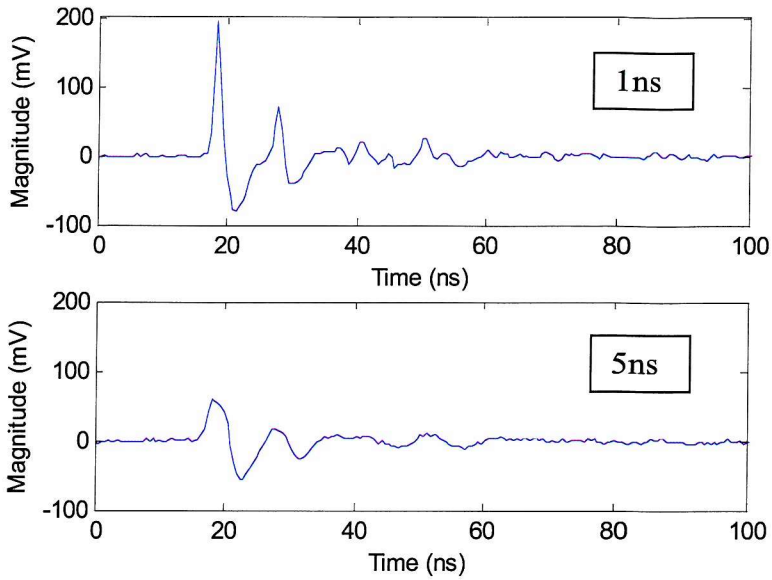

Figure 4.4 Typical coupler output under different rise time of 1ns and 5ns of calibration pulse

4.2 Evaluation of Injected Charge

The most fundamental issue regarding calibration of capacitive couplers is to determine the value of the injected charge. There are generally two methods available to determine the injected known charge depending on different applications, namely Q=CV method and $Q=A/R_m$ method. Both methods have been examined and their advantages and limitations will be discussed regarding their use in calibration of capacitive couplers.

4.2.1 Charge Equals Capacitance Times Voltage (Q=CV)

According to IEC 60270 [9], for conventional electrical PD measurement, the calibration process involves injecting a known amount of charge into test objects (e.g. cable) and determining the voltage or current magnitude that is produced by the PD measurement system in response to the injected charge. The quantity of injected charge comes from a fast rise time pulse generator (rise time < 60ns according to new edition IEC60270), which generates a step voltage V and is connected to the terminal of the cable via a calibration capacitor C. Under the condition that $C<<C_x$, the injected charge can be approximately calculated as Q = CV. If the detected pulse has a magnitude of X mV, then there is Q/X pC per milli-volt. Thus the magnitude

of each PD pulse can be measured in pC, independent of the capacitance of the test object.

Special emphasis should be given on the voltage source pulse generator to ensure that the output voltage amplitude V will not change under different external loads, i.e. test objects. Commercial calibrators are manufactured according to this standard with voltage source pulse generators in series with calibration capacitors. In fact, IEC Task Force 33.03.05 for 'Measurement of Partial Discharge' (1998) further recommends the voltage source pulse generator 'may be provided by a high accuracy DC voltage source whose output is switched by mercury whetted relay through a guarded capacitor having a known value between 50pF –150pF.'[129]. However, these calibrators are designed either for calibration of the conventional electrical measuring system or as reference calibrators for calibration of PD calibrators. Therefore the rise time of the pulse is much longer than required for calibration of VHF capacitive couplers. For example the rise time of Robinson calibrator 753 Simulator is 300ns; the rise time of high precision LEMKE reference calibrator LDC-5/R used for calibration of PD calibrators is 10ns. These calibrators are not fast enough for calibration of capacitive couplers as capacitive couplers work in VHF range and are very sensitive to the rise time of calibration pulses as discussed earlier. An alternative method using a fast commercial pulse generator in series with a capacitor may be adopted in order to get response from capacitive couplers with high sensitivity.

One problem using commercial pulse generators is that most of them are not voltage source generators as detailed by the IEC paper. On the contrary they are current source pulse generators, which means the output voltage changes with the external load while the output current is constant. Figure 4.5 shows the simplified output circuit of a PG product family (Agilent Technology 81110). It consists of a pulsating current source with selectable output impedance of 50Ω or 1kΩ. To calibrate using these pulse generators, the real output voltage of the PG under different external loads has to be calculated first in order to evaluate the exact known charge injected.

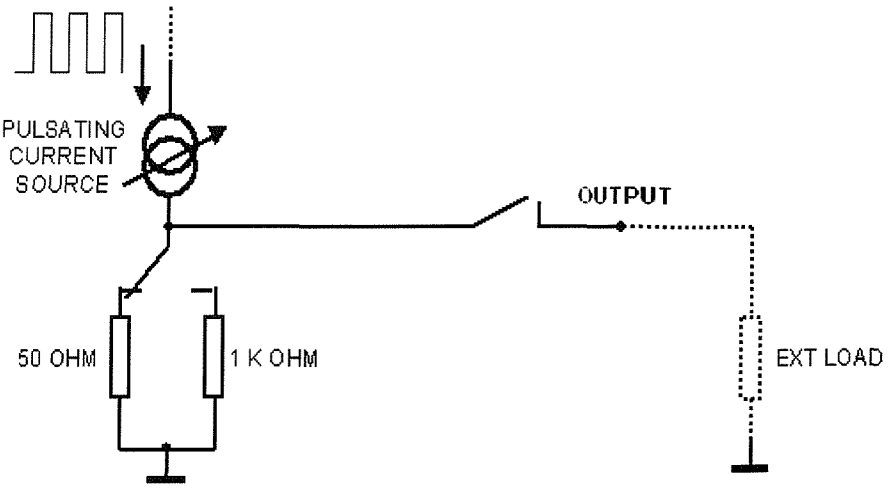

Figure 4.5 Simplified output circuit of a pulse generator (Agilent 81110 Family)

4.2.2 Alternative Method Suggested by IEC

An alternative method suggested by IEC 60270[9] to check the performance of PD calibrators can also be used for evaluation of the injected charge. This is $Q=A/R_m$ method, where A is the integration of the voltage $U_m(t)$ developed across a well defined load (high quality and low inductance resistor R_m having a value lying between 50 Ω and 200 Ω) as shown in Figure 4.6. The integration of this waveform can be performed numerically using a high precision digital oscilloscope in order to determine the charge value Q. Alternatively the integration can also be done in an analogue way using passive or active integration capacitors [130, 131].

$$Q = \int i(t)\,dt = \frac{1}{R_m}\int U_m(t)\,dt = \frac{A}{R_m} \qquad (4.2)$$

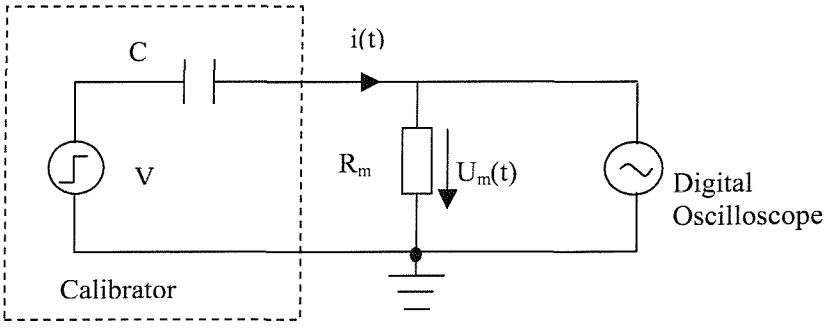

Figure 4.6 Calibration of PD calibrators

4.2.3 Practical Considerations for Calibration of VHF Couplers

The above two methods for evaluation of the injected known charge are equal and either of them can be employed in theory. In practice the Q=CV method has been more widely applied as it is more convenient if the voltage pulse amplitude V and the calibration capacitance C are known. The second method is not very convenient for calibration of the measuring system as the exact load resistance R_m of the test object is generally unknown and the integration A of the voltage $U_m(t)$ across the load is usually non-measurable. However, it can be used as a supplemental method to verify the value of output charge if directly connected to a digital oscilloscope and it is an efficient method for calibration of PD calibrators [130-133].

As for calibration of VHF capacitive coupler sensors, most commercial PD calibrators, which are used for calibration of conventional electrical PD measuring systems, or reference calibrators used for calibration of PD calibrators, are not suitable. This is because the frequency response of capacitive coupler sensors is generally above 100MHz and the rise time of the pulse has to be as short as a few nanoseconds in order to obtain a suitable output from the capacitive coupler.

In calibration experiments conducted in this thesis, a current source PG (HP8082A) has an output circuit similar to Figure 4.5 was used as it can provide fast pulses with rise time as short as 1ns. Figure 4.7 shows the interfacing circuit of the current source PG in series with an injection capacitor of 10pF when measured using a digital oscilloscope. To calculate the actual PG output voltage V_1 and voltage V_2 applied to the test object (the oscilloscope) under present external load, simulation models have been established in Matlab Simulink3.0. The present external load consists of a capacitor of 10pF and a resistor of 50Ω, which is the measuring impedance of the digital oscilloscope. Figure 4.8 shows the Simulink models for calculating V_1 and V_2, the relationships between V_1, V_2 and the input current I_2 are expressed in transfer function form, which is not difficult to obtain using the interfacing circuit model illustrated in Figure 4.7.

$$\frac{V_1}{I_2} = \frac{25s + 5\times10^{10}}{s + 10^9} \tag{4.3}$$

$$\frac{V_2}{I_2} = \frac{25s}{s + 10^9} \tag{4.4}$$

Where s represents Laplace operator. The input data is directly collected from the pulse generator using a fast digital oscilloscope and input into models through Matlab workspace. The outputs of these models can be either shown in the virtual scope in models or output to the Matlab workspace for further processing as shown in models.

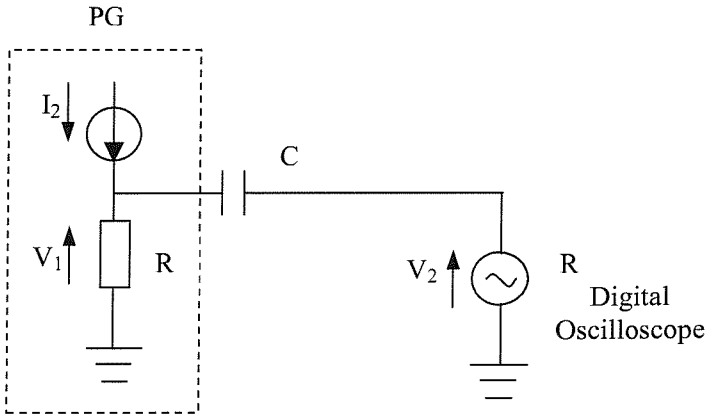

Figure 4.7 Current source PG in Series with a Capacitor used in the experiment

The computer-simulated results are shown in Figure 4.9 when the maximum output current of 0.2A from the PG is injected (the output voltage is 5Volts when connected directly to a 50Ω load). The results show that V_1 becomes 10Volts rather than 5Volts under the present load, i.e. it is exactly twice the measured value in this case. So the injected charge equals $Q=CV_1=10pF\times10Volts=100pC$. While the integral of V_2 equals 5nsV as can be seen from the simulation result when measured with a 50Ω load (input impedance of the oscilloscope). So injected charge can also be calculated as $Q = A/R_m = 5nsV/50\Omega = 100pC$. The simulated results V_2 and its integral have been measured using the digital oscilloscope (LC684DXL) and the results are in agreement with the simulated results. Therefore the same amount of injected charge can be obtained using both methods.

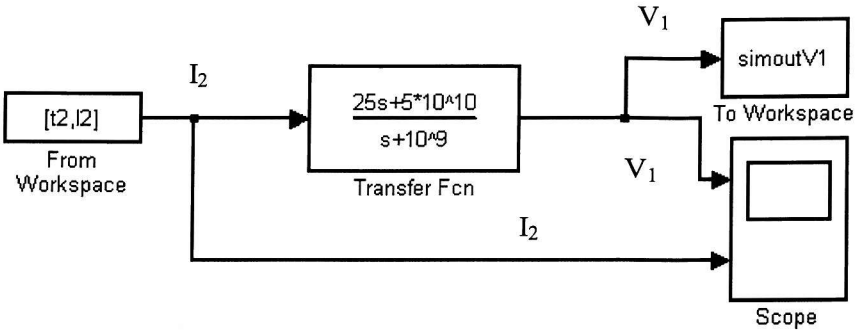

(a)

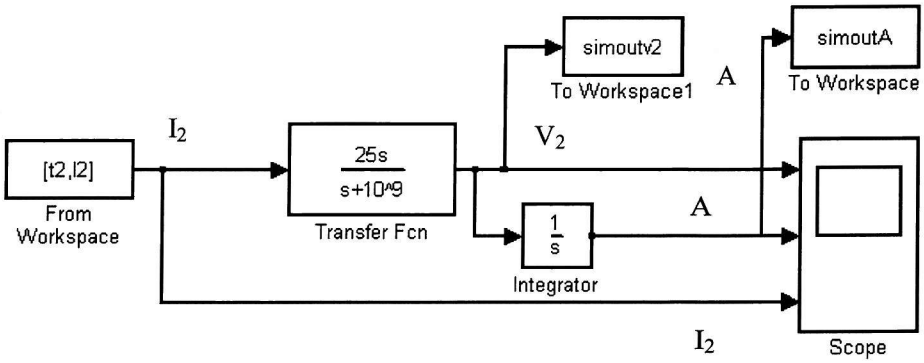

(b)

Figure 4.8 Simulation models to calculate V_1 (a) and V_2 (b) in Figure 4.7

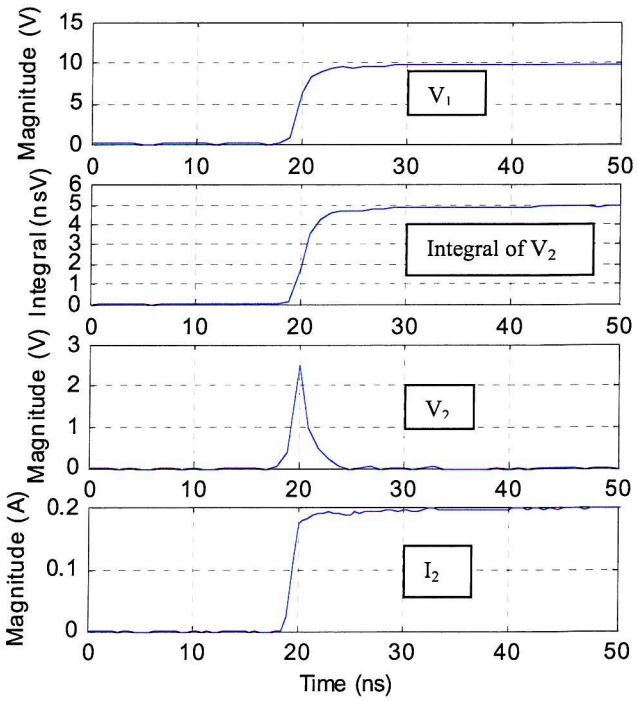

Figure 4.9 Simulated output of models shown in Figure 4.7 and Figure 4.8

Special consideration should be given when a different current source PG is used for calculation of the injected charge because the output circuit and supplied current of the current source PG may be different from that of HP8082A pulse generator.

4.2.4 Summary

Fundamentals regarding the calibration of PD measurements have been discussed. Both Q=CV method and $Q=A/R_m$ method can be used to evaluate the injected charge for calibration of PD measuring systems and calibrators. They have been shown to give identical results. However, Q=CV method is more practical than $Q=A/R_m$ method when used for calibration of a measuring system as the calibration capacitor and output voltage of PG are known or easy to obtain. The $Q=A/R_m$ is an efficient method for calibration of PD calibrators and can be used as a supplementary calibration method when the resistance of the test object is known and the integration, A, across the load can be determined.

The pulse generator used for calibration should ideally be a voltage source according to IEC 60270. However, for calibration of capacitive couplers, an alternative approach using a fast current source PG in series with a calibration capacitor has to be adopted as capacitive couplers work over the very high frequency range and are very sensitive to the rise time of the injected pulse. Special attention should be given when a current source pulse generator is used in order to evaluate the injected charge correctly.

4.3 Terminal Injection Calibration (Method 1)

This method is directly evolved from conventional PD measurement and has been accepted as a standard method for calibration of capacitive couplers. Its main disadvantage is that it can only be implemented under laboratory conditions and is therefore unsuitable for online calibration.

The terminal injection calibration method and its equivalent circuit model are shown in Figure 4.10, where C_0 is the injection capacitance, C_X is the capacitance of the whole cable and Z_M is the matching resistor (15Ω) to ensure that the input impedance of the circuit is matched to 50Ω and therefore the distortion error caused by

mismatching of impedances is minimized. In the experiment, a section of 2.96m length 66kV XLPE cable was terminated with its characteristic impedance Z_0(~35Ω) and a capacitive coupler of 0.02m was installed 0.62m apart from the injection terminal of the cable. The output of the coupler was connected to a fast digital oscilloscope (LC684DXL) with measuring impedance of 50Ω. The known charge was injected into the core conductor of the cable via an injection capacitor C_0 by applying a step voltage change using pulse generator HP8082A. The injected charge can be calculated as (see Figure 4.10):

$$Q_I = C_X V_X \tag{4.5}$$

Where the voltage V_X can be determined from the following relationship:

$$V_X = V_I \frac{C_0}{C_0 + C_X} \tag{4.6}$$

V_I is the magnitude of the step change voltage applied to the injection capacitor. By combining Equations 4.5 and 4.6 and under the condition that the capacitance of the test object (C_X) is much greater than the injection capacitance, C_0, the injected charge can be approximately determined as

$$Q_I = C_X V_I \frac{C_0}{C_0 + C_X} = V_I \frac{C_0}{\frac{C_0}{C_X} + 1} \approx C_0 V_I \tag{4.7}$$

A 10pF silver mica capacitor was chosen as the injection capacitor as the capacitance is relatively small compared to the capacitance of the test cable (~430pF) and the capacitance tolerance (<0.5pF) of silver mica capacitors is the smallest among polyethylene capacitors and ceramic capacitors. By varying the magnitude of the applied injection voltage from 1V to 5V (measured directly using an oscilloscope of 50Ω impedance, the real output voltage is twice this value when injected into the terminal via a capacitor as calculated in section 4.2.3), a varying charge of 20pC-100pC can be injected into the cable section. In the experiment the maximum output magnitude was measured as 4.8V rather than the exact 5V, therefore a range of injected charge from 20pC – 96pC was injected into the cable for the 0.02m length coupler. The corresponding output peak voltage measured values are shown in Figure 4.11 and a typical waveform obtained from the capacitive coupler is shown in Figure 4.12 when the injected charge was 96pC. The output pulse and its reflection can clearly be seen from the waveform. The first peak value is read as the output peak voltage. The rise time of injected pulses was 1ns to ensure the maximum

sensitivity was achieved. The relationship between the range of injected charge and corresponding output peak voltage has been linear-fitted to a straight line in order to minimise the possible error resulting from each measurement and a slope value of $1.9345 mVpC^{-1}$ has been obtained, which corresponds to a calibration ratio of 0.517 $pCmV^{-1}$, for an identical experimental arrangement any on-line calibration method should determine a similar calibration ratio.

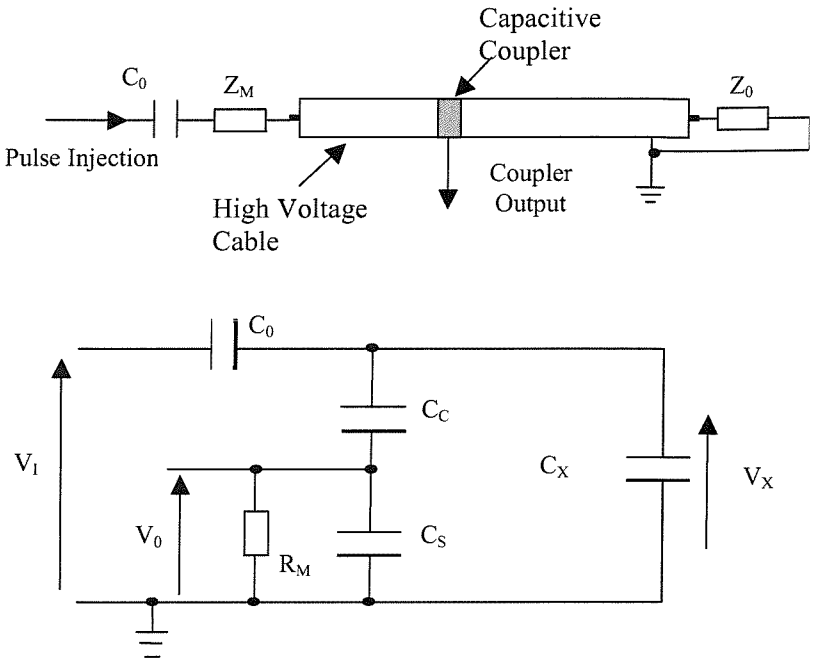

Figure 4.10 Terminal injection and equivalent circuit

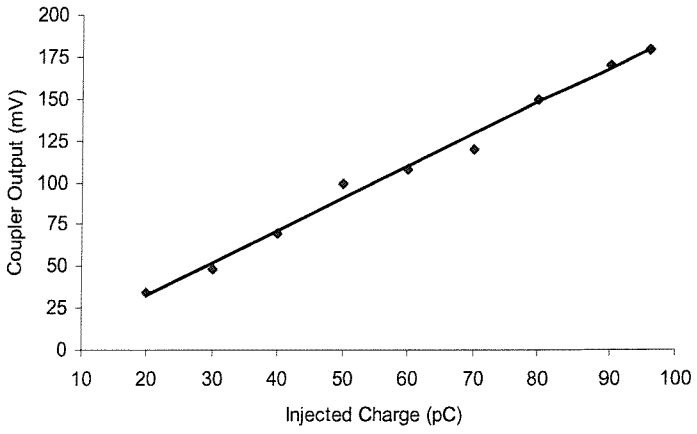

Figure 4.11 Terminal injection calibration results using a 10pF injection capacitance and pulses with 1ns rise time

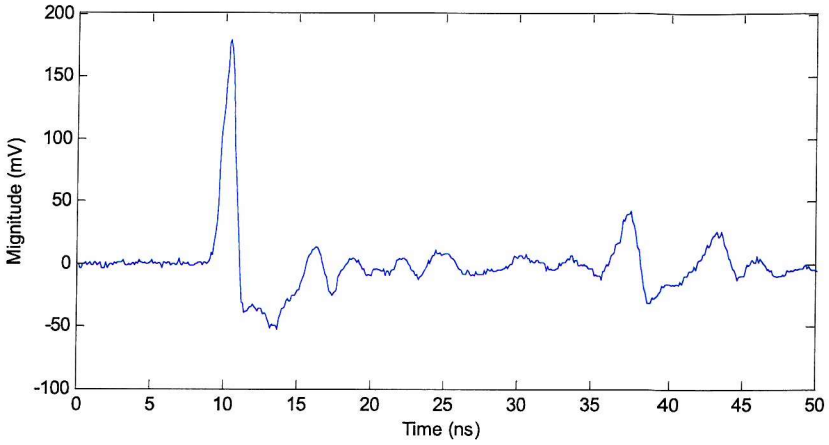

Figure 4.12 Typical terminal injection waveform measured from a capacitive coupler

4.4 Coupler Injection Methods for Online Calibration

For on-line calibration, as both terminals are not accessible, alternative methods have been developed in order to establish a relationship between measured voltage in mV and discharge magnitude in pC. Some coupler injection methods have been used for online calibration, however, their results have never been compared with that of the terminal injection calibration and the effectiveness of these methods has never been examined. In this section two different coupler injection methods have been investigated using the same experimental apparatus as method 1 and their results compared with the terminal injection calibration method.

4.4.1 Coupler Injection Method (Method 2)

This approach is to use two couplers, one acting as an injection coupler and the other as a measurement coupler. The coupler injection method and its equivalent circuit model are shown in Figure 4.13, where C_{C1} and C_{C2} are capacitances of the measurement and injection coupler respectively, each coupler also has an associated stray capacitance (C_{S1}, C_{S2}). Assuming that the capacitance of the cable under test is significantly larger than the capacitance of the injection capacitor and that stray capacitance can be ignored, then the injected charge, Q_2, can be estimated as:

$$Q_2 = C_X V_X \approx \frac{C_X C_{C2}}{C_X + C_{C2}} V_I = \frac{C_{C2}}{1 + \frac{C_{C2}}{C_X}} V_I \approx C_{C2} V_I \qquad (4.8)$$

The capacitance of the injection coupler C_{C2} can be approximately determined from the capacitance per unit length of the cable under test as expressed in Equation 4.9.

$$C_{C2} = \frac{2\pi\varepsilon_0\varepsilon_r}{\ln\left(\frac{D_2}{D_1}\right)} L \qquad (4.9)$$

Where L is the length of the coupler (0.02m in this case), ε_0 is the dielectric constant in vacuum (8.86×10^{-12} Fm^{-1}), ε_r is the relative dielectric constant of the insulating material (assumed to be 2.3 for XLPE), D_2 is the outer diameter of the insulation (54mm in this case), and D_1 is the inner diameter of the conductor (22.5mm). The resulting capacitance per unit length of the 66kV XLPE cable is 146 pFm^{-1}. The capacitance of coupler C_2 is therefore 2.92pF. Equation 4.9 is evolved from the coaxial structure communication cables where no semi-con layers are present. The existence of two semi-con layers is not taken into account when calculating the capacitance of the injection coupler using Equation 4.9.

The second coupler C_2, which is dimensionally identical to the first one C_1, was mounted 0.62m away from the measurement coupler C_1, which is 0.62m distant from the injection terminal of the cable. This is to ensure that same amount of signal attenuation compared to the terminal injection method. The magnitude of the injected pulse was varied from 1V to 5V if measured directly using a 50Ω impedance oscilloscope. But the injection capacitance according to the calculated coupler capacitance is only 2.92pF in this case, so the range of injected charge is from 5.84pC to 28.03pC. The corresponding coupler output peak values are shown in Figure 4.14 for the range of injected charge and a trend line with a slope value of 0.871 $mVpC^{-1}$ has been obtained, which corresponds a calibration ratio of 1.148 $pCmV^{-1}$. This does compare favourably with the value obtained using the terminal injection method due to the fact that in the case of coupler injection signals are propagated in both directions along the cable and hence there is a factor of two difference compared to the terminal injection method.

This would appear to be a quick and simple method for online calibration, but it is only an approximation in as much that the semicon layers are not taken into account. New methods to evaluate the capacitance of the injection coupler C_2 will also be determined in order to use this approach to calibrate capacitive couplers online.

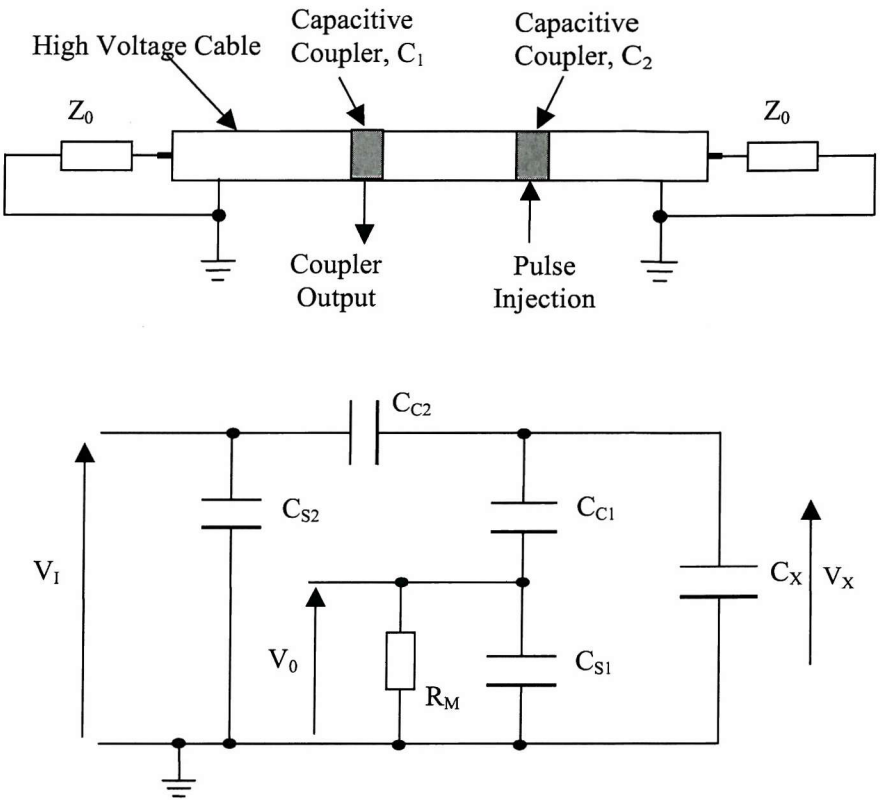

Figure 4.13 Coupler injection method and its equivalent circuit model

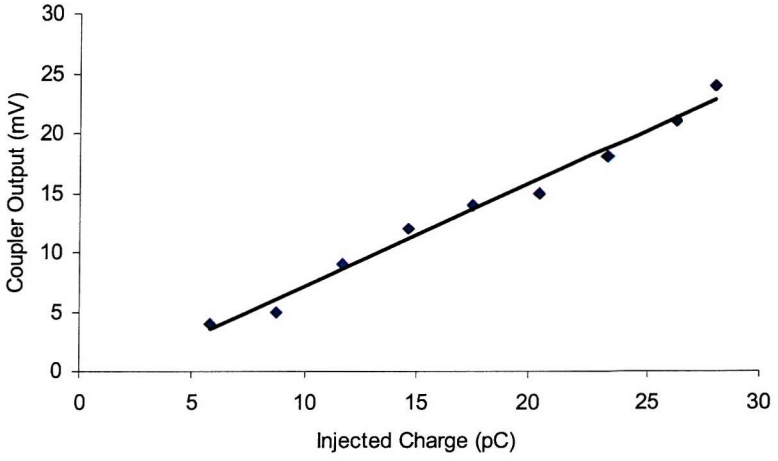

Figure 4.14 Coupler injection calibration results using a pulse with a 1ns rise time

4.4.2. Coupler Injection Via a Capacitor (Method 3)

This method is a modification of the above coupler injection method and comprises of two experiments. Firstly a pulse is injected directly into the injection coupler as per section 4.4.1 and secondly the pulse is injected into the injection coupler via an injection capacitor (C_0) as shown in Figure 4.15. With the additional injection capacitor and assuming that the cable capacitance is very large compared to the coupler capacitance, the injected charge can be estimated as

$$Q_3 = C_X V_X \approx \frac{C_X C_{C2}}{C_X + C_{C2}} V_S = \frac{C_X C_{C2}}{(C_X + C_{C2})} \frac{C_0}{(C_0 + C_{S2} + \frac{C_X C_{C2}}{C_X + C_{C2}})} V_I \qquad (4.10)$$

$$\approx \frac{C_{C2} C_0}{C_0 + C_{S2} + C_{C2}} V_I$$

Considered on its own it is impossible to use Equation 4.10 to evaluate the injected charge, as the stray capacitance, C_{S2} is unknown and C_{C2} cannot be determined accurately due to the existence of two semi-con layers. However, combining with results obtained by direct injection into the injection capacitor it is possible to determine an experimental value for C_{C2}.

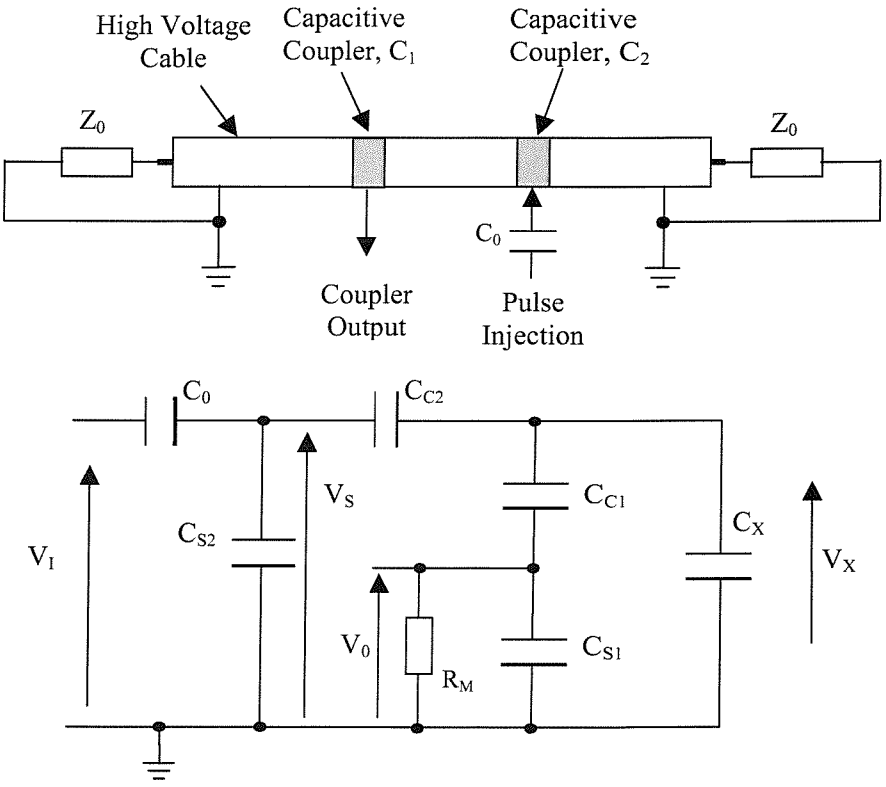

Figure 4.15 Coupler with capacitor injection experiment and equivalent circuit

Consider the application of a step change voltage, V_1, directly to the injection coupler that produces a peak voltage, V_2, at the output of the measurement coupler. From Equation 4.8 the calibration ratio, k, is defined as

$$k = \frac{C_{C2}V_1}{V_2} \tag{4.11}$$

If the experiment is repeated with an injection capacitor placed between the coupler and the voltage source, such that an identical step change voltage produces a peak voltage, V_3, at the output of the measurement coupler, then from Equation 4.10 the calibration ratio, k, is defined as

$$k = \frac{C_0 C_{C2} V_1}{(C_0 + C_{S2} + C_{C2})V_3} \tag{4.12}$$

Equating Equations 4.11 and 4.12, yields an expression for the coupler capacitance in terms of the two measured peak voltages, the known injection capacitance and the unknown stray capacitance, i.e.

$$C_{C2} = C_0\left(\frac{V_2}{V_3} - 1\right) - C_{S2} \tag{4.13}$$

Assuming that the stray capacitance is small enough to be ignored, then the injection coupler capacitance C_{C2} can be determined and the calibration ratio can be calculated using either Equation 4.11 or 4.12. The experiment was undertaken on the same arrangement as described in the previous section and the same 10pF injection capacitor was used. The rise time of injected pulses was still 1ns and the same range of step voltage from 1V to 5V was applied to the injection coupler with and without the injection capacitor. But this time the injection capacitance value C_{C2} was calculated from the measurements at each step pulse magnitude according to Equation 4.13 under the condition that the stray capacitance C_S could be ignored. The obtained capacitance value is therefore different at every voltage step as shown in Table 4.1. The range of 6.667pC to 32pC has been injected into cable according to the measured injection capacitance C_{C2}, which ranges from 2.5pF to 5.0pF from measurements at different injection magnitude under identical conditions. Figure 4.16 shows the corresponding output peak voltage values when evaluated using Equation 4.8 according to the experimentally obtained capacitance. The results at different magnitudes have been curve-fitted to a straight line once again and a slope value of $0.6826 mVpC^{-1}$ has been obtained, which corresponds to a calibration

coefficient of $1.465pCmV^{-1}$, this value is nearly three times greater than that determined using the terminal injection method.

Table 4.1 Calculated capacitance for different injection voltages and corresponding injected charge value

Injected Voltage(V)	Capacitance Cc (pF)	Injected Charge(pC)
4.8	3.333	32.000
4.5	3.125	28.125
4.0	3.846	30.769
3.5	3.636	25.455
3.0	4.000	24.000
2.5	5.000	25.000
2.0	5.000	20.000
1.5	2.500	7.500
1.0	3.333	6.667

The obtained result is still not in agreement with that obtained using the terminal injection method and the error is great. Compared to previous obtained results from terminal injection and coupler injection, the linearity and reproducibility of the results are poor. The main reason is that in Equation 4.13, ignoring stray capacitance C_{S2} is not reasonable as it maybe of the same order as the injection capacitance C_0 and the real capacitance of the injection coupler C_{C2}. In practice stray capacitance is related to many uncontrollable factors such as installation or location and is non-measurable. Consequently evaluation based on ignoring stray capacitance cannot give reasonable results. Figure 4.17 shows typical waveforms obtained using three injection methods when the same pulse was injected. Different waveforms and magnitudes have been obtained, meaning that the transfer characteristics among the three different injection methods are significantly different and consequently it is not accurate enough to describe these complicated processes using lumped parameter equivalent circuit models. Therefore coupler injection methods based on equivalent circuit models and some ideal assumptions are not applicable for calibration of VHF capacitive couplers.

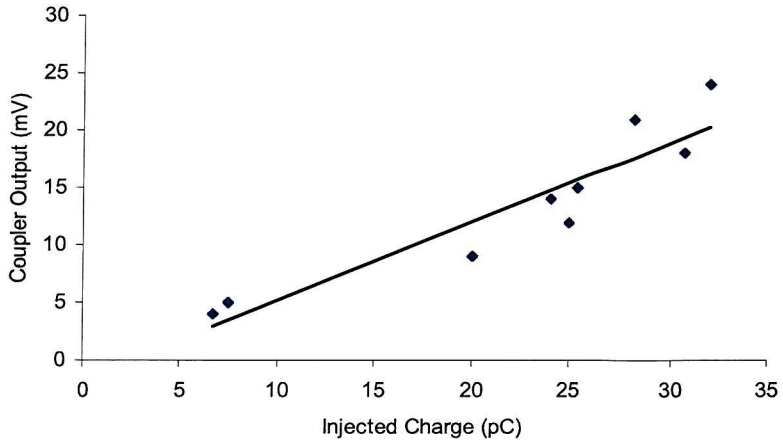

Figure 4.16 Coupler plus capacitor injection results using pulses with a 1ns rise time

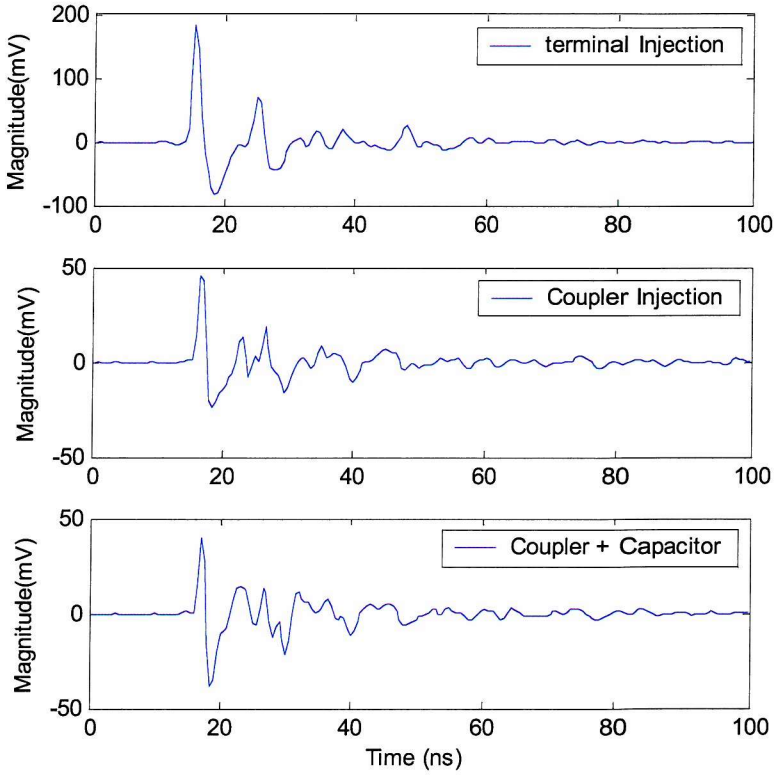

Figure 4.17 typical waveform comparison of three injection methods under same injection pulse

4.4.3 Discussion

The calibration errors of the two coupler injection methods are significant. This arises because the calculation of the coupler capacitance is based on the structure of a coaxial communication cable, which does not include semi-con material and usually

operates in the low voltage range. For HV power cables, semi-conducting layers are employed to smooth the interface between the conductor and dielectric, limiting stress enhancements and improving reliability. The existence of the semi-con material has little effect on power frequency characteristics of the cable as parameters of the semi-con material such as the dielectric constant and conductivity are negligible compared to those of cable dielectric. However these parameters are frequency dependent and vary greatly from low frequency range to very high frequency range [77], while PD pulses originate over a wide range of frequency and capacitive couplers work over very high frequency range. Consequently, the response of the capacitive coupler is highly frequency dependent and the evaluation of the capacitance based on Equation 4.9 and lumped circuit model is no longer reliable. Furthermore in method 3 ignoring stray capacitance C_S is not reasonable as it may of the same order as the injection capacitance and the capacitance of the coupler, given that C_S and C_C are generally non-measurable.

The coupler injection methods used for online calibration are generally unsatisfactory because the coupler capacitance cannot be accurately determined either by using Equation 4.9, which takes no account of the existence of the semiconducting polyethelene layers, or experimentally by a method that ignores stray capacitances possibly of the same order as the coupler capacitance and injection capacitor. The lumped parameter equivalent circuit approach is limited in its application and can at best approximate the behaviour of the capacitive coupler sensor.

Consequently a theoretical model of the capacitive coupler based on equivalent circuits is difficult to define and further research is needed in order to determine a method to calibrate capacitive couplers online.

4.5 Summary

The principle of the capacitive coupler and its characteristics has been discussed. Due to fundamental different coupling mechanisms compared to the conventional electrical method, measured results from VHF capacitive couplers are not comparable to results obtained using the conventional approach. So the concept of

'reduced charge' rather than 'apparent charge' has been proposed for VHF capacitive couplers.

Regarding calibration, it is of fundamental importance that the injected charge is determined correctly in order to calibrate any measuring instrument. According to IEC standards, Q=CV can be used to evaluate the injected charge if a voltage source pulse generator is used. Alternatively $Q=A/R_m$ method, which is usually used for calibration of PD calibrators, can also be used to evaluate the injected charge as long as the external load R_m is known and the integral A is measurable. For calibration of VHF capacitive couplers, a current source pulse generator, with a rise time as short as 1 nanosecond, has to be employed in order to match the frequency response range of the capacitive coupler sensor. As a result, special attention should be given when calculating the injected charge Q=CV, because the output voltage of the current source PG will change with different test objects.

Evolved from the conventional electrical PD detection method, the terminal injection method has been accepted as a standard approach for calibration of capacitive couplers. However, for online on-site calibration, alternative methods that approximate to the terminal injection method have to be used because terminals are generally either not accessible or too distant from the sensor.

Two coupler injection methods have been investigated as possible alternative methods to the terminal injection method. However due to difficulties in evaluation of coupler/cable parameters and limitations of equivalent circuit models as well as the existence of stray capacitance, obtained results are not in agreement with the terminal injection method and the resulting calibration errors are unacceptable.

Chapter 5

The Use of Frequency Response Analysis For Calibration of Capacitive Couplers

According to system theory, Frequency Response Analysis (FRA) is a nonparametric method to identify transfer characteristics of a linear time-invariant system [134]. It is often performed without significant prior knowledge of the system. In practice, the procedure for doing a frequency response test is simple; the system is treated as a 'black box' and a sinusoidal signal of varying frequency is applied to the system input and the corresponding system output is measured in terms of both magnitude and phase relative to the input. The system gain is then calculated at each frequency as the ratio of output magnitude divided by the input magnitude. Results are plotted either as a Nyquist diagram or as a Bode diagram, from which a model expressed in the form of a transfer function can be derived [135].

A frequency response test is an efficient experimental method to determine a system model when the exact mathematical model of a system is difficult to determine theoretically. It has been widely used in engineering to characterize and model devices such as sensors [136], transmission lines [137] and power transformers [138-141] as it can provide frequency dependent characteristics of these devices over a desired range of frequency. Transformer faults that alter the distributed capacitance and inductance parameters of its winding can be detected by measuring the frequency response at the terminals of the transformer windings. This provides vital information for preventive maintenance of important power transformers therefore has become an important means for condition monitoring of power transformers

[138-140]. It has also become a well-established method for characterization of electrical machines [142].

For capacitive coupler sensors, previous models based on lumped parameter electrical circuits have been initially proposed [23, 24]. These models are sufficient to study the transfer characteristics of capacitive couplers. However due to the complexity of the sensor geometry, cable/joint geometry and the presence of the semi-conductor PE layers, the relevant parameters are difficult to define, therefore obtained models are at best approximation and not suitable for calibration of capacitive couplers as discussed in Chapter 4. Improved accuracy has been achieved through numerical modelling and use of the Finite Difference Time Domain (FDTD) method [143, 144]. This is based on electromagnetic field theory and Maxwell Equations. A three-dimensional full-wave time domain model of a cable and capacitive coupler has been developed and the existence of semi-con layers are considered. The frequency dependent parameters of the semi-con materials are measured and verified by the propagation characteristics of the cable. However, semi-con materials have large frequency-dependent dielectric constants (εr from several 1000 down to several 10 in the frequency range up to 1GHz) and conductivity in the range of 0.1S/m to 10S/m [143]. Frequency dependent data and variable dielectric constant and conductivity require considerable computational effort, therefore only effective values are derived for certain frequency ranges or one value is used over the whole frequency range. Models based on these effective values and some other ideal assumptions are at best approximations. Furthermore, they are computationally intensive as sufficient accuracy can only be achieved through using enough FDTD grids. A model derived from frequency response analysis considers all frequency dependent characteristics of materials and factors that affect the behaviour of the coupler such as stray capacitance and environmental factors are reflected in the measured data. Consequently, the use of a simulation model based on FRA is promising for calibration of capacitive couplers.

5.1 FR Measurements of Capacitive Couplers

To investigate the possibility of establishing a model based on experimental frequency response analysis, it is necessary to first measure the frequency response data of a coupler installed on a section of cable.

5.1.1 Experimental Arrangement

All frequency response tests were undertaken on the same section of 66kV XLPE cable as used for the calibration experiment in Chapter 4. Figure 5.1(a) and (b) show the test arrangements for measuring frequency response data of a terminal to a coupler and a coupler to another coupler respectively. An Agilent 4395A Network Analyser was used to measure the frequency response of the cable/coupler system over the frequency range up to 500MHz. Similar to the experimental arrangement carried out for terminal injection calibration in Chapter 4, a matching resistor of 15Ω was connected to a terminal of the cable to ensure that the input impedance of the circuit was 50Ω, matching with the output impedance of the network analyser. To minimise any signal reflection from other end of the cable, it was terminated with its characteristic impedance (35Ω). For the coupler-to-coupler frequency response measurements both ends of the cable were terminated via a characteristic impedance to ground. The two identical couplers of 0.02m long were positioned 0.62m apart and the measurement coupler (coupler 1) was 0.62m distant from the injection terminal so that the signal attenuation is identical when comparing the frequency response data of a single coupler to that of two couplers.

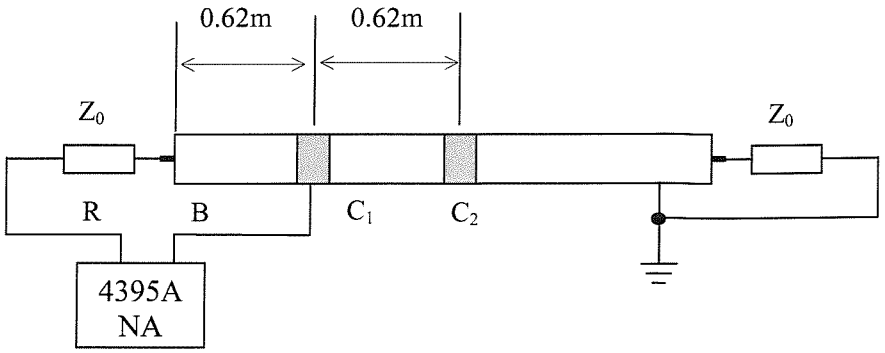

(a) From a terminal to a coupler

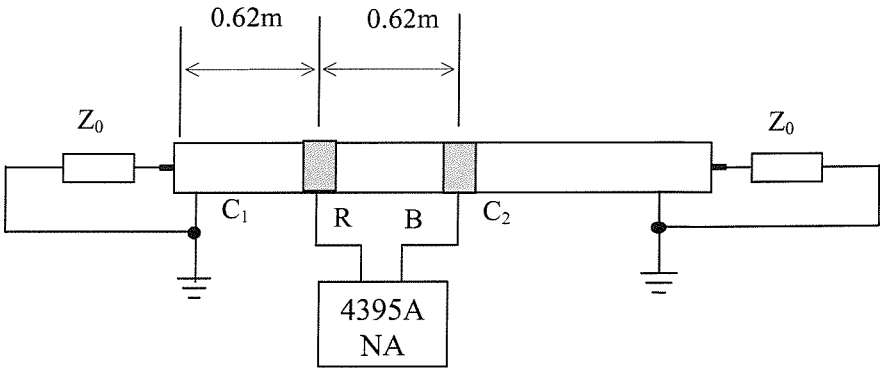

(b) From a coupler to another coupler

Figure 5.1 FR test arrangements

5.1.2 Relationship Between Terminal to Coupler FR Data and Two Coupler FR Data

Measurements have been undertaken on both test arrangements using the 4395A Network Analyser. To minimise the effect from external noise, an internal bandpass filter of 10Hz bandwidth was used over the frequency sweep range and measurements were averaged for 4 sweeps. The lowest frequency provided by the instrument is 10Hz, however it was set to 500Hz in the tests, as the frequency range of interest for capacitive couplers is much higher than that (>100MHz). Therefore a frequency range from 500Hz-500MHz was used to determine the coupler response. Obtained results for a terminal to coupler and for a coupler to another coupler are shown in Figure 5.2. The frequency response for the terminal to coupler 1 (T-C1, Figure 5.2) indicates that the coupler acts as a high pass filter and has a useful working frequency range from 10MHz-500MHz. Below 100kHz the data is

seriously contaminated by noise. This is due to the fact that the noise level (-85dB) of 4395A Network Analyser in the low frequency range is similar to or even greater than the actual frequency response data of the test object [145]. Over a very high frequency range (>100MHz) the frequency response data exhibits some oscillations and this is because that, strictly speaking, over a very high frequency range the cable system should be considered as a distributed parameter system consisting of inductance and capacitance per unit length rather than a lumped circuit system which is only capacitive [146]. The existence of inductance makes the coupler/cable system a resonant oscillating system. However, the oscillation is so small compared to the general trend of the frequency response curve that it can be ignored in the modelling process for simplicity. The coupler-to-coupler frequency response (C1-C2, Figure 5.2) data also exhibits a high pass filter characteristic; again measurement noise below 100kHz has corrupted the data and some oscillations over the higher frequency range can be observed.

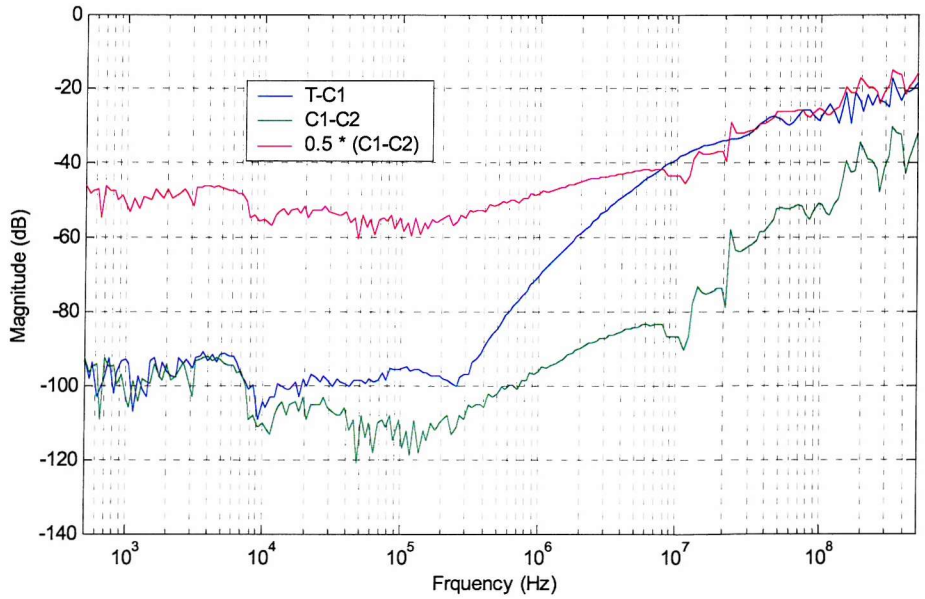

Figure 5.2 Frequency response measurement: terminal to coupler 1 vs. coupler 1 to coupler 2

Assuming that the system is linear and time invariant, two couplers are identical and the attenuation of the signal over such short distance (<1m) is negligible, then at a given frequency the coupler-to-coupler frequency response can be seen as the product of two terminal to coupler frequency responses and therefore the magnitude of the two couplers response should be twice the magnitude of the terminal to coupler response if expressed in decibels (dB). Figure 5.2 includes a plot of the

halved coupler-to-coupler frequency response curve and for frequencies above 10MHz there is good agreement with the terminal to coupler frequency response data. This infers that it is possible to approximate the terminal to coupler frequency response data by analysis of an experimental measurement of the frequency response between two identical couplers installed up to a few metres apart on a test cable. This is significant for online measurement as terminals are usually not accessible if the cable is in service.

5.2 Modelling of Capacitive Couplers Based on Frequency Response Analysis

Generally it is possible to obtain a mathematical representation of a system from measured frequency response results through a frequency domain curve-fitting process [147]. Various approaches and algorithms to obtain a transfer function model such as vector fitting [148], gradient searching [149] and subspace-based [150] methods as well as corresponding software have been reported. The complexity of the transfer function depends on the required accuracy of any given model. The accurate mathematical modelling and exact representation of the measured results is beyond the contents of this thesis. From a practical point of view and considering the physical meaning of the capacitive coupler only a simple model is required. If considering the general trend then the terminal to coupler frequency response can be approximated to a type 0 system containing a low frequency zero ω_z, a high frequency pole ω_p and a scalar gain G, i.e.

$$H(\omega) = \frac{G\left(1+\frac{j\omega}{\omega_Z}\right)}{\left(1+\frac{j\omega}{\omega_P}\right)} \qquad (5.1)$$

Where, $s=j\omega$, is the Laplace operator. Consequently, the system response can be described by three parameters G, ω_Z and ω_P.

From the terminal to coupler frequency response data it is possible to approximately determine the corner frequencies of the pole and zero as 200MHz and 200kHz respectively. It is more difficult to determine the low frequency scalar gain due to the high levels of measurement noise at low frequencies. However the output pulse of the coupler from the terminal injection can be measured as discussed in Chapter 4

and the output of above transfer function model for a range of possible scalar gain values can be simulated by building a transfer function model using Simulink3.0 in Matlab. By comparing the experimental terminal injection output waveform with that of the simulated transfer function output for the same input data it is possible to find a best fit value for G. G is varied over a range of possible values, the mean square error over the whole output waveform and the percentage difference in output peak values are determined for each value of G from –70dB to –90dB as illustrated in Figure 5.3. It is found that at –78dB or 1.259×10^{-4} the minimum output peak voltage error and minimum mean square error between the experiment and simulation model can be achieved. Therefore –78dB is the best-fit value of scalar gain G. And the corresponding transfer function model for the terminal to coupler arrangement can then be approximated as

$$H(\omega) = \frac{1.259\times10^{-4}\left(1+\frac{j\omega}{4\pi\times10^{5}}\right)}{\left(1+\frac{j\omega}{4\pi\times10^{8}}\right)} \qquad (5.2)$$

The corresponding Bode diagram for the above transfer function and experimentally measured Bode diagram are shown in Figure 5.4. As can be seen from the comparison of the two Bode diagrams, they are very close to each other over the very high frequency range, which is the working frequency range of the capacitive coupler. Therefore by approximating the measured Bode diagram, a model expressed in transfer function form can be derived.

(a)

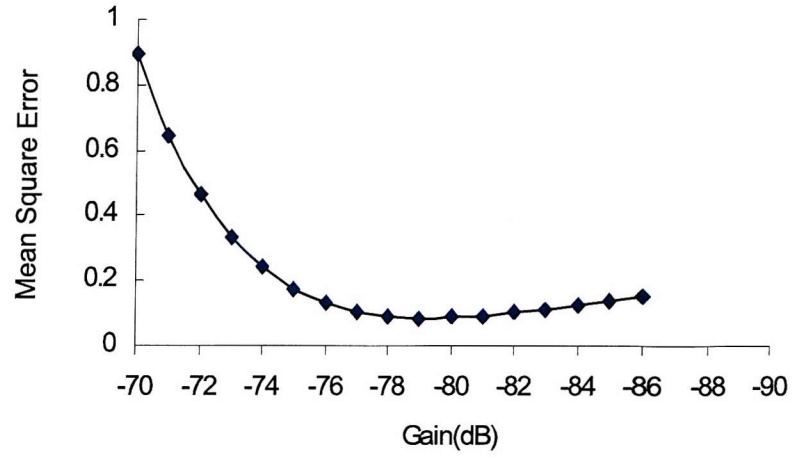

(b)

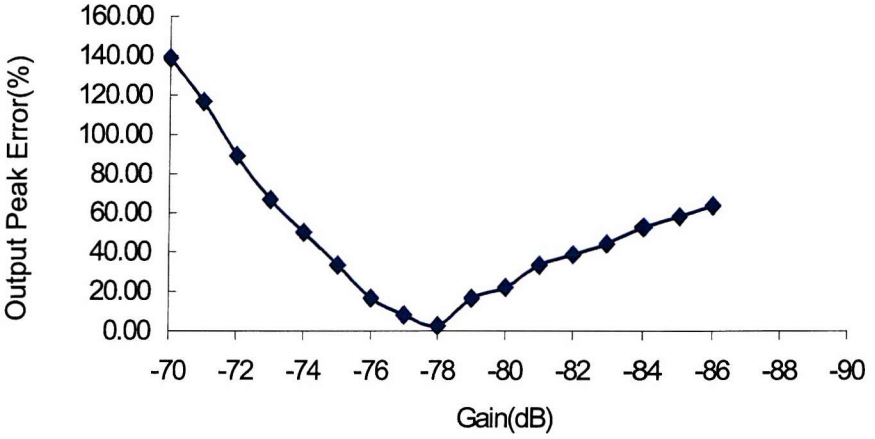

Figure 5.3 Error plots for a range of scalar gain, G (a) MSE (b) Output peak

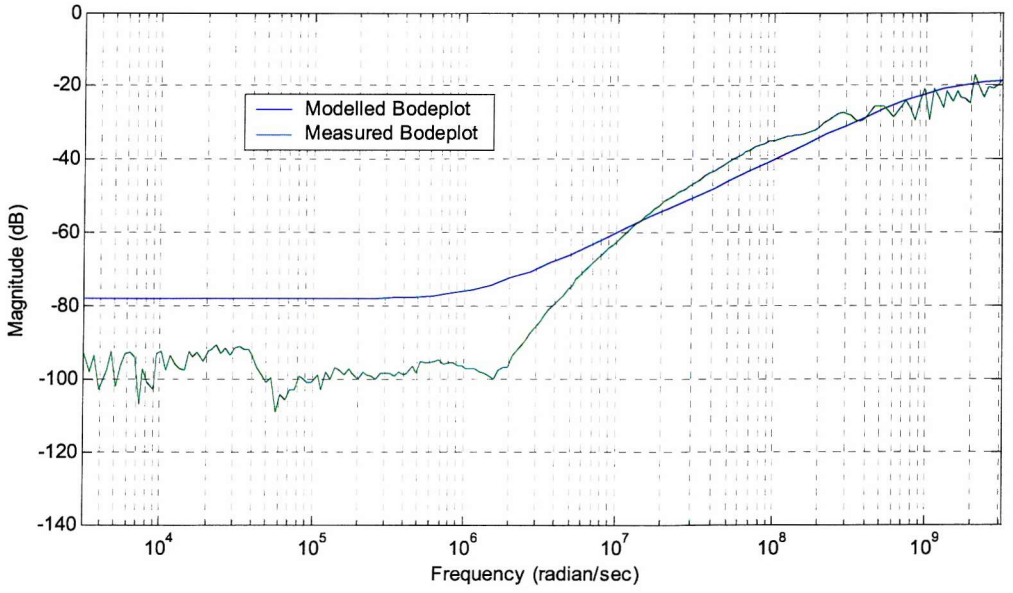

Figure 5.4 Modelled Bode diagram vs. measured Bode diagram

5.3 Simulation Results

The simulation model established for the transfer function defined in Equation 5.2 is shown in Figure 5.5, where the transfer function model of the capacitive coupler consists of a gain module and a type 0 module. The simulated input pulse data ([tn, sc1084]) is directly collected from the pulse generator in series with a capacitor using a fast digital oscilloscope. The integration of the input pulse has also been measured using an integrator module in order to confirm the magnitude of the input pulse using $Q=A/R_m$ method. The output of the model can either be shown on the virtual oscilloscope or output to Matlab workspace for further processing.

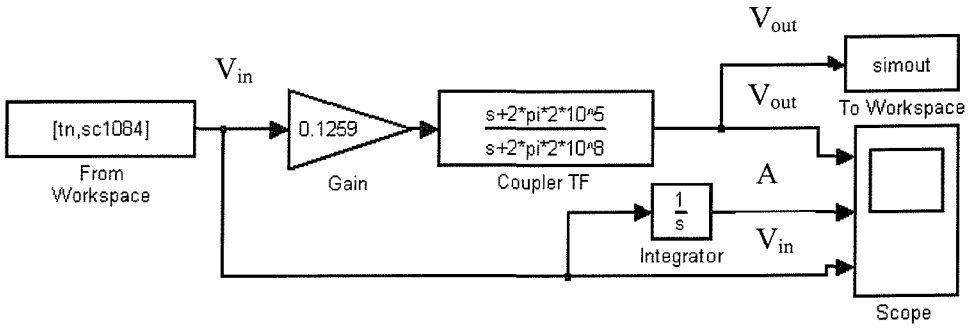

Figure 5.5 Simulation model of a terminal to coupler

Using the above model, it is possible to produce a simulation that determines the coupler output in mV for a predefined signal input. The simulated result is shown in Figure 5.6 when a 96pC pulse with 1ns rise time was modelled as the input injected into the model. The injected charge value has been confirmed using the alternative evaluation method $Q= A/R_m$. The simulated output and the measured output waveforms are close to each other except that the measured waveform has a reflected pulse near the end of the signal. Good agreement has been achieved between the simulation and the experimental output. Any discrepancy is most likely due to the fact that the model does not include the high frequency resonances observed in the FRA measurements. The model does not account for signal reflection but does closely match the initial response of the coupler.

Using this model it is possible to generate a calibration ratio through simulating a range of input pulses and calculating the corresponding output peak of the coupler,

Figure 5.7 shows the corresponding output peak voltage values when a series of pulses ranging from 20pC to 96pC were injected into the model. The same range of pulses has been injected into the test object and the resulting experimental values are compared with the simulated values as can be seen from Figure 5.7. The obtained values have been curve-fitted to straight lines and the reciprocals of the slope values are considered to be the calibration ratios. Good linearity has been obtained for both groups of results. From the simulation a calibration ratio of 0.542 $pCmV^{-1}$ has been obtained that is very close to the experimentally obtained value $0.517pCmV^{-1}$.

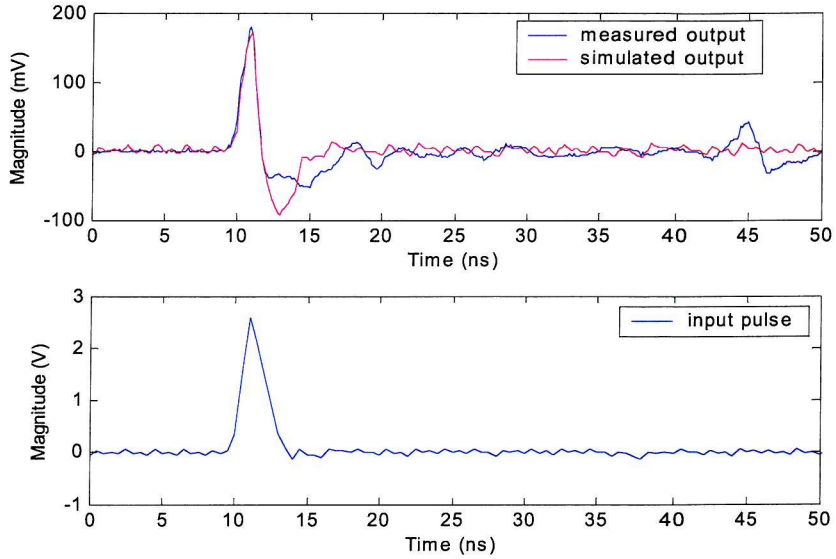

Figure 5.6 Simulated coupler output compared with experimental measurement for a terminal injection pulse of 96pC

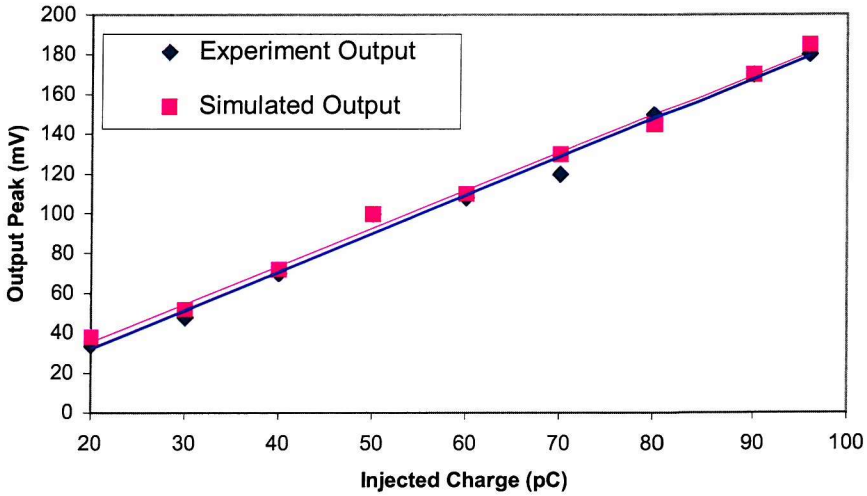

Figure 5.7 Comparison of simulated calibration with experimental terminal injection calibration

Besides output peak voltage values, the relationship between the output pulse area (integral of the output pulses) and the injected charge value has also been investigated. The integral of the output pulse has been conducted using a fast digital oscilloscope with built in integral algorithm. While the integral of the simulated output was implemented using the integrator shown in Figure 5.5. Figure 5.8 shows the simulated and experimental output integrals at various injected charge values. It can be seen that, similar to output peak values, the output areas (integral) are also proportional to the injected charge values and can be used to evaluate the discharge levels to some extent.

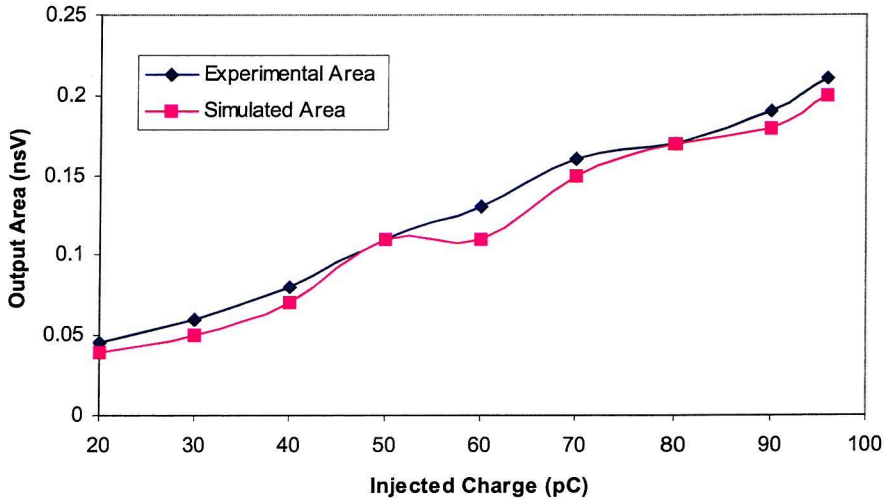

Figure 5.8 Output areas vs. injected charge

5.4 Using the Coupler to Coupler Frequency Response to Generate a Model Representing Terminal to Coupler Behaviour

Having established the relationship between the FR of the terminal to coupler and that of coupler to coupler as described in section 5.2, the possibility of deriving a terminal to coupler model based on the analysis of the coupler-to-coupler frequency response has been investigated. Figure 5.2 shows the coupler-to-coupler frequency response along with its halved value, there is reasonable agreement between the terminal to coupler response and the halved coupler-to-coupler response at higher frequencies. An approximate model of the form described by Equation 5.1 has been redefined as follows: ω_P is defined as the high frequency above which the magnitude

of the coupler-to-coupler frequency response is reasonably constant; ω_Z is defined as the low frequency above which the magnitude of the coupler-to-coupler frequency response starts to increase; and G is then chosen such that for higher frequencies the magnitude of the approximate model frequency response matches the halved coupler-to-coupler frequency response.

Applying these rules using the frequency responses shown in Figure 5.2 gives an approximate model, $H_a(\omega)$, of

$$H_a(\omega) = \frac{1.778\times10^{-4}(1+\frac{j\omega}{4\pi\times10^5})}{(1+\frac{j\omega}{2\pi\times10^8})} \qquad (5.3)$$

The corresponding Bode plot shown in Figure 5.9 is in good agreement with the halved frequency response data of coupler-to-coupler over very high frequency range. The same range of simulated input data (20pC-96pC) has been injected into the model and this in turn produces a calibration ratio of $0.589pCmV^{-1}$ as shown in Figure 5.10 using the same curve-fitting procedure as described in previous sections. This value is close to the value obtained using terminal to coupler frequency response data ($0.542pCmV^{-1}$) and close to the experimental terminal injection result ($0.517pCmV^{-1}$).

The above transfer function derived from the halved coupler-to-coupler frequency response data is different to the one derived from the terminal to coupler frequency response results (Equation 5.2). Yet very close calibration ratios have been obtained from both simulation models and these ratios are also close to the experimental value obtained in Chapter 4. This means that the calibration ratio can also be approximately generated from the frequency response data obtained for two identical couplers placed a short distance apart. This is significant for online calibration where terminals of the cable are usually not accessible and only frequency response from one coupler to another is available.

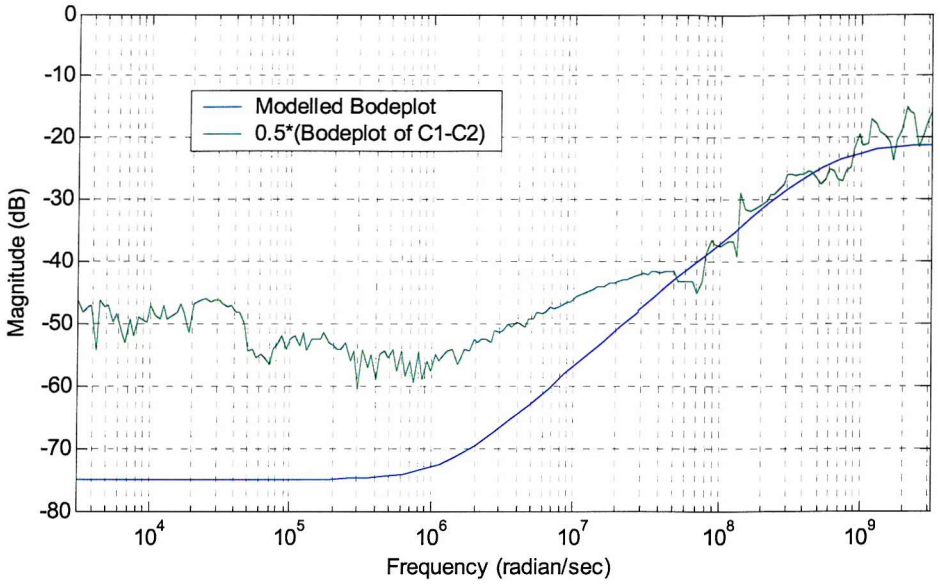

Figure 5.9 Modelled Bode plot from halved FR data of C1-C2

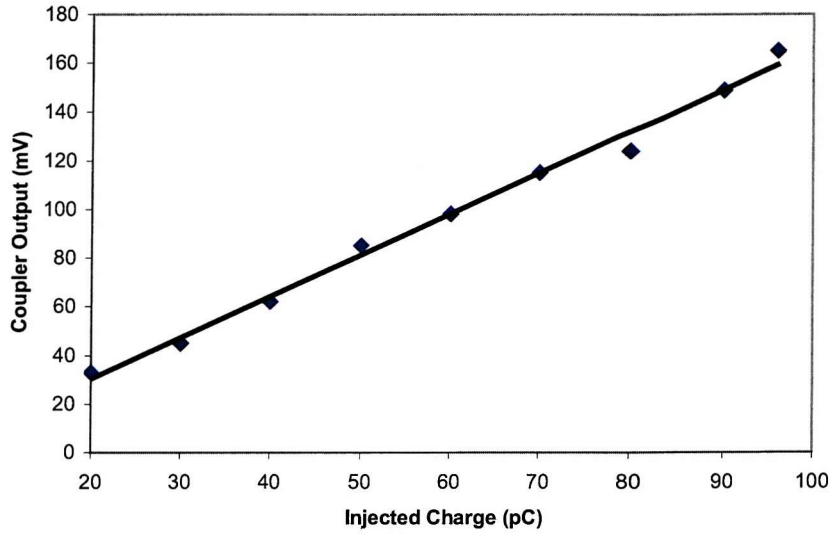

Figure 5.10 Simulation results using an approximate model based on the coupler to coupler frequency response

5.5 Discussion

5.5.1 Simulation Results Using Input Pulses With Different Rise Times

The simulation models were all obtained for 1-nanosecond rise time injection pulses. The maximum frequency component of such pulses is generally below 500MHz and

the frequency range of such pulses covers the working frequency range of the capacitive coupler. Therefore these models are also suitable for other frequency ranges. Figure 5.11 shows simulation results of the coupler model expressed in Equation 5.2 when the rise time of the injection pulse is 5 nanoseconds. The experimental arrangement was identical to that for the terminal injection calibration with the injected charge ranging from 20pC - 96pC. Only the rise time of the injected pulse was different. The output peak voltage values from both simulation and experiment are compared and their results are in reasonable agreement with each other.

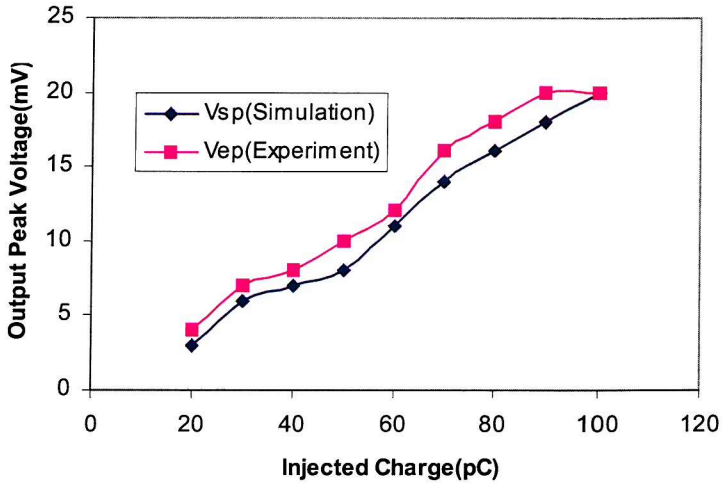

Figure 5.11 Simulation results for 5ns rise time input pulses

5.5.2 Simulation Models for Different Dimension Couplers

The models of Equation 5.2 and 5.3 were obtained for a 0.02m length coupler with a gap length between the coupler and the cable outer sheath of 0.03m. When different dimension couplers are employed the obtained output results should be different. Figure 5.12(a) shows the relationship between the output peak voltage and the coupler dimension (coupler length ranging from 0.02m to 0.09m, fixed gap length 0.03m). It is clear that the longer the coupler, the greater the output peak voltage of the coupler. Accordingly, this relationship is also reflected in the frequency domain and the measured frequency response data of the same couplers is shown in Figure 5.12(b). Corresponding transfer function models for these couplers can be obtained using the same procedure outlined in section 5.2.

The measurement sensitivity of the capacitive coupler is closely related to its dimensions. Better measurement sensitivity can be achieved with longer couplers, however the accuracy of PD source location will be compromised. In practice, the choice of coupler dimension is application dependent and in most cases it is a compromise between the detection sensitivity and location sensitivity.

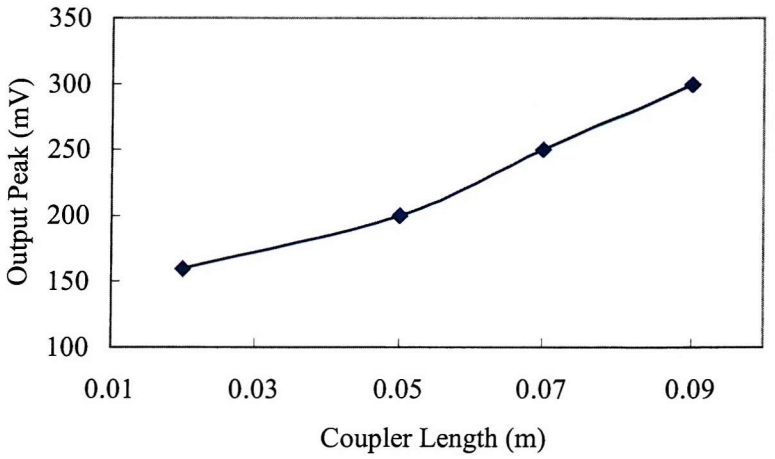

(a) Output peak voltages vs. coupler length

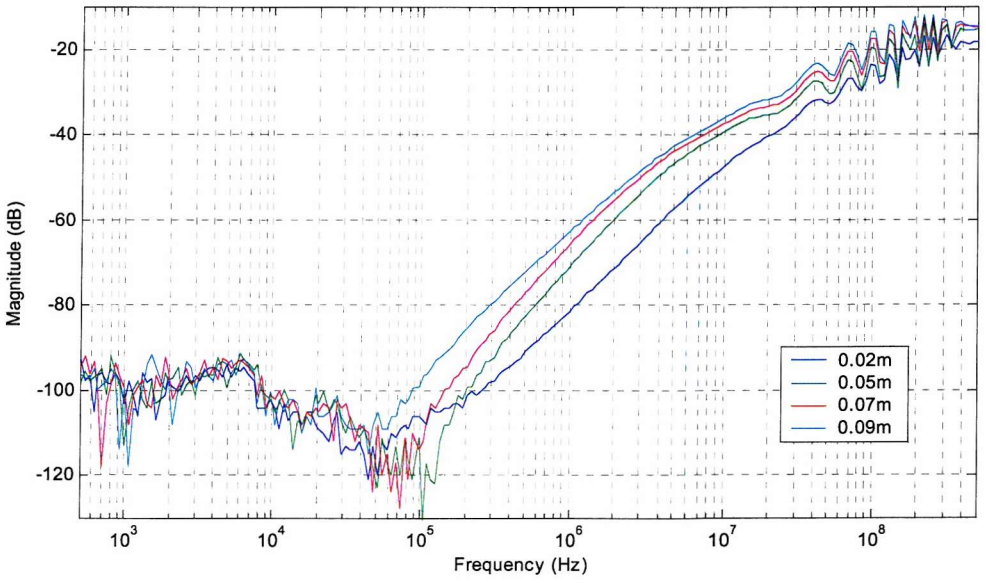

Figure 5.12 (b) Measured FR data for different dimension couplers from 0.02m to 0.09m (Terminal to Coupler)

5.5.3 Modelled as a Second Order System

To increase the accuracy of the model, the measured frequency response data can also be represented as a second order system with a pair of complex conjugate zeros in the lower frequency range and two poles in the high frequency range as expressed in Equation 5.4, where ζ is the damping ratio (0.1 in this case). The corresponding Bode diagram is shown in Figure 5.13. It is obvious that the second order system model is a better fit over the frequency range. But the determination of parameters is more complicated as five variables need to be defined. A procedure for obtaining a second order system transfer function can be found in [135]. This method has been used on the measurement data to yield the following transfer function:

$$H(\omega) = \frac{10^{-4.8}\left(1+\frac{2\zeta}{2\pi\times10^{6}}\,j\omega+\frac{1}{(2\pi\times10^{6})^{2}}(j\omega)^{2}\right)}{\left(1+\frac{j\omega}{2\pi\times10^{7}}\right)\left(1+\frac{j\omega}{2\pi\times10^{8}}\right)} \qquad (5.4)$$

The simulated second order model output waveform as well as the experiment output waveform is shown in Figure 5.14 when the same injection pulse of 96pC was injected into the model. Again good agreement has been achieved between the model and experiment and a calibration ratio of 0.523 ($pCmV^{-1}$) has been obtained from the model. This is close to the calibration result obtained from the first order model (0.542 $pCmV^{-1}$) and close to the experimental result for terminal injection. The second order system model fits the experimentally obtained Bode diagram better than the first order system especially over the low frequency range as can be seen from Figure 5.13. Comparison of the simulated output with experimental data (Figure 5.15) is in close agreement and any discrepancy is due to unmodelled higher order dynamics.

As the differences between the two simulation models are relatively small and the first order model is easier to define, the first order model approach has been adopted for this application.

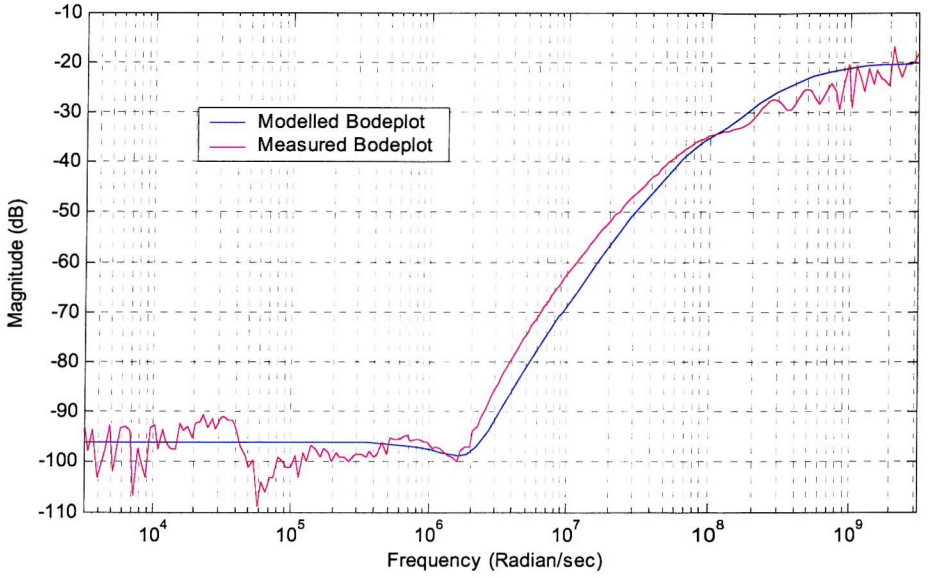

Figure 5.13 Modelled as a second order system

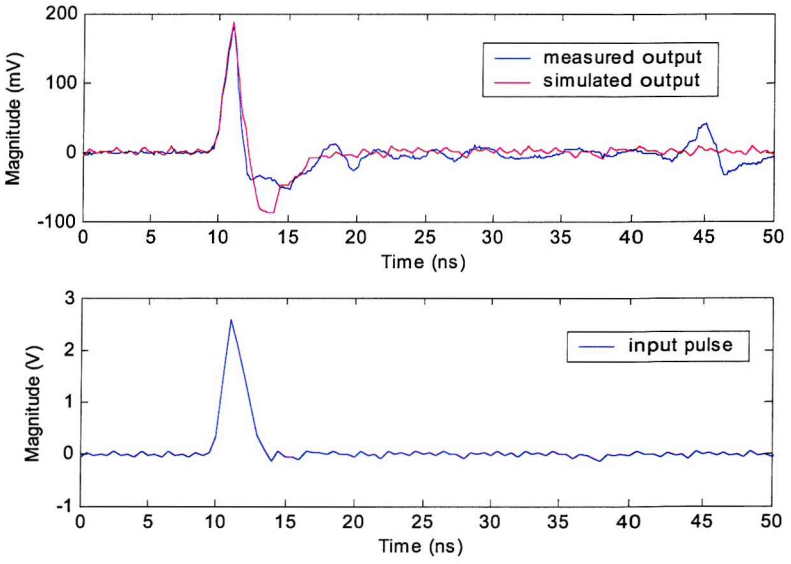

Figure 5.14 Simulated output waveform (second order) vs. experiment waveform

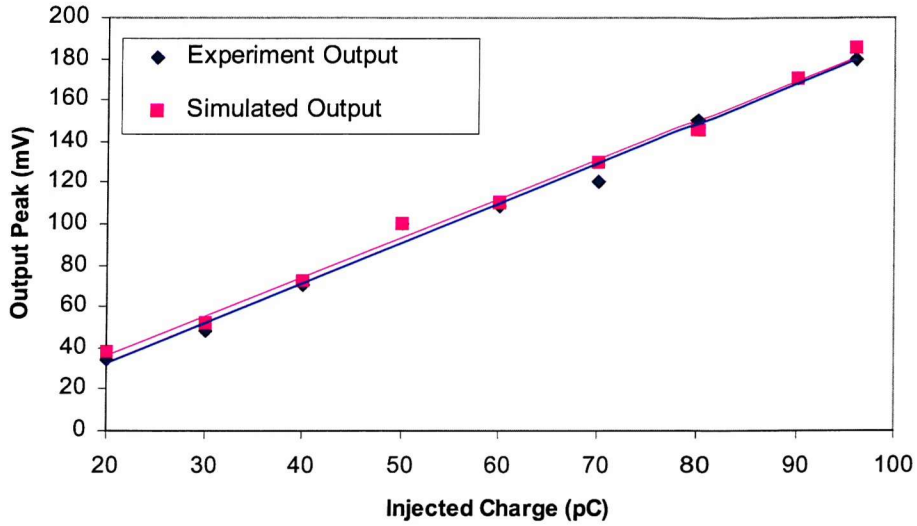

Figure 5.15 Experiment output vs. simulated output when modelled as a second order system

5.5.4 Effect of Attenuation

The signal attenuation effect over the distance between the two couplers has been ignored during the modelling process. To investigate the error resulting from this, attenuation measurements over the experimental cable section have been undertaken. Three identical couplers were installed on the cable at different distances as illustrated in Figure 5.16(a). A 96pC pulse (1ns rise time 10pF, 9.6V) was injected into a terminal and the response signal from the 3 couplers were measured using a digital oscilloscope. Obtained results are shown in Figure 5.16(b). The peak voltage value is slightly attenuated over the distance and the reflection of the original pulse can be seen clearly with different time positions due to the different locations of the couplers. However the difference in magnitude is quite small and could result from the difference in coupler installation as exactly identical couplers do not exist and stray capacitance due to installation is not controllable. Therefore the attenuation effect can be ignored over short distances of less than 2-3 metres.

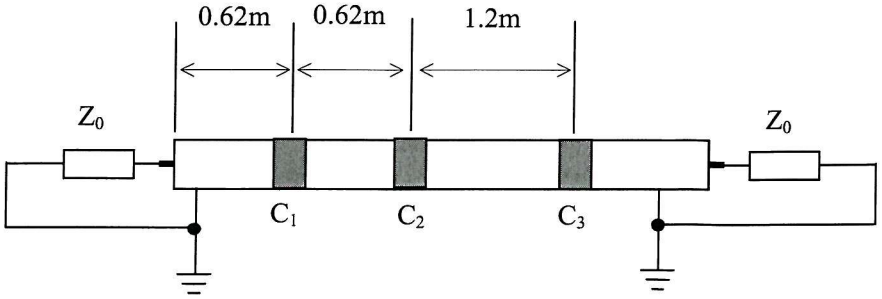

(a) Positions of Couplers

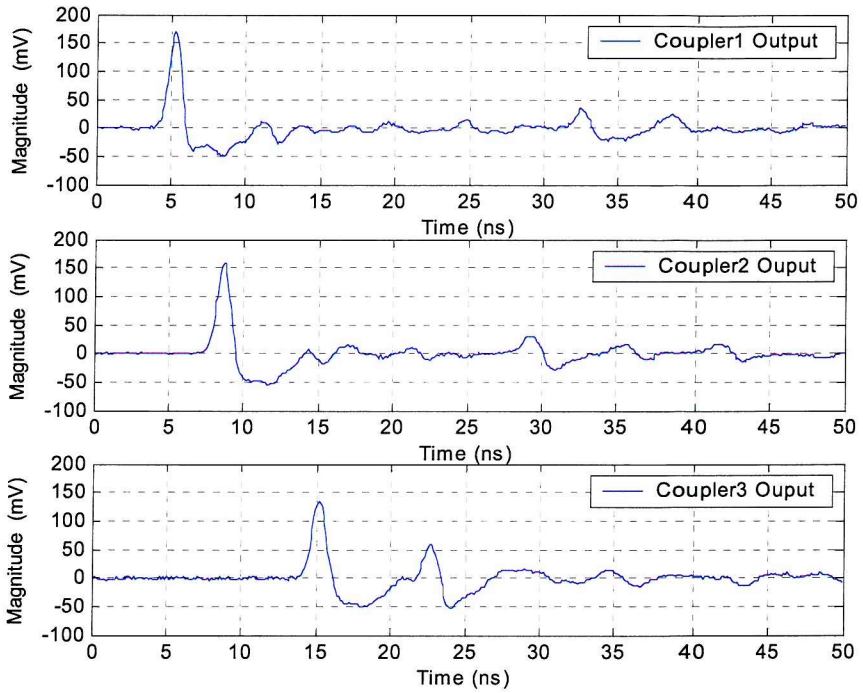

(b) Output waveforms from different couplers (Terminal Injection)

Figure 5.16 Attenuation Effect

5.6 Summary

Frequency response analysis is an efficient experimental method to determine the behaviour of a capacitive coupler. The result from FRA shows that the capacitive coupler works over a very high frequency range and acts as a high pass filter. The behaviour of a capacitive coupler mounted on a specific cable section can be approximately represented using a transfer function model. Based on the transfer function a simulation model has been established using Simulink3.0 and the

simulated results are in close agreement with the experimental ones. Basic calibration work has been carried out based on the simulation model and the result obtained is in good agreement with the experimental terminal calibration result.

Various approaches of determining a calibration ratio for a capacitive coupler have been investigated experimentally and the values obtained for one experimental arrangement are shown in Table 5.1. It can be seen that a model based on the frequency response from the terminal to coupler produces a calibration ratio that is very close to the value obtained using the terminal injection method. By approximating the model using data from the coupler-to-coupler frequency response a similar calibration ratio can also be achieved. Models obtained using both FRA results give far more accurate estimates of the reduced charge measured at the coupler than using pulse injection methods to determine the sensitivity of the measurement.

Table 5.1 Calibration ratios based on various methods

Method	Calibration ratio ($pCmV^{-1}$)	%age change from terminal injection result
Terminal injection	0.517	-
Coupler injection	1.148	122
Coupler/capacitor injection	1.465	183
Terminal-coupler simulation (first order)	0.542	4.8
Approximate model simulation (first order)	0.589	13.9
Terminal coupler simulation (second order)	0.523	1.2

The complexity of the transfer function model is determined by the required accuracy of the model. Both first order and second order models give good results compared to experiment results. However, for simplicity of modelling and practical application, a first order model gives sufficient accuracy for calibration purposes.

Chapter 6

Experimental Investigation of the Calibration Method Based on FRA

In order to investigate the feasibility of using an approximate simulation model based on FRA measurements of two identical couplers to estimate the calibration ratio of a capacitive coupler for online PD measurement, real PD tests have been undertaken on two different cable test sections containing different PD sources. On both test sections, terminals are not available; therefore the approximate modelling method based on the coupler-to-coupler frequency response measurement has been used. This chapter further investigates the application of this method when used for real PD online measurement and results obtained are compared with the conventional apparent charge measurements.

6.1 Needle loop PD Test

The needle loop PD test was undertaken on a short length of 66kV XLPE cable containing an earthed needle that acts as PD source as illustrated in Figure 6.1. A section of 3.5m length cable terminated with de-ionised water terminations has an earthed tungsten needle with a 1mm shank diameter and 3μm pin tip radius inserted into the cable insulation to within 3mm of the cable core conductor. Two couplers, with the same dimension as used in the previous experiments have been mounted on the cable outer semi-con layer as shown in Figure 6.1. The first coupler (C_1) is on the left hand side of the needle and 760mm away from it and the second one (C_2) is on the right hand side of the needle and 100mm away from it. The measurement apparatus is installed in a control room distant from the cable loop and includes two broadband amplifiers and a fast digital storage oscilloscope (LeCroy LC684DXL).

Signals from the couplers will pass through over-voltage protection (sgp-surge protector) before being amplified using 22dB broadband amplifiers and captured by the oscilloscope. Conventional electrical PD detection using a Robinson model 5 Type 700 Detector was also applied in order to determine the apparent charge of any PD activity and allow comparison with results obtained using the couplers.

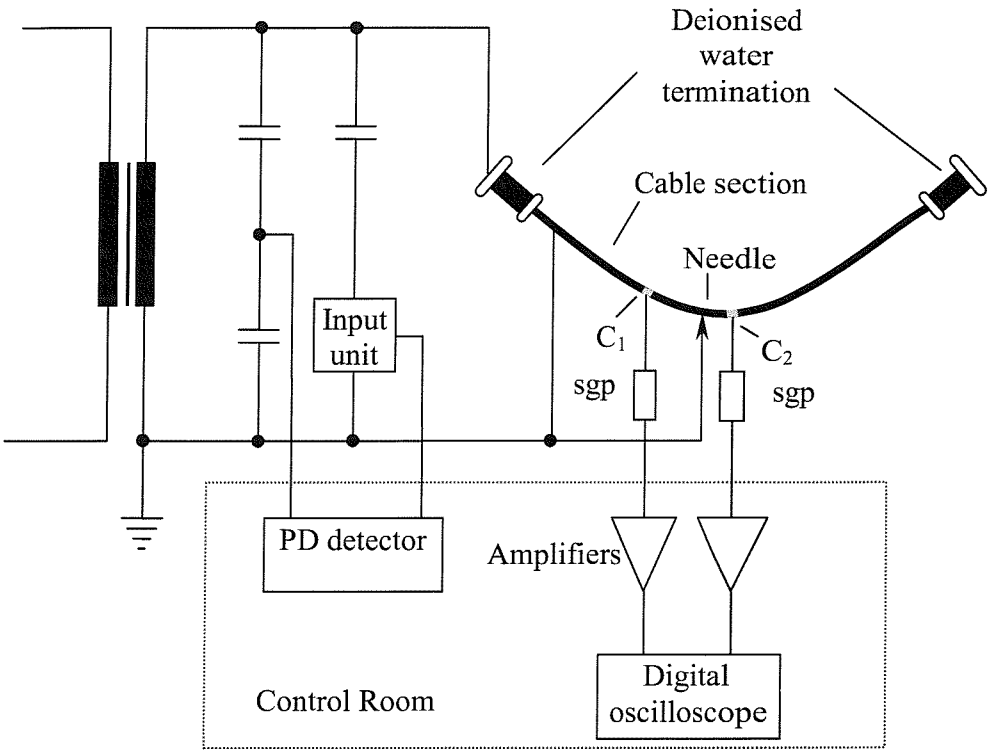

Figure 6.1 Test arrangements for a section of HV cable containing an earthed needle

Experiments revealed that the deionised water terminations significantly attenuate any injected high frequency thus making calibration of the couplers using the terminal injection method impossible and therefore the simulation model has been used to determine an estimate of the calibration coefficient. Two coupler to coupler frequency responses were obtained using Agilent 4395A Network Analyser over the frequency range from 500Hz to 500MHz, one response for the coupler to coupler only and the other one for a circuit that also included the over-voltage protectors and two 22dB broadband amplifiers connected to the output of the coupler as illustrated in Figure 6.2. In real PD tests, the coupler output has to travel a relative long distance before it reaches the control room. To ensure maximum measurement sensitivity signals have to be amplified. In order to protect the measuring instrument from any

damage caused by possible over-voltage from test objects, broadband surge protectors (sgp) are usually employed. To calibrate the output signal from such a measurement circuit, couplers together with surge protectors and amplifiers were taken as a black box system and frequency response measurement of such a system has been undertaken. The corresponding model will also include the surge protector and the amplifier for direct calibration based on the amplified signals. For the FRA measurements an internal bandpass filter of 10Hz bandwidth over the frequency sweep range was adopted and measurements were averaged for 4 sweeps. The results for coupler to coupler only and couplers with measurement circuit as well as halved data are shown in Figure 6.3. The amplified frequency response data are approximately 44dB greater than the coupler-to-coupler only frequency response data over the higher frequency range.

Similar to the procedure for obtaining an approximate model described in previous chapter, the three variables are redefined as follows: ω_P was defined as the high frequency above which the magnitude of the halved amplified coupler-to-coupler frequency response is reasonably constant; ω_Z was defined as the low frequency above which the magnitude of the coupler to coupler frequency response starts to increase; And G was then chosen such that for higher frequencies the magnitude of the approximate model frequency response matches the halved amplified coupler-to-coupler frequency response.

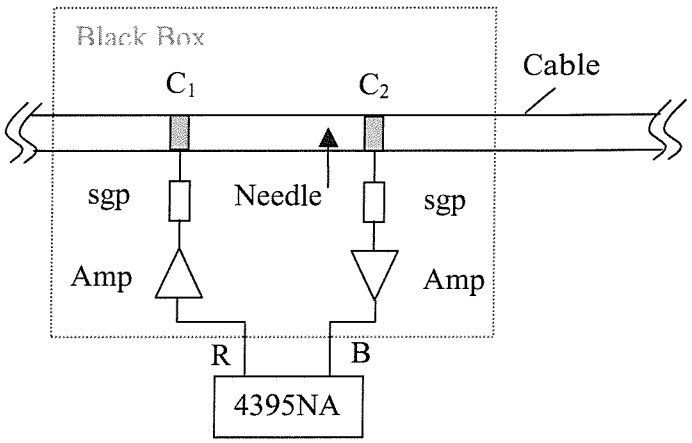

Figure 6.2 Frequency response measurement of two couplers with measurement circuit

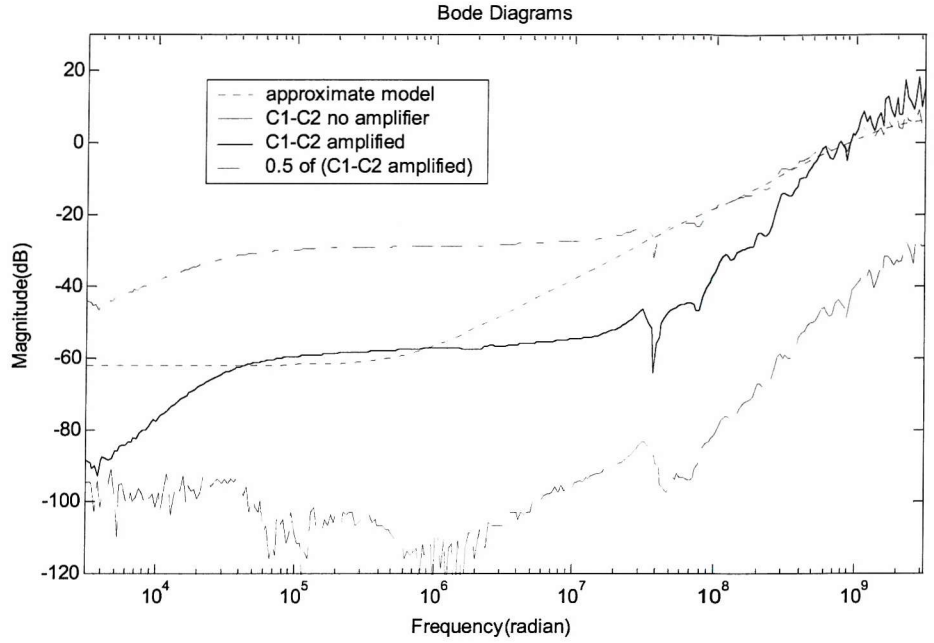

Figure 6.3 Coupler to coupler frequency response measurements and approximate model characteristics

ω_P can be approximately determined as 3×10^8 Hz from the amplified frequency response curve and ω_Z can be roughly determined as 1×10^5 Hz from the coupler-to-coupler frequency response curve (no amplifiers). The low frequency gain G was determined as –62dB through the magnitude matching process for the amplified frequency response data. This gave an approximate model for the terminal to coupler frequency response with amplifier of

$$H_a(\omega) = \frac{7.943\times10^{-4}(1+\frac{j\omega}{2\pi\times10^5})}{(1+\frac{j\omega}{6\pi\times10^8})} \qquad (6.1)$$

And the corresponding Bode plot shown in Figure 6.3 gives good agreement with the halved amplified frequency response curve over the very high frequency range. Similar to the simulation carried out in Chapter 5, the same range of input values from 20pC to 96pC was injected into the simulation model (Equation 6.1) and the outputs were curve fitted to a straight line in order to minimise any error. The relationship between the simulated output peak voltage and the injected charge over the range of the input values is shown in Figure 6.4, which yields a calibration ratio of 0.0364 $pCmV^{-1}$.

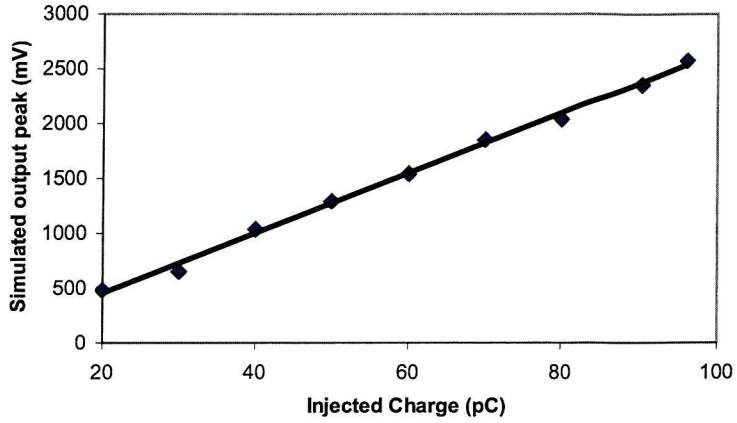

Figure 6.4 Simulated output peak voltage vs. injected charge

Besides the simulated output peak voltage, the simulated output pulse area and RMS value have also been investigated and their relationships to injected charge are illustrated in Figures 6.5 and 6.6 respectively, which yield calibration ratios of 30.675 pC/nsV for output area and 0.233 pC/mV for output RMS values respectively. The linearity of the RMS value versus the injected charge is better than the output area value versus the injected charge. They are both statistical values over the investigated time period of the pulse and are more affected by background noise than the output peak voltage. To calibrate using these values the time duration and the sampling rates of the calibrated pulse have to be the same as the calibrating pulse. Therefore this approach is not very convenient to use in practice.

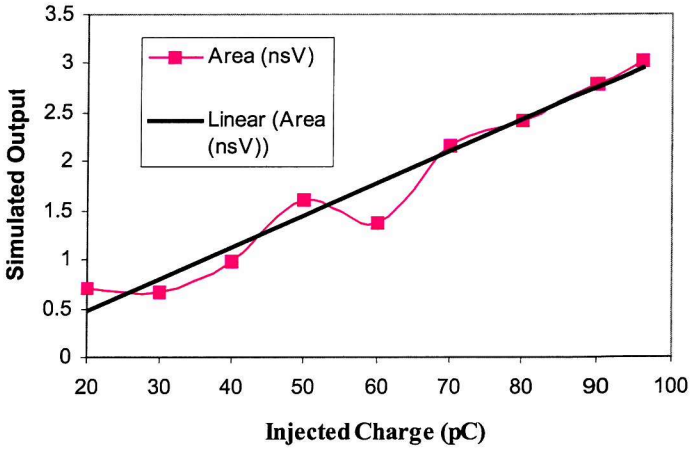

Figure 6.5 Simulated output pulse area vs. injected charge

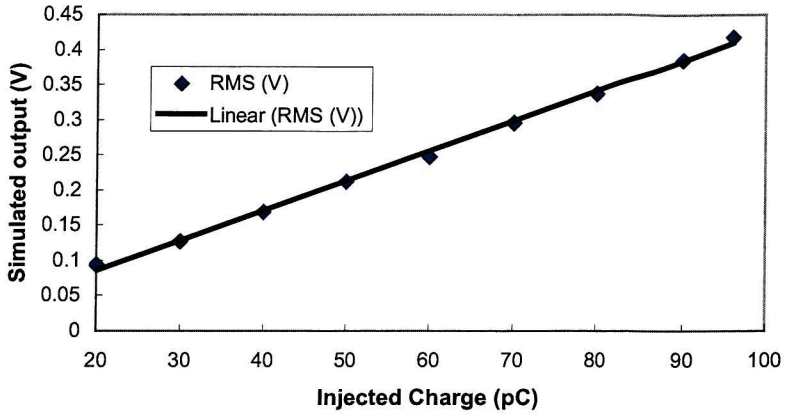

Figure 6.6 Simulated output RMS vs. injected charge

The determination of the three parameters in the first order model is by visual inspection and is dependent on the observer. To further investigate this problem, various values of pole corner frequency ω_P, and zero corner frequency ω_Z have been investigated over possible chosen ranges and the corresponding scalar gain, G, has been adjusted to match the measured frequency response data over the very high frequency range. Figure 6.7 shows the effect on calibration coefficient and the variation of scalar gain when the zero corner frequency is varied from 0.5×10^5 Hz to 5×10^5 Hz and the pole corner frequency is fixed at 3×10^8 Hz. It can be seen that by adjusting the scalar gain from –68dB to –48dB very close calibration coefficients are obtained. Similar to the variation of zero corner frequency, Figure 6.8 shows the effect on calibration coefficient and variation of scalar gain when the pole corner frequency is varied from 2×10^8 Hz to 4×10^8 Hz with a fixed zero corner frequency at 1×10^5 Hz. The scalar gain is varied from –60dB to –63dB and very close calibration coefficients have been achieved. Both Figures show that by adjusting the scalar gain G to match the halved frequency response curve over the high frequency range models produce a similar estimate of calibration ratio for a reasonable range of both pole corner frequency ω_P and zero corner frequency ω_Z. That means that small variations of ω_P and/or ω_Z do not significantly affect the calibration ratio as long as the simulation model matches the measured frequency response data over the high frequency range.

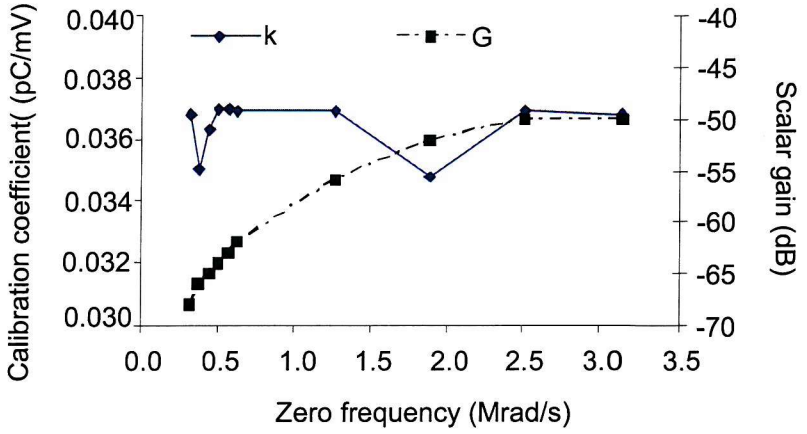

Figure 6.7 Variation in both calibration coefficient and scalar gain for a range of zero corner frequency

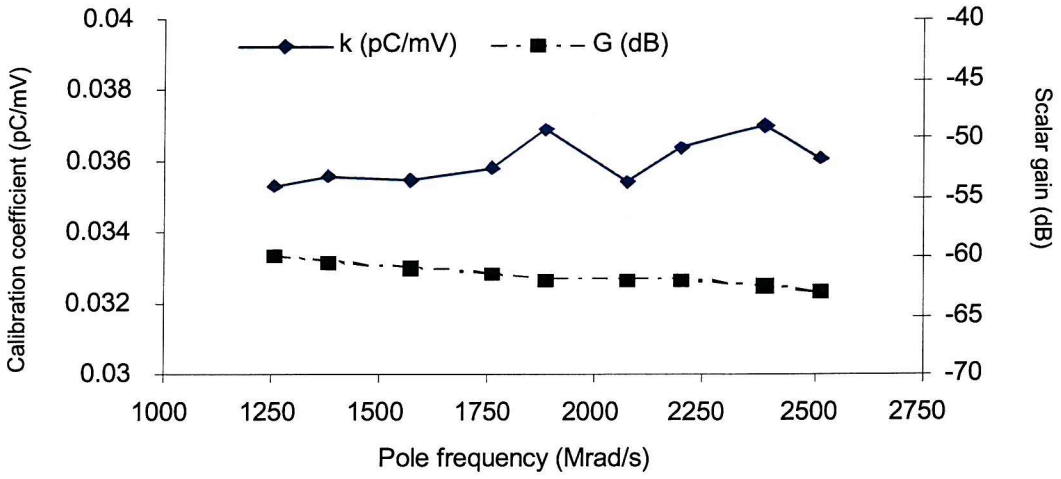

Figure 6.8 Variation in both calibration coefficient and scalar gain for a range of pole corner frequency

6.1.1 Calibration Results

To calibrate the conventional electrical PD detector a low frequency calibration pulse equivalent to 50pC was injected into one of the deionised water terminations. Figure 6.9 shows the calibration pulse captured by Robinson PD Detector giving a calibration ratio of 1/70 pC/mV. AC high voltage was then applied to the cable loop at increasing magnitudes until regular PD activity was observed. The PD inception voltage was 9kV in this case. Figure 6.10 shows two typical PD measurements obtained both from Coupler C_2 and the conventional electrical PD detector

(Robinson) simultaneously at different applied high voltages. A sampling rate of 500M/s was adopted here. The pulse captured by the coupler leads the pulse captured by the conventional PD Detector by about 10μs in this case due to the very different working frequency range and integration process of the conventional PD detector. With reference to Figure 6.9 for an applied voltage of 11.8kV the Robinson Detector gives an apparent PD magnitude of 4.7pC whereas the simulated reduced charge value from the coupler is 3.7pC, increasing the applied voltage to 14kV produces PD apparent charge of 9pC according to conventional detection and a reduced charge of 4.7pC from the coupler measurement.

Figure 6.11 shows the comparison of a PD pulse captured by the two capacitive couplers, a time of flight of approximately 4ns can be observed between the two signals, thus the location of the PD source can be estimated if the propagation velocity of the PD pulse is known and vice versa. The signal attenuation can also be estimated if the differences between the constructions of the couplers are negligible.

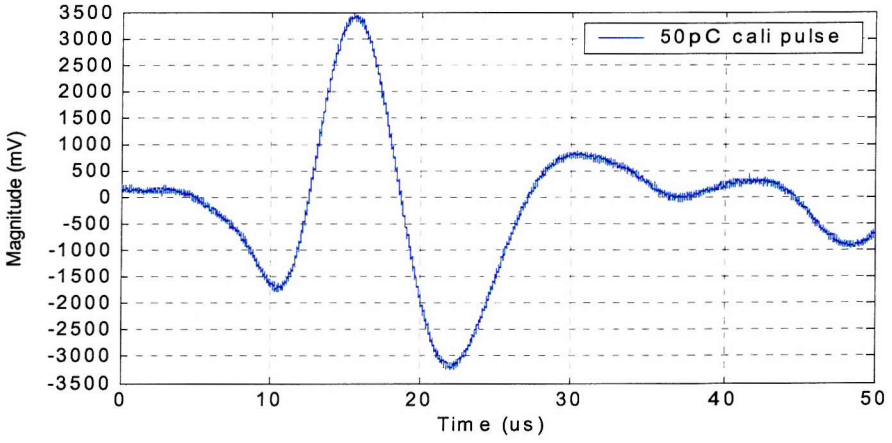

Figure 6.9 50pC calibration pulse captured by PD Detector

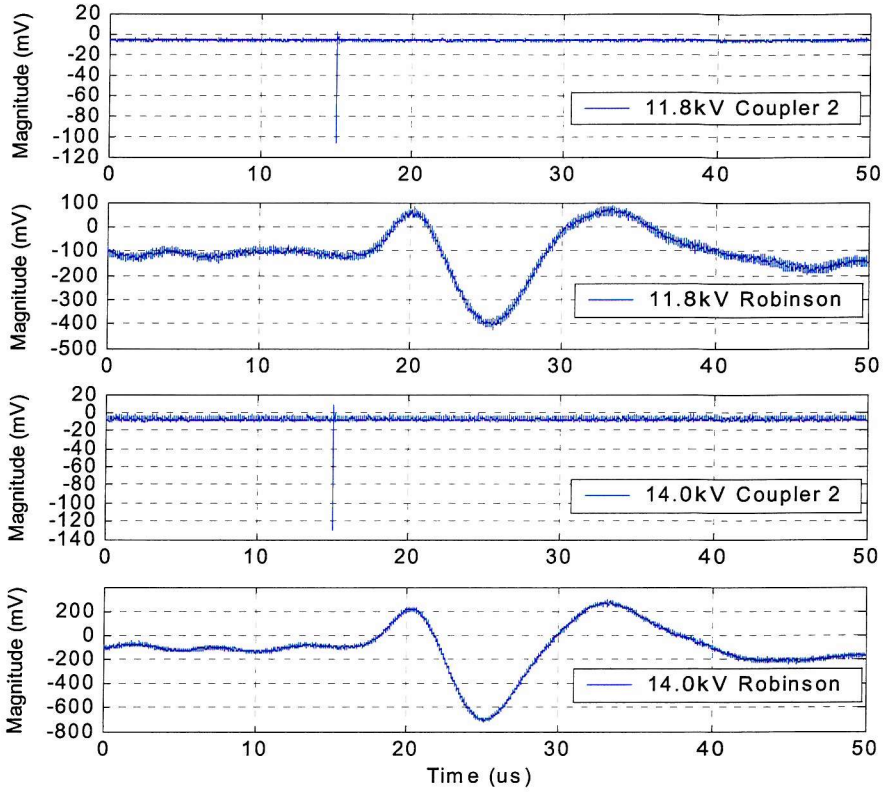

Figure 6.10 PD measurements from Coupler 2 and conventional PD Detector

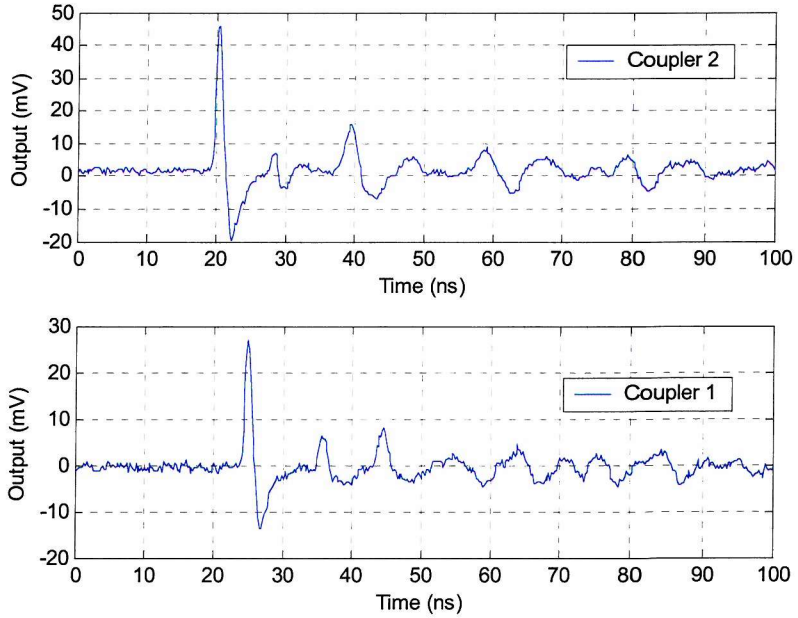

Figure 6.11 Comparison of a PD pulse captured by Coupler 2 and Coupler 1

6.2 132kV loop PD Test

The second experiment was conducted on a 132kV cable joint where a known defect is inside. The test arrangement is illustrated in Figure 6.12, two sections of cross-linked cable are connected with a prefabricated cable joint, and a known defect made of conducting paint is located inside the joint. Two identical couplers with the same dimension as used in the needle loop experiment were installed on each side of the joint in order to measure the frequency response of the coupler to coupler and to detect PD activities inside. The distance between the two couplers is 1 meter and any attenuation within this short distance will not be taken into account when deriving the frequency response based model of a single coupler from FRA measurements between two couplers. The ends of the cable are terminated with oil-filled cable terminations to minimise the reflection from the cable ends.

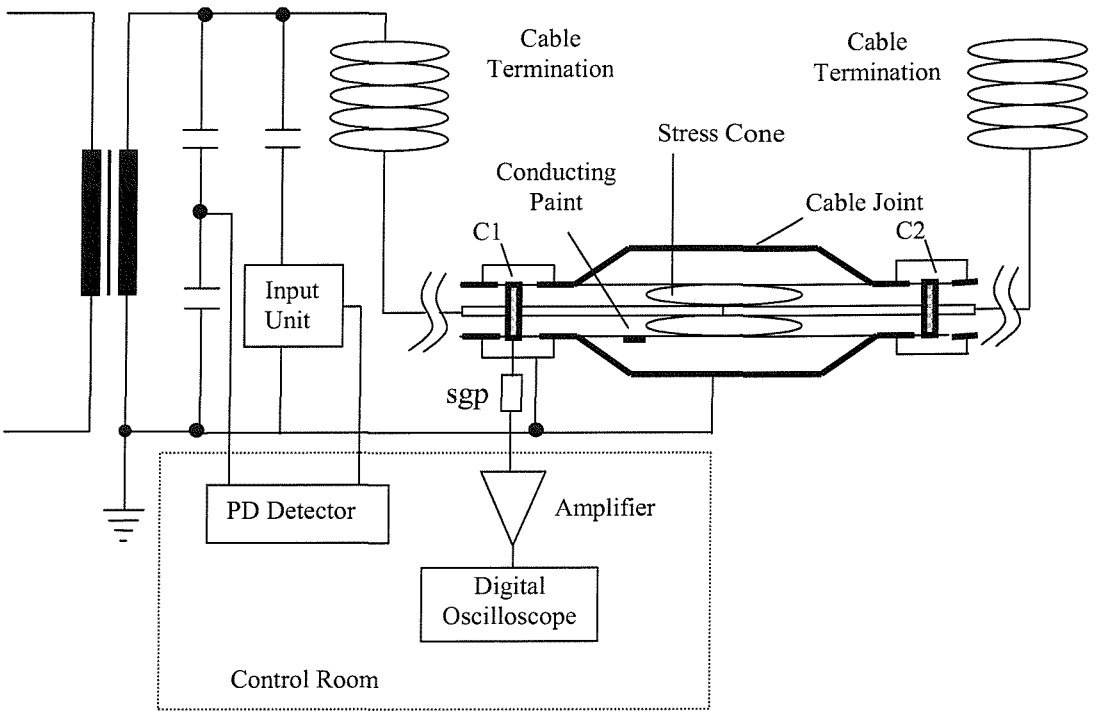

Figure 6.12 Test Arrangement of 132kV cable joint loop

Similar to the first experiment, a conventional PD detection system using a coupling capacitor of 1000pF, input unit of 400-6000pF and Robinson model 5 type 700 PD Detector was also applied in order to measure the apparent charge and provide comparison with the PD levels obtained using the capacitive coupler.

As with the needle loop test section, coupler calibration based on the direct terminal injection method is not available as both terminals are too distant from the coupler (~5 meters) and the injection pulse would suffer unacceptable signal distortion and attenuation due to the structure of the termination. Therefore calibration based on the approximate model from FRA measurements has been used. Once again as the output signal passes through the surge protector and amplifier before being measured using a digital oscilloscope, frequency response measurements for coupler to coupler only and coupler-to-coupler with amplifiers and surge protectors included have been undertaken (Figure 6.2) using the Agilent 4395A Network Analyser. The obtained results for both frequency response tests as well as the halved value of coupler-to-coupler frequency response data with amplifiers are shown in Figure 6.13. As with the previous frequency response measurements, the internal bandpass filter of 10Hz bandwidth was set and the measured results were averaged for 4 sweeps. A zero corner frequency of 0.6×10^5 Hz and a pole corner frequency of 0.9×10^8 Hz were determined from the measured frequency response curves and the matching low frequency gain was determined as -60dB. Applying the same approach as previously discussed, an approximate model was obtained as

$$H_a(\omega)=\frac{0.001\times\left(1+\frac{j\omega}{2\pi\times0.6\times10^5}\right)}{\left(1+\frac{j\omega}{2\pi\times0.9\times10^8}\right)} \qquad (6.2)$$

And its corresponding Bode plot is shown in Figure 6.13. Based on this model the relationship between the injected charge and simulated output peak voltage over a range of simulated injection charge from 20pC to 96pC has been obtained as shown in Figure 6.14 and gives a calibration ratio of 0.034pC/mV.

The measured coupler-to-coupler frequency response is more oscillatory over the high frequency range than that obtained from the needle test section as can be seen from Figure 6.13. This is probably due to the influence of the structure of the cable joint and its material characteristics over the high frequency range. For simplicity it is still modelled as a first order system without oscillation. But errors resulting from this approximation will be bigger than those for the previous model. Over the higher frequency range the frequency response data for two couplers with amplifiers is about 44dB greater than the frequency response data for two couplers only. Over the

lower frequency range the measured frequency response data for two couplers with amplifiers is contaminated by noise due to the higher noise levels of the network analyser.

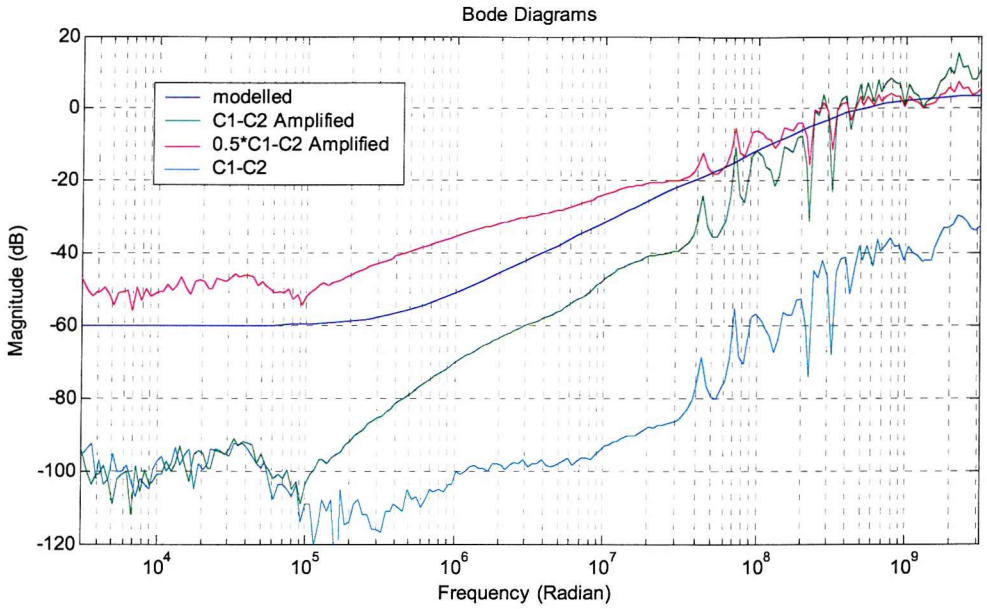

Figure 6.13 Coupler to coupler frequency response measurements and approximate model characteristics

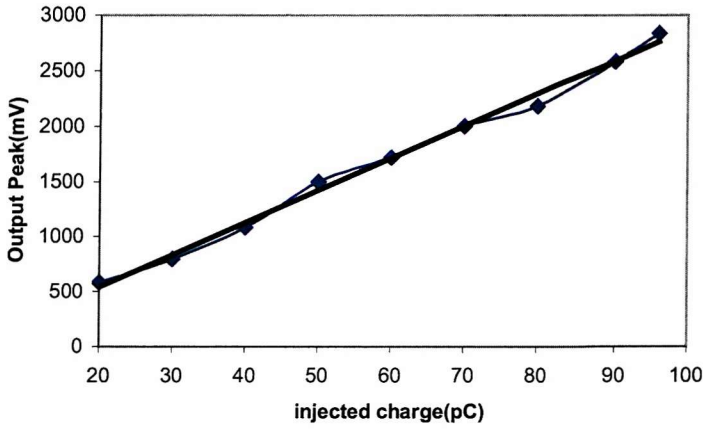

Figure 6.14 Simulated output vs. injected charge

6.2.1 Calibration Result

The conventional PD detection system was first calibrated with a 50pC pulse before high voltage was applied. The calibration pulse captured by the PD Detector is shown in Figure 6.15. Then AC high voltage was applied at an increasing magnitude until regular PD activity was observed. Figure 6.16 shows the comparison of the

same PD pulse detected by the capacitive coupler and Robinson PD Detector respectively when the applied high voltage was 32kV. The output signals from both sensors were captured using a fast digital oscilloscope with a sample rate of 1G/s. From the PD detector apparent charge of 35pC has been obtained, while from the capacitive coupler reduced charge of 16pC has been obtained according to the calibration ratio obtained using the simulation result.

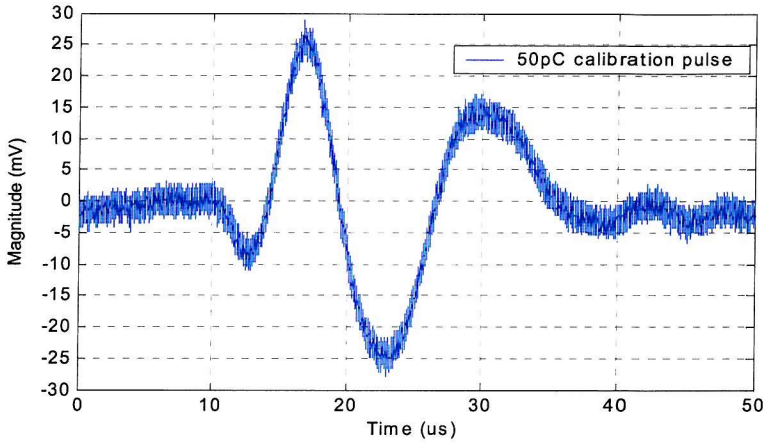

Figure 6.15 50pC calibration pulse for Robinson PD Detector

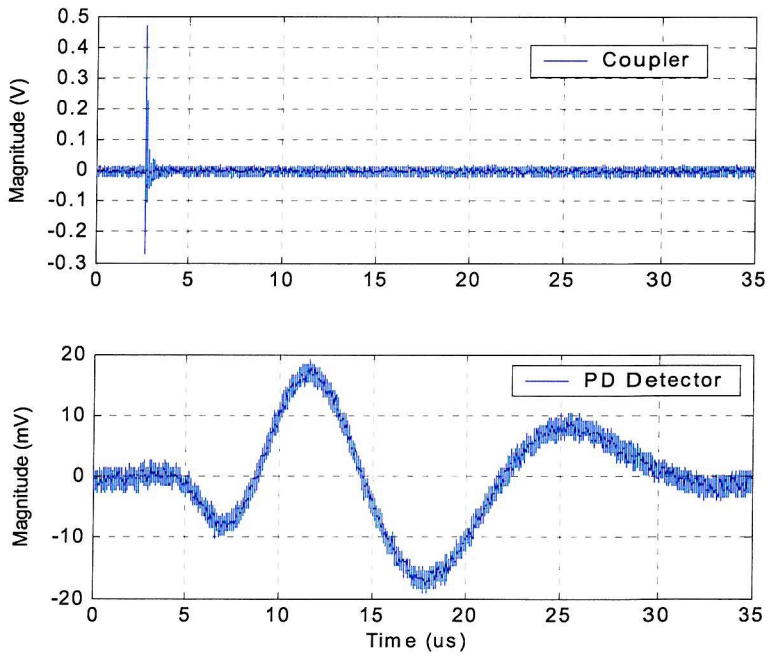

Figure 6.16 Coupler output vs. conventional PD detector output under HV of 32kV

6.3 Discussion

For the experiments carried out for both test sections, the calibration ratio determined from the estimated model yields charge values for coupler signals that are lower than the conventional apparent charge measured using a Robinson PD detector. Other researchers have carried out similar research work for comparison of PD quantity apparent charge with respect to the PD probe measurement and similar results have been obtained [151]. Differences are due to the fundamental different coupling mechanisms between the two detection systems as well as their distinct working frequency ranges. For narrow-band conventional PD coupling, PD signals are detected with a bandwidth of 100kHz or less and the PD detector acts as a low pass filter or integrator [152]. While for VHF capacitive couplers, PD pulses are directly coupled to the coupler with a bandwidth range from a few MHz to a few hundreds MHz as can be seen from frequency response measurements. So the minimum detectable input frequency of the capacitive coupler is relatively high. The measuring error due to this is only negligible for very fast pulses. Differences between apparent charge and reduced charge could also result from ignoring any signal attenuation from the PD source to the point of measurement and the modelling process ignores high frequency resonances could also introduce errors. However for online measurement, the simulation method provides a reasonable estimate of the reduced charge and a comparison of the corresponding apparent charge. For most on-line condition monitoring applications the measured PD activity trend over a long time interval is considered to be more important than absolute charge values at a single moment [28].

6.4 Summary

To further investigate the calibration method based on using a simulation model derived from frequency response analysis, real PD tests on two different cable test sections have been undertaken. On both test sections terminals are not available, therefore frequency response measurements from one coupler to another coupler have been undertaken. An approximate transfer function determined from frequency response measurements of coupler-to-coupler and corresponding measuring circuits provides an estimate of the calibration ratio for the coupler installed on specific sections of a cable/joint. The resulting PD magnitudes are less than those obtained

using conventional electrical PD detection in both cases. The difference is due to the different coupling modes and working frequency ranges between the two measurement systems. However these values reflect the reduced charge measured by VHF capacitive couplers.

Chapter 7

Extraction of PD Signals from Noise data by Wavelet Analysis for Online PD detection

One of the main challenges associated with online PD measurements is coping with background noise and interference. It is important for accurate online PD measurements as they are usually carried out onsite where no specific de-noising measures are taken. Offline PD measurements usually take place in well-controlled laboratories or factories where no external interference is present. With the advancement of several non-conventional detection techniques such as capacitive couplers and inductive couplers the application of online PD measurements became popular and dealing with background noise has become a necessary aspect for long-term service condition monitoring of HV cables.

A wide range of noise and interference can be encountered during onsite PD tests, according to their characteristics it can be classified as either [1, 99] Discrete Spectral Interference (DSI) from radio transmissions and power line carrier communication systems or periodic pulse shaped interference from power electronics or other periodic switching or stochastic pulse shaped interference from power system PD, corona and surface discharges or random noise similar to white noise from amplifiers.

The existence of the noise and interference corrupts the PD signals and may result in false indication. In the extreme case, this can make PD tests impossible. Therefore the reduction of noise and recovery of PD signals from noisy data is very important.

This chapter presents issues relating to the signal and noise characteristics associated with capacitive coupler measurements. Based on the different characteristics of the signal and interference, wavelet analysis has been found to be very efficient in discriminating internal PD activities from external pulse-shaped narrow-band interference and corona discharge as well as random noise. Furthermore, de-noising can be realized with a minimum loss of pulse amplitude or distortion of pulse shape.

7.1 Wavelet Analysis Basics and De-noising

To use wavelet analysis it is necessary to look into the basic theory of wavelet analysis and the de-noising principles first. The mathematical theory behind wavelet transforms can be found in [153-159], therefore only a brief introduction will be given here.

7.1.1 Wavelet Basics

Wavelets are relatively recent development in applied mathematics. Their name itself was coined in the 1980s [153]. Since then the interest in wavelets has grown. The concept of wavelets has been seen to be applicable to many areas of science and engineering and applications include signal processing (sound and image) and numerical analysis [154, 155]. Recently, wavelet based approaches have extended to HV engineering [160-164], and PD signal discrimination [99, 111-115].

A wavelet is a small waveform with limited duration and a zero mean value. Similar to the Fourier Transform, which breaks up a signal into sine waves of various frequencies, the wavelet transform breaks up a signal into shifted and scaled versions of the original (or mother) wavelet. A continuous wavelet transform is defined as the sum over all time of the signal s(t) multiplied by scaled and shifted version of wavelet function ψ.

$$C(a, b) = |a|^{-1/2} \int s(t)\, \psi\left(\frac{t-b}{a}\right) dt \qquad (7.1)$$

Where, ψ is the mother wavelet, b is the shift operator and a is the scaling function. The result is a two-dimensional coefficient array of scale a (related to frequency) and position b (related to time) of the time domain signal s(t). A continuous wavelet

transform is computationally intensive and generates a lot of redundant data. Therefore the discrete wavelet transform (DWT) is usually employed at $a = 2^j$ and $b = k2^j$ (j, k are positive integers) for speed and convenience. Furthermore, Multi-resolution Signal Decomposition (MSD) which breaks up a signals into several sub-bands of non-overlapping frequencies can be implemented based on the DWT, which made the wavelet transform practical and popular.

Single level signal discrete wavelet decomposition produces a series of approximation coefficients (cA) and detail coefficients (cD) through a low-pass filter (low-D) and a high-pass (High-D) filter respectively as illustrated in Figure 7.1. The approximation (A) and detail (D) of a signal can be reconstructed using reconstruction filters (High-R, Low-R) based on these coefficients, which correspond to the low frequency and high frequency components of the signal(s). MSD up to level j produces series of approximation and detail coefficients through a multi-level digital filtering technique, which corresponds to the multi frequency sub-bands of the signal. Figure 7.2 shows a 3-level decomposition and reconstruction procedure of a signal. The exact reconstruction of the original signal can be obtained through the reversed procedure - inverse wavelet transform [159].

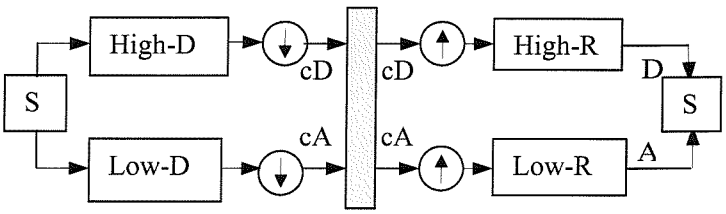

Figure 7.1 One stage decomposition and reconstruction

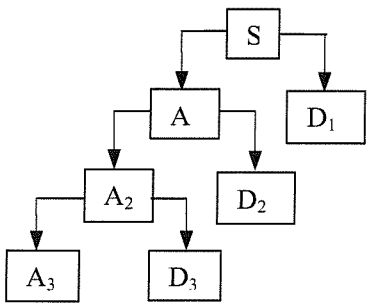

$S = A1 + D1$

$= A_2 + D_2 + D_1$

$= A_3 + D_3 + D_2 + D_1$

Figure 7.2 A 3-level signal decomposition and reconstruction

7.1.2 De-noising procedures

The principle of de-noising based on MSD wavelet analysis is simple; first the original signal is decomposed into approximation and detail components up to a desired number of levels. This is done by first choosing a suitable mother wavelet according to the signal and noise characteristics. The next phase is to identify those components corresponding to the PD signal, interference or random noise at each level by visual inspection and knowledge of the frequency characteristics of each signal type. Finally those coefficients corresponding to the interference and random noise are discarded while the coefficients corresponding to the PD signal are retained by setting threshold values accordingly, allowing reconstruction of the signal based on the modified coefficients to produce an interference-free signal.

The selection of mother wavelets, number of decomposition levels and determination of threshold values and methods (hard or soft threshold) are application dependent. The next section considers these issues regarding signals obtained using capacitive couplers.

7.2 Characteristics of the signal detected by capacitive couplers and issues in application of wavelet method

7.2.1 Signal Characteristics Compared to Conventional PD Detectors

The capacitive coupler is one of the most popular non-conventional PD coupling techniques. Compared to conventional narrow-band PD detection method, capacitive couplers are very sensitive and broadband. Figure 7.3 shows the comparison of the same PD pulse detected by a capacitive coupler and a conventional PD detector (Robinson 700) respectively (sampling rate, 1G/s). The zoomed PD pulse (500ns) and its frequency spectrum are given in Figure 7.4.

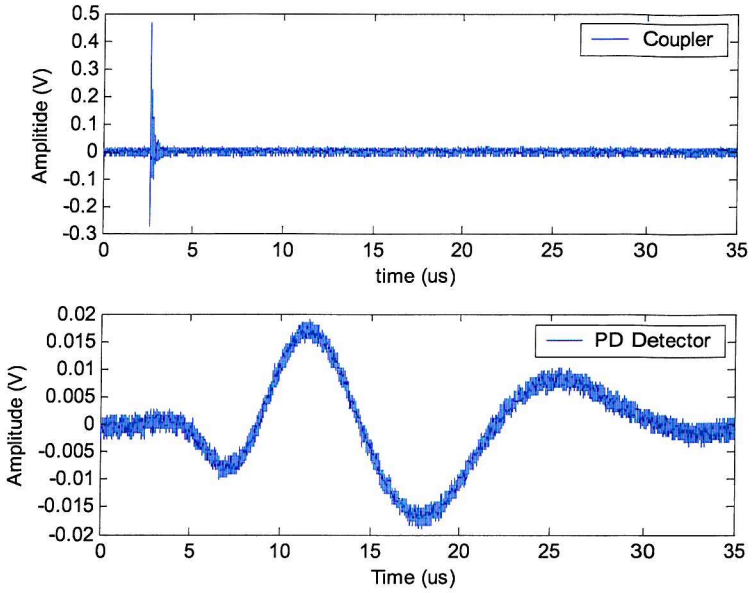

Figure 7.3 Same PD pulse captured by coupler and PD detector

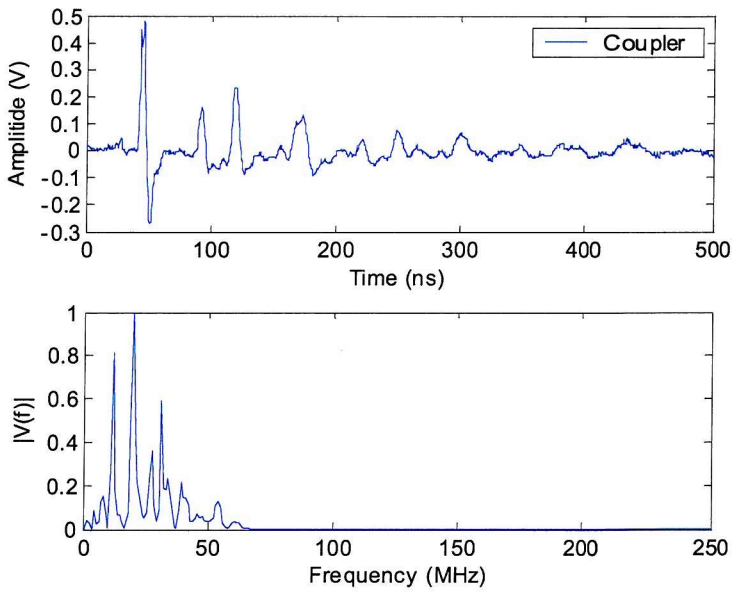

Figure 7.4 Typical coupler PD pulse and its power spectrum

PD activity inside a void is a very fast event and usually lasts for only a few nanoseconds or less. The detected PD magnitude and pulse shape depend on the coupling and measurement system. As can be seen from the time domain the PD pulse captured by a capacitive coupler lasts for less than 100ns (depending on the size and shape of the defects and distance between the PD source and the coupler), while the same activity captured by the conventional PD detector lasts for much

longer (30 microseconds). The pulse detected by the capacitive coupler also leads the pulse detected by conventional PD detector by a certain amount of time due to the quasi-integral procedure of the conventional PD measurement and different working frequency range between the two coupling modes. In the frequency domain a conventional PD detector usually works below 1MHz, while the frequency band of the capacitive coupler is very wide up to several hundreds of MHz (about 70MHz in this particular case). In general, the signals detected by capacitive couplers are quite different in both the time domain and frequency domain compared with that of conventional PD detectors, therefore special consideration should be given during the post-processing of these signals if using wavelet analysis.

7.2.2 Selection of mother wavelet

The selection of the suitable mother wavelet function is essential in using wavelet analysis. Best wavelets are those that can represent the signal of interest as effectively as possible. This is not an easy decision to make in practice. In most cases, a trial and error method is used. Ma et al [111, 112] have discussed the optimal wavelet selection based on the calculation of the cross-correlation coefficients between PD pulses and wavelet shapes for signals obtained using conventional PD detectors. They found that db2 and db8 are the best wavelets for analysing exponential PD pulses and damped resonant PD pulses respectively. From a frequency point of view, consideration in choosing the wavelet is based on the central frequency of the wavelet compared to that of the signal of interest. In this application, db1 has been chosen as it has the highest central frequency of the Daubechies family. Some other wavelets with sharp waveforms such as lower order biorthogonal wavelets bior1.1 and reverse biorthogonal wavelets rbio1.1 and rbio1.3 also give good results.

7.2.3 Number of decomposition levels

The number of decomposition levels depends on the lowest interference frequency bands that need to be eliminated from the signal. The goal is to have sufficient resolution in the low frequency range in order to suppress interference completely. Initially a trial and error method has to be used. 10 levels were chosen and found to be sufficient for this application.

7.2.4 Thresholds

The de-noising procedure involves thresholding of those coefficients corresponding to the signal and interference as mentioned above. The determination of threshold values is based on the identification and evaluation of these coefficients corresponding to the signal and interference. Some automatic threshold rules such as Stein's unbiased risk estimate (SURE) and fixed threshold are well suited for white noise. However for suppressing the pulse-shaped interference, no automatic rules are available as it is difficult to estimate the magnitude of the interference in an unknown environment, where the magnitude of interference could be larger than that of the signal. In this application threshold values have been manually determined. The hard threshold method was adopted as it can maintain the PD pulse magnitude better than the soft threshold method. This is significant for further quantification of the processed signals.

7.3 Test Arrangement

HV tests were carried out on the 132kV cable loop system as illustrated in Figure 7.5. Two sections of cable are connected through a prefabricated cable joint with a known defect (conducting paint). The main insulation material of the joint is ethylene propylene rubber (EPR), while the cable insulation is cross-linked polyethylene (XLPE). Both ends of the cable are terminated with oil-filled cable terminations. A capacitive coupler (C) was installed near the defect side of the cable in order to detect the internal PD activities caused by the conducting paint inside the cable joint. A surge protector (sgp) with maximum operating frequency up to 1GHz and response time of less then 10ns was connected to the output of the coupler to protect the measuring system from possible over-voltage. The measuring system consists of a digital oscilloscope and a personal computer. A 20dB broadband (up to 1GHz) amplifier was used to amplify the signal before it was fed to the digital oscilloscope (LeCroy LC684DXL). The personal computer is connected to the oscilloscope via a GPIB board to collect the data for further processing.

Based on the frequency spectra shown in Figure 7.4, in which a sampling rate of 1GHz was used to comply with Shannon's sampling theorem. It can be seen that the power spectrum of the PD pulse detected by the capacitive coupler has a bandwidth of less than 100MHz. So a lower sampling rate of 250MHz was used to ensure manageable amounts of data were collected over one power cycle.

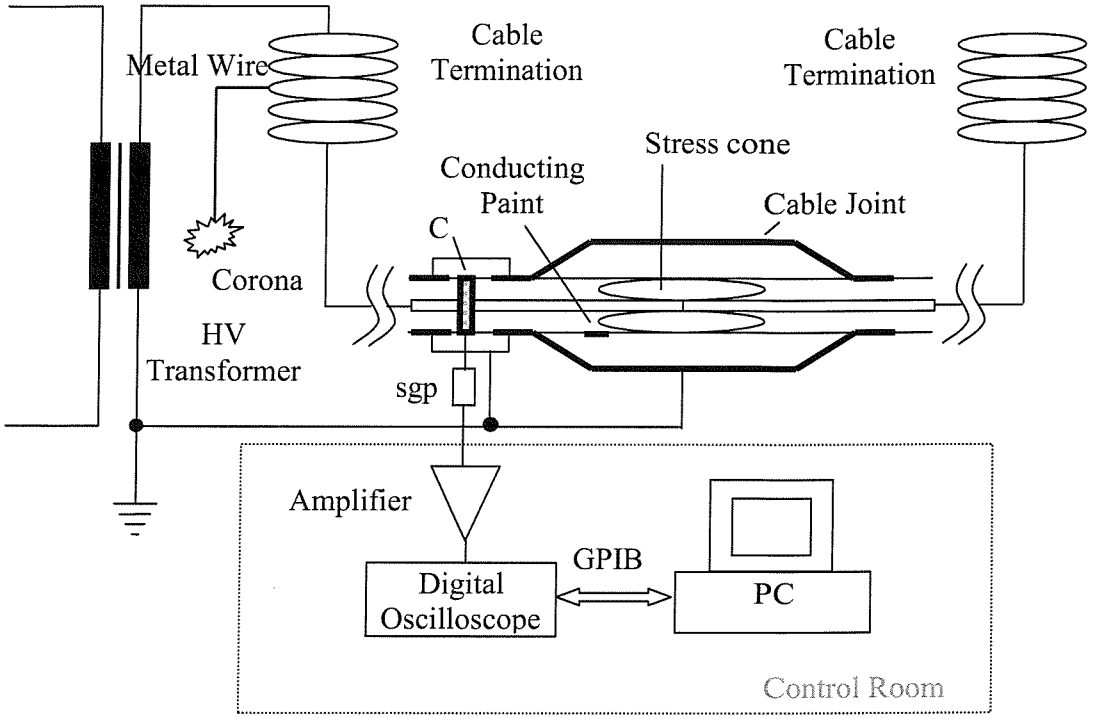

Figure 7.5 HV Test arrangement

Corona discharges are the most common source of interference during online PD measurements. In this experiment external corona discharge pulses were produced using a length of metal wire connected to the system HV end as shown in Figure 7.5.

7.4 Results

7.4.1 PD activities without corona interference

The test was first carried out without corona interference present. Figure 7.6 shows the PD activities over one power cycle (20ms) and its persistence plot under an applied high voltage of 35kV. Two fixed phase interference pulses located approximately at 10ms and 20ms have been detected as can be seen from the

persistence plot. The pulses located in first and third quadrants are internal PD pulses.

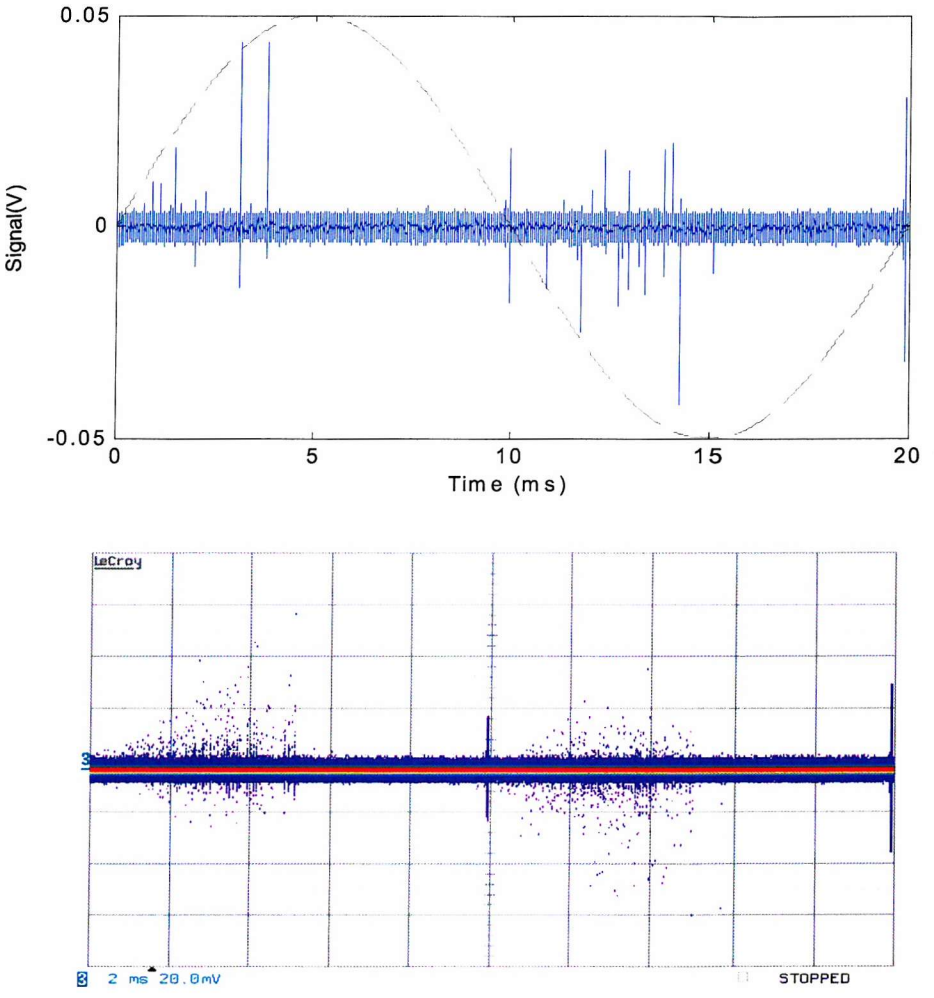

Figure 7.6 PD activities without corona interference and the persistence plot at 35kV

7.4.2 Wavelet de-noising of PD with corona interference

Corona discharge interference was introduced into the system by increasing the applied high voltage until regular PD activities and corona discharges were observed. The corona discharges can be judged from the persistence plot of the one power cycle signal. Figure 7.7(a) and (b) show the original signal and its persistence plot over one power cycle when applied the high voltage was 30kV. The persistence plot in Figure 7.7(b) clearly shows the corona discharge pulses around the negative half peak as well as the two other pulse-shaped interference pulses at 10ms and 20ms. However from the original signal shown in Figure 7.7(a), internal PD pulses and

external corona discharge pulses are mixed together and it is difficult to discriminate between them just by visual inspection.

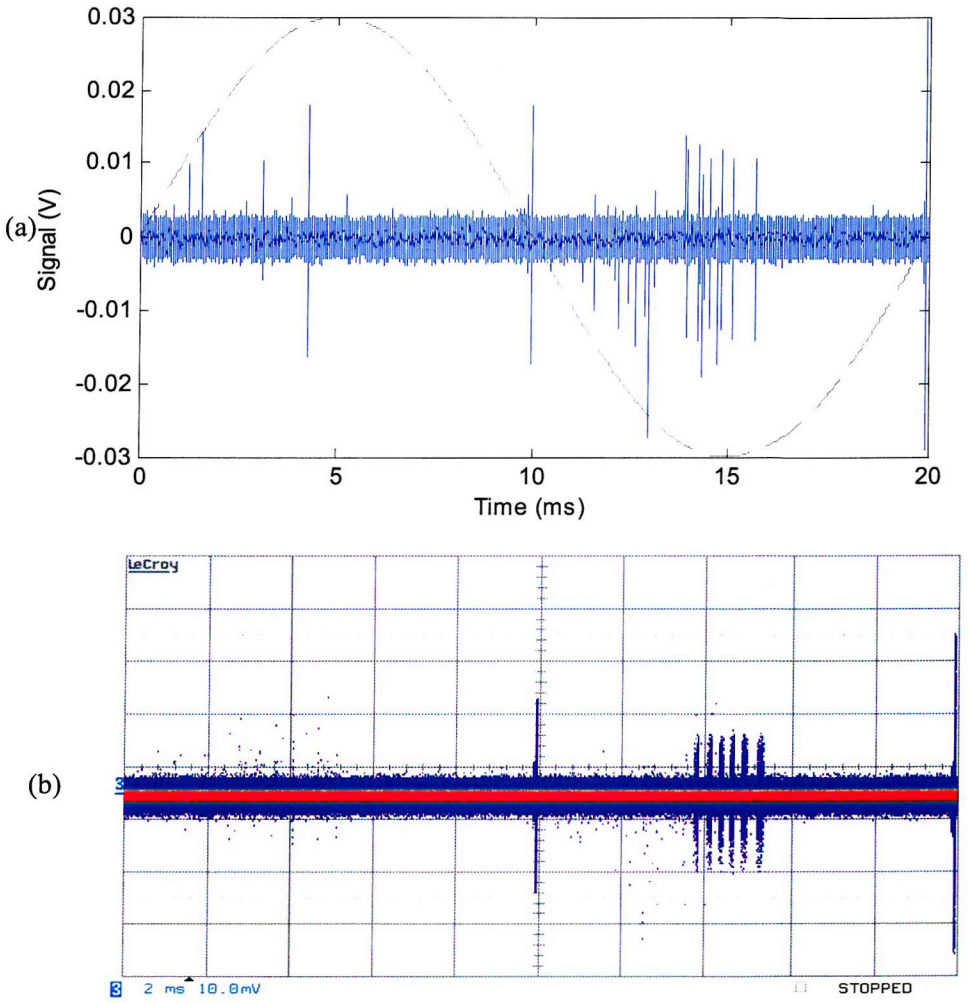

Figure 7.7 PD activities with corona interference and the persistence plot at 30kV

The signal shown in Figure 7.7(a) has been decomposed into details and approximations up to 10 levels using db1 wavelet as shown in Figure 7.8 and 7.9. The detail level D1 clearly shows all of the internal PD pulses, while the corona pulses are mostly concentrated in detail level D3 and extend to detail level D6. This indicates that corona discharge pulses have lower frequency components compared to internal PD pulses. The two pulse-shaped interference pulses located at 10ms and 20ms cannot be seen in D1 and D2 at all. They are distributed among several levels from D3 to D9; this indicates their frequency components are even lower than that of corona pulses and internal PD pulses. This kind of pulse interference is very common

in PD measurements. Köpf et al. [165] reported similar kind of pulse-shaped interference called synchronous pulses during onsite PD tests. Similar interference called periodic pulse-shaped interference has also been reported [166]. The prominent character of this kind of interference is that it always occurs at specific phase angles. They are caused by facilities that are operating synchronously with the mains such as rotating machines with communtators, rectifiers as well as other power electronic devices. Random noise similar to white noise can be seen in each decomposition level but it is not the main source of noise in this case as the magnitude of the pulse-shaped interference is much higher than that of random noise.

The wavelet decomposition of Figure 7.8 and 7.9 has effectively discriminated internal PD pulses among the external corona discharge interference and two synchronous pulses. The final procedure is de-noising by setting threshold values at each level. This has been done manually in this case and the following threshold values have been used from level 1 to level 10: [0.006, 0.01, 0.017,0.038, 0.088, 0.166, 0.063, 0.026, 0.018, 0.019]. The comparison of original signal and de-noised signal is shown in Figure 7.10. All pulse-shaped interference and random noise have been effectively suppressed and only internal PD pulses are left.

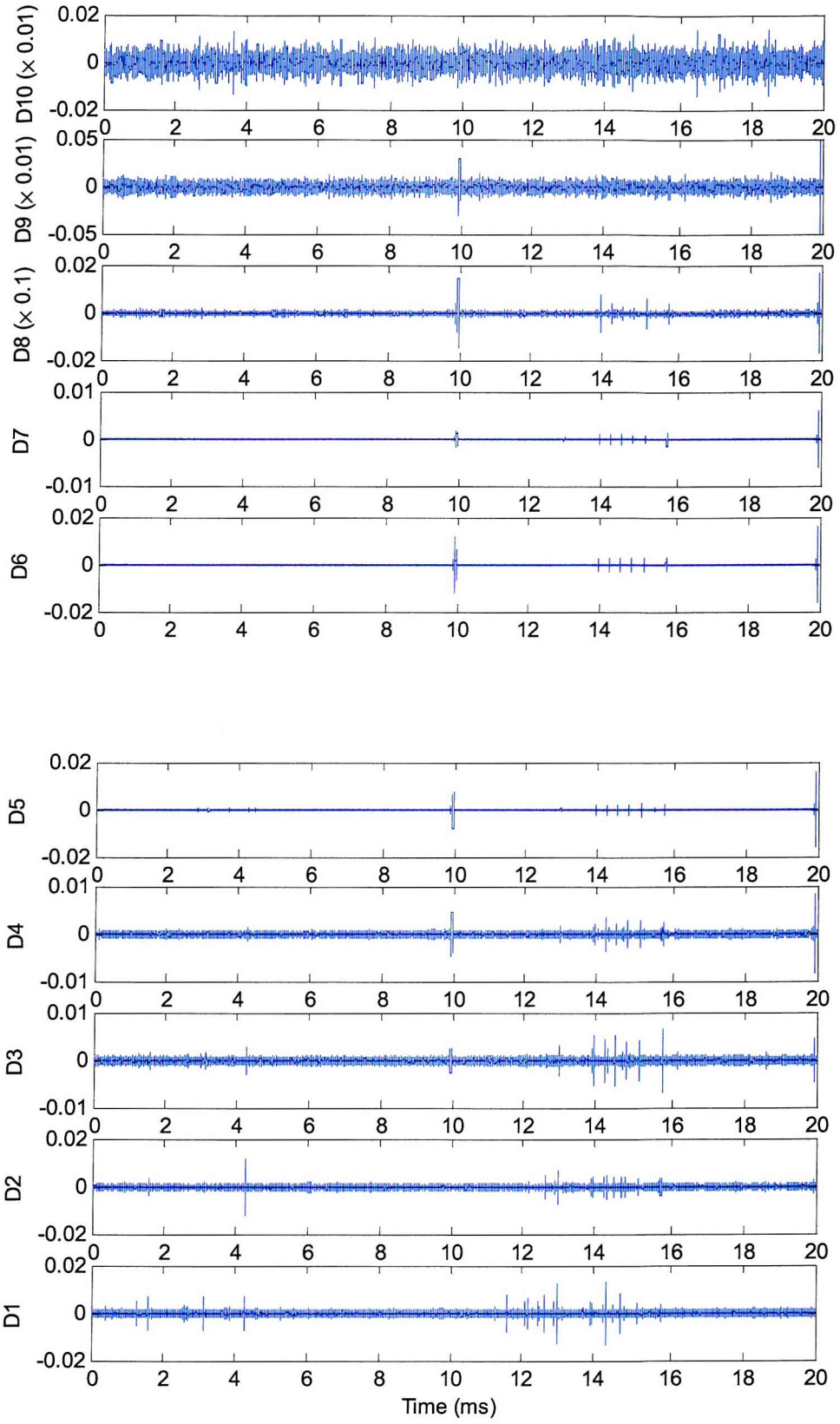

Figure 7.8 Details level 1-10

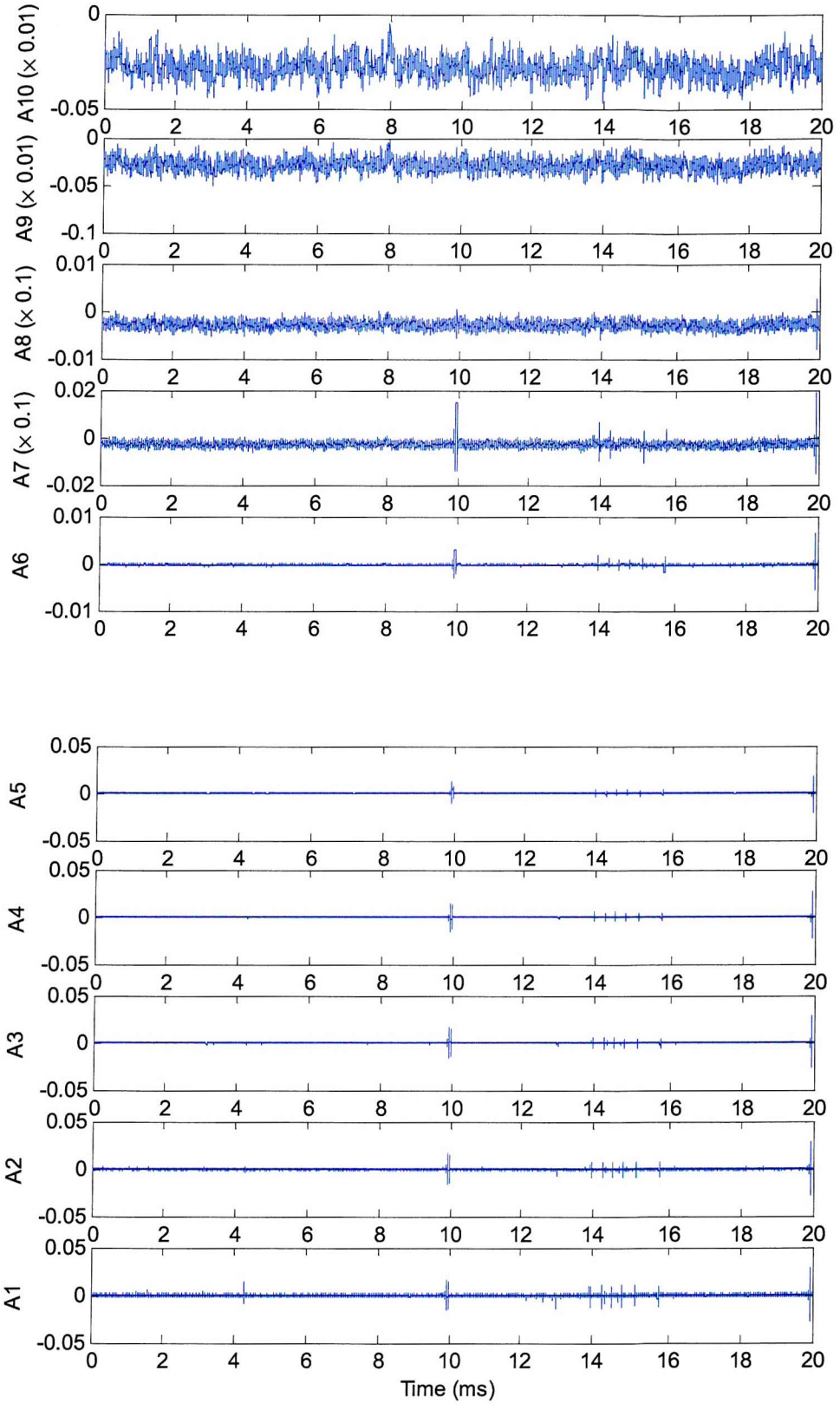

Figure 7.9 Approximation level 1-10

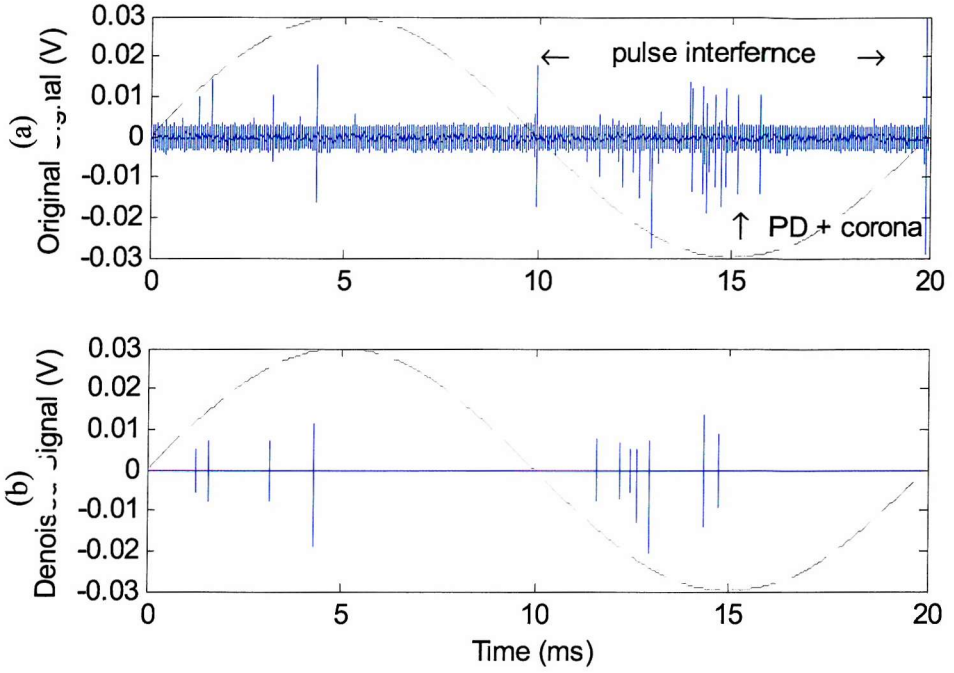

Figure 7.10 Original (a) vs. de-noised (b) signal for 1 power cycle at 30kV

7.4.3 Frequency components of PD, corona and synchronous interference

To further verify the effectiveness of the de-noising procedure, Fast Fourier Transforms (FFT) have been applied to the PD waveforms before and after de-noising. An original PD pulse in Figure 7.6 and a de-noised PD pulse in Figure 7.10(b) show similar power frequency distributions except at the lower frequency range around 25MHz as shown in Figure 7.11(a) and (d). The loss of the frequency peak in the de-noised pulse is due to the high threshold values selected for lower frequency bands (higher levels) in order to suppress the corona pulse interference. A corona pulse presented in Figure 7.11(b) shows lower frequency peaks than the internal PD pulse and the synchronous pulse (Figure 7.11(c)) shows even lower frequency components. This is in agreement with the wavelet decomposition results. So it can be safely concluded that the wavelet de-noising procedure is effective in discriminating between internal PD pulses among corona discharge and synchronous interference pulses.

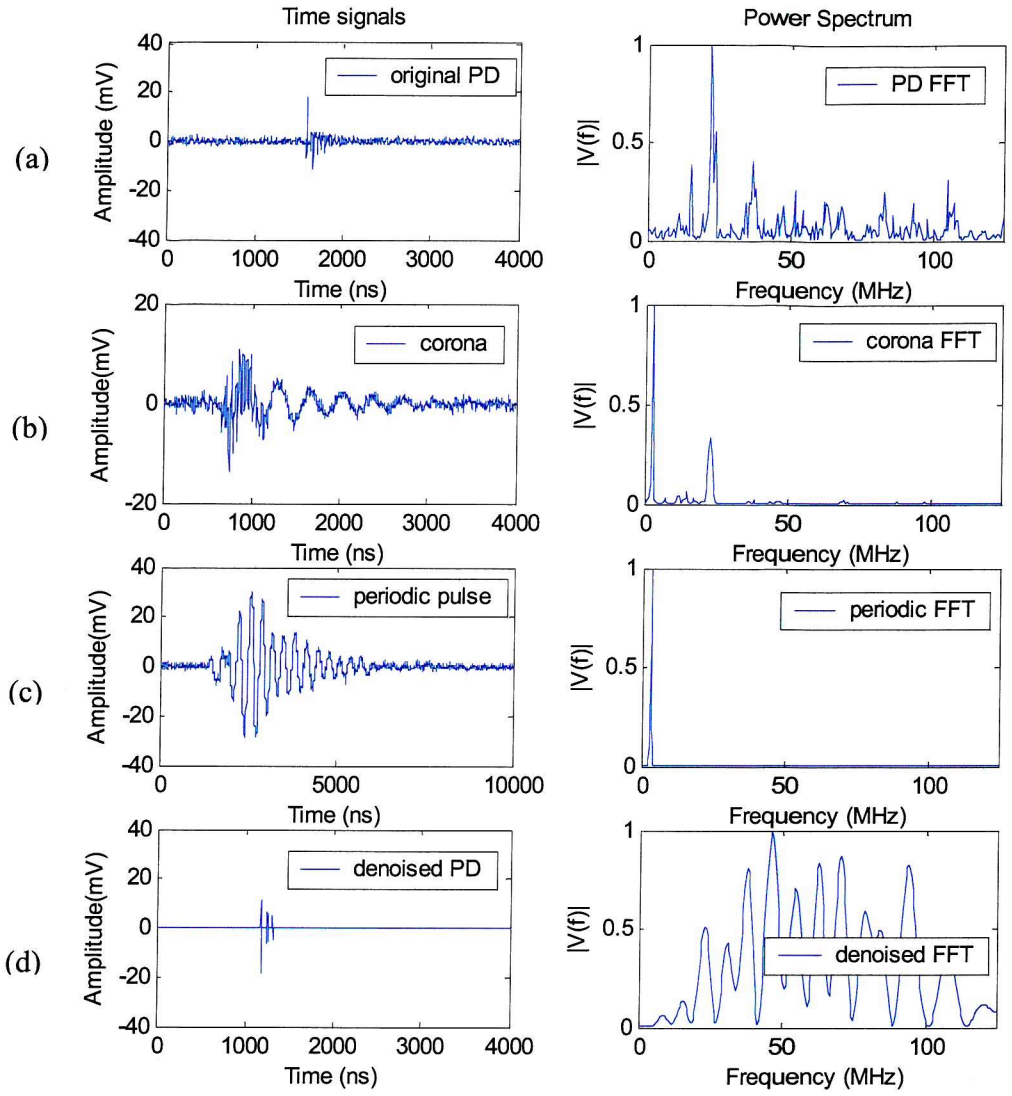

Figure 7.11 Frequency components of the PD signals, corona and synchronous interference pulse (Sampling rate: 250MHz)

7.4.4 Hard Threshold and Soft Threshold

Hard thresholding is the process of setting to zero the coefficients whose absolute values are lower than a threshold and keeping the coefficients whose absolute values are greater than the threshold value. Soft thresholding is an extension of hard thresholding, first setting to zero the coefficients whose absolute values are lower than the threshold, and then shrinking the nonzero coefficients towards zero. The hard threshold is defined as:

$$\delta_{\lambda}^{H}(t) = x(t), \ |x(t)| > \lambda$$

$$\delta_{\lambda}^{H}(t) = 0, \ |x(t)| \leq \lambda \quad (7.1)$$

Where λ is the threshold value, x(t) the coefficient before thresholding and δ is the coefficient after thresholding. The soft threshold is defined as:

$$\delta_{\lambda}^{S}(t) = \mathrm{sgn}(x(t))(|x(t)| - \lambda), \ |x(t)| > \lambda$$

$$\delta_{\lambda}^{S}(t) = 0, \ |x(t)| < \lambda \quad (7.2)$$

Soft thresholding has better mathematical properties and is preferred for some applications [167], hard thresholding is more straightforward to implement and has been preferred in PD measurements [111, 112, 115].

Hard threshold denoising offers an improved signal to noise ratio and can maintain the magnitude of original coefficients therefore minimizes any loss of pulse magnitude, this is significant for further quantification of the measured results. Figure 7.12 shows a comparison of de-noised signals obtained through hard thresholding and soft thresholding using identical threshold values.

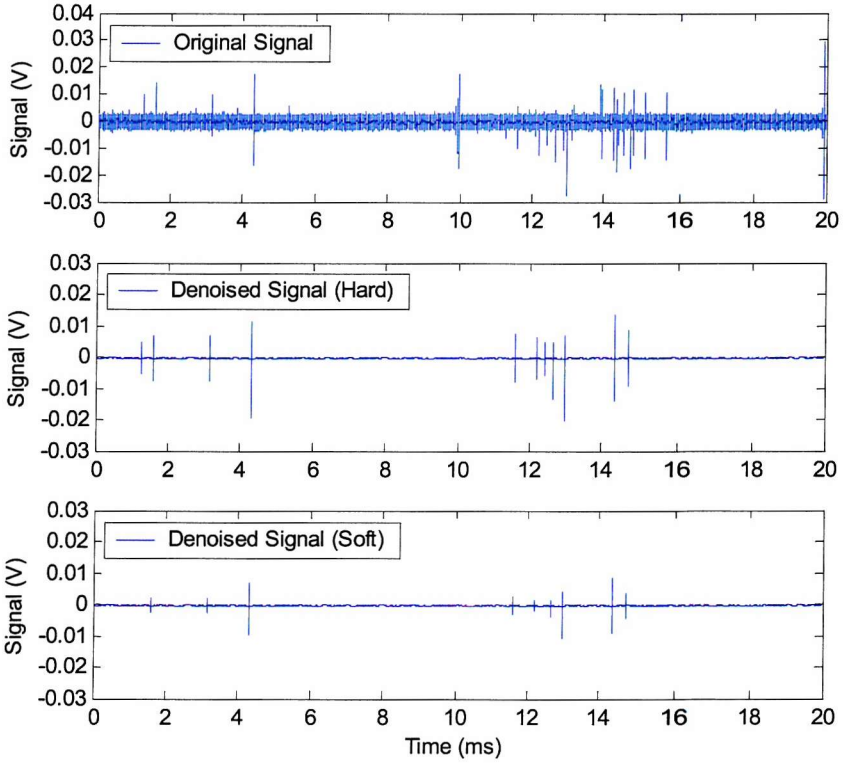

Figure 7.12 Hard threshold vs. soft threshold

7.5 Discussion

Among all the possible noise and interference encountered in online onsite PD detection pulse-shaped interference are reported to be difficult to distinguish and eliminate; especially the stochastic interference pulses such as corona discharge pulses and system discharge pulses as their time and frequency characteristics are similar to internal PD discharges. Previously, several methods have been proposed and reported effective in distinguishing the external PD pulse from internal PD activities on cable accessories such as directional coupling sensors (DCS) applied to the both sides of the cable joint [45]. Two capacitive coupler sensors placed on both sides of the cable joint and differential sensors have also been reported [14, 21]. More recently, some techniques of pattern recognition based on artificial intelligent methods such as neural networks and genetic algorithms have been found helpful in separation of the internal PD from other interference pulses [168-171]. However these approaches are not directly applicable to many online monitoring applications because knowledge is required to effectively 'train' the system to recognise PD.

Each method has its own advantages and limitations. Directional coupling sensors are effective in discriminating between various external PD pulses but the system is bulky and expensive. Wavelet methods discussed in the thesis use only one single coupler which is cheap and easy to apply. However, they are obviously less effective for some pulse-shaped interference whose frequency components are very close to the internal PD pulses such as system PD and surface discharges. Another advantage of wavelets analysis is that it can possibly be used for real time processing, as the processing time is short compared to some time domain techniques such as adaptive filtering and some PD pattern recognition algorithms such as neural networks which usually take longer time in learning and computation. In practice the choice of the post-processing algorithms and de-noising methods depends on the characteristics of the signal and noise presented in the environment and sometimes several techniques have to be used at the same time.

7.6 Summary

Capacitive coupling is one of several popular non-conventional PD detection techniques suitable for PD online onsite detection and long-term service condition

monitoring of HV cables. Compared to signals obtained using the conventional PD detection method, signals obtained using capacitive couplers are quite different in both time domain and frequency domain. Regarding the characteristics of the capacitive coupler, wavelet analysis has been applied to the signals obtained using capacitive couplers. Results shows that it can effectively discriminate internal PD pulses among pulse-shaped interference such as corona discharges and synchronous interference pulses as well as random noise through careful selection of the mother wavelet function and decomposition levels. Further removal of the interference has been accomplished by setting threshold values for each level. Greatly improved signal to noise ratio has been achieved with minimum loss of pulse magnitude and distortion.

Further work will focus on the practical application of the technique. More than one de-noising technique may be needed in order to achieve the maximum signal to noise ratio. For online application of these techniques, real time processing speed is also an important consideration and wavelet analysis is considered to be advantageous. It also facilitates PD location and further quantification of the measured results in term of reduced charge.

Chapter 8

Conclusions and Further Work

8.1 Conclusions

Partial discharge detection has become an important metric for condition monitoring of high voltage cables and accessories as it is both a dominant symptom and a cause of deterioration within solid electric insulation. For long-term maintenance of high voltage cables and accessories, condition based maintenance (CBM) strategies based on the online condition monitoring have been accepted as the best strategy from both an economical and technical point of view.

It is well accepted that acoustic emission (AE) detection is one of the most important non-destructive methods for partial discharge detection and the conventional acoustic emission method based on the use of ceramic piezoelectric materials has been successfully applied to the partial discharge detection in cables and accessories. With the advent of a new piezoelectric polymer material - Polyvinylidene fluoride (PVDF), the possibility of partial discharge detection based the PVDF film sensor has been investigated. It can be used to monitor mechanical vibration with higher sensitivity than ceramic sensors. However, unfortunately it also acts as electrically coupled sensor rather than an acoustic sensor when used for PD detection on HV cables due to the strong HF electrical field environment. Therefore the present PVDF film sensors are not suitable for on-line PD monitoring or general PD detection. Further measures similar to be those used for ceramic AE sensors such as complete electrical shielding, differential input sensors and amplifiers for rejecting the common mode noise need to be economically developed in the future.

Another widely used online partial discharge detection technique is capacitive coupling. It is sensitive, cheap and easy to apply. By using more than one coupler at the same time, partial discharge location can be achieved. However as a non-conventional method the calibration of capacitive couplers according to conventional apparent charge has not been achieved. Another problem associated with the capacitive coupler is post-processing of measured signals, as it is very sensitive to electrical noise and interference especially when applied on energized cable systems.

The principles of the capacitive coupler and its characteristics have been discussed in detail. Due to fundamentally different coupling mechanisms compared to the conventional electrical method, the measured results of the VHF capacitive coupler are not comparable with those of the conventional electrical method. So the concept of 'reduced charge' rather than 'apparent charge' has been proposed.

Regarding calibration, it is of fundamental importance that the injected charge is determined correctly in order to calibrate any measuring instrument. According to IEC standards, Q=CV is usually used to evaluate the injected charge if a voltage source pulse generator is used. Alternatively $Q=A/R_m$ method, which is usually used for calibration of PD calibrators, can also be used for evaluation of the injected charge as long as the external load R_m is known and the integral A is measurable. For calibration of VHF capacitive couplers, a current source pulse generator, with a rise time as short as a few nanoseconds, has to be used in order to match the frequency response range of the capacitive coupler sensor. As a result, special attention should be given when calculating the injected charge using the Q=CV method, because the output voltage of the current source PG will change with test object input impedance.

Evolved from the conventional electrical PD detection method, the terminal injection method has been accepted as a standard approach for calibration of capacitive couplers. However, for online on-site calibration alternative methods that approximate to the terminal injection method have to be developed because both terminals are generally not accessible if the cable is in service.

Two coupler injection methods based on the lumped circuit model have been investigated as possible alternative methods to the terminal injection calibration method. However due to the difficulties in evaluation of coupler/cable parameters and the limitations of the equivalent circuit model as well as the influence of the stray capacitance, obtained results are not in agreement with that of the terminal injection method and the errors are unacceptable. Further investigation based on frequency response analysis (FRA) has yielded a possible solution to this problem.

Frequency response analysis is an experimental method that can be used in order to determine a system model when the exact mathematical model of the system is difficult to determine theoretically. It is an efficient method to determine the behaviour of a specific coupler installed on a section of cable. The simulation model based on FRA gives good agreement with the experiment results and can be used to calibrate capacitive couplers. Various approaches of determining a calibration ratio for a capacitive coupler have been investigated experimentally and the values obtained for one experimental arrangement are shown in Table 5.1. It can be seen that a transfer function model based on the frequency response from the terminal to coupler produces a calibration ratio that is very close to the value obtained using the terminal injection method. By approximating the model using data from the coupler-to-coupler frequency response a similar calibration ratio can also be achieved. In general calibration based on FRA results in a far more accurate estimate of the reduced charge measured at the coupler than using pulse injection methods to determine the sensitivity of the measurement.

The complexity of the transfer function model is determined by the required accuracy of the model. Both first order and second order models give good agreement with the experiment results. Therefore, for simplicity of modelling and practical use, a first order model can be assumed to give sufficient accuracy for calibration purposes.

To further investigate the calibration method based on the simulation model of frequency response analysis, HV PD tests on two different cable test sections have been undertaken. The measured results from two capacitive couplers can provide approximate PD site location, the propagation velocity of the PD signal and

estimated attenuation of the PD pulse. An approximate transfer function determined from frequency response measurements of coupler-to-coupler and corresponding measuring circuits provide an estimate of the calibration ratio for couplers installed on specific sections of cable. The resulting PD magnitudes are less than those obtained using conventional electrical PD detection in both cases. However these values reflect the reduced charge measured at the sensor and the changing trend over a relatively long time provide an important quantity for long-term condition monitoring of HV cables.

Capacitive coupling is one of the several popular non-conventional PD detection techniques suitable for online onsite PD detection and long-term service condition monitoring of HV cables. Compared to signals obtained using the conventional PD detection method, signals obtained using capacitive couplers are quite different in both time domain and frequency domain. Capacitive couplers are also very sensitive to the electrical interference and noise that can be experienced during onsite online measurement. Special shielding and proper earthing measures are needed for couplers installed on onsite conditions. In addition signal post-processing techniques are also necessary. Regarding the characteristics of the capacitive coupler, wavelet analysis has been applied to the signals obtained. Results show that it can effectively discriminate internal PD pulses among pulse-shaped interference such as corona discharges and synchronous interference pulses as well as random noise through careful selection of the mother wavelet function and choice of decomposition levels. Further removal of interference has been accomplished by setting threshold values for each level. Greatly improved signal to noise ratio has been achieved with minimum loss of pulse magnitude and distortion of pulse shapes. This is a significant result for online PD measurement and further quantification of discharge magnitude.

8.2 Further Work

Acoustic partial discharge detection using PVDF film sensor is still a promising method for online partial discharge detection. However, further de-noising measures such as completely shielding from high frequency electrical noise and common mode noise rejection method using differential inputs similar to the conventional ceramic

sensor need to be further investigated if applied to such an electrically noisy environment as found online partial discharge detection.

Online calibration of capacitive couplers has been investigated in the thesis and the calibration method based the FRA and the corresponding simulation model is proved to be effective. Further work should be focus on automation of calibration procedures and possibility of practical use based on the original measurements of the frequency response and automatic determination of critical parameters and software modelling. Various aspects of online onsite situations also need to be considered.

Signal post-processing based on the wavelet analysis is very effective in discriminating internal PD pulses among some forms of pulse-shaped interference and random noise. However, every method has its own advantages and limitations to some specific kinds of interference. In order to achieve the maximum signal to noise ratio more than one de-noising techniques maybe needed depending on characteristics of the signal and noise. For online application of these techniques, real time processing speed is also an important consideration. Wavelet analysis is suitable for the real time situation and further work will focus on the practical application of the technique.

References

1. G.C Stone, Practical Discharge – Part VII: Practical Techniques for Measuring PD in Operating Equipment, IEEE Electrical Insulation Magazine, July/August 1991-Vol.7, No.4, pp9-19.

2. Johan J. Smit, Edward Gulski and Frank J. Wester, Economical and Technical Aspects of Advanced PD Diagnostics to Support Condition Based Maintenance of HV Assets, IEEE/PES 2002 Asia Pacific Conference and Exhibition on Transmission and Distribution, Volume, 2, 6-10 Oct. 2002, pp1110-1115.

3. Z. Yan, Ming Dong and Minghua Li, Development and Prospect of Insulation Monitoring and Diagnosis Technology, Proceedings of the 2nd International Conference on Insulation Condition Monitoring of Electrical Plant (ICMEP-ACEID 2003), 27-30, Oct. 2003, Chongqing, China, pp1-8.

4. Ben Quak, Johan J. Smit, Edward Gulski, Frank J. Wester and Edwin R.S. Groot, Database Support for Condition Assessment of Distribution Power Cables, IEEE/PES 2002 Asia Pacific Conference and Exhibition on Transmission and Distribution, Volume, 2, 6-10 Oct. 2002, pp1100-1104.

5. Johan J. Smit, Insulation Condition estimation of Distribution Power Cables by Online and Offline Diagnostics, Proceedings of 2001 International Symposium on Electrical Insulating Materials, 2001(ISEIM 2001), 19-22 Nov. 2001, pp513-517.

6. Q. Su and K. Sack, New Techniques for Online Partial Discharge Measurements, IEEE Proceedings of International Multi Topic Conference, 2001, Technology for 21st Century (INMIC 2001), 28-30 Dec. 2001, pp49-53.

7. K. Abdolall, G. L. Halldorson and D. Green, Condition Assessment and Failure Modes of Solid Dielectric Cables in Perspective, IEEE Transactions on Power Delivery, Vol. 17, No. 1, January 2002, pp18-24.

8. E. Gockenbach, Condition Monitoring and Diagnosis of Insulation systems Separable Tasks? Proceedings of the 2nd International Conference on Insulation Condition Monitoring of Electrical Plant (ICMEP-ACEID 2003), 27-30, Oct. 2003, Chongqing, China, pp25-27.

9. IEC 60270, High-voltage Test Techniques – Partial Discharge Measurements, International Electrotechnical Commission, Third edition, 2000-12.

10. J. P. Zondervan, E. Gulski, J. J. Smit, T. Grun and M. Turner, A New Multipurpose Partial Discharge analyser for On-site and On-line Diagnosis of HV Components, 11th International Symposium on High Voltage Engineering (ISH), London, 23-27 August 1999, pp.5.348.P5-5.351.P5.

11. A.J.M. Pemen, W.R. Rutgers, T. J.M. van Riji, and Y.H. Fu, Online Partial Discharge Monitoring of HV Components, 11th International Symposium on High Voltage Engineering, 23-27 August 1999, London, pp. 5.136.S16-5.139.S16.

12. N. Ahmed and N. Srinivas, On-line versus Off-line Partial Discharge Testing in Power Cables, Transmission and Distribution Conference and Exposition, 2001 IEEE/PES, Vol. 2, 28 Oct.-2. Nov. 2001, pp865-870.

13. G.C. Stone, Importance of Bandwidth in PD Measurement in Operating Motors and Generators, IEEE Transactions on Dielectrics and Electrical Insulation, Vol. 7 No. 1 Feb 2000, pp6-11.

14. G. Katsuta, A. Toya, K. Muraoka, T. Endoh, Y. Sekii and C. Ikeda, Development of a Method of Partial Discharge Detection in Extra-High Voltage Cross-linked Polyethylene Insulated Cable Lines, IEEE Transactions on Power Delivery, Vol. 7, No. 3, July 1992, pp1068-1074.

15. H. Ota, M. Ichihara and N. Miyamoto, Application of Advanced After-laying Test to Long-Distance 275 kV XLPE Cable Lines, IEEE Transactions on Power Delivery, Vol. 10, No. 2, April 1995, pp567-576.

16. M. Chen, Koji Urano, Atsushi Nishizawa, Atsuhide Jinno, Jiang Yun, Wei zhen Yu, Zhang Wen Feng, Tang Jian, Li Zhi Jian and Liu Yi Gang, Online Partial Discharge Measurement of Directly-buried Power Cable in China, ICMEP-ACEID 2003, pp113-117.

17. Th. Heizmann, Th. Aschwanden, H. Hahn, M. Laurent and L. Ritter, On-site Partial Discharge Measurements on Premoulded Cross-Bonding Joints of 170kV XLPE and EPR Cables, IEEE Transactions on Power Delivery, Vol. 13, No. 2, April 1998, pp330-335.

18. M. M. De A. Olivieri, W. A. Mannnheimer and A. P. Ripper-Neto, On the Use of Acoustic Signals for Detection and location of Partial discharges in Power Transformers, Conference Record of the 2000 IEEE International Symposium on Electrical Insulation, Anaheim, CA USA, April 2-5, 2000, pp259-262.

19. S. L. Jones, The Detection of Partial Discharge in Power Transformers Using Computer Aided Acoustic Emission Techniques, Conference Record of the 1990 IEEE International Symposium on Electrical Insulation, Toronto, Canada, June 3-6, 1990, pp106-110.

20. Md. E. Haque, A. B. Darus, M. M. Yaacob and F. Ahmed, Application of Acoustic Sensing and signal Processing for PD Detection in GIS, International Conference on Information, Communications and Signal Processing, ICICS'97 Singapore, 9-12 September 1997, pp745-749.

21. R. Morin, R. Bartnikas and G, Lessard, In-Service Location of Partial Discharge Sites in Polymeric Distribution Cables using Capacitive and Inductive Probes, IEEE Transmission and Distribution Conference, Piscataway, NJ, USA; 1999, Vol. 1, pp120-127.

22. Y. Tian, P. L. Lewin, A. E. Davies, S. J. Sutton, S. G. Swingler and G. M. Hathaway, Comparison of On-line Partial Discharge Detection Methods For HV Cable Joints, IEEE Transactions on Dielectrics and Electrical Insualtion, Vol. 9, No. 4, August 2002, pp604-615.

23. L. Zhong, Y. Xu, G. Chen, A.E. Davies, Z. Richardson and S. G. Swingler, Use of Capacitive Couplers for Partial Discharge Measurements in Power Cables and Joints, Proceedings of the 2001 IEEE 7th International Conference on Solid Dielectrics (ICSD '01), 25-29 June 2001, Eindhoven, the Netherlands, pp412 – 415.

24. Y. Tian, P. L. Lewin, A. E. Davies, S. J. Sutton and S. G. Swingler, Partial Discharge Detection in Cables Using VHF Capacitive Couplers, IEEE Transactions on Dielectrics and Electrical Insulation, Vol. 10, No. 2; April 2003, pp343-353.

25. H. Borsi, A PD Measuring and Evaluation System Based on Digital Signal Processing, IEEE Transactions on Dielectrics and Electrical Insulation, Vol. 7 No. 1, February 2000, pp21-29.

26. H. Zhu, V. Green, M. Sasic and S. Halliburton, Increased Sensitivity of Capacitive Couplers for In-service PD Measurement in Rotating Machines, IEEE Transactions on Energy Conversion, Vol. 14, No. 4, December 1999, pp1184-1192.

27. R. Bartnikas, Partial Discharges Their Mechanism, Detection and Measurement, IEEE Transaction on Dielectrics and Electrical Insulation, Vol. 9, No. 5, October 2002, pp763-808.

28. C. R. Qiu and N.Q. Wang, Partial Discharge and its Detection in Electrical Equipment, Mechanical industry Press, China, 1993.

29. Y. Tian, Partial Discharge Detection in Cable Systems, Ph.D. Thesis, University of Southampton, Department of Electronics and Computer Science, 2001.

30. F. H. Kreuger, Discharge Detection in High Voltage Equipment, Temple Press Books ltd., London 1964.

31. S. A. Boggs, Partial Discharge: Overview and Signal Generation, IEEE Electrical Insulation Magazine, Vol.6, No. 4 July/August 1990, pp33-39.

32. S. A. Boggs, Partial discharge- Part III: Cavity Induced PD in Solid Dielectrics, IEEE Electrical Insulation Magazine, Nov. /Dec. 1990-Vol.6, No. 6, pp11-20.

33. J. P. Steiner, Partial Discharge – Part IV: Commercial PD Testing, IEEE Electrical Insulation Magazine, Jan./Feb. 1991, Vol.7, No. 1, pp20-33.

34. S. A. Boggs, Partial Discharge-Part II: Detection Sensitivity, IEEE Electrical Insulation Magazine, Vol. 6, No. 5 September/October 1990, pp35-42.

35. G. C Crichton, P. W. Karlsson and A. Pedersen, Partial Discharges in Ellipoidal and Spheroidal Viods, IEEE Transactions on Electrical Insulation, Vol. 24 No. 2, April 1989, pp335-342.

36. E. Gulski and F. H. Kreuger, Computer-aided Recognition of Discharge Sources, IEEE Transactions on Electrical Insulation, Vol. 27, No. 1, Feburary 1992, pp82-92.

37. E. Gulski, Computer-aided Measurement of Partial Discharges in HV Equipment, IEEE Transactions on Electrical Insulation, Vol. 28, No. 6, December 1993, pp969-983.

38. J. P. Zondervan, E. Gulski and J. J. Smit, Fundamental Aspects of PD Patterns of On-line Measurements on Turbogenerators, IEEE Transactions on Dielectrics and Electrical Insulation, Vol. 7, No. 1, February 2000, pp59-70.

39. R. Candela, G. Mirelli and R. Schifani, PD Recognition by Means of Statistical and Fractal Parameters and a Neural Network, IEEE Transactions on Dielectrics and Electrical Insulation, Vol. 7, No. 1, February 2000, pp87-94.

40. G. C. Stone, The Use of Partial Discharge Measurements to Asses the Condition of Rotating Machine Insulation, IEEE Electrical Insulation Magazine, Vol. 12, No. 4, July/August 1996, pp23-27. [29] Y. Tian, Partial Discharge Detection in Cable Systems, Ph.D. Thesis, University of Southampton, Department of Electronics and Computer Science, 2001.

41. C. Huang, W. Yu and W. Wei, Development of PD Online Monitoring System for Large turbine Generators, IEEE International Symposium on Electrical Insulation, Boston, MA USA, April 7-10, 2002, pp23-26.

42. Y. Ming and S. Birlasekaran, Characterization of Partial Discharge Signals Using Wavelet and Statistical Techniques, IEEE International Symposium on Electrical Insulation, Boston, MA USA, April 7-10, 2002, pp9-13.

43. N. Hozumi, T. Okamoto and T. Imajo, Discrimination of Partial Discharge Patterns Using a Neural Network, IEEE Transactions on Electrical Insulation, Vol. 27 No. 3, June 1992, pp550-555.

44. E. Lemke and P. Schmiegel, Fundamentals of PD Probe Measuring Technique, LEMKE DIAGNOSTICS GmbH, Dresden, Germany, 1993.

45. D. Pommerenke, T. Strehl, R. Heinrich, W. Kalkner, F. Schmidt and W. WeiBenberg, Discrimination between Internal PD and Other Pulses Using Directional Coupling Sensors on HV Cable Systems, IEEE Transaction on Dielectrics and Electrical Insulation Vol. 6 No. 6 December 1999.

46. E. Lemke and P. Schmiegel, Progress in PD-probe Measuring Technique, 7th International Symposium on High Voltage Engineering, Technische Universititat Dresden, August 26-30, 1991, pp43-46.

47. E. Pultrum, Onsite Testing of Cable Systems After Laying, Monitoring With HF Partial Discharge Detection, IEE Two Day Colloquium on Supertension, 20-21 November 1995, pp21/1-21/4.

48. H. N. Bidhendi and Q. Su, Partial Discharge Location for Cables with Helical Earth Screens, 10th International Conference on High Voltage Engineering, 25-29 August 1997, Canada.

49. U. Schichler, A Sensitive Method for On-site Partial discharge Detection on XLPE Cable Joints, Proceedings of 5th International Conference on Properties and Applications of Dielectric Materials, Vol. 2, 25-30 May 1997, pp1099-1102.

50. U. Schichler, H. Borsi and E. Gockenbach, Problems and New Solutions for Partial Discharge Measurement on High Voltage Cables under Noisy Conditions, Conference Record of the IEEE International Symposium on Electrical Insulation, Pittsburgh, PA USA, June 5-8, 1994, pp66-69.

51. N. H. Ahmed and N. N. Srinivas, Online Partial Discharge Detection in Cables, IEEE Transaction on Dielectrics and Electrical Insulation, Vol. 5, No. 2, April 1998, pp181-188.

52. N. H. Ahmed and N. N. Srinivas, Partial Discharge Measurements in Distribution-Class Extruded Cables, IEEE Transmission and Distribution Conference, 11-16 April 1999, Vol. 1, pp46-51.

53. N. Ahme, O. Morel and N. Srinivas, Partial Discharge Measurement in Transmission-Class Cable Terminations, IEEE Transmission and Distribution Conference, 11-16 April 1999, Vol. 1, pp2-7.

54. E. Lemke, T. Strehl and D. Ru wurm, New Development in the Field of PD Detection and Location in Power Cables Under On-site Condition, 11th International Symposium on High Voltage Engineering, ISH 99 Vol. 5 pp5.106-110.

55. D. Pommerenke and K. Masterson, A Novel Concept for Monitoring Partial Discharge on EHV-Cable System Accessories Using Components at the Accessories, IEE 2000 Proceedings of Dielectric Material, Measurements and Applications, pp145-149.

56. C. G. Henningsen, K. Polster, Bernhard A. Fruth and Detlev W. Gross, Experience with an Online Monitoring system for 400kV XLPE Cables, IEEE Proceedings of Transmission and Distribution Conference, 15-20 September 1996, pp515-520.

57. K. Fukunaga, M. Tan and H. Takehana, New Partial Discharge Detection Method for Live UHV/EHV Cable Joints, IEEE Transactions on Electrical Insulation, Vol. 27, No. 3 June 1992, pp669-675.

58. N. N. Srinivas and N Ahmed, Condition Assessment of Distribution and Transmission Class Voltage Cable systems, IEEE 10th International Conference on Transmission and Distribution Construction, Operation and Live-line Maintenance, 2003, 6-10 April 2003, pp194-201.

59. Y. Tian, P. L. Lewin, A. E. Davies, S. J. Sutton and S. G. Swingler, Partial discharge Detection in High Voltage Cables using VHF Capacitive Coupler and Screen Interruption Techniques, Conference Record of the 2002 IEEE International Symposium on Electrical Insulation, Boston, MA USA, April 7-10, 2002, pp87-90.

60. L. E. Lundgaard, Partial Discharge –part XIII: Acoustic Partial Discharge Detection-Fundamental considerations, IEEE Electrical Insulation Magazine, Vol.8, No.4 July/August 1992, pp25-31.

61. D. A. Nattrass, Partial Discharge XVII: The Early History of Partial Discharge Research, IEEE Electrical Insulation Magazine, July/August 1993, Vol. 9, No. 4, pp27-31.

62. L. E. Lundgaard, Partial Discharge –part XIV: Acoustic Partial Discharge Detection-Practical Application, IEEE Electrical Insulation Magazine, Vol.8, No.5 September/October 1992, pp34-43.

63. E. Grossmann and K. Feser, Comparison of the Sensitivity of an Acoustic and Electrical PD-Measurement on Transformers in the Laboratory and Onsite, 2000 conference on Electrical Insulation and Dielectric Phenomena, pp690-693.

64. D. Zhu, K. Tan, C. Wang and X. Jin, Computer-Aided Online Detection of Partial Discharge in Power Transformer, Proceedings of the 3rd International Conference on Properties and Application of Dielectric Materials, July 8-12, 1991, Tokyo, Japan, pp1128-1131.

65. P. M. Eleftherion, Partial Discharge XXI: Acoustic Emission-Based PD Source Location in Transformers, IEEE Electrical Insulation Magazine, November/December 1995, pp22-26.

66. S. Gao, L. Zhang, K. Tan and F. Li, Partial discharge Acoustic Emission Detector Based on Computer for Power Capacitor, Proceedings of 2001 International Symposium on Electrical Insulating Materials (ISEIM 2001), 19-22 November 2001, pp761-764.

67. L. Ghirelli, W. Koltunowicz, A. Pigini, S. Rama and A. Yellaiah, Acoustic Method for Partial Discharge Detection in high Power Capacitors, International Conference for Partial discharge, 28-30 September 1993, pp92-93.

68. M. Chen, K. Urano, A. Kato, M. Okada and N. Yoshikawa, Study of Partial Discharge Localization Methods for EHV Prefabricated Joint, IEEE Power Engineering Society Summer Meeting, 2000, Volume 1, 16-20 July 2000, pp475-479.

69. L. E. Lundgaard and W. Hansen, Acoustic Method for Quality Control and In-Service Periodic Monitoring of Medium Voltage Cable Terminations, Conference Record of the 1998 IEEE International Symposium on Electrical Insulation, Arlington, Virginia, USA, June 7-10, 1998, pp130-133.

70. Y. Tian, P. L. Lewin, A. E. Davies and G. M. Hathaway, Acoustic Emission Techniques for Partial Discharge Detection Within Cable Insulation, IEE 2000 Conference on Dielectric Materials, Measurements and Applications, pp503-508.

71. Y. Tian, P. L. Lewin, A. E. Davies, G. M. Hathaway, S. J. Sutton and S. G. Swingler, Acoustic Emission Measurement of Partial Discharges During electrical Tree Growth in XLPE Cable Insulation, 2001 IEEE 7th International Conference on Solid Dielectrics, June 25-29, 2001, Eindhoven, the Netherlands, pp477-480.

72. M. Duval, A Review of Faults Detectable by Gas-in-oil Analysis in Transformers, IEEE Electrical Insulation Magazine, May/June 2002, pp8-17.

73. B. H. Ward and S. Lindgren, A Survey of Developments in Insulation Monitoring of Power Transformers, Conference Record of the 2000 IEEE International Symposium on Electrical Insulation, Anaheim, CA USA, April 2-5, 2000, pp141-147.

74. N. Singh, O. Morel and S. Singh, The condition assessment through Dissolved-Gas Analysis of 138kV Extruded Cable Terminations, Detroit Edison® Report for EPRI and NEETRAC, centre of Georgia Institute of Technology, USA, TR-112676, 1999, pp9.16-9.20.

75. J. C. Chan. P. Duffy, L.J. Hiivala, and J. Wasik, Partial Discharge-Part VIII: PD testing of Solid Dielectric Cable, IEEE Electrical Insulation Magazine, Vol.7 No.5 September/October 1991, pp9-20.

76. S. A. Boggs and G. C. stone, Fundamental Limitations in the Measurement of Corona and Partial Discharge, IEEE Transaction on Electrical Insulation, Vol. EI-17, No. 2, April 1982, pp143-150.

77. S. A. Boggs, Ash Pathak and Philip Walker, Partial Discharge XXII: High Frequency Attenuation in Shielded Solid Dielectric Power Cable and Implications Thereof for PD Location, IEEE Electrical Insulation Magazine, Vol. 12, No, 1 January/February 1996, pp9-16.

78. F. H. Kreuger M.G. Wezelenbury, A. G. Wiemer and W. A. Sonneveld, Partial Discharge Part XVIII: Errors in the Location of Partial Discharges in High Voltage Solid Dielectric Cables, IEEE Electrical Insulation Magazine, November/December 1993 Vol. 9 No 6, pp15-23.

79. M. S. Mashikian, R. Bansal and R. Northrop, Location and Characterization of Partial Discharge Sites in Shielded Power Cables, IEEE Transactions on Power Delivery, Vol. 5, No. 2, April 1990, pp833-839.

80. M. S. Mashikian, R. Luther, J. C. Mclver, J. Jurcisin and P W. Spencer, Evaluation of Field Aged Crosslinked Polyethylene Cables by Partial discharge Location, IEEE Transactions on Power Delivery, Vol. 9, No. 2, April 1994, pp620-628.

81. H. Borsi, Digital location of Partial Discharges in HV Cables, IEEE Transactions on Electrical Insulation, Vol. 27, No. 1, February 1992, pp28-36.

82. E. Gockenbach and W. Hauschild, The Selection of the Frequency Range for High-Voltage On-site Testing of Extruded Insulation Cable Systems, IEEE Electrical Insulation Magazine, November/December 2000, Vol. 16, No. 6, pp11-16.

83. S. V. Heyer, A. J. Jushchyshyn, W. Boone and T. Aabo, Diagnostic Testing Comes to Rescue, Transmission and Distribution World, July 1998, pp81-83.

84. E. Pultrum and E. Hetzel, Dutch Experience With VLF Partial Discharge Detection, IEE Colloquium on: MV paper cables: asset or liability? Capenhurst, 21 April 1998, pp7/1-7/5.

85. D. W. Gross and J. G. Herbig, Partial Discharge Fault Location and Diagnosis on HV Cables, 2000 Annual Report Conference on Electrical Insulation and Dielectric Phenomena, 15-18 Oct 2000, Vol. 2, pp630-633.

86. E. F. Steennis, R. Ross, N. van Schaik, W. boone and D. M. van Aartrijk, Partial Discharge Diagnostics of Long and Branched Medium-Voltage Cables, 2001 IEEE 7th International Conference on Solid Dielectrics, 25-29, 2001, Eindhoven, Netherlands, pp27-30.

87. E. Gulski, J. J. Smit, P. N. Seitz and J. C. Smit, PD Measurements On-site Using Oscillating Wave Test System, Conference Record of the 1998 IEEE International Symposium on Electrical Insulation, Arlington, Virginia, USA, June 7-10, 1998, pp420-423.

88. F. J. Wester, E. Gulski, J. J. Smit, P. N. Seitz and M. Turner, Application of Advanced PD Diagnostics for Condition Based Maintenance of MV Power Cable Systems, Conference Record of the 2000 IEEE International Symposium on Insulation, Anaheim, CA USA, April 2-5, 2000, pp115-118.

89. B. Quak, E. Gulski, J. J. Smit, F. J. Wester and P. N. Seitz, Conference Record of the 2002 IEEE International Symposium on Electrical Insulation, Boston, MA USA, April 7-10, 2002, pp83-86.

90. E. Gulski, F. J. Wester, J. J. Smit, P. N. Seitz and M. Turner, Advanced Partial discharge Diagnostic of MV Power Cable system Using Oscillating Wave Test System, IEEE Electrical Insulation Magazine, March/April 2000, Vol. 16, No. 2, pp17-25.

91. W. Schufft, P. Coors, W. Hauschild and J. Spiegelberg, Frequency-Tuned Resonant Test Systems for On-site Testing and Diagnostics, IEE High Voltage Symposium, 22-27 August 1999.

92. P. Mohaupt, M. Gamlin, R. Gleyvod and J. K. G. Voigt, High Voltage Testing Using Series Resonance with Variable Frequency, ISH 97, Montreal.

93. S. Schierig and D. Russwurm, HV Onsite Testing on Cables by Alternating Voltage of Variable Frequency, IEEE Insulated Conductors Committee (ICC) Meeting 2000, 29 Oct.-1 Nov. 2000, Florida.

94. R. Bodega, A. Cavallini, P. H. F. Morshuis and F. J. Wester, The Effect of Voltage Frequency on Partial Discharge Activity, 2002 Annual Report Conference on Electrical Insulation and Dielectric Phenomena, 20-24 Oct. 2002, pp685-689.

95. R. Miller and I. A. Black, Partial Discharge Measurement Over the Frequency Range 0.1Hz to 50Hz, IEEE Transactions on Electrical Insulation, Vol. EI-12, No. 3, June 1977, pp224-232.

96. R. Miller and I. A. Black, Partial Discharge Energy Measurement on Electrical Machine Insualtion When Energized at Frequencies between 0.1Hz and Power Frequency, IEEE Transactions on Electrical Insulation, Vol. EI-14, No. 3, June 1979, pp127-135.

97. B. Oyegoke, P. Hyvonen, M Aro and N. Gao, Selectivity of Damped ac (DAC) and VLF Voltages in After-layering Tests of Extruded MV Cable Systems, IEEE Transactions on Dielectrics and Electrical Insulation, Vol. 10, No. 5, October 2003, pp874-882.

98. N. Srinivas, N. Ahmed and G. Raju, On Line Measurement of Partial Discharges, 2000 Conference on Electrical Insulation and Dielectric Phenomena, 15-18 Oct. 2000, Vol. 2, pp678-681.

99. L. Satish and B. Nazneen, Wavelet-based Denoising of Partial Discharge Signals buried in Excessive Noise and Interference, IEEE Transaction on Dielectrics and Electrical Insulation, Vol. 10, No. 2, April 2003, pp354-367.

100. I. Shim, J.J. Saraghan and W.H. Siew, Digital Signal Processing applied to the Detection of Partial Discharge: An Overview, IEEE Electrical Insulation Magazine, May/June 2000, Vol. 16, No. 3, pp6-12.

101. A. Hariri, Z. Du, S. Dong, S. Mashikian and David Jordan, Field Location of Partial Discharge in Power Cables Using an Adaptive Noise Mitigating system, Conference Record of the 1996 IEEE International Symposium on Electrical Insulation, Montreal, Quebec, Canada, June 16-19, 1996, pp121-125.

102. M. S. Mashikian, F. Palmieri, R. Bansal and R. B. Northrop, Location of Partial Discharges in Shielded Cables in the Presence of High Noise, IEEE Transactions on Electrical Insulation, Vol. 27 No. 1, February 1992, pp37-43.

103. Sher Zaman Khan, Zhu Deheng, Jin Xiahe and Tan Kexiong A New Adaptive Technique for Online Partial Discharge Monitoring, IEEE Transaction on Dielectrics and Electrical Insulation, Vol. 2 No. 4, August 1995, pp700-707.

104. B. Widrow and S. D. Stearns, Adaptive Signal Processing, Prentice-Hall, Inc., 1985.

105. A. Zargari and T. R. Blackburn, Application of Adaptive Filters for the Estimation of Partial Discharge Signals in Noise Environment, Proceedings of the 5th International conference on Properties and Applications of Dielectric Materials May 25-30, 1997, Seoul, Korea, pp212-215.

106. A. Zargari and T. R. Blackburn, Detection of Partial Discharge Signals in Unknown Noisy Environment, 1996 IEEE Annual Report- Conference on Electrical Insulation and Dielectric Phenomena, San Francisco, October 20-23, 1996, pp472-475.

107. V. Nagesh and B. I. Gururaj, Evaluation of Digital Filters for Rejecting Discrete Spectral Interference in On-site PD Measurements, IEEE Transactions on Electrical Insulation, Vol. 28 No. 1, February 1993, pp73-85.

108. Z. Du and M. S. Mashikian, Self-learning Digital Filter for the Field Location of Partial Discharge in Cables, Conference Record of the 1994 IEEE International Symposium on Electrical Insulation, Pittsburgh, PA USA, June 5-8, 1994, pp245-248.

109. Q. Su, An adaptive Filtering Method for Noise Suppress in Partial Discharge Measurement, Conference on Electrical Insulation and Dielectric Phenomena, Annual Report, 17-20 Oct. 1993, pp481-486.

110. Q. Su, Application of Digital Signal Processing Techniques for Noise Suppression in Partial Discharge Measurements, Proceedings of the 4th International Conference on Properties and Application of Dielectric Materials, July 3-8, 1994, Brisbane Australia, pp602-605.

111. X. Ma, C. Zhou and I. J. Kemp, Interpretation of Wavelet Analysis and Its application in Partial Discharge Detection, IEEE Transactions on Dielectrics and Electrical Insulation, Vol. 9, No. 3, June 2002, pp446-457.

112. X. Ma, C. Zhou and I.J. Kemp, Automated Wavelet Selection and Thresolding for PD Detection, IEEE Electrical Insulation Magazine, March/April 2002, Vol. 18, No. 2, pp37-45.

113. X. Ma, C. Zhou and I.J. Kemp, Investigation into the Use of Wavelet Theory for Partial Discharge Pulse Exaction in Electrically Noisy Environments, Eighth International Conference on Dielectric Materials, Measurements and applications, 17-21 Sep. 2000, pp123-126.

114. C. Zhou, X. Ma, and I.J. Kemp, Optimal algorithm for Wavelet-based Denoising in PD Measurement, XIIIth International Symposium for High Voltage Engineering, Netherlands 2003, pp1-4.

115. I. Shim, J.J. Soraghan and W. H. Siew, Detection of PD Utilizing Digital Signal Processing Methods Part 3: Open-loop Noise Reduction, IEEE Electrical Insulation Magazine, January/February 2001, Vol. 17, No. 1, pp6-13.

116. H. Borsi, A PD Measuring and Evaluation System Based on Digital Signal Processing, IEEE Transactions on Dielectrics and Electrical Insulation, Vol. 7 No. 1, February 2000, pp21-25.

117. C. Wang, X. Jin and T. C. Cheng, Analysis and Suppression of Continuous Periodic Interference for Online PD Monitoring of Power Transformers, IEE Proceedings of High Voltage Engineering Symposium, 22-27 August 1999, pp 5.212.P5-5.215.P5.

118. J. Luo, J Feng, J. Yuan, C. Ma and Y. Qiu, Partial Discharge Detection in XLPE Power Cable With CT Sensor, 2001 IEEE 7th International Conference on Solid Dielectrics, June 25-29, 2001, Eindhoven, the Netherlands, pp400-403.

119. X. Wang, D. Zhu, F. Li and S. Gao, Analysis and Rejection of Noises from Partial Discharge (PD) On-site Testing Environment, Proceedings of the 7th International Conference on Properties and Applications of Dielectric Materials, June 1-5 2003, Nagoya, pp1104-1107.

120. U. Schichler, H. Borsi and E. Gockenbach, Problems and New solutions for Partial Discharge Measurement on High Voltage Cables under Noisy Conditions, Conference Record of the IEEE International Symposium on Electrical Insulation, Pittsburgh, PA USA, June 5-8, 1994, pp66-69.

121. U. Schichler, H. Borsi and E. Gockenbach, Application of Digital Filters for On-site Partial Discharge Detection on High Voltage Cables, Proceedings of the 4th International Conference on Properties and Applications of Dielectric Materials, July 3-8, 1994, Brisbane, Australia, Vol. 2, pp618-621.

122. U. Schichler, A Sensitive Method for Onsite Partial Discharge Detection on XLPE Cable Joints, Proceedings of the 5th International Conference on Properties and Applications of Dielectric Materials, May 25-30, 1997, Seoul, Korea, pp1099-1102.

123. X. Wang, D. Zhu and F. Li, Interference Analysis and Rejection of Partial Discharge (PD) Monitoring Signal Onsite, Proceedings of 2001 International Symposium on Electrical Insulating Materials, 2001 (ISEIM 2001), 19-22 November 2001, pp111-114.

124. Y. Tian, P. L. Lewin, A.E. Davies and Z. Richardson, Acoustic Emission Detection of Partial Discharge in Polymeric Insulation, IEE High Voltage Engineering Symposium, 22-27 August 1999, pp1.82S23-1.85.S23.

125. Y. Tian, P. L. Lewin, A.E. Davies, S. J. Sutton and S. G. Swingler, Application of Acoustic Emission Techniques and Artificial Neural Networks to Partial Discharge Classification, Conference Record of the 2002 IEEE International Symposium on Electrical Insulation, Boston, MA USA, April 7-10, 2002, pp119-123.

126. M. F. Barsky, D. K. Lindner and R. O. Claus, Robot Gripper Control System Using PVDF Piezoelectric Sensors, IEEE Transactions on Ultrosonics, Ferroelectrics and Frequency Control, Vol. 36, No. 1, January 1989, pp129-134.

127. Measurement Specialties, Piezo Film Sensors Technical Manual, Internet version, 1998.

128. S. W. Or, H. L. W. Chan and C.L. Choy, P(VDF-TrFE) Copolymer Acoustic Emission Sensors, Sensors and Actuators 80(2000), pp 237-241.

129. Task Force 33.03.05: "Measurement of partial discharge", Calibration Procedures for Analog and Digital Partial Discharge Measuring Instruments, Electra No.180 October 1998, pp122-144.

130. W. Lucas, K. Schon and E. Lemke, H. Elze, Comparison of Two Techniques for Calibrating PD Calibrators, 10th International Symposium on High Voltage Engineering, Montreal Canada, August 25-29, 1997, pp1-4.

131. E. Lemke, P. Schmiegel, H. Elze and D. Russwurm, Experience in the Calibration Technique for PD Calibrators, 3rd European Conference and Exhibition, High Voltage Measurements and Calibration, CESI Auditorium, Milan, Italy: 9-11 October 1996, pp6.1.1-6.1.7.

132. K. Schon, W. Lucas, E. Lemke, H. Elze, A. Bergman, Q. Gunnarsson, F. Garnacho, P. Simón, M. Muhr, S. Pack, G. Rizzi, A. Sardi, P. A. Giorgi, G. Pesavento, R. Gobbo, F. N. Gomez, F. Domimgues, I. Blanc, J. Hällström, J. Piiroinen, W. Zaengl and R. Brooks, Intercomparison on PD Calibrators and PD Instruments, 11th International Symposium on High Voltage Engineering, 22-27 August 1999, pp1.5.S1-1.8.S1.

133. O. Gunnarsson, A, Bergman and K Rydler, A Method for Calibration of Partial Discharge Calibrators, Transactions on Instrumentation and Measurement, Vol.48 No.2 April 1999, pp453-456.

134. L. Ljung, System Identification theory for the user, Second Edition, Prentice Hall PTR, 1999.

135. K. Dutton, S. Thompson and B. Barraclough, The Art of Control Engineering, England: Addison-Wesley 1997.

136. Y. Liu, F. Lu, Y. Li and N. Wang, The Transfer Characteristic of Partial Discharge Current Sensor Based on Vector Fitting, Proceedings of the 2nd International Conference on Insulation Condition Monitoring of Electrical Plant, 27-30 Oct. 2003, Chongqing, China, pp187-189.

137. L. R Marti, Accurate Modelling of Frequency-Dependent Transmission Lines in Electromagnetic Transient Simulations, IEEE Transactions on PAS, Vol. 101, No.1, January 1982, pp147-157.

138. S. Birlasekaren and Fred Fetherston, Off/Online FRA Condition Monitoring Technique for Power Transformer, IEEE Power Engineering Review, Volume 19, Issue 8, August 1999, pp54-56.

139. X. Liu and Q. Sun, Test Research on Power Transformer Winding Deformation by FRA Method, Proceedings of 2001 International Symposium on Electrical Insulating Materials [ISEIM 2001], 19-22 Nov. 2001, pp837-840.

140. Jorge Pleite, Emilio Olías, Andrés Barrado, Antonio Lázaro and Ramón Vázquez, Frequency Response Modeling for Device Analysis, IEEE 2002 28th Annual Conference of the Industrial Electronics Society [IECON02], Vol. 2, 5-8 November 2002, pp1457-1462.

141. Jorge Pleite, Emilio Olías, Andrés Barrado, Antonio Lázaro and Juan Vázquez, Transformer Modeling for FRA Techniques, Transmission and Distribution Conference and Exhibition 2002, Asia Pacific, IEEE/PES, Volume 1, 6-10 Oct. 2002, pp64-72.

142. F. S. Sellschopp and Marco A. Arjona, An Automated system for Frequency Response Analysis With Application to an Undergraduate Laboratory of Electrical Machines, IEEE Transactions on Education, Accepted for Future Publication, 2003.

143. R. Heinrich, R. Jobava, W. Kalkner and A. Gheonjian, Numerical Modelling for Investigation and Optimisation of a Sensor for Sensitive Partial Discharge Detection on High-Voltage XLPE Cables, European Transaction on Electrical Power (ETEP) Vol. 10 No. 3, May/June 2000, pp161-166.

144. D. Pommerenke, R. Jobava and R. Heinrich, "Electromagnetic Finite Differences Time Domain (FDTD) Modelling of Partial discharge Coupling Applied to High Voltage Cables and Cable Joints", Dielectric Materials, Measurements and Applications, Conference Publication No. 473, IEE 2000, pp497-502.

145. Agilent Technologies, 4395A Network/Spectrum/Impedance Analyser Operation Manual, 2002.

146. Z. Zhao, High Voltage Technologies, Electrical Power Press, China, 1999.

147. G. M. Sandquist, Introduction to System Science, Prentice Hall, Inc.1985.

148. B. Gustavsen and A. Semlyen, Rational Approximation of Frequency Domain Responses by Vector Fitting, IEEE Transactions on Power Delivery, Vol. 14, No. 3, July 1999, pp1052-1061.

149. M. D. Sidman, F. E. DeAngelis and G. C. Verghese, Parametric System Identification on Logarithmic Frequency Response Data, IEEE Transactions on Automatic Control, Vol. 36, No. 9, September 1991, pp1065-1070.

150. H. Akcay, S. M. Islam and B. Ninness, Subspace Based Identification of Power Transformer models from Frequency Response Data, Proceedings of American Control Conference, Philadelphia, Pennsylvania, June 1998, pp3398-3402.

151. S. Zollner and E. Lemke, On the evaluation of the PD Quantity Apparent Charge with Respect to PD Probe Measurement, 7th International Symposium on High Voltage Engineering, August 26-30,1991, 87-90, Vol. 7, Dresden, Germany, pp87-90.

152. S. A. Boggs and J. Densley, Fundamentals of Partial Discharge in the Context of Field Cable Testing, IEEE Electrical Insulation Magazine, Vol. 16, No. 5 September/October 2000, pp13-18.

153. I. Daubechies, Ten Lectures on Wavelets, CBMS-NSF Regional Conference Series in Applied Mathematics, Society for Industrial and Applied Mathematics, Philadelphia, Pennsylvania, 1992.

154. Charles K. Chui, Wavelets: A Tutorial in Theory and applications, Academic Press, Inc. 1992.

155. L. L. Schumaker and G. Webb, Recent Advances in Wavelet Analysis, Academic Press, Inc. 1994.

156. C. K. Chui, An Introduction to Wavelets, Academic Press, Inc. 1992.

157. Gerald Kaiser, A Friendly Guide to Wavelets, Birkhäuser Boston 1994.

158. Donald B. Percival and Andrew T. Walden, Wavelet Methods for Time Series analysis, Cambridge University Press, 2000.

159. Wavelet Toolbox 2.2 Manual - User's Guide The Math Works Inc. 2002.

160. S. Fujimori, T. Endoh, K. Mitsuboshi, K. Ishiwata and S. Hirute, Wavelet Analysis of Tree Development, IEEE 5th International Conference on Conduction and Breakdown in Solid Dielectrics, Leicester, UK, 1995, pp376-380.

161. L. Angrisani and P. Daponte, A Proposal for the Automatic Evaluation of the Mean Curve Required by the ANSI/IEEE Std4-1978, IEEE Transactions on Instrumentation and Measurement, Volume 47, Issue 5, Oct. 1998, pp1180 -1186.

162. X. Hu, F. Wang, H. Zhao and Y. Ji, The Mechanical Fault Diagnosis for HV Breakers on the Wavelet Packet Analysis, Proceedings of the 20th IEEE Instrumentation and Measurement Technology Conference, IMTC '03, Volume 1, Vail, CO, USA, 20-22 May 2003, pp415-419.

163. L. Angrisani, P. Daponte, C. Dias, and A.A. do Vale, Advanced processing techniques of high-voltage impulse test signals, IEEE Transactions on Instrumentation and Measurement, Volume 47, Issue 2, April 1998, pp439-445.

164. Y. Tu, Z. D. Wang, P. A. Crossley, Partial discharge pattern recognition based on 2-D wavelet transform and neural network techniques, 2002 IEEE Power Engineering Society Summer Meeting, Volume 1, 21-25 July 2002, pp411-416.

165. U. Köpf and K. Feser, Rejection of Narrow-band Noise and Repetitive Pulses in On-site PD Measurements, IEEE Transactions on Dielectrics and Electrical Insulation, Vol. 2 No. 6, December 1995, pp1180-1191.

166. V. Nagesh and B.I. Gururaj, Automatic Detection and Elimination of Periodic Pulse Shaped Interferences in Partial Discharge Measurements, IEE Proceedings of Science, Measurements and Technology, Vol.141, No. 5, September 1994, pp335-342.

167. D.L. Donoho, Denoising by Soft Thresholding, IEEE Transactions on Information Theory, Vol. 41, 1995, pp 613-627.

168. H. Borsi, E. Gockenbach and D. Wenzel, Separation of Partial Discharges from Pulse-shaped Noise Signals with the Help of Neural Networks, IEEE Proceedings of Science, Measurements and Technology, Volume, 142, Issue: 1, January, 1995, pp 69-74.

169. H. Suzuki, and T. Endoh, Pattern Recognition of Partial Discharge in XLPE Cables Using a Neural Network, IEEE Transactions on Electrical Insulation, Vol. 27, No. 3, June 1992, pp543-549.

170. D. Wenzel, H. Borsi and E. Gockenbach, A New Approach for Partial Discharge Recognition on Transformers On-site by Means of Genetic Algorithms, IEEE International Symposium on Electrical Insulation, Montreal, Quebec, Canada, June 16-19, 1996, pp57-60.

171. G. Wu, X. Jiang and H. Xie, A Neural Network Used for Pattern Recognition with Genetic Algorithm, Proceedings of the 6th International Conference on Properties and applications of Dielectric Materials, June 21-26 2000, Xi'an Jiaotong University, Xi'an, China, pp451-454.

Appendix 1

CALIBRATION OF CAPACITIVE COUPLERS FOR ONLINE PD DETECTION IN HV CABLES USING FREQUENCY RESPONSE ANALYSIS

P Wang, P L Lewin and S J Sutton*
Electrical Power Engineering Group, Department of Electronics and Computer Science, University of Southampton, Southampton, SO17 1BJ, UK
*National Grid Company plc, National Grid House, Kirby Corner Road, Coventry, Warwickshire, CV4 8JY, UK

Accepted by IEEE Electrical Insulation Magazine

ABSTRACT

On-line partial discharge (PD) detection for high voltage cable systems is important as it ensures that possible faults can be detected and remedied before catastrophic failure occurs. Of growing interest is the use of non-conventional field coupling techniques to detect PD signals and the VHF capacitive coupler sensor is finding increasing application in PD detection systems due to its low cost, reliability and applicability to online detection. However, it has a major disadvantage as it is very difficult to quantify the sensor output voltage in terms of the conventional PD quantity, apparent charge. Proposed methods rely on pulse injection either at the cable termination or via another coupler in order to obtain a calibration ratio, these approaches have been assessed experimentally. In addition, frequency response (FR) measurements have been taken and used to generate a transfer function relating the coupler output to signals present on the cable core conductor. The transfer function has been used as the central component of a simulation model that estimates the calibration ratio. Good agreement has been achieved between the simulation model output and experimental results. PD tests have also been undertaken on a section of 66kV HV cable, containing an earthed needle within the cable dielectric. Obtained results have been compared with measurements using the conventional electrical detection method. Results indicate that a better estimation of reduced charge is possible using a frequency response measurement to provide coefficients for a simulation model than existing pulse injection calibration methods.

1.0 INTRODUCTION

Conventional partial discharge (PD) measurement as specified by IEC 60270[1] has been used as a tool for the quality control of HV cables for more than 50 years. With the introduction of polyethylene (PE) extruded cables into the power distribution sector in 1950s, a rapid development of PD detection techniques and testing standards to assess the reliability of these cables occurred. Recently PD measurements have been used not only by manufacturers but also by end-users in order to monitor cable condition during normal service. As conventional PD detection is not ideally suited to on-line monitoring, non-conventional field coupling PD detection techniques using sensors such as inductive couplers (high frequency current transducers) [2,3], directional couplers [4,5,6] and capacitive couplers have been developed. Capacitive coupler sensors have gained popularity and been widely used for PD detection [7-12] within HV cable systems. Capacitive couplers produce a signal due to the coupling between the sensor and the high frequency electrical field generated by PD sources during normal service conditions. The presence of a capacitive coupler does not affect the internal electrical field of the HV cable and it can easily be incorporated into the design of cable joints and terminations during manufacture. The capacitive coupler generally has a useful bandwidth of around 200MHz.

However, quantification of the measured output signal relating the signal magnitude in mV to the apparent discharge magnitude in pC of the PD source has yet to be satisfactorily established. The main reason is that the performance of capacitive couplers is related to several factors. These factors include coupler parameters such as its overall dimensions and shape, cable parameters such as its dimensions and dielectric properties as well as the unknown stray capacitance that will exist between the cable and the coupler due to its installation. The electrical parameters (permittivity and conductivity) of the semi-conducting layers of a high voltage cable are frequency dependent and vary significantly between different cables [13,14]. Consequently, any measured signal is sensor and cable specific and there is no general standard method for coupler calibration.

According to IEC 60270[1], for conventional PD measurement, calibrating pulses should be injected into the terminals of the test object with the additional requirement that the rise time of the calibrating pulse must be less than 60ns to ensure that the pulse is similar to that of a real PD source signal. The purpose of this calibration is to ensure that if two different systems are used to measure the same sample, they measure the same 'apparent PD magnitude', which is the charge transfer at the sample electrodes. Evolved from

conventional electrical PD measurement, the terminal injection method has been accepted as a useful approach for calibrating capacitive couplers. It involves the injection of a pulse into the cable terminal and measurement of the installed coupler output. Compared to conventional calibration there is a fundamentally different coupling mechanism between the injected pulse and the measured signal and a new calibration quantity called 'reduced charge' was introduced by Lemke and Schmiege in order to distinguish between the standard PD quantity 'apparent charge' and the calibration procedure applied to capacitive couplers [15]. However, 'reduced charge' does not identically correspond to 'apparent charge' when the same PD event is considered.

For online calibration, both terminals are generally not accessible, and alternative methods have been developed in order to determine calibration online. One method is the use of two couplers [12, 15, 16], where one coupler is used to inject a calibration pulse that is measured using the other coupler. This paper investigates possible on-line calibration methods used for capacitive couplers and compares the obtained results. The advantages and limitations as well as the sources of error are discussed in detail.

Models have been developed in order to analyse capacitive coupler performance. A lumped parameter model [16, 17] was initially proposed but due to the complexity of the sensor geometry, cable/cable joint geometry and the presence of semi-con PE layers obtained results were at best approximations. More accurate models can be achieved using electromagnetic theory and the Finite Difference Time Domain (FDTD)[18,19] method. The improved accuracy is because the effects of semi-con layers are considered and the calculation uses values obtained from measured results. However, it is based on ideal assumptions and is computationally intensive. Therefore, the development of a simulation model based on practical frequency response measurements has been considered.

Frequency response tests have been undertaken on capacitive couplers in order to determine their performance over their operational bandwidth. According to linear systems theory, this is an efficient experimental method to determine system behaviour when the theoretical model of the system is difficult to obtain. Approximated transfer function models can be obtained from analysis of the frequency response data. Using these transfer functions a simulation model has been established. There is very good agreement between the simulation model output and obtained experimental results. This has been extended to consider calibration based on a simulation model. Real partial discharge tests on a section of 66kV HV cable containing a known PD source show that it is possible to obtain a good

estimation of reduced charge when compared with apparent charge measurements using a conventional electrical PD detector.

2.0 CALIBRATION METHODS FOR CAPACITIVE COUPLERS

The capacitive coupler consists of an insulated metallic electrode placed between the outer semicon and the metallic earth sheath of a HV cable. The coupler electrode can either be a patch or completely wrap around the cable (Figure 1). The couplers used for these experiments were implemented on a section of 66kV XLPE cable. The cable has a core conductor, inner and outer semi-conducting layers, insulation and outer sheath. The capacitive coupler sensor was placed on the outer semi-con layer and consisted of an insulation layer (PE film), the electrode (tin tape) and a dielectric substrate (bubble wrap) above the electrode. The sensor is completely covered by the outer earth sheath of the HV cable in order to keep the integrity of the cable coaxial structure and minimize the effect of any external noise on the measurement signal.

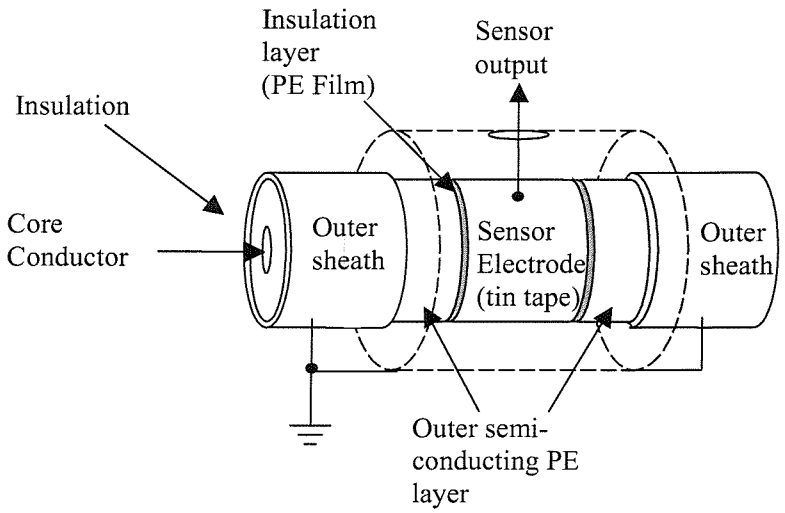

Figure 1 Capacitive coupler construction

A simplified lumped parameter equivalent circuit of the cable and coupler is shown in Figure 2, where CC is the capacitance between the coupler and cable inner conductor, Z0 is the cable characteristic impedance, CS is the stray capacitance between the coupler electrode and the cable sheath and RM is the input impedance of the digital oscilloscope (50Ω). The stray capacitance is unknown and will be different at each coupler installation, consequently practical calibration is required in order to quantify the magnitude of any detected discharge event.

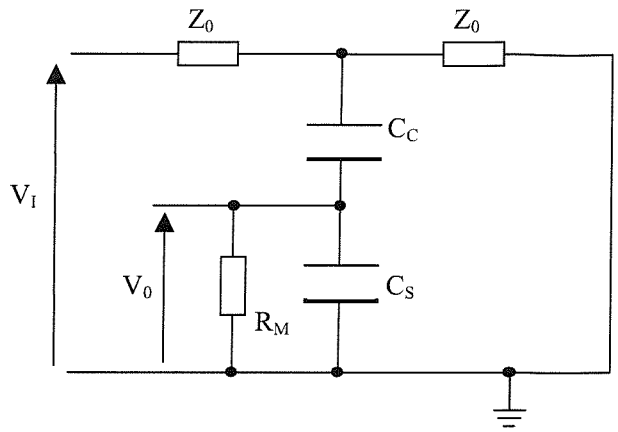

Figure 2 Lumped parameter equivalent circuit of cable and capacitive coupler

2.1 The terminal injection method

This method has been directly evolved from conventional PD measurement and has been widely accepted as a method for calibration of capacitive couplers. Its main disadvantage is that it can only be implemented under laboratory conditions and is therefore unsuitable for online calibration. The terminal injection calibration method and its model are shown in Figure 3. In this case C0 is the injection capacitance, CX is the capacitance of the whole cable and ZM is a matching resistance to ensure that the input impedance of the circuit is 50Ω. In the experiment, a 2.96m length of 66kV XLPE cable was terminated with its characteristic impedance, Z0, and a coupler installed 0.62m from the injection terminal of the cable was connected to a digital oscilloscope having an input impedance of 50Ω. A known charge was injected into the core conductor of the cable via an injection capacitor, C0, by applying a step change in voltage using a pulse generator. According to IEC 60270[1], under the condition that the capacitance of the test object (CX) is much greater than the injection capacitance, C0, then the injected charge can be calculated as:

$$Q_1 = C_X V_X \tag{1}$$

Where the voltage VX can be determined from

$$V_X = V_I \frac{C_0}{C_0 + C_X} \tag{2}$$

VI is the magnitude of the step change voltage applied to the injection capacitor. Hence by combining Equations 1 and 2 and assuming that CX is very large compared to C0 an approximation for injected charge can be determined i.e.

$$Q_I = C_X V_I \frac{C_0}{C_0 + C_X} = V_I \frac{C_0}{\frac{C_0}{C_X} + 1} \approx C_0 V_I \qquad (3)$$

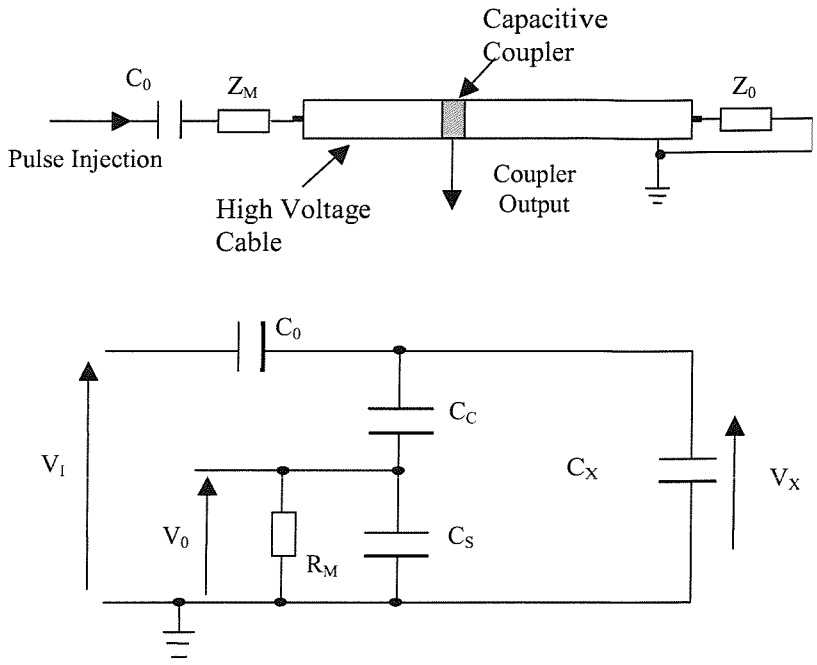

Figure 3 Experimental arrangement and model for terminal injection

Obtained calibration measurements for a 20mm wide coupler are shown in Figure 4, for a range of injected charge from 20pC to 96pC. This gives a calibration ratio of 0.517 pCmV-1, for an identical experimental arrangement any on-line method should determine a similar calibration ratio.

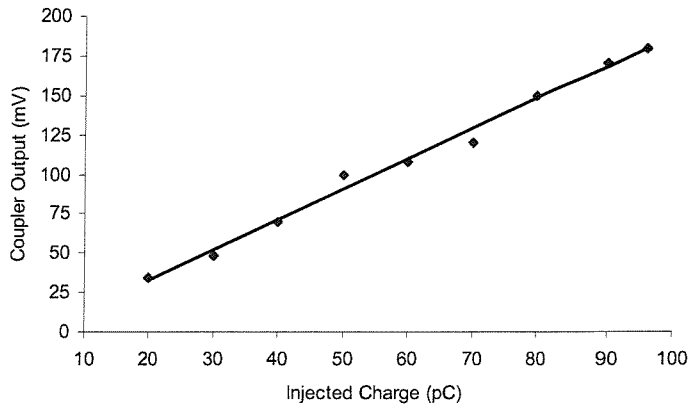

Figure 4 Terminal injection calibration results using a 10pF injection capacitance and a pulse with a 1ns rise time.

2.2 Coupler Injection

For on-line calibration, as both terminals are not accessible, alternative methods have been developed in order to establish a relationship between measured voltage and discharge magnitude. One approach is to use two couplers, one acting as an injection coupler and the other as a measurement coupler. The coupler injection method and its model are shown in Figure 5. Where CC1 and CC2 are the capacitances of the measurement and injection coupler respectively, each coupler also has an associated stray capacitance (CS1, CS2). Assuming that the capacitance of the cable under test is significantly larger than the capacitance of the injection capacitor and that stray capacitance can be ignored, then the injected charge, Q2, can be estimated as:

$$Q_2 = C_X V_X \approx \frac{C_X C_{C2}}{C_X + C_{C2}} V_I = \frac{C_{C2}}{1 + \frac{C_{C2}}{C_X}} V_I \approx C_{C2} V_I \tag{4}$$

The capacitance of the injection coupler can be determined from the capacitance per unit length of the cable under test i.e.

$$C_{C2} = \frac{2\pi\pi_0\varepsilon_r}{\ln\left(\frac{D_2}{D_1}\right)} 1 \tag{5}$$

Where L is the length of the coupler (20mm in this case), ε0 is the dielectric constant (8.86×10-12 Fm-1), εr is the relative dielectric constant of the insulating material (assumed to be 2.3 for XLPE), D2 is the outer diameter of the insulation, (54mm in this case) and D1 is the outer diameter of the conductor (22.5mm). Therefore, the capacitance per unit length of the 66kV XLPE cable is 146 pFm-1. The capacitance of coupler C2 is therefore 2.92pF. In order to obtain a calibration ratio the 20mm long couplers were implemented on the cable 620mm apart with the measurement coupler 620mm distant from one end of the cable. The obtained calibration measurements are shown in Figure 6 for a range of injected charge from 5.84 to 28.03pC and the corresponding calibration ratio is 1.148 pCmV-1. This does not compare favourably with the value obtained by terminal injection due to the assumptions made; in particular stray capacitances are ignored and the frequency dependent characteristics of the two semi-conducting polyethylene layers are not taken into consideration at all.

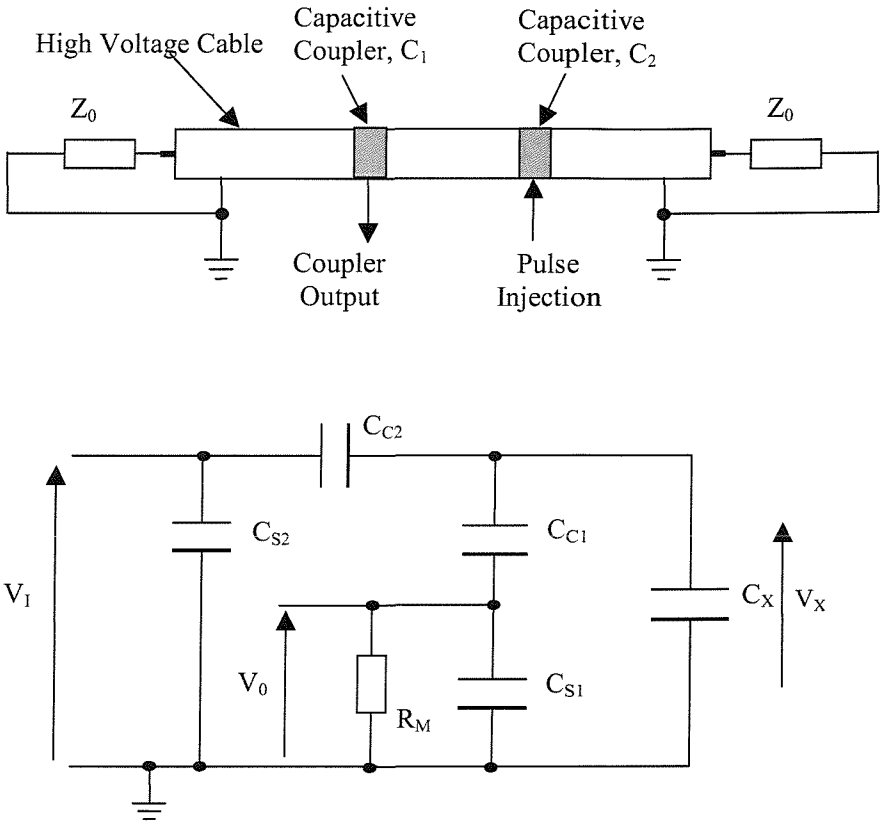

Figure 5 Experimental arrangement and model for coupler injection

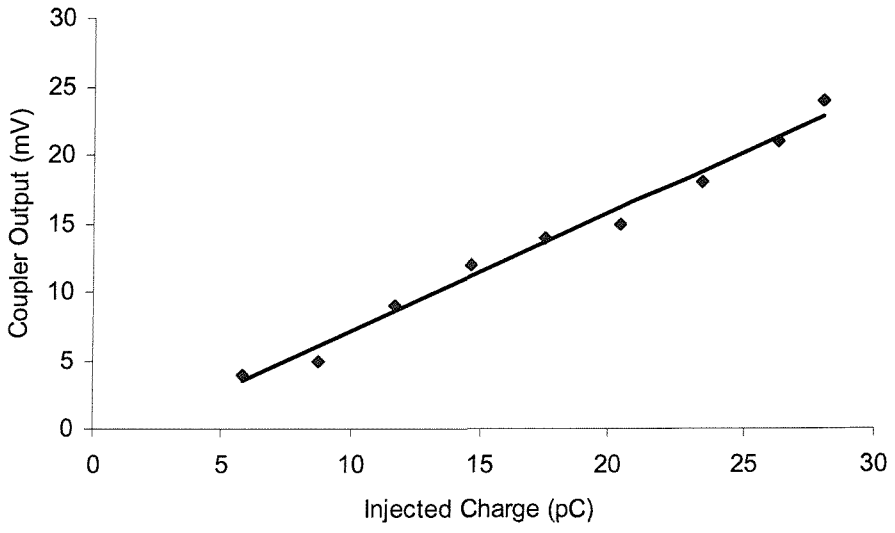

Figure 6 Coupler injection calibration results using a pulse with a 1ns rise time

2.3 Coupler Injection with Capacitor Injection

This method is a modification of the coupler injection method and comprises of two experiments. Firstly a pulse is injected directly into the injection coupler as per section 2.2 and secondly the pulse is injected into the injection coupler via an injection capacitor (C0) a shown in Figure 7. With the additional injection capacitor and assuming that the cable capacitance is very large compared to the coupler capacitance the injected charge is defined as

$$Q_3 = C_X V_X \approx \frac{C_X C_{C2}}{C_X + C_{C2}} V_S = \frac{C_X C_{C2}}{(C_X + C_{C2})} \frac{C_0}{\left(C_0 + C_{S2} + \frac{C_X C_{C2}}{C_X + C_{C2}} \right)} V_I \approx \frac{C_{C2} C_0}{C_0 + C_{S2} + C_{C2}} V_I \tag{6}$$

Considered on its own it is impossible to use Equation 6 to evaluate the injected charge, as the stray capacitance, CS2 is unknown and CC2 cannot be determined accurately. However, combined with results obtained by direct injection into the injection capacitor it is possible to determine an experimental value for CC2.

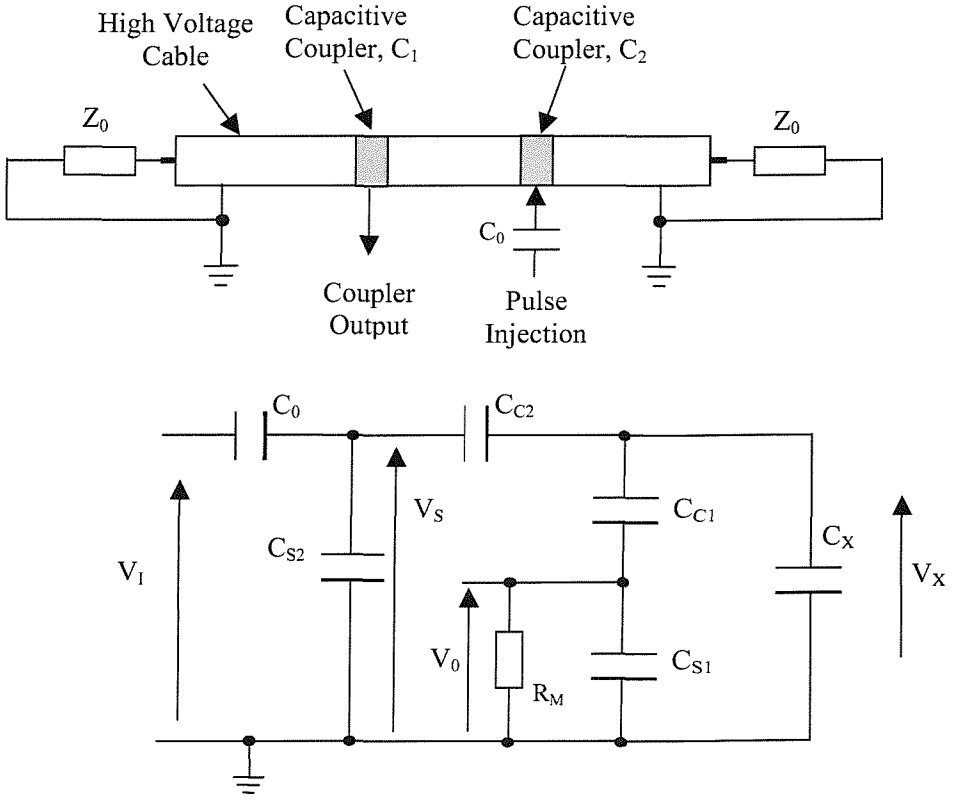

Figure 7 Experimental arrangement and model for coupler plus capacitor injection

Consider the application of a step change voltage, VI, directly to the injection coupler that produces a peak voltage, V2, at the output of the measurement coupler. From Equation 4 the calibration ratio, k, is defined as

$$k = \frac{C_{C2} V_I}{V_2} \tag{7}$$

If the experiment is repeated with an injection capacitor placed between the coupler and the voltage source, such that an identical step change voltage produces a peak voltage, V_3, at the output of the measurement coupler, then from Equation 6 the calibration ratio, k, is defined as

$$k = \frac{C_0 C_{C2} V_I}{(C_0 + C_{S2} + C_{C2}) V_3} \tag{8}$$

Equating Equations 7 and 8, yields an expression for the coupler capacitance in terms of the two measured peak voltages, the known injection capacitance and the unknown stray capacitance, i.e.

$$C_{C2} = C_0 \left(\frac{V_2}{V_3} - 1 \right) - C_{S2} \tag{9}$$

Assuming that the stray capacitance is small enough to be ignored, then the injection coupler capacitance can be determined and the calibration ratio calculated using either Equation 7 or 8. Figure 8 shows the results obtained using a 10pF injection capacitor, applying a step voltage input with a rise time of 1ns and using the same coupler arrangement as described in the previous section. The obtained calibration coefficient is 1.465 pCmV-1, this value is nearly three times greater than that determined using the terminal injection method. Experiments using a range of injection capacitor values have been undertaken and under identical experimental conditions each produces a different value of calibration coefficient.

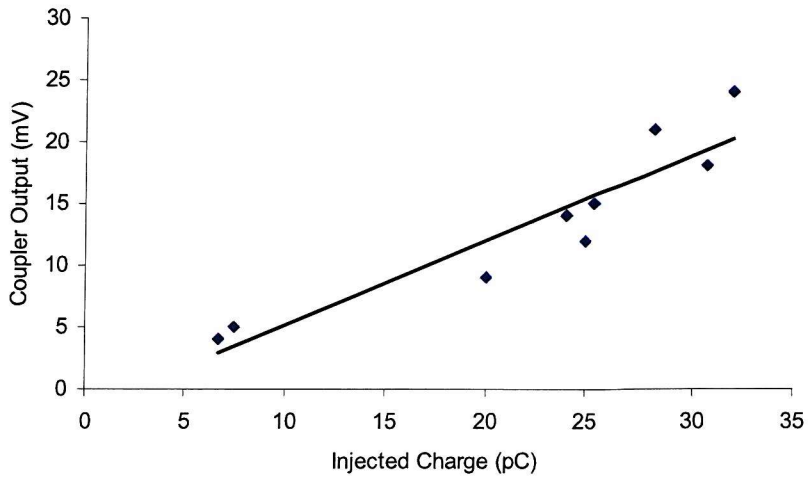

Figure 8 Coupler plus capacitor injection results using a pulse with a 1ns rise time

The coupler injection methods are generally unsatisfactory because the coupler capacitance cannot be accurately determined either by using Equation 5, which takes no account of the existence of the semiconducting polyethelene layers, or experimentally by a method that ignores stray capacitances possibly of the same order as the coupler capacitance and/or injection capacitor. The lumped parameter equivalent circuit approach is limited in its application and can at best approximate the behaviour of the capacitive coupler sensor.

3.0 FREQUENCY RESPONSE ANALYSIS OF CAPACITIVE COUPLERS

Frequency response measurements on the cable and coupler arrangement have been undertaken in order to experimentally determine the frequency dependent behaviour of the system under test. The principle of the frequency response test to determine system behaviour is simple; the system is treated as a 'black box' and a sinusoidal signal of varying frequency is applied to the system input and the corresponding system output is measured in terms of both magnitude and phase relative to the input. The system gain is then calculated at each frequency as the ratio of output magnitude and the input magnitude. Results are plotted either as a Nyquist diagram or as a Bode diagram, from which a model expressed in the form of a transfer function can be derived [20]. In order to obtain an accurate model, it must be assumed that the system under test is both linear and time invariant.

The frequency response tests were undertaken on the same section of 66kV XLPE cable and couplers as used for the calibration experiment. An Agilent 4395A Network Analyser was used to determine the frequency response of the system over the range 500Hz to 500MHz. As with the terminal injection calibration method a matching impedance was used to ensure that the input impedance of the circuit was 50Ω and to minimise any signal reflection the other end of the cable was terminated with its characteristic impedance. For coupler to coupler frequency response measurements both ends of the cable were terminated via its characteristic impedance to ground. The two couplers both 20mm long were positioned 620mm apart with the measurement coupler (coupler 1) 620mm distant from the injection terminal. Obtained results are shown in Figure 9. The frequency response between the terminal and coupler 1 (T-C1, Figure 9) indicates that the coupler acts as a high pass filter for frequencies greater than 10MHz. Over the lower frequency range the data is contaminated by noise, mainly because the 4395A Network Analyser noise level (-85dB) in low frequency range is similar to or greater than the true data. The coupler to coupler

frequency response (C1-C2, Figure 9) also exhibits a high pass filter characteristic, again measurement noise below 10kHz has corrupted the data. Assuming that the system is linear time invariant, the couplers are identical and that the attenuation of signals by the cable over a distance of a meter is negligible, then at a given frequency the coupler to coupler response should be double the magnitude (in dB) of the terminal to coupler response. Figure 9 includes a plot of the halved coupler to coupler frequency response and for frequencies above 10MHz there is good agreement with the terminal to coupler frequency response. This infers that it is possible to approximate the terminal to coupler frequency response by analysis of an experimental measurement of the frequency response between two identical couplers installed up to a few metres apart on a test cable.

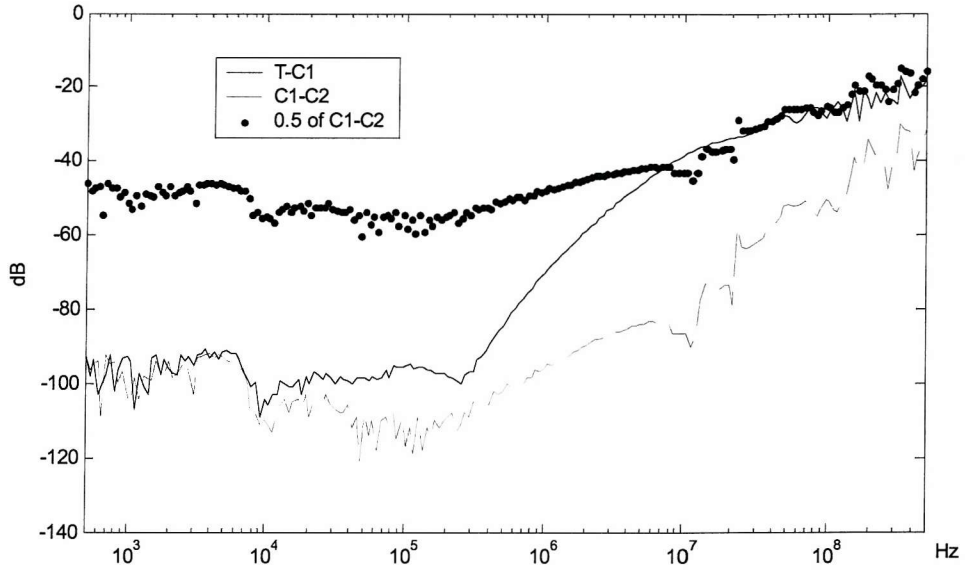

Figure 9 Frequency response measurements; terminal to coupler 1 and coupler 1 to coupler 2

3.1 Calibration Based on Frequency Response Analysis

It is possible to model the system by using transfer functions derived from analysis of the frequency response data. The complexity of the transfer function is determined by the required accuracy of any given model. If considering general trends then the terminal to coupler frequency response can be approximated to a first order system containing a low frequency zero, a high frequency pole and a scalar gain, i.e.

$$H(\omega) = \frac{G\left(1+\frac{j\omega}{\omega_Z}\right)}{\left(1+\frac{j\omega}{\omega_P}\right)} \tag{10}$$

Consequently, the system response can be described by the three parameters G, ω_Z and ω_P. From the terminal to coupler results it is possible to define the corner frequencies of the pole and zero as 200MHz and 200kHz respectively. It is more difficult to define the scalar gain, due to the high levels of measurement noise at low frequencies, however by comparing the experimental terminal injection output waveform with the transfer function output for the same input data it is possible to find a best fit value for G. G is varied over a range of suitable values, the mean square error over the whole output waveform and the percentage difference in peak output value are determined for each value of G (Figure 10). In this case the best fit value of G is -78dB or $1.259.10^{-4}$. Therefore the frequency response between the terminal and coupler can be approximated as

$$H(\omega) = \frac{1.259.10^{-4}\left(1+\frac{j\omega}{4\pi.10^{5}}\right)}{\left(1+\frac{j\omega}{4\pi.10^{8}}\right)} \tag{11}$$

The model has been used to simulate the output of the coupler for a given signal injected into the termination and obtained results are in very good agreement. A typical result is shown in Figure 11, the model does not account for signal reflection but does closely match the initial response of the coupler.

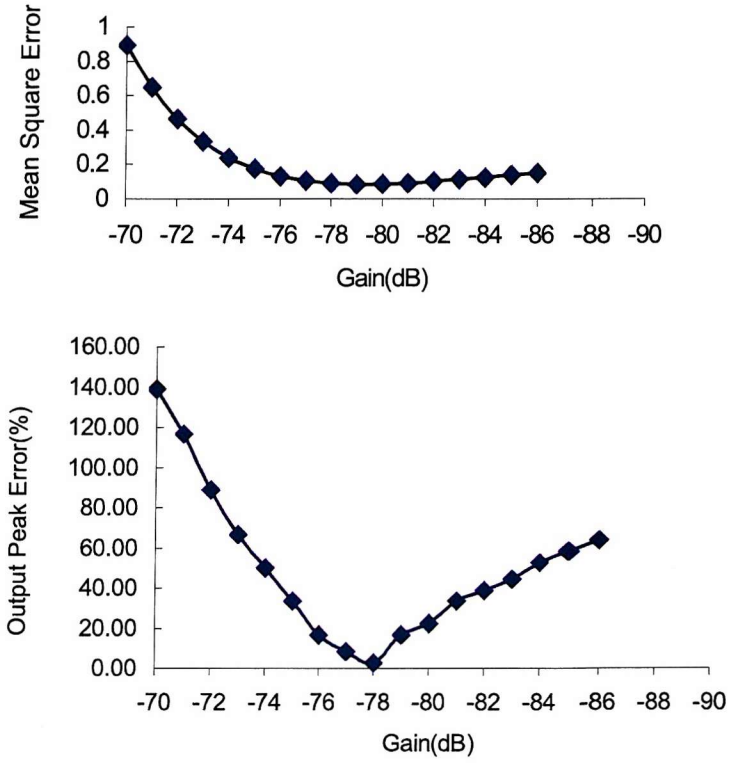

Figure 10 MSE and output peak error plots for a range of scalar gain, G.

Using the model it is possible to generate a calibration ratio through simulating a range of input pulses and calculating the corresponding peak output of the coupler, results in a calibration ratio of 0.542 $pCmV^{-1}$ that is very similar to the value obtained experimentally (Figure 12).

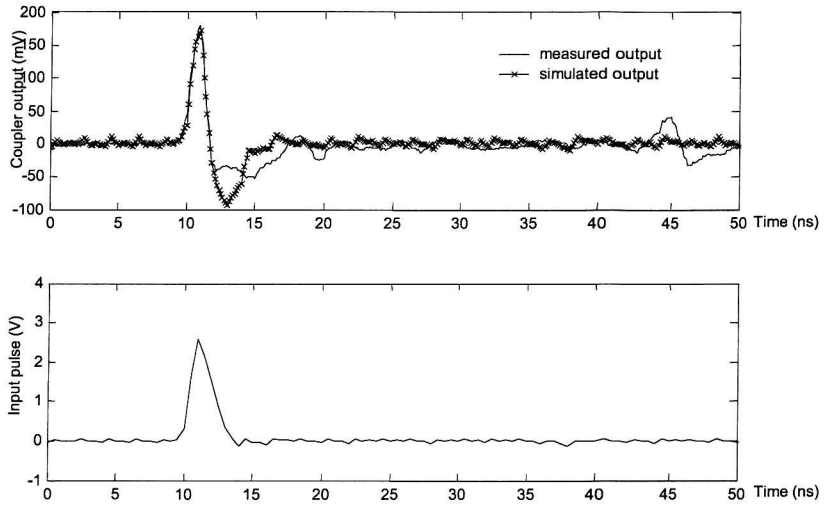

Figure 11 Simulated coupler output compared with experimental measurement for a terminal injection pulse of 96pC

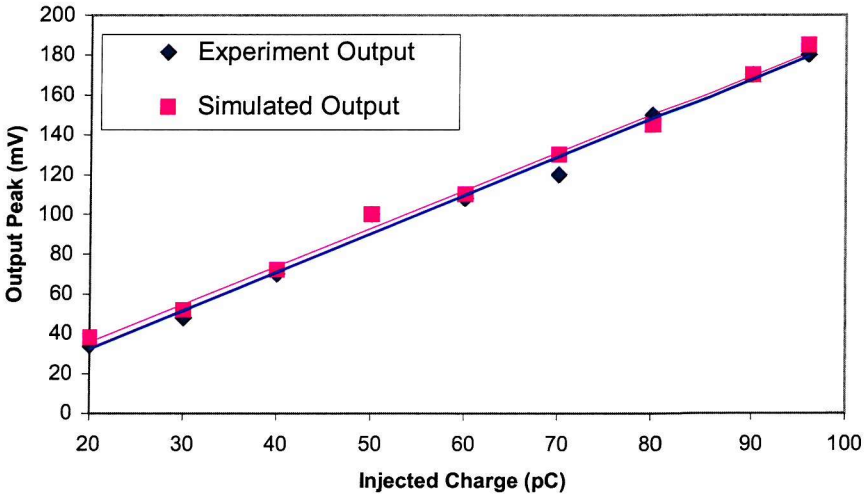

Figure 12 Comparison of simulated calibration with experimental terminal injection calibration

3.2 Using the coupler to coupler frequency response to generate a model representing terminal to coupler behaviour

Having established that a reduced order model can effectively represent terminal to coupler behaviour, the possibility of deriving a terminal to coupler model based on analysis of the coupler to coupler frequency response has been investigated. Figure 9 shows the coupler to coupler frequency response along with its halved value, there is reasonable agreement between the terminal to coupler response and the halved coupler to coupler response at higher frequencies. An approximate model of the form described by Equation 10 has been defined as follows:

- ω_P is defined as the high frequency above which the magnitude of the coupler to coupler frequency response is reasonably constant.
- ω_Z is defined as the low frequency above which the magnitude of the coupler to coupler frequency response starts to increase.
- G is then chosen such that for higher frequencies the magnitude of the approximate model frequency response matches the halved coupler to coupler frequency response.

Applying these rules using the frequency responses shown in Figure 9 gives an approximate model, $H_a(\omega)$, of

$$H_a(\omega) = \frac{1.778.10^{-4}\left(1+\frac{j\omega}{4\pi.10^5}\right)}{\left(1+\frac{j\omega}{2\pi.10^8}\right)} \tag{12}$$

This in turn produces a calibration ratio of $0.589 pCmV^{-1}$ as shown in Figure 13.

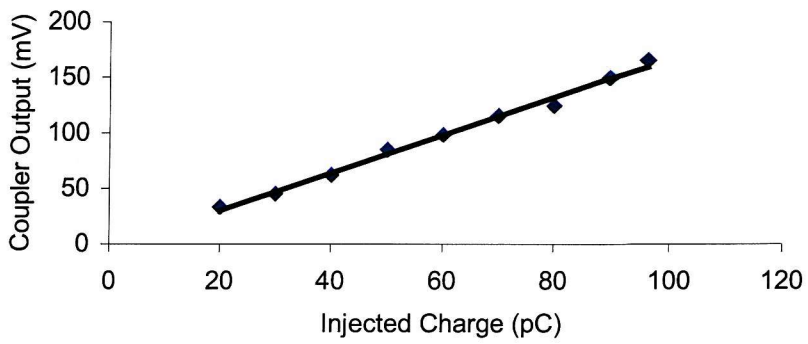

Figure 13 Simulation results using an approximate model based on the coupler to coupler frequency response

3.3 Summary

Various approaches of determining a calibration ratio for a capacitive coupler have been investigated experimentally and the values obtained for one experimental arrangement are shown in Table 1. It can be seen that a model based on the frequency response from the terminal to coupler produces a calibration ratio that is very close to the value obtained using the terminal injection method. By approximating the model using data from the coupler to coupler frequency response a similar calibration ratio can be achieved and results in a far more accurate estimate of the reduced charge measured at the coupler than using pulse injection methods to determine the sensitivity of the measurement.

Table 1 Calibration Ratios

Method	Calibration ratio ($pCmV^{-1}$)	%age change from terminal injection
Terminal injection	0.517	-
Coupler injection	1.148	122
Coupler/capacitor injection	1.465	183
Terminal-coupler simulation	0.542	4.8
Approximate model simulation	0.589	13.9

4.0 PRACTICAL PD MEASUREMENT

In order to establish the feasibility of using an approximate simulation model to estimate the calibration ratio for a capacitive coupler used for on-line PD measurement, experiments have been undertaken on a short length of 66kV XLPE cable containing a known PD source (Figure 14). A 3.5m length of cable terminated with de-ionised water terminations has an earthed tungsten needle with a 1mm shank diameter and 3μm pin tip radius inserted into the cable insulation to within 3mm of the cable core conductor. Two couplers, with the same dimensions as used in the previous experiment have been installed on the cable 760mm (C_1) and 100mm (C_2) from the needle respectively. The measurement apparatus is installed in a control room distant from the cable loop, consequently the signals from the couplers pass through overvoltage protection before being amplified using 22dB broadband amplifiers and captured using the digital storage oscilloscope. Conventional electrical PD detection

according to IEC 60270 [1] using a Robinson model 5 type 700 detector was also applied in order to determine the apparent charge of any PD activity and allow comparison with results obtained using the two couplers.

Experiments revealed that the deionised water terminations significantly attenuate any injected high frequency thus making calibration of the couplers using the terminal injection method impossible and therefore the simulation model was used to determine an estimate of the calibration coefficient. Two coupler to coupler frequency responses were obtained using the Agilent 4395A Network Analyser over the range 500Hz to 500MHz, one response for the coupler to coupler only and the other one for a circuit that also included the overvoltage protector and 22dB broadband amplifier connected to the output of the measurement coupler (Figure 15).

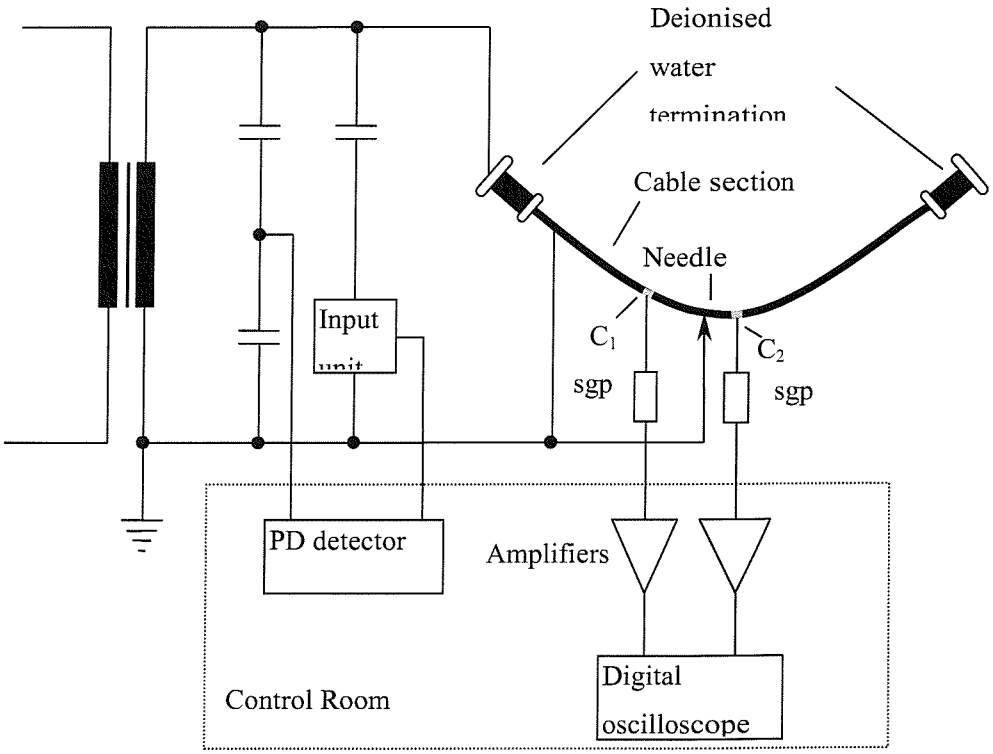

Figure 14 Test arrangement for a HV cable containing an earthed needle

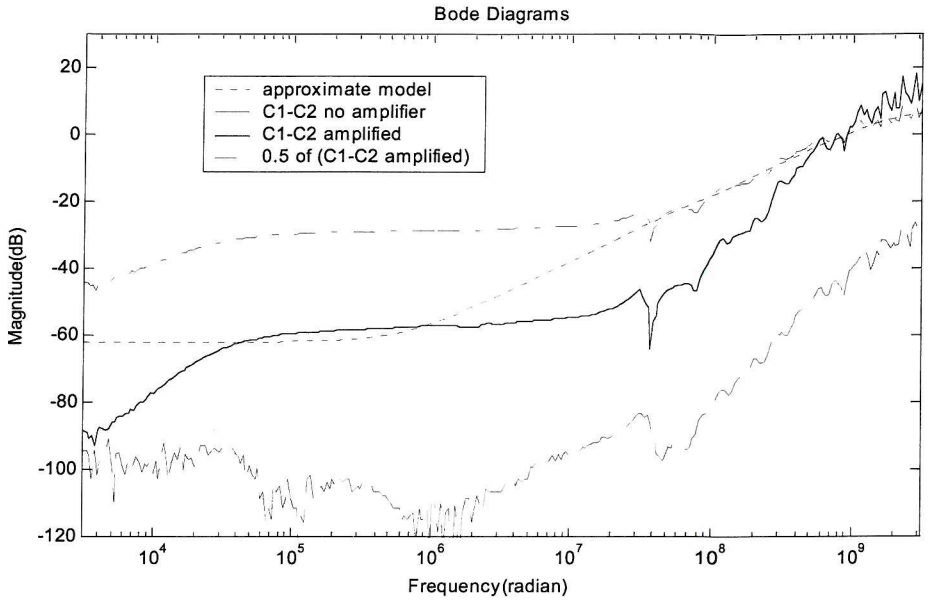

Figure 15 Coupler to coupler frequency response measurements and approximate model characteristic.

The three variables for the approximate model were defined as follows:

- ω_P was defined as the high frequency above which the magnitude of the halved amplified coupler to coupler frequency response is reasonably constant.
- ω_Z was defined as the low frequency above which the magnitude of the coupler to coupler frequency response starts to increase.
- G was then chosen such that for higher frequencies the magnitude of the approximate model frequency response matches the halved amplified coupler to coupler frequency response.

This gave an approximate model for the terminal to coupler frequency response of

$$H_a(\omega) = \frac{7.943.10^{-4}\left(1+\frac{j\omega}{2\pi.10^5}\right)}{\left(1+\frac{j\omega}{6\pi.10^8}\right)} \tag{13}$$

which yields a calibration ratio of $0.0369 pCmV^{-1}$. The effect on both the calibration ratio and the choice of scalar gain, G, for variations in the chosen values of ω_P and ω_Z has been investigated and obtained results are shown in Figure 16. Results obtained indicate that by adjusting the value of G to match the halved frequency response the model produces a similar estimate of calibration ratio for a reasonable range of both ω_P and ω_Z.

To calibrate the conventional electrical PD detector a low frequency calibration pulse equivalent to 50pC was injected into one of the deionised water terminations. AC high voltage was then applied to the cable loop at increasing magnitudes until regular PD activity

was observed. The PD inception voltage was 9kV and Figure 17 shows typical measurements obtained from Coupler 1 and the conventional electrical PD detector. Comparing the results obtained from both couplers revealed that there was a time of flight of approximately 4ns between the two signals, thus identical couplers can be used to estimate the location of the PD source, the propogation velocity of the PD signal and indicate the reduced charge. With reference to Figure 17 for an applied voltage of 11.08kV the Robinson Detector gives an apparent PD magnitude of 4.7pC whereas the coupler value is 3.7pC, increasing the applied voltage to 14kV produces PD of 9pC according to conventional detection and a value of 4.7pC from the coupler measurement.

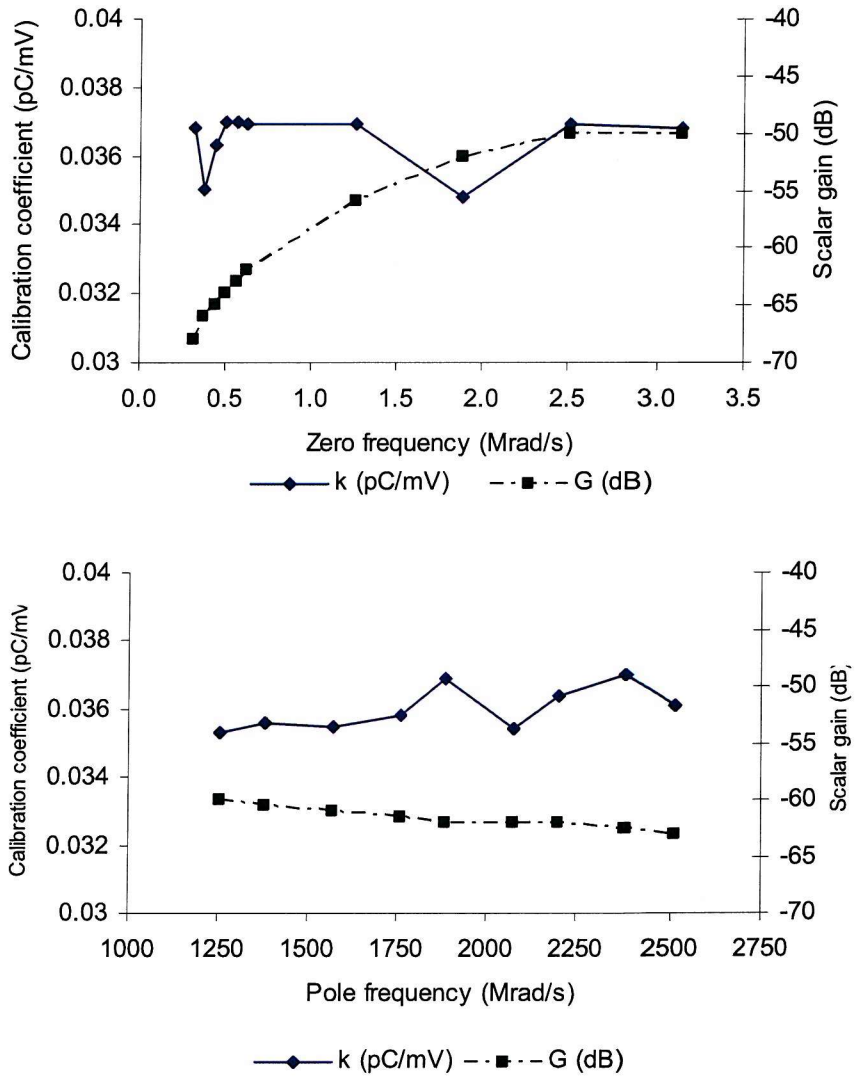

Figure 16 Variation in both calibration coefficient and scalar gain for a range of estimates of the zero corner frequency and pole corner frequency

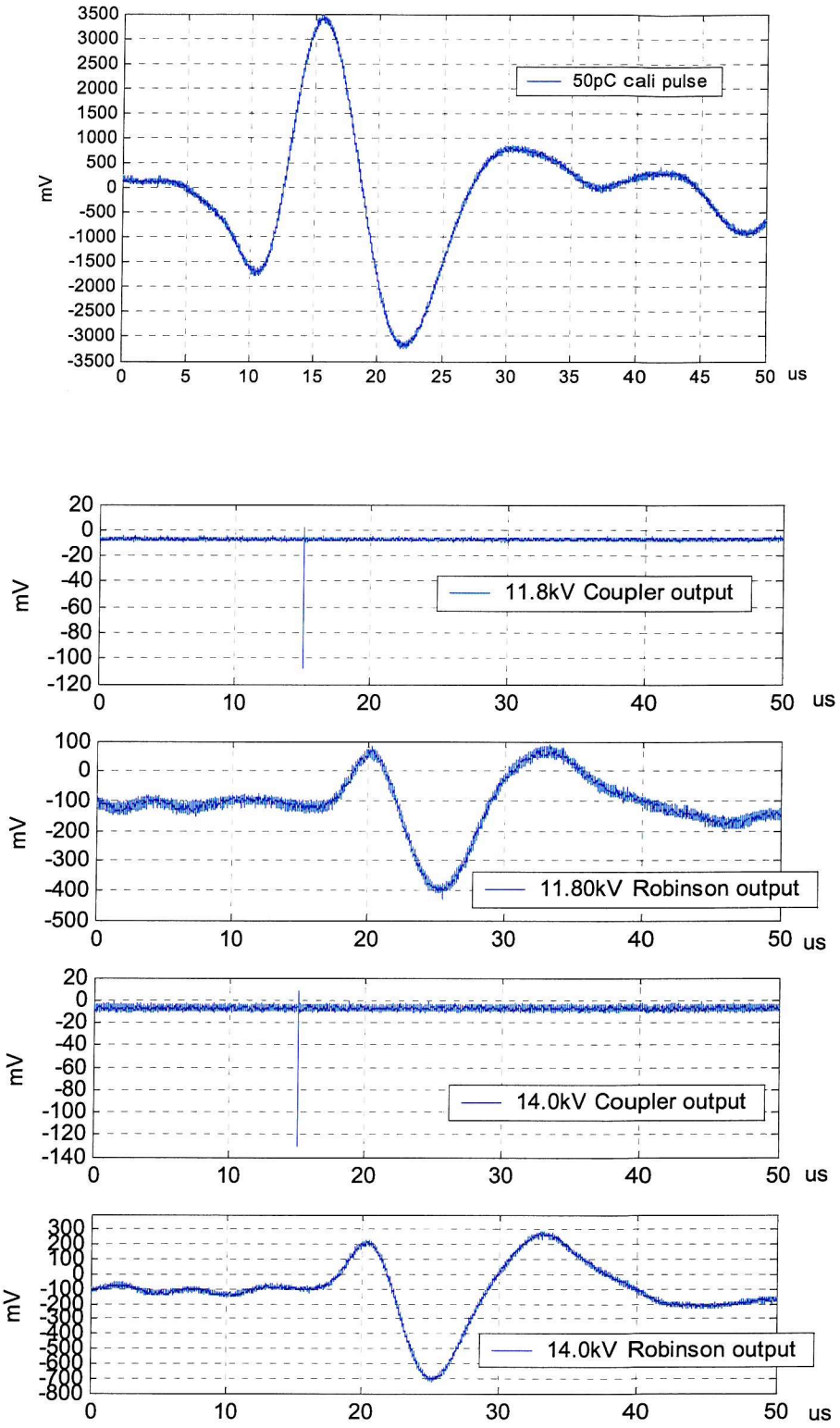

Figure 17 Conventional calibration pulse and PD measurements

The calibration ratio determined from the estimated model yields charge values for coupler signals that are smaller than the conventional apparent charge measured using the Robinson detector. Differences are due to the detection systems coupling mechanisms and the frequency response range of each measurement. For narrow-band conventional PD coupling, PD signals are detected with a bandwidth of 100kHz or less and the PD detector acts as a low pass filter or integrator [21]. While for VHF capacitive couplers, PD pulses are directly coupled to the coupler with a bandwidth range from a few hundred kHz to a few hundreds of MHz as can be seen from frequency response measurements (Figures 9 and 15). However for online calibration, the simulation method provides a reasonable estimate of the reduced charge. For many on-line applications the PD measurement trend over a time interval is more important than absolute charge values [22].

5.0 CONCLUSIONS

Possible on-line quantification and calibration methods for capacitive couplers have been investigated experimentally. Evolved from the conventional electrical method, the terminal injection method for calibration of capacitive couplers has been accepted as a standard approach. However, for online on-site calibration alternative methods that approximate to the terminal injection method have to be used because the terminals are generally either not accessible or are too distant from the sensor.

Calibration methods using two couplers have been investigated as possible alternative methods to terminal injection. These methods are based on equivalent circuit lumped parameter models that do not truly represent the behaviour of the system due to the frequency dependence of some parameters and the existence of unknowns such as stray capacitance. Therefore obtained results are not in agreement with values obtained using the terminal injection method and the resulting error is large.

The behaviour of capacitive couplers installed on a specific cable arrangement can be determined through frequency response measurements. It is an efficient experimental method when the theoretical model of a system is difficult to define. A coupler/cable model expressed in the form of transfer function has been established based on analysis of coupler to coupler frequency response measurements. Good agreement has been achieved between the calibration ratio determined using the transfer function and that derived from experimental terminal injection measurements.

Real PD tests have been undertaken on a high voltage cable containing an earthed needle within its bulk insulation. The measured results from two capacitive couplers can provide PD site location, the propagation velocity of the PD signal and estimate the attenuation of the PD pulse. A transfer function determined from frequency response measurements provided an estimate of the calibration ratio for the couplers and resulting PD magnitudes are less than those obtained using conventional electrical PD detection. However these values reflect the reduced charge measured at the sensor, further work will investigate data processing techniques that will determine the apparent magnitude of the discharge taking into account signal attenuation from the discharge source to the points of measurement.

6.0 ACKNOWLEDGEMENTS

The financial support and permission to publish from the National Grid Company is greatly appreciated for this project. This paper is dedicated to the memory of Professor Tony Davies.

REFERENCES

1. IEC 60270, High-voltage Test Techniques - Partial Discharge Measurements, Third edition 2000.
2. N. H. Ahmed and N. N. Srinivas, "Online Partial Discharge Detection in HV Cables", IEEE Transaction on Dielectrics and Electrical Insulation, Vol. 5 No. 2, April 1998.
3. Th. Heizmann, Th. Aschwanden, H. Hahn, M. Laurent and L. Ritter " On-site Partial Discharge Measurements on Premoulded Cross-Bonding Joints of 170kV XLPE and EPR Cables", IEEE Transactions on Power Delivery, Vol. 13, No. 2, April 1998, pp330-335.
4. D. Pommerenke, T. Strehl, R. Heinrich, W.Kalkner, F.Schmidt and W. WeiBenberg, "Discrimination between Internal PD and Other Pulse Using Directional Coupling Sensors on HV Cable Systems", IEEE Transactions on Dielectrics and Electrical Insulation, Vol. 6 No. 6, December 1999.
5. D. Pommerenke and Keith Masterson, "A Novel Concept For Monitoring Partial Discharge on EHV-cable System Accessories Using no Active Components at the Accessories", Dielectric Material, Measurements and Applications Conference Publication No. 473, IEE 2000.

6. E. Lemke, T. Strehl and D. RuBwurm, "New Development in the Field of PD Detection and Location in Power Cables under On-site Condition", 11th International Symposium on High Voltage Engineering, 22-27, August 1999, 5.106-5.111, London.
7. R. Bartnikas, "Partial Discharges Their Mechanism, Detection and Measurement", IEEE Transaction on Dielectrics and Electrical Insulation, Vol. 9 No. 5, October 2002, pp763-808.
8. K. Fukunage, M. Tan and H. Takehana, "New Partial Discharge Detection Method for Live UHV/EHV Cable Joints," IEEE Transactions on Electrical Insulation, Vol. 27 No. 3 June 1992.
9. R. Morin, R. Bartnikas and G. Lessard, "In-service Location of Partial Discharge Sites in Polymeric Distribution Cables using Capacitive and Inductive Probes," IEEE Transmission and Distribution Conference, IEEE Piscataway, NJ, USA, 1999; Vol. 1 pp120-7.
10. Katsuta Ginzo, Atsushi Toys, Keiichi Muraoka, Takeshi Endoh, Yasuo Sekii and Chuki Ikeda, "Development of Partial Discharge Detection in Extra-High Voltage Cross-Linked Polyethylene Insulated Cable Lines," IEEE Transactions on Power Delivery, Vol. 7, No. 3 July 1992.
11. E. Lemke and Schmiegel P., "Progress in PD-probe Measuring Techniques," 7th International Symposium on High Voltage Engineering, August 26-30, 1991.
12. Y. Tian, P.L. Lewin, A.E.Davies, S.G.Swingler, S.J.Sutton and G.M. Hathaway, "Comparison of On-line Partial Discharge Detection Methods for HV Cable Joints" IEEE Transactions on Dielectrics and Electrical Insulation, Vol. 9 No. 4, August 2002.
13. S.A. Boggs, A. Pathak, and P. Walker, "Partial Discharge XXII: High Frequency Attenuation in Shielded Solid Dielectric Power Cable and Implications Thereof for PD Location," IEEE Electrical Insulation Magazine, Vol.12, January/February 1996,pp.9-16.
14. S. A. Boggs and G. C. Stone, "Fundamental Limitations in Measurement of Corona and Partial Dicharge", IEEE Transaction on Electrical Insulation Vol. EI-17 No. 2, April 1982, pp143-150.
15. E. Lemke. and Schmiegel P., "Fundamentals of the PD Probe Measuring Technique" LEMKE DIAGNOSTICS GmbH, Dresden, German (1993).
16. Y. Tian, "Partial Discharge Detection in Cable Systems," Ph.D Thesis, University of Southampton, Department of Electronics and Computer Science, 2001.
17. L. Zhong, Y Xu, G. Chen, A.E. Davies, Z. Richardson and S.G. Swingler, "Use of Capacitive Couplers for Partial Discharge Measurements in Power Cables and Joints" 2001 IEEE 7th International Conference on Solid Dielectrics, June 25-29, 2001, Eindhoven, the Netherlands.

18. R. Heinrich, R. Jobava, W. Kalkner and A. Gheonjian, "Numerical Modelling for Investigation and Optimisation of a Sensor for Sensitive Partial Discharge Detection on High-Voltage XLPE Cables" ETEP Vol. 10 No. 3, May/June 2000.
19. D. Pommerenke, R. Jobava and R. Heinrich, "Electromagnetic Finite Differences Time Domain (FDTD) Modelling of Partial discharge Coupling Applied to High Voltage Cables and Cable Joints", Dielectric Materials, Measurements and Applications, Conference Publication No. 473, IEE 2000.
20. Dutton K., Thompson S. and Barraclough B. "The Art of Control Engineering", England: Addison-Wesley (1997).
21. S.A. Boggs and John Densley, "Fundamentals of Partial Discharge in the Context of Field Cable Testing", IEEE Electrical Insulation Magazine, Vol. 16, No. 5 September/October 2000.
22. S. Zollner and E. Lemke, "On the evaluation of the PD Quantity Apparent Charge with Respect to PD Probe Measurement", 7th International Symposium on High Voltage Engineering, August 26-30,1991, 87-90, Vol. 7, Dresden, Germany.

Appendix 2

MODELLING OF CAPACITIVE COUPLERS THROUGH FREQUENCY RESPONSE ANALYSIS FOR PD ONLINE DETECTION IN HV CABLES

P Wang, P L Lewin, Y Tian, S J Sutton* and S G Swingler*

Electrical Power Engineering Group, Department of Electronics and Computer Science, University of Southampton, Southampton, SO17 1BJ

*National Grid, Surrey, KT22 7ST

Published in The 2nd International Conference on Insulation Condition Monitoring of Electrical Plant, October 27-30, 2003, University of Chongqing, Chongqing, China

ABSTRACT

Partial Discharge (PD) online detection is of increasing importance to condition monitoring of HV cables. PD online detection using non-conventional field coupling techniques i.e. VHF capacitive coupling is finding increasing application due to its low cost and applicability to online measurement. The performance of the capacitive coupler varies with many factors and its theoretical model is difficult to obtain. Frequency response (FR) tests have been undertaken in order to determine the performance of the capacitive coupler experimentally. The results show for a specific coupler installed on a section of 66kV power cable that there is good performance over a wide range of frequency (0-500MHz). An approximate simulation model based on system theory and FR analysis has been established. Good agreement has been achieved between the simulation model and the experimental results. This makes it possible to quantify the measured signal in mV with a discharge magnitude in pC. This approach may be useful for online calibration of capacitive couplers.

INTRODUCTION

Partial Discharge (PD) detection and measurement is one of the techniques used to monitor the insulation condition for HV cables as PD activity is both a dominant symptom and cause of deterioration in solid electric insulation. Traditionally, PD tests are carried out offline under laboratory conditions. Recently some non-conventional PD detection techniques such as capacitive couplers, inductive couplers and directional couplers have been developed and partly put into use due to their low cost and suitability for online measurement [1-8]. Among them, the capacitive coupler technique is one of the most popular approaches and can be widely used for PD detection.

The performance of the capacitive coupler is related to many factors including the structure and material of the cable itself, dimensions of the coupler and some uncertain factors such as stray capacitance. In order to understand the capacitive coupler characteristic, Models based on electrical circuits and the electromagnetic field have been established [8,9,10,11]. However, due to unknown parameters and the frequency dependence of these factors these models are only an approximation and have the disadvantage of being computationally intensive.

This paper presents a new modelling method based on system analysis theory and frequency response tests. It is an efficient experimental method to determine system behaviour when the theoretical model of the system is difficult to obtain. Simulation results show good agreement with experimentally obtained results.

FREQUENCY RESPONSE TEST OF CAPACITIVE COUPLERS

Capacitive Couplers

The capacitive coupler and XLPE cable system schematic is shown in Figure1. A HV cable consists of the inner conductor, inner and outer semi-conducting layers, insulation and outer sheath. The capacitive coupler sensor is placed on the outer semi-con layer and consists of an insulation layer (PE film), the electrode (tin tape) and a dielectric substrate (bubble wrap) above the electrode. The sensor is completely covered by the outer earth sheath of the HV cable in order to minimize effect of the external disturbance.

An equivalent circuit of the coupler and cable is shown in Figure 2, where C_c represents the capacitance between the coupler and cable inner conductor, Z_0 represents the cable characteristic impedance, C_s is the stray capacitance between coupler electrode and cable sheath and R_m is the measuring impedance of the digital oscilloscope (50Ohms). The capacitance, C_c, is generally unknown and frequency dependent due to the frequency dependence of the two semi-conducting layers, and the stray capacitance C_s is non-measurable. Therefore the simple equivalent circuit may only provide an approximation of the coupler output for a given input.

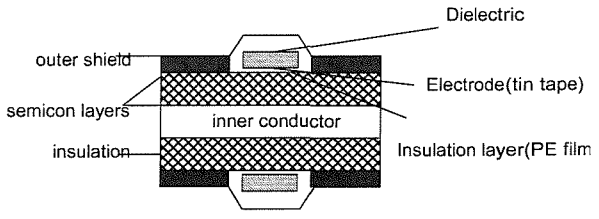

Figure 1. XLPE cable and Coupler Structure

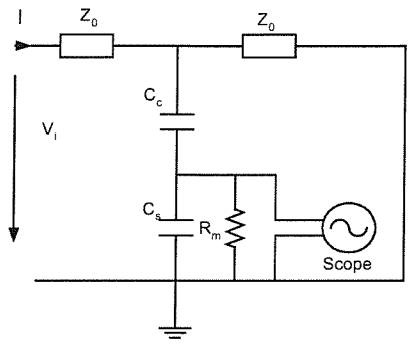

Figure 2. Equivalent circuits for coupler cable system

Frequency Response Test of Couplers

If the PD pulse propagation is considered as signal transmission within a linear system, system theory maybe applied. As a whole physical system, the cable coupler combination can be treated as a 'black box', which has an inherent frequency response characteristic. The interrelation of the system input and output can be described in the form of transfer function.

The experimental arrangement for the frequency response (FR) test of a single coupler and two couplers are shown in Figure 3 and Figure 4 respectively. The Agilent 4395A Network Analyser was used for the FR test up to 500MHz. For a terminal to a coupler FR test, a 15 Ohms matching resistor was used to match the test circuit. For a coupler to another coupler FR test two resistors equal to the characteristic Z_0 (35 Ohms) were used to minimize signal reflection. The FR test results are shown in Figure 5. For the terminal to coupler FR test, the same coupler at different positions (see Figure 4) was tested in order to measure the attenuation effect of the cable.

As can be seen from the results shown in Figure 5, the coupler acts as a high pass filter above 100MHz. In the low frequency range the FR data is seriously contaminated by noise. This is mainly because the 4395A Network Analyser noise level (-85dB) in low frequency range is similar with the actual value of the FR data. The results for different positions show very little difference in FR value. It can therefore be assumed that the attenuation caused over short distance (<3m) is negligible.

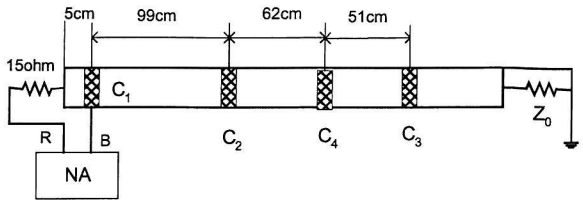

Figure 3. FR test arrangement for a terminal to coupler test

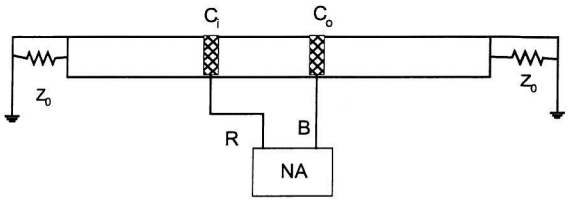

Figure 4. FR test arrangement for a coupler-to-coupler test

Relationship Between Single Coupler FR and Two-coupler FR

In linear system theory two coupler FR data should be half of a single FR data, and the test results confirm the theory in high frequency range (>100MHz) as can be seen from Figure 5. In low frequency range however the results are contaminated by noise and any difference is negligible.

So based on the experiment results, we can assume that the fixed relationship between the FR data of a single coupler and two-coupler always exists if two identical couplers are used and any attenuation is ignored. That means a single FR result can be inferred from the two-coupler FR result. This is significant for online PD measurement as both terminals of the cable are generally not accessible if it is in service.

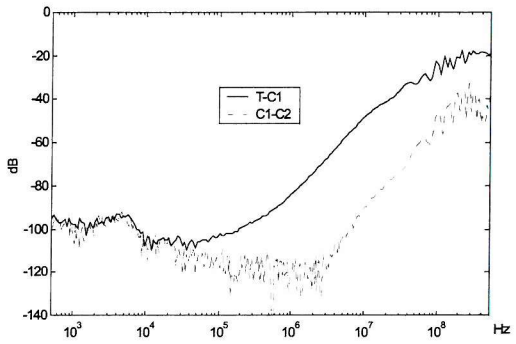

Figure 5. Relationship between a single coupler FR and two-coupler FR

MODELLING OF COUPLERS

Transfer Function of The Coupler

The measured FR results can be easily transferred to Bode diagram by changing the frequency unit in Hz to frequency in radian/second. The Bode diagram of a system corresponds to a transfer function (TF). Thus approximate TF of the coupler can be obtained from the Bode diagram [12].

According to the measured FR result, the single coupler FR can be approximately modelled as a first order system with one zero in the low frequency range (around 10KHz), one pole in the high frequency range (around 100MHz) and a low frequency gain G as expressed in Formula (1).

$$TF1 = \frac{G(s + z_0)}{(s + p_0)} \tag{1}$$

So three parameters need to be determined in order to obtain the TF of a single coupler.

The system pole can be obtained from both FR results at around 2×10^8 Hz, and the system zero can be determined around 2×10^5 Hz. While the gain G has to be corrected as the measured results are noisy and the real value of the FR result in low frequency range has to be found. The corrected gain G can be obtained by comparing the error of measured output and the simulation output. It shows that at G=-81dB, minimum mean square error can be achieved. So the TF of single coupler can approximated expressed as following formula:

$$TF1 = \frac{0.1122(s+2\pi\times2\times10^5)}{(s+2\pi\times2\times10^8)} \tag{2}$$

The corrected Bode diagram as well as measured Bode diagram of the single coupler is shown in Figure 6.

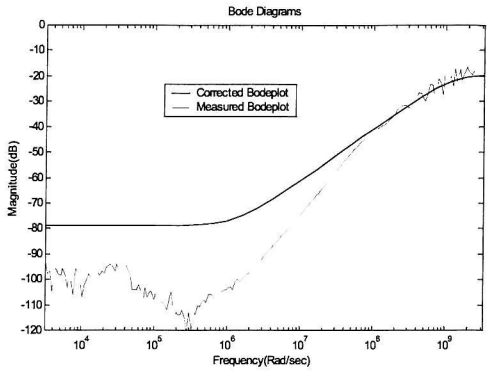

Figure 6. Corrected Bode diagram and measured Bode diagram for a single coupler

The reason for correction of the low frequency gain G is that the measured FR results in low frequency range are noisy if the real value of the FR data is of the same order as the instrument noise level (-85dB).

Simulation Results

A simulation model was established using the above transfer function in Matlab Simulink 3.0. The simulated result is shown in Figure 7 for a 1-nanosecond rise time input pulse. Good agreement is achieved between the simulation and experiment.

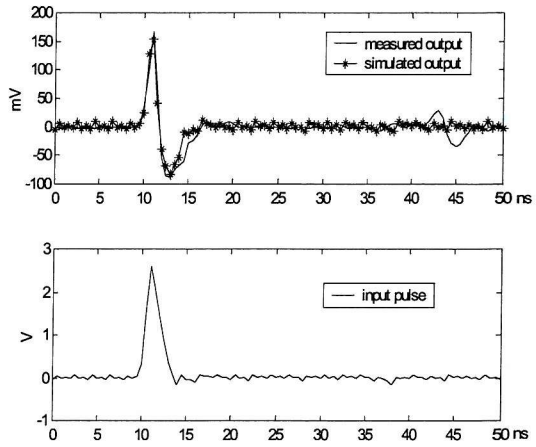

Figure 7. Simulated output and experiment output (1ns)

Models for Different Couplers

The above model is for a 20mm length coupler and the gap between the coupler and cable sheath is 30mm. For different length couplers, FR tests were also undertaken. Figure 8 shows the difference in FR results for different coupler lengths. As can be seen the longer the coupler the greater the response. This is in agreement with the experiment. Models for these couplers can be obtained by similar procedures described above.

CONCLUSIONS

- FR tests show the coupler performance over a wide range of frequency especially at high frequency.

- A simulation model has been established for a 20mm length coupler placed on the 66KV HV cable. The simulated results agree with experimental measurements.

- The simulation model is suitable over the measurement frequency range.

- Similar models can be obtained for couplers having different dimensions.

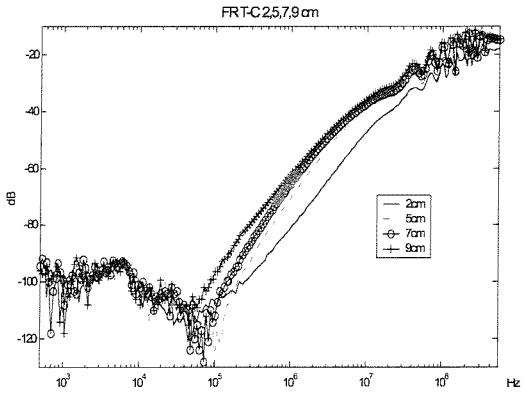

Figure 8 FR results for different dimension couplers

ACKNOWLEDGEMENT

The financial support from National Grid Company is greatly appreciated for this project. This paper is dedicated to the memory of Professor Tony Davies.

REFERENCES

[1] Pommerenke D. and Keith Masterson, "A Novel Concept For Monitoring Partial Discharge on EHV-cable System Accessories Using no Active Components at the Accessories" Dielectric Material, Measurements and Applications Conference Publication No. 473, IEE 2000.

[2] Pommerenke D., T. Strehl, R. Heinrich, W.Kalkner, F.Schmidt and W. WeiBenberg, "Discrimination between Internal PD and Other Pulse Using Directional Coupling Sensors on HV Cable Systems", IEEE Transactions on Dielectrics and Electrical Insulation, Vol. 6 No. 6, December 1999.

[3] Fukunage K., M. Tan and H. Takehana, "New Partial Discharge Detection Method for Live UHV/EHV Cable Joints," IEEE Transactions on Electrical Insulation, Vol. 27 No. 3 June 1992.

[4] Morin R., R. Bartnikas and G. Lessard, "In-service Location of Partial Discharge Sites in Polymeric Distribution Cables using Capacitive and Inductive Probes," IEEE Transmission and Distribution Conference, IEEE Piscataway, NJ, USA, 1999; Vol. 1 pp120-7.

[5] Katsuta Ginzo, Atsushi Toys, Keiichi Muraoka, Takeshi Endoh, Yasuo Sekii and Chuki Ikeda, "Development of Partial Discharge Detection in Extra-High Voltage Cross-Linked Polyethylene Insulated Cable Lines," IEEE Transactions on Power Delivery, Vol. 7, No. 3 July 1992.

[6] Lemke E. and Schmiegel P., "Fundamentals of the PD Probe Measuring Technique" LEMKE DIAGNOSTICS GmbH, Dresden, German (1993).

[7] Lemke E. and Schmiegel P., "Progress in PD-probe Measuring Techniques," 7th International Symposium on High Voltage Engineering, August 26-30, 1991.

[8] Tian Y, P.L. Lewin, A.E.Davies S.G.Swingler, S.J.Sutton and G.M. Hathaway, "Comparison of On-line Partial Discharge Detection Methods for HV Cable Joints" IEEE Transactions on Dielectrics and Electrical Insulation, Vol. 9 No. 4, August 2002.

[9] Tian Y, "Partial Discharge Detection in Cable Systems," Ph.D Thesis, University of Southampton, Department of Electronics and Computer Science, 2001.

[10] Heinrich R, R. Jobava, W. Kalkner and A. Gheonjian, "Numerical Modelling for Investigation and Optimisation of a Sensor for Sensitive Partial Discharge Detection on High-Voltage XLPE Cables" ETEP Vol. 10 No. 3, May/June 2000.

[11] Zhong L, Y Xu, G. Chen, A.E. Davies, Z. Richardson and S.G. Swingler, "Use of Capacitive Couplers for Partial Discharge Measurements in Power Cables and Joints" 2001 IEEE 7th International Conference on Solid Dielectrics, June 25-29, 2001, Eindhoven, the Netherlands.

[12] Dutton K., Thompson S. and Barraclough B. "The Art of Control Engineering", England: Addison-Wesely (1997).

Appendix 3

APPLICATION OF WAVELET-BASED DE-NOISING TO ONLINE MEASUREMENT OF PARTIAL DISCHARGES

P Wang, P L Lewin, Y Tian, S J Sutton* and S G Swingler
High Voltage Laboratory, School of Electronics and Computer Science, University of Southampton,
Southampton, SO17 1BJ, Hampshire, UK
*The National Grid Transco, Warwickshire, UK

Published in 2004 IEEE International Conference on Solid Dielectrics (ICSD 2004)
July 5-9, 2004, Toulouse, France

ABSTRACT

For online detection of partial discharge (PD) activity within power cables and cable accessories, one of the non-conventional PD detection techniques, VHF capacitive coupling has been proved to be suitable. However, the existence of excessive interference will significantly influence the measurement sensitivity and reliability. This paper investigates the application of wavelet transforms for de-noising signals obtained using capacitive couplers. The experimental work has been carried out on a 132kV cable loop with a known defect within the cable joint. Obtained results indicate that the wavelet analysis technique can effectively discriminate internal PD pulses among corona discharges and pulse-like interference. Further, removal of interference has been achieved by applying level dependent threshold values.

INTRODUCTION

Online partial discharge (PD) detection using non-conventional PD techniques such as capacitive couplers, inductive couplers and acoustic emission methods, has recently become popular. However, the big challenge of onsite PD tests is to cope with excessive noise and interference.

A wide range of noise and interference can be experienced during onsite PD measurements, according to their characteristics they can be classified using the following [1]

- Discrete Spectral Interference (DSI) from radio transmissions and power line carrier communication systems
- Periodic pulse-shaped interferences from power electronics and other periodic switching etc.
- Stochastic pulse-shaped interferences due to the discharges from other power equipment
- Random noise similar to the white noise from amplifiers

Various methods for post-processing of PD signals have been reported with the advancement in digital signal processing techniques during the last two decades. These methods include designing of suitable filters (FIR and IIR), Fast Fourier Transform (FFT) based approaches, moving averages, adaptive filtering as well as wavelet analysis. Among them wavelet analysis has recently been found to be an extremely efficient tool in partial discharge detection as it can provide both time and frequency domain information [1-4]. However most published

work is concerned with the processing of signals acquired by conventional PD detection method. For online PD detection, signal post-processing techniques have only been applied to a few non-conventional PD detection sensors so far such as Rogowski coils and current transducers (CT)[5]. It is necessary to investigate the de-noising of signals obtained using capacitive couplers.

WAVELET BASICS AND DENOISING

Basics

A wavelet is a small waveform with limited duration and a zero mean value. Similar to the Fourier Transform, which breaks up a signal into sine waves of various frequencies, the wavelet transform breaks up a signal into shifted and scaled versions of the original (or mother) wavelet. A continuous wavelet transform is defined as the sum over all time of the signal s(t) multiplied by a scaled and shifted version of the wavelet function ψ [6]

$$C(a, b) = |a|^{-1/2} \int s(t)\, \psi\left(\frac{t-b}{a}\right) dt \qquad (1)$$

Where, ψ is the mother wavelet, b is the shift operator and a is the scaling function. The result is a two-dimensional coefficient array of scale a (related to frequency) and position b (related to time) of the time domain signal s(t). The continuous wavelet transform is computationally intensive and generates a lot of redundant data. Therefore the discrete wavelet transform (DWT) is usually employed at $a = 2^j$ and $b = k2^j$ (j, k are positive integers) for speed and convenience.

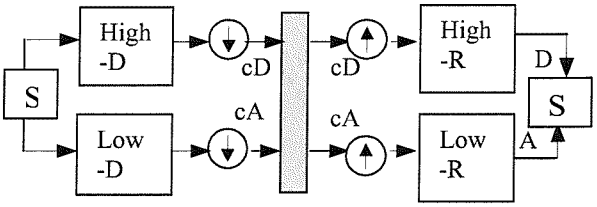

Figure 1. One stage decomposition and reconstruction

Single level signal discrete wavelet decomposition produces a series of approximation coefficients (cA) and detail coefficients (cD) through a low-pass filter (low-D) and a high-pass (High-D) filter respectively as illustrated in Figure 1. The approximation (A) and detail (D) of a signal can be reconstructed using reconstruction filters (High-R, Low-R) based on these coefficients, which correspond to the low frequency and high frequency components of

the signal(s). Multi-resolution Signal Decomposition (MSD) up to level j produces series of approximation and detail coefficients corresponding to multi frequency sub-bands of the signal [6].

De-noising Procedures

The principle of de-noising based on MSD wavelet analysis is simple; first the original signal is decomposed into approximation and detail components up to desired number of levels. This is done by first choosing a suitable mother wavelet according to the signal and noise characteristics. Then those components corresponding to PD signals, interference and random noise are identified at each level by visual inspection and knowledge of frequency characteristics. Finally those coefficients corresponding to interference and random noise are discarded while retaining those coefficients corresponding to PD signals by setting threshold values accordingly. The reconstruction of the signal based on the modified coefficients gives an interference-free signal.

CHARACTERISTICS OF SIGNALS DETECTED BY CAPACITIVE COUPLERS AND ISSUES IN APPLICATION OF WAVELET METHOD

Signal Characteristics Compared to Conventional PD Detection

Compared to the conventional narrow-band PD detection method, capacitive couplers are very sensitive and broadband. Figure 2 shows a PD pulse captured by a capacitive coupler and a conventional PD detector (Robinson 700). The zoomed PD pulse and its frequency distribution are given in Figure 3.

The PD activity itself inside a void is very fast and usually lasts only a few nanoseconds or less. The detected pulse depends on the coupling and measuring system. As can be seen from time domain the PD pulse captured by CC lasts less than 50ns, while the same activity captured by conventional PD detector lasts much longer (30 microseconds) due to its quasi-integral procedure in the measurement. In the frequency domain a conventional PD detector usually works below 1MHz, while the frequency band of the CC is very wide up to several hundreds of MHz. In general, signals detected by CCs are quite different in both time domain and frequency domain with conventional PD detectors, therefore special considerations should be given in the post-processing of these signals using wavelet analysis.

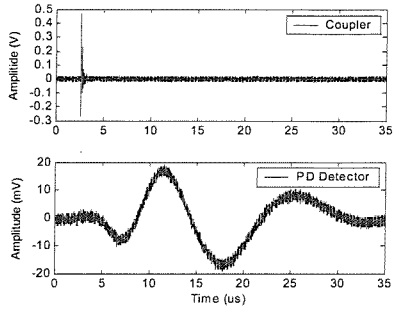

Figure 2 Same PD pulse captured by a CC and a PD Detector

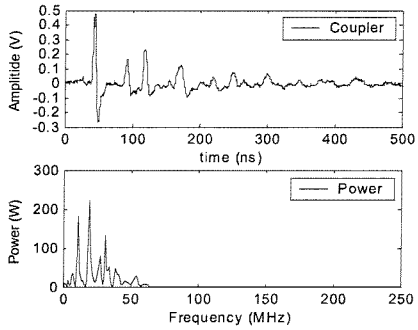

Figure 3 Typical CC PD pulse and its power spectrum

Selection of Mother Wavelet

The selection of the suitable mother wavelet function is essential in using the wavelet analysis. Best wavelets are those that can represent the signal of interest as effective as possible. This can be difficult to implement in practice. In most cases, a trial and error method is used. Ma et al. [3,4] discussed optimal wavelet selection based on calculation of the cross-correlation coefficients between PD pulses and wavelet shapes regarding signals obtained using conventional PD detectors; db2 and db8 are thought to be the best wavelet for analysing an exponential PD pulse and a damped resonant PD pulse respectively. From the frequency point of view, the main consideration in choosing the wavelet is the central frequency of the wavelet compared to the signal of interest. In this application, db1 was chosen as it has the highest central frequency in Daubeches family. Some other wavelets with sharp waveform such as lower order biorthogonal wavelets bior1.1 and reverse biorthogonal wavelets rbio1.1 and rbio1.3 can also give good results.

Number of Decomposition Levels

The determination of the number of decomposition levels depends on the lowest interference frequency bands to be eliminated from the signal. The goal is to have sufficient resolution in the low frequency range in order to suppress the interference completely. 10 levels were chosen and found to be sufficient for this application.

Threshold

The de-noising procedure involves thresholding of those coefficients corresponding to signals and interference as mentioned above. The determination of threshold values is based on the identification and evaluation of these coefficients corresponding to the signal and interference. In this application threshold values are manually determined as no automatic threshold rules are available for pulse-shaped interference. Hard-threshold method was adopted as it can maintain the PD pulse magnitude better than the soft-threshold method.

TEST ARRANGEMENT

The HV test was carried out on a 132kV cable loop system as illustrated in Figure 4. Two sections of cable are connected through a prefabricated cable joint with a known defect (conducting paint). Both ends of the cable are terminated with oil-filled cable terminations. A capacitive coupler (CC) is installed near the defect side of the cable in order to detect the internal PD activities caused by the conducting paint inside the joint. A surge protector (sgp) with maximum operating frequency up to 1GHz and response time less then 10ns is connected to the output of the coupler to protect the measuring system from possible over-voltage. The measuring system consists of a digital oscilloscope (LC684DXL) and a personal computer. A 20dB broadband amplifier (up to 1GHz) is used to amplify the signal before it is fed to the digital oscilloscope. The personal computer is connected to the oscilloscope via a GPIB board to collect the data for post-processing.

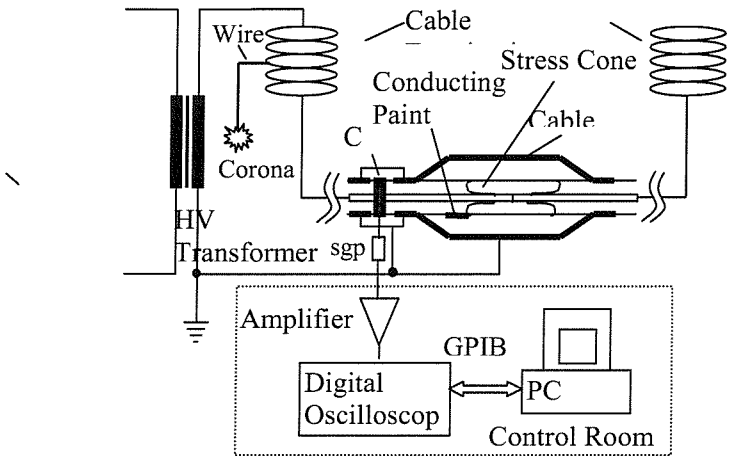

Figure 4 Experiment arrangement

Based on the frequency components shown in Figure 3, in which sampling rate of 1GHz was used to ensure the sampling complies with Shannon's sampling theorem. As can be seen from it, the power frequency components of the PD pulse detected by CC is below 100MHz. So a lower sampling rate of 250MHz was used to ensure manageable amounts of data are collected over a power cycle.

Corona discharges are the most common interference during online PD measurements. In this case corona discharges were produced using a metal wire connected to the HV side (Figure 4).

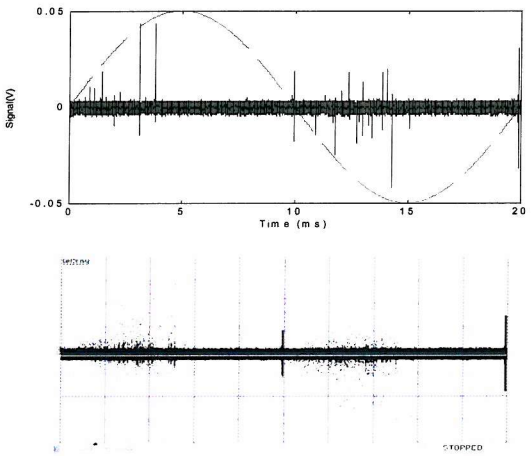

Figure 5 PD activities without corona interference and their persistence plot at 35kV

RESULTS

PD Activities Without Corona Interference

The test was first carried out without introducing corona interference. Figure 5 shows the obtained PD activities over one power cycle (20ms) and their persistence plot under high voltage of 35kV. Two fixed phase interference pulses located approximately at 10ms and 20ms have been detected as can be seen from the persistence plot. The pulses in the first and third quadrants are internal PD pulses.

Wavelet De-noising of PD with Corona Interference

Corona discharges were introduced into the system as external interference. Figure 6a and Figure 7 show the result and its persistence plot over one power cycle at an applied high

voltage of 30kV. The persistence plot clearly shows corona discharge pulses around the negative peak and two other pulse-shaped interference pulses. However from the original signal shown in Figure 6a, internal PD pulses and external corona discharge pulses are mixed together and it is difficult to discriminate between them just by visual inspection.

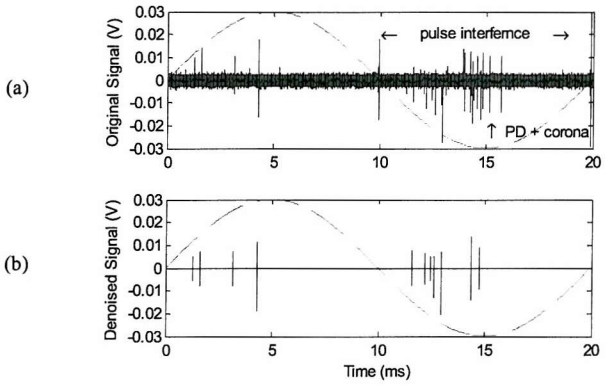

Figure 6 (a) original and (b) de-noised signals for 1 power cycle

The original signal has then been decomposed into details and approximations up to 10 levels using the db1 wavelet (Figure 8). The detail level 1 D1 clearly shows all of the internal PD pulses, while the corona pulses are mostly concentrated in detail level 3 D3. The two pulse-shaped interference pulses located at 10ms and 20ms cannot be seen in D1 and D2 at all. They are distributed among several levels from D3 to D9. This indicates that their frequency components are much lower than that of corona pulses and internal PD pulses. This kind of pulse interference always occurs at specific phase angles and is very common in PD tests. Köpf et al. [7] have reported similar interference pulses. They are caused by facilities that are operating synchronously with the mains such as rotating machines with commutators, rectifiers as well as other power electronic devices.

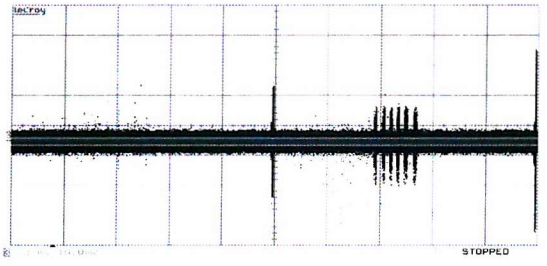

Figure 7 Persistence plot of Figure 6a

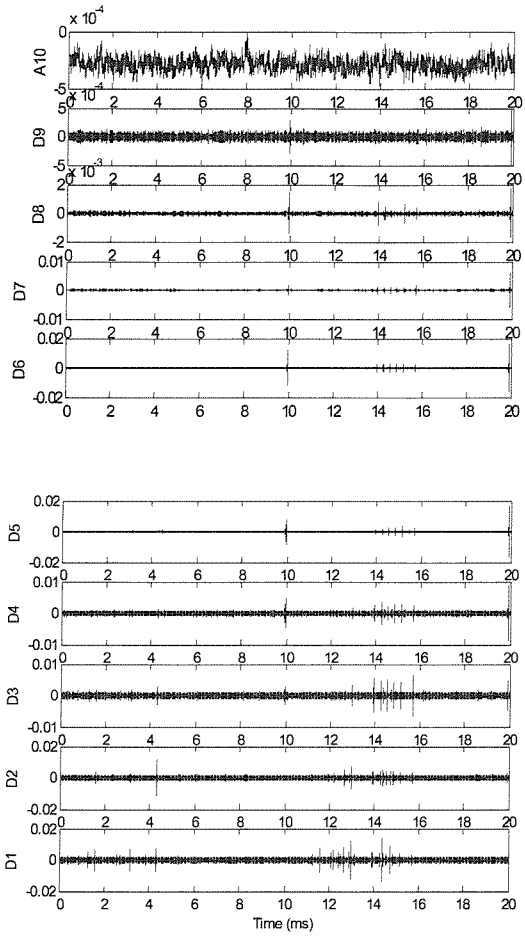

Figure 8 Decomposition results of the original signal in Figure 6a

The above wavelet decomposition has effectively discriminated internal PD pulses among external corona discharges and two synchronous interference pulses. The final procedure is de-noising by setting threshold values at each level. This has been done manually in this case with the following threshold values from level 1 to level 10 ([0.006, 0.01, 0.017,0.038, 0.088, 0.166, 0.063, 0.026, 0.018, 0.019]). All pulse-shaped interference and random noise have been effectively removed as can be seen from Figure 6b.

CONCLUSIONS

Regarding the characteristics of the capacitive coupler, wavelet analysis has been applied to the signals obtained using capacitive couplers. Results shows that it can effectively discriminate internal PD pulses among pulse-shaped interference such as corona discharge and synchronous pulse interference as well as random noise through carefully selection of the mother wavelet function and decomposition levels. Further removal of interference has been accomplished by setting threshold values for each level. Signal to noise ratio has been

significantly increased with minimum loss of pulse magnitude and distortion of the pulse shape. This is significant considering online PD measurements and further quantification of measured results.

REFERENCES

[1] L. Satish and B. Nazneen, "Wavelet-based Denoising of Partial Discharge Signals buried in Excessive Noise and Interference," *IEEE Trans. Dielec. Electr. Insul.,* Vol. 10, pp354-367, Apr. 2003.

[2] X. Ma, C. Zhou and I. J. Kemp, "Interpretation of Wavelet Analysis and Its application in Partial Discharge Detection," *IEEE Trans. Dielec. Electr. Insul.,* Vol. 9, pp446-457, June 2002.

[3] X. Ma, C. Zhou and I.J. Kemp, "Automated Wavelet Selection and Thresholding for PD Detection," *IEEE Electr. Insul. Mag.,* Vol. 18, No. 2. pp37-45, Mar./Apr. 2002.

[4] I. Shim, J.J. Soraghan and W. H. Siew, "Detection of PD Utilizing Digital Signal Processing Methods Part 3: Open-loop Noise Reduction," *IEEE Electr. Insul. Mag.,,* Vol.17, No.1 pp6-13, Jan./Feb. 2001.

[5] H. Borsi, "A PD Measuring and Evaluation System Based on Digital Signal Processing," *IEEE Trans. Dielec. Electr. Insul.,* Vol. 7 No. 1, pp21-29, Feb. 2000.

[6] Wavelet Toolbox 2.2 Manual - User's Guide The Math Works Inc. 2002.

[7] U. Köpf and K. Feser, "Rejection of Narrow-band Noise and Repetitive Pulses in On-site PD Measurements," *IEEE Trans. Dielec. Electr. Insul.,* Vol. 2 No. 6, pp1180-1191, Dec. 1995.